Performance bounds in terms of estimation and resolution and applications in array processing

Nguyen Duy Tran

THESE DE DOCTORAT

DE L'ÉCOLE NORMALE SUPÉRIEUR DE CACHAN

Présentée par

Monsieur TRAN Nguyen Duy

pour obtenir le grade de

DOCTEUR DE L'ÉCOLE NORMALE SUPÉRIEUR DE CACHAN

Domaine

Électronique - Électrotechnique - Automatique

Sujet de la thèse :

Performances limites en termes d'estimation et de résolution et applications aux traitements d'antennes

Thèse présentée et soutenue à ENS de Cachan le 24 Septembre 2012 devant le jury composé de :

Mr.	Yannick BERTHOUMIEU	ENSEIRB-MATMECA	Rapporteur
Mr.	Pascal CHARGE	Université de Nantes	Rapporteur
Mr.	Pascal CHEVALIER	CNAM	Examinateur
Mr.	Pascal LARZABAL	ENS de Cachan	Directeur de thèse
Mr.	Alexandre RENAUX	Université Paris-Sud XI	Encadrant
Mr.	Rémy BOYER	Université Paris-Sud XI	Encadrant

Laboratoire des Systèmes et Applications des Technologies de l'Information et de l'Énergie (SATIE)
École Normale Supérieure de Cachan / CNRS / UMR 8029
61, avenue du Président Wilson, 94235, Cachan Cedex, France

Laboratoire des Signaux et Systèmes (LSS)
Université Paris-Sud / SUPELEC / CNRS / UMR 8506
3 rue Joliot Curie,91192, Gif-sur-Yvette, France

Résumé

Cette thèse porte sur l'analyse des performances en traitement du signal et se compose de deux parties :

- Premièrement, nous étudions les bornes inférieures dans la caractérisation et la prédiction des performances en termes d'erreur quadratique moyenne (EQM). Les bornes inférieures de l'EQM donne la variance minimale qu'un estimateur peut atteindre et peuvent être divisées en deux catégories : les bornes déterministes pour le modèle où les paramètres sont supposés déterministes (mais inconnus), et les bornes Bayésiennes pour le modèle où les paramètres sont supposés aléatoires. En particulier, nous dérivons les expressions analytiques de ces bornes pour deux applications différentes : (i) La première est la localisation des sources en utilisant un radar multiple-input multiple-output (MIMO). Nous considérons les bornes inférieures dans deux contextes c'est-à-dire avec ou sans erreurs de modèle. (ii) La deuxième est l'estimation de phase d'impulsion de pulsars à rayon X qui est une solution potentielle pour la navigation autonome dans l'espace. Pour cette application, nous avons calculé plusieurs bornes inférieures de l'EQM dans le contexte de données modélisées par une loi de Poisson (complétant ainsi les travaux disponibles dans la littérature où les données sont modélisées par une loi gaussienne).
- Deuxièmement, nous étudions le seuil statistique de résolution limite (SRL), qui est la distance minimale en termes des paramètres d'intérêts entre les deux signaux permettant de séparer / estimer correctement les paramètres d'intérêt. Plus précisément, nous dérivons le SRL dans deux contextes : le traitement d'antenne et le radar MIMO en utilisant deux approches basées sur la théorie de l'estimation et sur la théorie de l'information. Finalement, nous proposons des expressions compactes du SRL dans le cas d'erreurs de modèle.

Mots clés : Traitement d'antenne, théorie de l'estimation, théorie de la détection, multiple-input multiple-output radar, navigation espace autonome, analyse de performance, borne inférieure de l'erreur quadratique moyenne, estimation de direction d'arrivée, seuil statistique de résolution limite, signaux multidimensionnels.

Abstract

This manuscript concerns the performance analysis in signal processing and consists into two parts :

– First, we study the lower bounds in characterizing and predicting the estimation performance in terms of mean square error (MSE). The lower bounds on the MSE give the minimum variance that an estimator can expect to achieve and it can be divided into two categories depending on the parameter assumption : the so-called deterministic bounds dealing with the deterministic unknown parameters, and the so-called Bayesian bounds dealing with the random unknown parameter. Particularly, we derive the closed-form expressions of the lower bounds for two applications in two different fields : (i) The first one is the target localization using the multiple-input multiple-output (MIMO) radar in which we derive the lower bounds in the contexts with and without modeling errors, respectively. (ii) The other one is the pulse phase estimation of X-ray pulsars which is a potential solution for autonomous deep space navigation. In this application, we show the potential universality of lower bounds to tackle problems with parameterized probability density function (pdf) different from classical Gaussian pdf since in X-ray pulse phase estimation, observations are modeled with a Poisson distribution.
– Second, we study the statistical resolution limit (SRL) which is the minimal distance in terms of the parameter of interest between two signals allowing to correctly separate/estimate the parameters of interest. More precisely, we derive the SRL in two contexts : array processing and MIMO radar by using two approaches based on the estimation theory and information theory. We also present in this thesis the usefulness of SRL in optimizing the array system.

Keywords : Array processing, estimation theory, detection theory, multiple-input multiple-output radar, space navigation, statistical resolution limit, asymptotic and non-asymptotic performance analysis, lower bounds on the mean square error, multidimensional signals.

Table des matières

Chapitre 1

Introduction

Statistical signal processing is a vast area with applications in many fields of science and engineering. One important object of signal processing is to extract relevant information, generally referenced as parameters of interest, from a set of noisy measured observations. These unknown parameters can be an angle of arrival (in radar or sonar), a phase (in space navigation) or a time-delay (in telecommunications), etc.... The estimation theory provides a formal framework for solving this type of problems. More particularly, in the so-called parametric estimation, we first fix a physical observation model which is usually a nonlinear function of the parameters of interest. Then, from the probability distribution of this model, we employ an estimator, i.e. an estimation rule, to estimate the parameters of interest. In the literature, there are two categories of estimator : the optimal and the sub-optimal estimators which are distinguished by how close the estimated values of the unknown parameters are to the real ones. Experience shows that while the former category is more accurate, the latter requires less computational complexity.

The parameter estimation is usually done by finding a global maximum of a criterion depending on the estimator. The accuracy of an estimator or the difference between the estimated and the real values of the parameter of interest can be quantified via its mean square error (MSE). One can see in the literature [Van68] that the MSE of an estimator for a non-linear problem can be divided into three regions with respect to (w.r.t) the signal-to-noise ratio (SNR) or the number of observations (see figure 1.1 where the MSE of the maximum likelihood estimator for the spectral analysis is presented with 1000 snapshots). The first region is where the SNR or the number of observations is high, the MSE is small and this region is called asymptotic. Next, when the SNR or the number of observations reduces, the estimation error raises rapidly due to the appearance of outlier in the searching criterion. There appears the so-called threshold effect, hence, this region is call threshold region. Finally, the so-called non-information region is where the SNR or the number of observations is very low so that the observation is mainly the noise component. So, the estimation has a quasi-uniform distribution on the support of the parameter and the MSE becomes a flat line.

In general, the MSE of an estimator is evaluated by using Monte Carlo trials. In each trial, the estimated parameter is searched as the global maximum of a criterion depending on the estimator. Consequently, when a multi unknown parameter problem involves, it requires a multidimensional search, leading to a very high computational complexity. In addition, employing the Monte Carlo method does not allow us to have an analytical expression of the MSE which is essential to optimize the system performance. This demands another solution that is independent of any estimators and can give a panorama

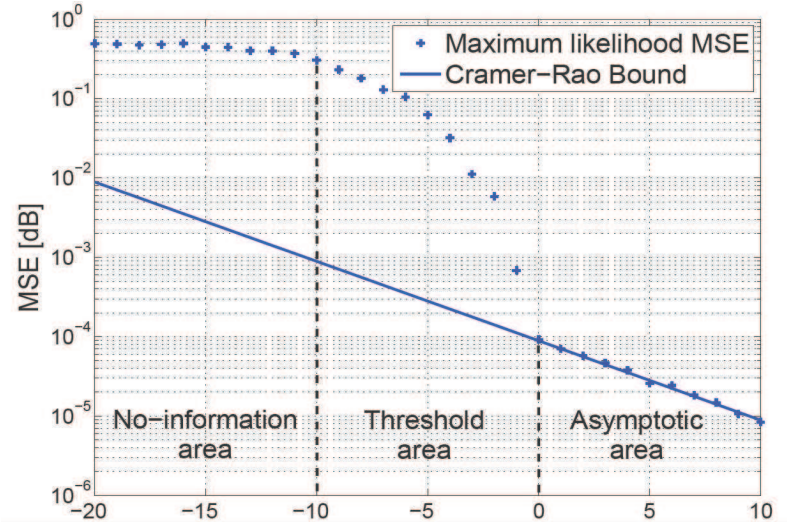

FIGURE 1.1 – Three zones of operation of the MSE of the maximum likelihood estimator.

view of the estimation performance in terms of MSE. In signal processing, the so-called lower bound on the MSE which gives the minimum variance that an estimator can expect to achieve, can fill this lack. The lower bound on the MSE can be divided into two categories depending on the parameter assumptions [TB07]. When the unknown parameters are assumed to be deterministic, the so-called deterministic bounds that evaluate the "locally best" behavior of the estimators have been proposed. An example of this category is the well-known Cramér-Rao bound (CRB) [Cra46, Rao45] which is also showed in figure 1.1. The other category, the so-called Bayesian bounds, deal with the random parameter and presume an *a priori* probability density function (pdf) so that they can evaluate the "globally best" performance of an estimator.

As aforementioned, in estimation theory, the lower bound on the MSE appears to have the capabilities to investigate the estimation performance of the system instead of using the Monte Carlo simulations. However, in practice, many questions come out. Can we derive the closed-form expressions of the lower bound for practical problems ? How can the lower bound be used to optimize the system ? How can we predict the threshold point using the lower bound ? Motivated by these questions, the first part of this thesis is dedicated to study specifically practical problems to demonstrate the usefulness of lower bounds in characterizing, predicting and optimizing the estimation performance in terms of MSE.

In the literature, another approach to investigate the performance of a system, beside the MSE criterion, is the statistical resolution limit (SRL). The SRL is the minimal distance in terms of the parameter of interest between two signals allowing to correctly separate/estimate the parameters of interest. The problem of SRL for two closely spaced sources has attached many interests with applications such as radar, sonar, image processing. There are many ways to describe and derive the SRL in the literature. The earliest way is based on the concept of the mean null spectrum concerning the specific estimation algorithms [Cox, KB86, AD08]. While the concept of this approach is quite simple, its application is limited to the used estimation algorithm. Hence, the second part of this thesis considers other approaches, independent of the algorithm, to derive the closed-form expressions of the SRL and to optimize the system using these expressions. Particularly, we

examine the SRL based on estimation accuracy*i. e.* the CRB [Lee92, Lee94, Smi05, Dil98] and the SRL based on the Stein's lemma [CT, Che56] for some array processing problems.

1.1 Results and thesis outline

The results of this thesis are presented in two parts

- In Chapter 2, we have examined the lower bounds in two different contexts. The first one is the target localization using the MIMO radar for which we have developed the Weiss-Weinstein bound [WW85] for Bayesian parameter and the CRB for deterministic parameter in the presence of modeling errors. For the Bayesian case, we have shown that the Weiss-Weinstein bound for the parameter of interest provides a good prediction of the MSE in all regions. It also predicts the threshold SNR location near the threshold SNR indicated by the maximum *a posteriori* estimator. We also introduced a numerical procedure to optimize antenna geometry of MIMO radar in terms of the MSE. For the case with modeling errors, we have derived closed-form expressions of the Fisher information matrix and shown its block diagonal structure to deduce the Cramér-Rao bounds expressions of the angle-of-arrival and of the angle-of-departure. We have shown that, under a certain signal-to-noise ratio, the performance of the system can not be improved. Finally, we have proposed a simple formula to evaluate this critical value of the signal-to-noise ratio. The second context is the pulse phase estimation of X-ray pulsars for which we have derived the closed-form expressions of the Quinlan-Chaumette-Larzabal bound [CGQL08] for the deterministic parameter and the Weiss-Weinstein bound for the Bayesian parameter. We have shown that both types of lower bound provide good prediction of the threshold location depending on the estimation framework while the computational complexity remains very low in comparison to the maximum likelihood estimator.

- In Chapter 3, we derived the closed-form expressions of the SRL based on estimation accuracy and the SRL based on the Stein's lemma. First, we derived and analyzed the angular resolution limit (ARL) based on the Lee's criterion and the Smith's criterion in the context of array processing in the presence of modeling errors. We showed that, as the signal-to-noise ratio increases, the ARL does not fall into zero (contrary to the classical case without modeling errors) and converges to a fixed limit depending on the method for which we gave a closed-form expression. It can be seen that at high SNR, the ARL in the Lee and Smith sense are linear in the error variance. We have also investigated the influence of array geometry on the ARL based on the Lee's and Smith's criteria. Second, we followed the approach based on the Stein's lemma to derive the SRL. We examined this approach in two difference contexts : (i) in the context of array processing, the ARL based on the Stein's lemma is derived and compared to the ARL based on the Lee's and Smith's criteria. It has been seen that the ARL based on the Chernoff distance and the Smith's criterion have a similar behavior and they are proportional by a factor which depends on the probabilities of false alarm and of detection and not of the signal parameters. We also show that for orthogonal sources and/or a large number of snapshots, it is possible to give a unified expression of the ARL for the three considered approaches. (ii) In the context of MIMO radar, the ARL is derived when the transmitting array and the receiving array are either widely spaced or collocated. It has been seen that the behavior of resolution limit is different when the amplitudes of the targets are

identical or not. Numerical results have shown that the resolution limit is better when the amplitudes of two targets are not identical.

The contributions of this thesis are published (or submitted) in :

International journal

- [TRBML12] N. D. Tran, A. Renaux, R. Boyer, S. Marcos and P. Larzabal, "Weiss-Weinstein bound for MIMO radar with colocated linear arrays for SNR threshold prediction", Elsevier Signal Processing, Volume : 92, Issue : 5, May 2012, pp. 1353-1357.
- [TRBML] N. D. Tran, A. Renaux, R. Boyer, S. Marcos and P. Larzabal, "Performance Bounds for The Pulse Phase Estimation of X-Ray Pulsars", IEEE Transactions on Aerospace and Electronic Systems, in minor revision.
- [TBRMLb] N. D. Tran, R. Boyer, S. Marcos and P. Larzabal, "Angular Resolution Limit for array processing in the presence of modeling errors", IEEE Transactions on Signal Processing, accepted for publication with mandatory minor revision.

Conference

- [TRBML11a] N. D. Tran, A. Renaux, R. Boyer, S. Marcos and P. Larzabal, "MIMO radar in the presence of modelling error : a Cramér-Rao bound investigation", in Proc. of IEEE International Conference on Acoustics, Speech, and Signal Processing, ICASSP-11, Prague, Czech Republic.
- [TRBML11b] N. D. Tran, A. Renaux, R. Boyer, S. Marcos and P. Larzabal, "Radar MIMO en présence d'erreurs de modèles : une approche par les bornes de Cramér-Rao", in Proc. of Colloque GRETSI 2011, Bordeaux, France.
- [TBRMLc] N. D. Tran, R. Boyer, A. Renaux, S. Marcos and P. Larzabal, " Theoretical Multidimentional Resolution Limit for MIMO Radar based on the Chernoff distance", in Proc. of IEEE Workshop on Statistical Signal Processing, SSP-2012, Chicago, USA.
- [TBRMLd] N. D. Tran, R. Boyer, S. Marcos and P. Larzabal, "Angular Resolution Limit for array processing : estimation and information theory approaches", in Proc. of 20th European Signal Processing Conference, EUSIPCO-2012, Bucharest, Rumania.

Chapitre 2

Applications of performance bounds on the mean square error in MIMO radar and Pulse Phase Estimation of X-ray Pulsars

2.1 Introduction

In the literature of signal processing, the lower bound on the MSE is a solution that is independent of any estimators and can give a panorama view of the estimation performance in terms of MSE. Rigorously, the lower bound on the MSE gives the minimum variance that an estimator can expect to achieve and it can be divided into two categories depending on the parameter assumptions [CGQL08]. When the unknown parameters are assumed to be deterministic, the so-called deterministic bounds that evaluate the "locally best" behavior of the estimators have been proposed. Examples of this category are the well-known Cramér-Rao bound (CRB) and bounds on the Barankin family as Mcaulay–Seidman bound [MS69] and Quinlan-Chaumette-Larzabal (QCL) bound [CGQL08]. The other category, the so-called Bayesian bounds, deal with the random parameter and presume an *a priori* probability density function (pdf) so that they can evaluate the "globally best" performance. The representatives of this category are the Weiss-Weinstein bound (WWB) [WW85] and the Ziv-Zakai bound [ZZ69].

In deterministic bounds, the CRB is the first and also the most popular due to its simplicity of calculation and the fact that in the asymptotic region, this bound can be achieved by the maximum likelihood estimator (MLE). However, the limitation of the CRB shows up when the SNR or the number of observations reduces to a critical limit, the so-called threshold phenomenon in terms of MSE performance appears. This phenomenon can be explained by the distorted cost function used by estimators whose global extremum appears at a far point from the true value [RB74]. Typically, the threshold value can be predicted by using other bounds tighter than the CRB such as the Barankin family. Mathematically, the Barankin bound (BB) [Bar49] is known to be tighter than the CRB, however, it is not computable. In classical array processing, to obtain a computable BB, several approximations of BB were proposed [CGQL08] and one of the tightest bounds among the Barankin family is the QCL bound [CGQL08] which, along with the CRB, will be considered in this work.

As an alternative to the deterministic case, the Bayesian bound provides a tight minimal bound over all the range of SNR or observation time and a good prediction of the SNR or observation time threshold. The Bayesian bounds deal with the random parameter and presume an *a priori* pdf on the support of the parameters. Hence, the advantage of Bayesian bounds over the deterministic bounds is their capability to give the fundamental limits of an estimator in terms of MSE over all the MSE range. However, the usefulness of the deterministic bound still remains when the parameter is deterministic. One can find in the literature various types of Bayesian bounds including the Ziv-Zakai bound [ZZ69], the Bell-Steinberg-Ephraim-Van Trees bound [BSET97], the Bobrovsky-Zakai bound [BZ76], the Bayesian Abel bound [RFLR06], and the Weiss-Weinstein bound [WW85, RO07a, RO07b]. Note that not all the Bayesian bounds proposed in the literature are able to take into account the case when the parameters of interest are supposed to be uniformly distributed.

The primary goal of this chapter is demonstrate the usefulness of lower bounds in characterizing and predicting the estimation performance in terms of MSE, both for deterministic and random parameters. Therefore, we here consider two applications in two different fields. The first one is the target localization using the MIMO radar, which is an emerging technology in array processing. The other one is the pulse phase estimation of X-ray pulsars which is a potential solution for autonomous deep space navigation. Note that the works in this chapter also show the potential universality of lower bounds to tackle problems with parameterized pdf different from classical Gaussian pdf since in X-ray pulse phase estimation, observations are modeled with a Poisson distribution. To the best of our knowledge, there are very few results on lower bounds relevant to this kind of pdf. We can cite here the works in [AL01] and in [Mar97] where the behavior of the CRB and a simple approximation of the Barankin bound are studied respectively in emission tomography. However, those articles do not consider the Bayesian case.

The first contribution of this chapter is to investigate the estimation performance of the MIMO radar in terms of MSE. Since it was first introduced [FHB$^+$04], MIMO radar has been receiving the attention of researchers and practitioners. A MIMO radar (see figure 2.1) is a system that uses simultaneously multiple antennas which transmit and receive a set of probing waveforms to collect information of targets. The probing waveforms can be chosen freely and can be fully uncorrelated or partially correlated. The conventional phased array radar (see figure 2.2) is a case of MIMO radar where all the transmitted waveforms are correlated. Besides, the positions of antennas of MIMO radar can be set to be collocated or widely separated. Thank to these additional degrees of freedom, it is known that a MIMO radar system has many advantages in comparison with a phased-array radar in terms of detection/estimation (see, *e.g.* [LS09] and [FHB$^+$04]). Depending on the positions of antennas (collocated or widely separated), each configuration of MIMO radar has its own interests such as improving parameter identifiability [LS09] [LSXR07] ; offering higher flexibility in transmit beam pattern designs : improving the angular resolution, lowering sidelobes, or decreasing the spatial power density of transmitted signals [LS09] ; increasing detection performance, and allowing direct applicability of adaptive techniques for parameter estimation [XLS08].

If we focus on target localization, the superiority of MIMO radar's performance w.r.t. the phased-array radar has been shown in terms of lower bound on the MSE. To the best of our knowledge, all the existing works available in the literature concern only the case of deterministic parameter for the location of the target. In [FHB$^+$04], preliminary calculations of the CRB have been introduced. The considered model was the collocated uniform linear array (ULA) for both transmitting and receiving arrays. In [GHB08] and

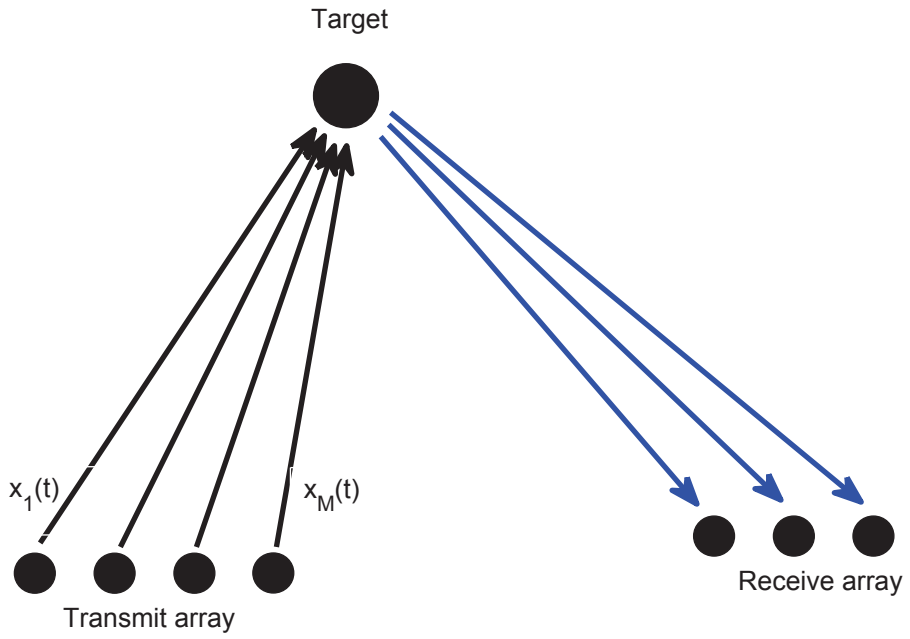

FIGURE 2.1 – MIMO radar

[HBGH08], a MIMO radar with widely-separated antennas was studied and the CRB has been calculated for target position and velocity. Besides, Jian Li *et al.* have investigated the waveform optimization of MIMO radar based on the CRB using collocated ULA transmitting and receiving antennas [LXS+08, Boy11]. While all the above works have exploited the asymptotic region of the MSE over SNR performance, the Barankin bound has been shown to give a SNR threshold approximation in the scenario of collocated circular array configuration [Tab06, LS09](chapter 4).

All these above investigations handle only the cases where the unknown parameters are assumed to be deterministic. To have a complete analysis of the MIMO radar performance, among various types of Bayesian bounds, we concentrate, in Section 2.2, on the WWB, which can deal with the uniformly distributed prior assumption and is one of the tightest bound of the Weiss and Weinstein family [RFL05, RFL+08]. The scenario under investigation is a MIMO radar estimating the direction-of-arrival (DOA) of a target and the complex radar-cross-section (RCS) in the Swerling 0 case. Our results are derived in the case of linear (possibly non-uniform) collocated arrays at emission and reception. We first propose a strict bound for which it is not possible to obtain a closed-form expression. While a numerical integration is still possible, we also propose a closed-form expression based on an approximation.

As aforementioned, the MIMO radar system has superior capabilities compared with a phased-array radar. However such good performance can be achieved only when the observation model of the MIMO radar is well known because the powerful detection/estimation techniques used are often based on statistically optimal algorithms such as the maximum

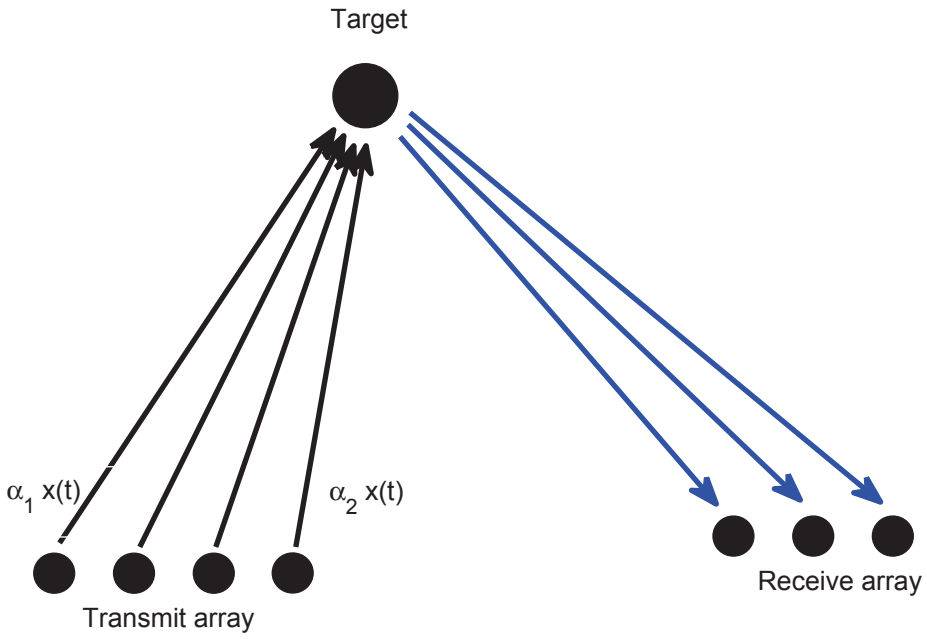

FIGURE 2.2 – Phased array radar

likelihood technique. Indeed, in the literature, the system model is supposed to be correct, *i.e.* the array response is supposed to be precisely known. However, in practice, the assumed model is different from the true one due to the variation of array element positions or the differences in element patterns. Even though this mismatch is usually regulated by a calibration procedure, the imperfections in the array still exist and degrade the system performance. Besides, a precious calibration procedure is expensive and time consuming. Hence, it is important to investigate the modeling errors in MIMO radar to reduce the requirements without a noticeable degradation in the performance. This is why, in this work, we focus on the influence of modeling error at the receiver of a MIMO radar on the localization of a target. We consider for this analysis the so-called widely separated MIMO radar with linear arrays (possibly non-uniform or lacunar) where the localization parameter of the target are the angle-of-departure and the angle-of-arrival. In the literature, there is few result for the behavior of MIMO radar in the presence of modeling errors. Mainly, an analysis via performance bounds of MIMO radar affected by modeling errors can be found in [GHP09, HB10, GHP10, AN10]. However, in these work only phase synchronization errors are studied. Also, some works have been done in passive array processing. One can cite [RP87], [VS94] and recently [FLV10]. Our approach follows the idea presented in [FLV10] where the error is modeled by a Gaussian random vector added to the true steering vector.

In Section 2.3, we derive the CRB w.r.t unknown target parameters in the context of MIMO radar in which the receiver suffers from an array response error. Then, the proposed closed-form expressions are analyzed and it is shown that the Cramér-Rao bound and the

mean square error of the maximum likelihood estimator of the angle-of-arrival do not fall into zero (contrary to the classical case without modeling error) and converge to a fixed limit for which we give a closed-form expression. Moreover, we give a simple closed-form expression of the critical value of the SNR where this limitation of performance appear.

The final contribution of this chapter is to give a insight of the pulse phase estimation of X-ray pulsars which is a potential solution for autonomous deep space navigation. One can find that the development of deep space operation requires accurate and autonomous navigation solutions for the purpose of orienting and controlling a spacecraft. The actual solution, the ground-based navigation, is very accurate but highly depends on the communication with the ground station, and therefore, is not robust to a loss of contact. Besides, large errors can occur in shadowing areas or at large distance from the ground. While satellite navigation systems, such as the Global Positioning System (GPS), are helping devices operating inside the orbit of the GPS constellation to internally determine their location within a few meters or even less, a similar solution for spacecraft is still an open question. In this context, the celestial-based system that uses signals from celestial sources is a potential candidate to solve this problem. Among various types of celestial sources, pulsars, discovered in 1967, are the subset that emits highly regular, stable, and periodic signals. Their behavior has been observed for years, so the shape and period of their pulse profile are known very accurately. This property could be of the utmost interest for navigation objectives. Therefore, in this contribution, we focus on pulsars among other celestial sources. In the literature, two kinds of pulsars were examined for navigation purposes : sources that emit in the radio band and sources that emit in the X-ray band. We here consider the X-ray pulsars for their feasibility in implementation (thanks to the smaller sized detectors compared to those of radio band) and better accuracy [RWP06].

In pulsar-based navigation, the observed signal is the pulse time-of-arrival (TOA) (or the pulse phase) at the detector. Processing this signal with respect to the recorded database gives us the specific information of the location of the spacecraft. The main problem in this kind of navigation is to estimate very precisely the pulse initial phase, and this challenge has been examined in the literature. In [GS07], the statistical model of the pulse TOA has been developed and the pulse phase estimation is investigated by deriving and analyzing the maximum likelihood estimator (MLE) and the Cramér-Rao bound (CRB). In [ES10], the nonlinear least-squares (NLS) estimator of the pulse phase is proposed and compared to the MLE in terms of computational complexity and the MSE over the observation time. In both papers, one can observe, in terms of MSE performance, the so-called threshold phenomenon which appears as the observation time is below a critical limit. As the CRB can not be used to observed this phenomenon, in Section 2.4, we exploit both different deterministic and Bayesian bounds to analyze the behavior of the MSE and to predict the threshold position. Particularly, we derive the closed-form expression of the QCL bound (deterministic case) and the WWB (Bayesian case), then we present some simulations to confirm the good ability of the derived bounds to predict the performance of the MLE.

2.2 Weiss-Weinstein Bound for MIMO Radar with collocated linear arrays for SNR threshold prediction

This Section is organized as follows : Section 2.2.1 presents the general problem setup with collocated linear arrays. In Section 2.2.2, we calculate the corresponding WWB matrix (and its approximation) for the DOA and the complex RCS and we prove its diagonal

structure. In Section 2.2.3, simulations are presented to confirm the good ability of WWB to predict the MSE of the maximum *a posteriori* (MAP) in all range of SNR (asymptotic and threshold regions). Numerical procedure is introduced to analyze the MIMO radar system in terms of antenna geometry. Finally, Section 2.2.4 draws some summaries of this Section.

2.2.1 Problem Setup

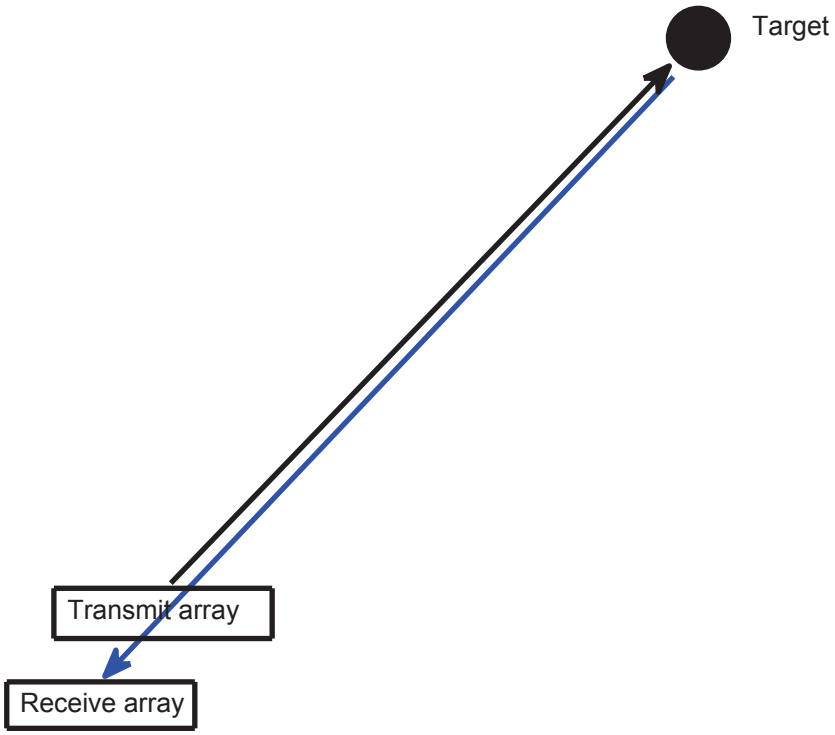

FIGURE 2.3 – Collocated MIMO radar

We consider a single-target localization scenario with a MIMO radar system (see figure 2.3) formed with collocated linear (possibly non-uniform) transmitting and receiving arrays with M and N antennas, respectively. Each transmitting antenna sends out a different waveform, which is known. The $N \times 1$ complex received signal is then given by [LXS+08] :

$$\mathbf{y}(t) = \beta \mathbf{b}(\theta)\mathbf{a}^T(\theta)\mathbf{x}(t) + \mathbf{n}(t) = \beta \mathbf{C}(\theta)\mathbf{x}(t) + \mathbf{n}(t) \ , t = 1 \dots T, \tag{2.1}$$

where T is the number of snapshots. Since both transmitting and receiving arrays are linear, the steering vectors have the following forms $\mathbf{a}(\theta) = [\exp(-j\frac{2\pi}{\lambda}a_1 \sin\theta), \dots, \exp(-j\frac{2\pi}{\lambda}a_M \sin\theta)]^T$, and $\mathbf{b}(\theta) = \left[\exp(-j\frac{2\pi}{\lambda}b_1 \sin\theta), \dots, \exp(-j\frac{2\pi}{\lambda}b_N \sin\theta)\right]^T$, where λ denotes the wavelength, where a_i, $i = 1 \dots M$, and b_j, $j = 1 \dots N$, are the positions of the elements (w.r.t. a reference point) of the transmitting and receiving arrays, respectively. Note that for the colocated scenario, the DOA is the same as the direction-of-departure (DOD), hence θ is the only one location parameter of the target. Moreover, θ is assumed

to have an *a priori* uniform distribution over the support $[0, \pi]$. For simplicity in the derivation, we define $u = \sin(\theta)$ as the parameter of interest instead of working directly with θ. Note that, the pdf for u is $p(u) = \frac{1}{\pi\sqrt{1-u^2}}$. We denote $\mathbf{C}(\theta) = \mathbf{b}(\theta)\mathbf{a}^T(\theta) \in \mathbb{C}^{N\times M}$. The elements of $\mathbf{C}(\theta)$ are given by $[\mathbf{C}(\theta)]_{k,l} = \left[\exp(-j\frac{2\pi}{\lambda}(a_l + b_k)\sin\theta)\right]$. $\mathbf{x}(t)$ is the vector of each transmitted waveform. We suppose that these waveforms are independent and have the following empirical covariance matrix : $\mathbf{R}_x = \frac{1}{T}\sum_{t=1}^{T}\mathbf{x}(t)\mathbf{x}^H(t) = Diag(\boldsymbol{\sigma}_s^2)$, where $\boldsymbol{\sigma}_s^2 = [\sigma_1^2, \ldots, \sigma_M^2]^T$. We also define $\{\mathbf{n}(t)\}_{t=1}^{T}$ as the noise vectors, which are assumed to be independent and identically distributed circularly complex Gaussian with zero-mean and covariance matrix $\mathbf{R} = \sigma_n^2\mathbf{I}$. β is the target complex amplitude related to the RCS of the target in the Swerling 0 case, and has an *a priori* circular complex Gaussian distribution with zero mean and variance σ_β^2, namely $\beta \sim \mathcal{CN}(0, \sigma_\beta^2)$. The elements of the unknown parameter vector $\boldsymbol{\Theta} = [u, \beta_R, \beta_I]^T$ with $\beta_R = Re\{\beta\}, \beta_I = Im\{\beta\}$, are considered to be statistically independent such that the joint pdf $p(\boldsymbol{\Theta}) = p(u)p(\beta_R)p(\beta_I)$.
Under the assumption of independent observations, the likelihood of the full set of observations $\mathbf{Y} = [\mathbf{y}(1), \mathbf{y}(2), \ldots, \mathbf{y}(T)]$ is given by

$$p(\mathbf{Y};\boldsymbol{\Theta}) = \frac{1}{\pi^{NT}\sigma_n^{NT}}\exp\left(-\frac{1}{\sigma_n^2}\sum_{t=1}^{T}(\mathbf{y}(t) - \beta\mathbf{C}(\theta)\mathbf{x}(t))^H(\mathbf{y}(t) - \beta\mathbf{C}(\theta)\mathbf{x}(t))\right). \tag{2.2}$$

2.2.2 Weiss-Weinstein Bound for MIMO radar 's parameter estimation

2.2.2.1 Numerical WWB

The Weiss-Weinstein bound [WW85], denoted by **WWB**, of the unknown target parameters $\boldsymbol{\Theta} = [u, \beta_R, \beta_I]^T$ is a 3×3 matrix such that the following relation holds

$$E\left\{\left(\hat{\boldsymbol{\Theta}} - \boldsymbol{\Theta}\right)\left(\hat{\boldsymbol{\Theta}} - \boldsymbol{\Theta}\right)^T\right\} \geq \mathbf{WWB} = \sup_{\substack{\mathbf{h}_i, s_i \\ i=1,2,3}} \mathbf{H}\mathbf{G}^{-1}\mathbf{H}^T, \tag{2.3}$$

where $E\left\{\left(\hat{\boldsymbol{\Theta}} - \boldsymbol{\Theta}\right)\left(\hat{\boldsymbol{\Theta}} - \boldsymbol{\Theta}\right)^T\right\}$ is the MSE of any Bayesian estimator $\hat{\boldsymbol{\Theta}}$ and $\mathbf{H} = [\mathbf{h}_1, \mathbf{h}_2, \mathbf{h}_3]$ is the 3×3 matrix of test-points. The elements of the 3×3 matrix $\mathbf{G}$ are given by

$$[\mathbf{G}]_{kl} = \frac{E\left\{[L^{s_k}(\mathbf{Y};\boldsymbol{\Theta} + \mathbf{h}_k, \boldsymbol{\Theta}) - L^{1-s_k}(\mathbf{Y};\boldsymbol{\Theta} - \mathbf{h}_k, \boldsymbol{\Theta})][L^{s_l}(\mathbf{Y};\boldsymbol{\Theta} + \mathbf{h}_l, \boldsymbol{\Theta}) - L^{1-s_l}(\mathbf{Y};\boldsymbol{\Theta} - \mathbf{h}_l, \boldsymbol{\Theta})]\right\}}{E\left\{L^{s_k}(\mathbf{Y};\boldsymbol{\Theta} + \mathbf{h}_k, \boldsymbol{\Theta})\right\}E\left\{L^{s_l}(\mathbf{Y};\boldsymbol{\Theta} + \mathbf{h}_l, \boldsymbol{\Theta})\right\}}, \tag{2.4}$$

where $L(\mathbf{Y};\boldsymbol{\Theta} + \mathbf{h}_i, \boldsymbol{\Theta}) = \frac{p(\mathbf{Y},\boldsymbol{\Theta}+\mathbf{h}_i)}{p(\mathbf{Y},\boldsymbol{\Theta})}$, and $s_i \in [0, 1], i = 1, 2, 3$. The expectations are taken over the joint pdf $p(\mathbf{Y}, \boldsymbol{\Theta})$.

Rigorously, the quantity $\mathbf{H}\mathbf{G}^{-1}\mathbf{H}^T$ must be maximized w.r.t. $\mathbf{h}_i$ and s_i leading to a high computational complexity. However, it has been shown [WW88] [Xu01] that choosing $s_i = \frac{1}{2}, \forall i = 1, 2, 3$, and a diagonal matrix $\mathbf{H}$ leads to a bound still tight. Therefore, we assume here that $s_i = 1/2, \forall i$, and that $\mathbf{H} = Diag([h_1, h_2, h_3]^T)$. In this case, the elements of the matrix $\mathbf{G}$ can be written as

$$[\mathbf{G}]_{kl} = \frac{\eta(\mathbf{h}_k, \mathbf{h}_l) + \eta(-\mathbf{h}_k, -\mathbf{h}_l) - \eta(\mathbf{h}_k, -\mathbf{h}_l) - \eta(-\mathbf{h}_k, \mathbf{h}_l)}{\eta(\mathbf{h}_k, \mathbf{0})\eta(\mathbf{h}_l, \mathbf{0})}, \tag{2.5}$$

where we define $\eta(\boldsymbol{\alpha},\boldsymbol{\gamma}) = \int_{\boldsymbol{\Upsilon}}\int_{\boldsymbol{\Omega}} p(\mathbf{Y},\boldsymbol{\Theta}+\boldsymbol{\alpha})^{\frac{1}{2}} p(\mathbf{Y},\boldsymbol{\Theta}+\boldsymbol{\gamma})^{\frac{1}{2}} d\mathbf{Y} d\boldsymbol{\Theta}$, where $\boldsymbol{\Omega}$ and $\boldsymbol{\Upsilon}$ are the observation and parameter spaces, respectively, and where $\boldsymbol{\alpha} = [\alpha_1,\alpha_2,\alpha_3]^T$, and $\boldsymbol{\gamma} = [\gamma_1,\gamma_2\gamma_3]^T$.
By denoting

$$\eta'(\boldsymbol{\Theta},\boldsymbol{\alpha},\boldsymbol{\gamma}) = \int_{\boldsymbol{\Omega}} p(\mathbf{Y};\boldsymbol{\Theta}+\boldsymbol{\alpha})^{\frac{1}{2}} p(\mathbf{Y};\boldsymbol{\Theta}+\boldsymbol{\gamma})^{\frac{1}{2}} d\mathbf{Y}, \tag{2.6}$$

$\eta(\boldsymbol{\alpha},\boldsymbol{\gamma})$ can be rewritten as

$$\eta(\boldsymbol{\alpha},\boldsymbol{\gamma}) = \int_{\boldsymbol{\Upsilon}} \eta'(\boldsymbol{\Theta},\boldsymbol{\alpha},\boldsymbol{\gamma}) p(\boldsymbol{\Theta}+\boldsymbol{\alpha})^{\frac{1}{2}} p(\boldsymbol{\Theta}+\boldsymbol{\gamma})^{\frac{1}{2}} d\boldsymbol{\Theta}. \tag{2.7}$$

Plugging (2.2) into (2.6), we obtain a closed-form expression for η' as follows (see **Appendix** 2.6.1 for details)

$$\eta'(\boldsymbol{\Theta},\boldsymbol{\alpha},\boldsymbol{\gamma}) = \exp\left(-\frac{1}{4\sigma_n^2}\sum_{t=1}^{T}\left[\mathbf{f}(\boldsymbol{\Theta}+\boldsymbol{\alpha},t)-\mathbf{f}(\boldsymbol{\Theta}+\boldsymbol{\gamma},t)\right]^H\left[\mathbf{f}(\boldsymbol{\Theta}+\boldsymbol{\alpha},t)-\mathbf{f}(\boldsymbol{\Theta}+\boldsymbol{\gamma},t)\right]\right), \tag{2.8}$$

where $\mathbf{f}(\boldsymbol{\Theta},t) = \beta\mathbf{C}(\theta)\mathbf{x}(t)$. Consequently,

$$\eta(\boldsymbol{\alpha},\boldsymbol{\gamma}) = \int_{\boldsymbol{\Upsilon}} \eta'(\boldsymbol{\Theta},\boldsymbol{\alpha},\boldsymbol{\gamma}) \frac{1}{\pi((1-(u+\alpha_1)^2))^{\frac{1}{4}}((1-(u+\gamma_1)^2))^{\frac{1}{4}}} \frac{1}{\pi\sigma_\beta^2} \tag{2.9}$$

$$\exp\left(-\frac{(\beta_R-\alpha_2)^2+(\beta_R-\gamma_2)^2}{\sigma_\beta^2}\right)\exp\left(-\frac{(\beta_I-\alpha_3)^2+(\beta_I-\gamma_3)^2}{\sigma_\beta^2}\right) du d\beta_R d\beta_I. \tag{2.10}$$

Unfortunately, in this case, no closed-form expression of the WWB can be obtained (see also [NT94] where the same thing appears in the context of classical bearing estimation). This is why we propose in the following an approximation for which we will have a closed-form expression of the bound. A closed-form expression is always interesting because it allows an easy interpretation of the bound, i.e., we can study the performance of the MIMO radar system w.r.t. some design parameters.

2.2.2.2 Analytical approximation of the bound

In this Section, with the intention of obtaining a closed-form expression of the WWB, we propose a different approach where we assume a uniform *a priori* pdf on u. Note that this approach has already been successfully used in [Ath01] [AE01] [XBB04] and [BET96]. We also show by simulation (in Section 2.2.3.2) that the two approaches give very close bounds and the same prediction of the SNR threshold.

Assuming a uniform *a priori* pdf on u, the structure of the matrix **WWB** is given as follows (see **Appendix** 2.6.2 for more details) :

$$\mathbf{WWB} = Diag\left(\sup_{h_1}\frac{h_1^2}{[\mathbf{G}]_{11}}, \frac{1}{2\left(TASNR+\frac{1}{\sigma_\beta^2}\right)}, \frac{1}{2\left(TASNR+\frac{1}{\sigma_\beta^2}\right)}\right), \tag{2.11}$$

where the array signal to noise ($ASNR$) is defined as PN/σ_n^2 where $P = \sum_{k=1}^{M} \sigma_k^2$ is the total transmitted power, and where $[\mathbf{G}]_{11}$ is given by

$$[\mathbf{G}]_{11} = 4\frac{[(2-h_1)f(2,h_1) - 2(1-h_1)]\, f(1,h_1)^2}{(2-h_1)^2 f(2,h_1)}, \tag{2.12}$$

where we define $f(\varphi, h_1) = \sigma_\beta^2 \frac{1}{2} T \sum_{k=1}^{M} \sum_{r=1}^{N} \frac{\sigma_k^2}{\sigma_n^2} \left[1 - \cos\left(\frac{\varphi 2\pi}{\lambda} h_1 (a_k + b_r)\right)\right] + 1$. In the following, we analyse the proposed bound in terms of SNR threshold prediction and array geometry design.

2.2.3 Analysis

2.2.3.1 Properties of the bound

There are three properties of the WWB matrix (2.11) :

1. Due to the diagonal structure of the WWB matrix, the lower bounds on estimation errors are decoupled.
2. Thanks to this derivation, the initial multidimensional optimization problem w.r.t. h_1, h_2, and h_3 has been reduced to a monodimensional optimization problem w.r.t. h_1 only.
3. The WWB for β_R and β_I are the same as their Bayesian CRB in the case where u is assumed to be known (the proof is straightforward).

2.2.3.2 WWB performance in predicting the global MSE and the SNR threshold

The aim of this part is to examine the usefulness of using the WWB to predict the ultimate global MSE and the SNR threshold. For that reason, we consider the empirical global MSE of the MAP estimator, which is evaluated over 1000 Monte Carlo trials. The simulation is performed for 3 scenarios with configurations as follows : the transmit array is sparse with $M = 8$ (scenario A and B) and $M = 5$ (scenario C) sensors and with inter-element spacing (in unit of wavelengths) equals to $0.5M$ and the receive array is an ULA with $N = 8$ (scenario A and B) and $N = 5$ (scenario C) sensors and with inter-element spacing (in unit of wavelengths) equals to 0.5. Such array configuration is well-known in MIMO radar ([LS09] p.76) to create a Nyquist virtual array with good performance. The uncorrelated MIMO radar waveforms are generated using Hadamard codes with $T = 64$ (scenario A) and $T = 32$ (scenario B and C) snapshots. The transmitted power is assumed to be uniformly distributed on all transmit antennas. h_1 is chosen on the support $[-1, 1]$. Figure 2.4 shows the approximated WWB with $s_i = 1/2$ and the MAP of the parameter of interest θ versus ASNR for 3 scenarios. We also draw the numerical optimization of approximated WWB over s_i. It can be seen that the WWB provides a good prediction of the MSE in all regions. It predicts the threshold SNR location to be 4 dB below the threshold SNR indicated by the MAP.

In Figure 2.5, we compare, under the three aforementioned scenarios, the true WWB (computed with numerical integration) and our approximation of the WWB. Both bounds are very close and lead to the same prediction of the SNR threshold. Note that, in our simulation, time needed to calculate the bound with numerical integration is over 100 times longer than that in the other case. Consequently, to have a (still tight) bound with an efficiently computational cost and an easy interpretation, our WWB approximation should be preferred especially for designing a MIMO radar system.

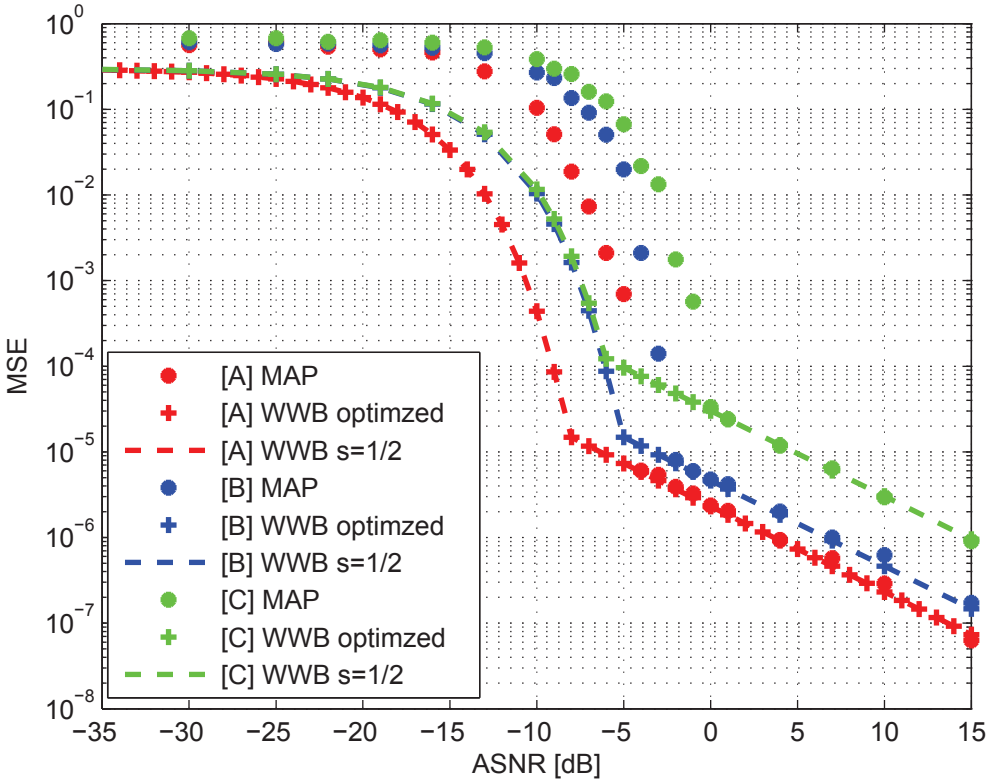

FIGURE 2.4 – MAP estimator empirical global MSE and approximated WWB of θ versus SNR

2.2.3.3 MIMO array geometry investigation

This part investigates the behavior of the derived WWB w.r.t. the array geometry of both the receiver and transmitter. Note that the proposed bound has been derived in the context of linear arrays but possibly non-uniform. Consequently, it remains a degree of freedom to enhance the performance. We first analyze the impact of the receiver array geometry while the transmitter is made from a classical ULA. Both transmitter and receiver are made with $M = N = 8$ sensors. The transmitter is a fixed ULA (half-wavelength inter-element spacing) array. The receiver has different linear array geometries keeping the array aperture $D = 23$ (in unit of $\frac{\lambda}{2}$) fixed (i.e. the positions of the 2 extreme sensors of the linear array are fixed). In other words, their is 22 positions available for the 6 other sensors (74613 possibilities). The number of observations is $T = 64$. We have generated all the array configurations and computed the associated WWB. In Figure 2.6, among these 74613 bounds we have plotted the bound which leads to the lowest SNR threshold (denoted bound A) and the bound which has the lowest MSE in the asymptotic area (denoted bound B). We have noticed that both geometries leading to bound A and B are not with minimum redundancy or minimum gap. Indeed, for this configuration, it can be seen that it exists four minimum-redundancy arrays. We have computed the bounds associated to these four possibilities and plotted the best one in terms of MSE for comparison purpose. The bound A (i.e. the bound with the lowest SNR threshold) shows that better asymptotic performance can be obtained. It exists a geometry configuration leading to slightly better

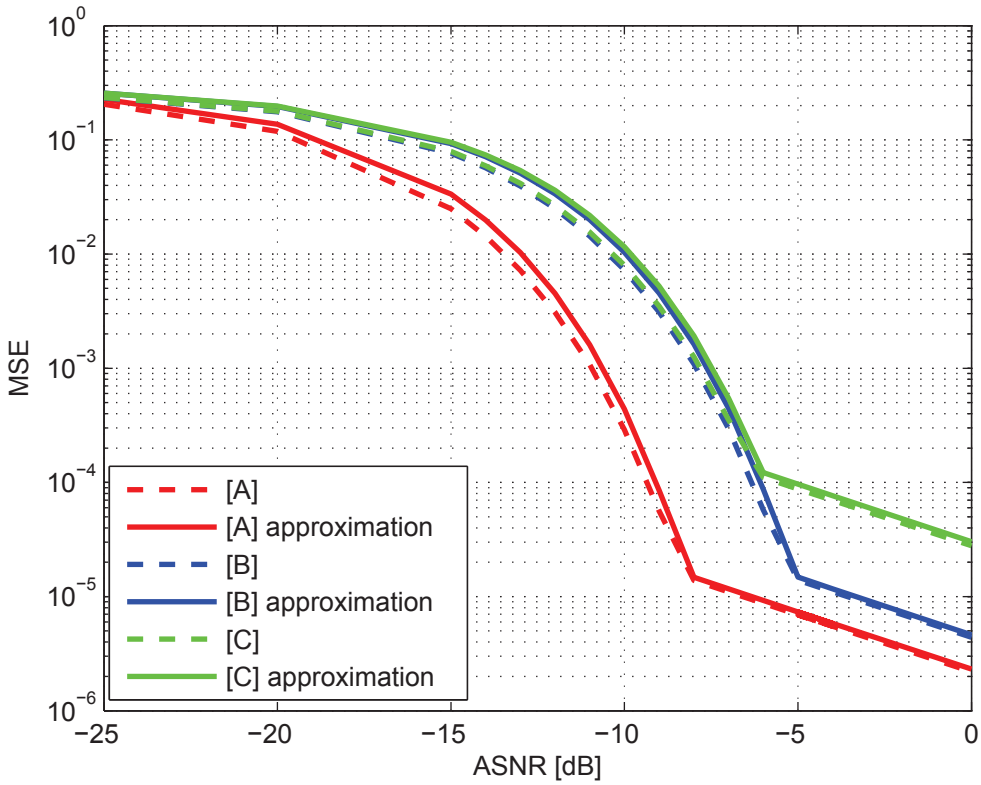

FIGURE 2.5 – WWB of θ and its approximation versus SNR

asymptotic performance (bound B) but with a worst SNR threshold. Note that, we have obtained the same results, i.e. same bounds associated to the same optimal geometries, in the opposite case where the receiver is a fixed ULA and where the transmitter array geometry is optimized following the same aforementioned way.

2.2.4 Summary

In this Section, we have derived a closed-form expression of the Weiss-Weinstein bound for MIMO Radar with collocated linear arrays. It has been seen that the Weiss-Weinstein bound for the parameter of interest provides a good prediction of the MSE in all regions. It also predicts the threshold SNR location near the threshold SNR indicated by the MAP. We have also investigated the influence of array geometry on the behavior of the Weiss-Weinstein bound.

2.3 MIMO radar in the presence of modeling errors : A Cramér-Rao bound investigation

This Section is organized as follows : Section 2.3.1 presents the general problem setup with MIMO radar equipped with well separated transmitting and receiving arrays in the presence of modeling errors. In Section 2.3.2, we derive the corresponding CRB matrix for the DOA and the complex RCS. In Section 2.3.3, simulations are presented to analyze the

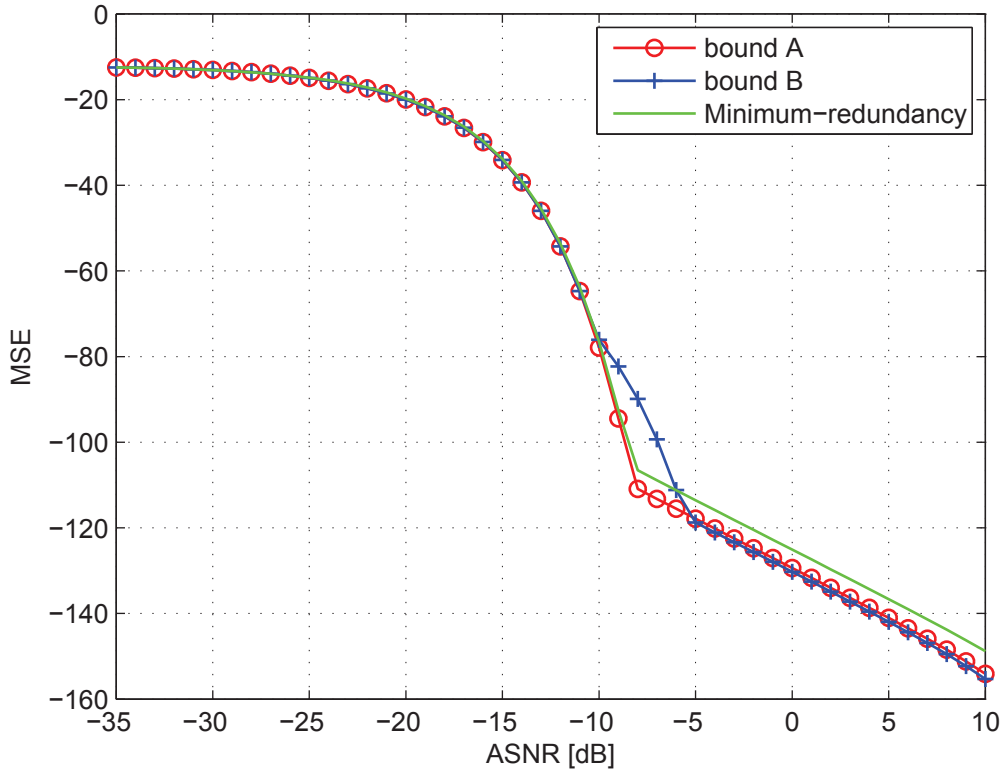

FIGURE 2.6 – Receiver geometry investigation : WWB for the the lowest-threshold-point, the lowest-asymptotic-region, and the minimum-redundancy arrays.

proposed closed-form expressions. It is shown that the CRB and the MSE of the maximum likelihood estimator of the angle-of-arrival do not fall into zero (contrary to the classical case without modeling error) and converge to a fixed limit for which we give a closed-form expression. Moreover, we give a simple closed-form expression of the critical value of the signal-to-noise ratio where this limitation of performance appear.

2.3.1 Problem setup

We consider a MIMO radar equipped with well separated transmitting and receiving arrays (see figure 2.7). Both arrays are assumed to be central-symmetric linear arrays where the numbers of transmit and receive antennas are denoted M and N, respectively. In this context, a point target is located by two parameters : the angle-of-departure denoted by θ_D and the angle-of-arrival denoted by θ_A. Consequently, the observation model is given by :

$$\mathbf{y}(t) = \beta \mathbf{b}_t(\theta_A)\mathbf{a}_t^T(\theta_D)\mathbf{x}(t) + \mathbf{n}(t),\ t = 1 \dots T, \tag{2.13}$$

where T is the number of snapshots. $\mathbf{a}_t(\theta_D)$ and $\mathbf{b}_t(\theta_A)$ are the observed steering vectors of transmitting and receiving arrays, respectively. The complex quantity β is the target complex amplitude related to the radar-cross-section (RCS) of the target. The vector $\mathbf{x}(t)$

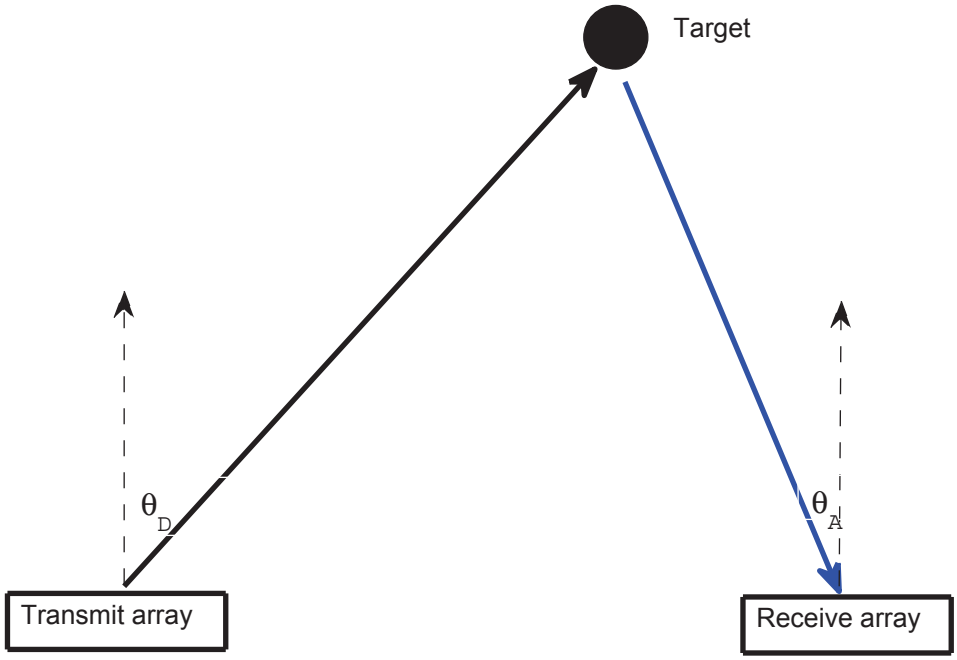

FIGURE 2.7 – Widely separated MIMO radar

contains M transmitted waveforms. We assume that these waveforms are orthogonal and have the following empirical covariance matrix :

$$\mathbf{R}_x = \frac{1}{T}\sum_{t=1}^{T}\mathbf{x}(t)\mathbf{x}^H(t) = \sigma_x^2\mathbf{I}_M, \tag{2.14}$$

Finally, the noise vectors $\{\mathbf{n}(t)\}_{t=1}^{T}$ are assumed to be independent and identically distributed circularly symmetric complex Gaussian with zero-mean and covariance matrix $\mathbf{R}_n = \sigma_n^2\mathbf{I}_N$. In this section, we consider that only the observed steering vector of the receiving array, $\mathbf{b}_t(\theta_A)$, is subject to a modeling error represented by an additive random vector $\mathbf{e}$. In other words,

$$\mathbf{b}_t(\theta_A) = \mathbf{b}(\theta_A) + \mathbf{e}, \tag{2.15}$$
$$\mathbf{a}_t(\theta_D) = \mathbf{a}(\theta_D), \tag{2.16}$$

where $\mathbf{a}(\theta_D)$ and $\mathbf{b}(\theta_A)$ are the theoretical steering vectors which have the following structures

$$\mathbf{a}(\theta_D) = \left[\exp\left(-j\frac{2\pi}{\lambda}a_1\sin\theta_D\right),\ldots,\exp\left(-j\frac{2\pi}{\lambda}a_M\sin\theta_D\right)\right]^T, \tag{2.17}$$

and

$$\mathbf{b}(\theta_A) = \left[\exp\left(-j\frac{2\pi}{\lambda}b_1\sin\theta_A\right),\ldots,\exp\left(-j\frac{2\pi}{\lambda}b_N\sin\theta_A\right)\right]^T, \tag{2.18}$$

where λ is the wavelength, where the quantities a_i, $i = 1\ldots M$, and b_j, $j = 1\ldots N$, are the nominal sensor positions (w.r.t. a reference point) of transmitting and receiving arrays, respectively. The modeling error vector $\mathbf{e}$ is assumed to be jointly circular and Gaussian distributed, namely $\mathbf{e} \sim \mathcal{CN}(0, \sigma_e^2\mathbf{I}_N)$. Moreover, $\mathbf{e}$ is assumed to be statistically independent of the noise vector $\mathbf{n}(t)$, $\forall t$. Consequently, the complex data vector received by such a MIMO radar can be written as

$$\mathbf{y}(t) = \beta\mathbf{b}(\theta_A)\mathbf{a}^T(\theta_D)\mathbf{x}(t) + \beta\mathbf{e}\mathbf{a}^T(\theta_D)\mathbf{x}(t) + \mathbf{n}(t). \tag{2.19}$$

The unknown parameters vector is $\mathbf{\Theta} = [\theta_D, \theta_A, \beta_R, \beta_I]^T$ where β_R and β_I denote the real part of β and the imaginary part of β, respectively.

Finally, note that [1] in this case the likelihood of the observations is complex circular Gaussian distributed with both parameterized mean and covariance matrix, *i.e.*, by letting $\mathbf{y} = \left[\mathbf{y}^T(1)\ldots\mathbf{y}^T(T)\right]^T \in \mathbb{C},^{NT}$, $\mathbf{y}|\,\mathbf{\Theta} \sim \mathcal{CN}(\mathbf{m}(\mathbf{\Theta}), \mathbf{R}(\mathbf{\Theta}))$ where

$$\mathbf{m}(\mathbf{\Theta}) = vec\left(\left[\beta\mathbf{b}(\theta_A)\mathbf{a}^T(\theta_D)\mathbf{x}(1)\ldots\beta\mathbf{b}(\theta_A)\mathbf{a}^T(\theta_D)\mathbf{x}(T)\right]\right), \tag{2.20}$$

where $vec\,(.)$ denotes the vec operator and

$$\mathbf{R}(\mathbf{\Theta}) = |\beta|^2\,\sigma_e^2\mathbf{s}(\theta_D)\mathbf{s}^H(\theta_D) \otimes \mathbf{I}_N + \sigma_n^2\mathbf{I}_{NT}, \tag{2.21}$$

where

$$\mathbf{s}(\theta_D) = \left[\mathbf{a}^T(\theta_D)\mathbf{x}(1)\ldots\mathbf{a}^T(\theta_D)\mathbf{x}(T)\right]^T. \tag{2.22}$$

We note that the full parameter vector parameterizes the mean while only θ_D, β_R, and β_I parameterize the covariance matrix of the observations.

2.3.2 Cramér-Rao bound

For a general Gaussian parameterized model such that $\mathbf{y}|\,\mathbf{\Theta} \sim \mathcal{CN}(\mathbf{m}(\mathbf{\Theta}), \mathbf{R}(\mathbf{\Theta}))$, it is well known that the element (i, j) of the Fisher information matrix $\mathbf{F}\,(\mathbf{\Theta})$ is given by the Slepian-Bang formula (see, *e.g.*, [Kay93])

$$[\mathbf{F}\,(\mathbf{\Theta})]_{i,j} = Tr\left\{\mathbf{R}^{-1}(\mathbf{\Theta})\frac{\partial\mathbf{R}(\mathbf{\Theta})}{\partial[\mathbf{\Theta}]_i}\mathbf{R}^{-1}(\mathbf{\Theta})\frac{\partial\mathbf{R}(\mathbf{\Theta})}{\partial[\mathbf{\Theta}]_j}\right\} + 2\mathcal{R}\left\{\frac{\partial\mathbf{m}^H(\mathbf{\Theta})}{\partial[\mathbf{\Theta}]_i}\mathbf{R}^{-1}(\mathbf{\Theta})\frac{\partial\mathbf{m}(\mathbf{\Theta})}{\partial[\mathbf{\Theta}]_j}\right\}, \tag{2.23}$$

1. This is quite different from the classical case (in the MIMO radar context or in the array processing context) where only the mean or the covariance matrix are parameterized. Note also that the analysis of modeling error on both transmitter and receiver seems to be a very complex work. Indeed, in this case the observations vector is the sum of a deterministic vector plus a Gaussian vector plus the product of two Gaussian vectors which depend on the first Gaussian vector.

where $[\mathbf{\Theta}]_{i=1,\ldots,4}$ denotes the i^{th} element of the vector $\mathbf{\Theta}$. Without loss of generality, the reference points for the transmitting and receiving arrays are chosen such that

$$\mathbf{a}^H(\theta_D)\dot{\mathbf{a}}(\theta_D) = 0 \text{ and } \mathbf{b}^H(\theta_A)\dot{\mathbf{b}}(\theta_A) = 0, \tag{2.24}$$

where we define $\dot{\mathbf{a}}(\theta_D) = \frac{\partial \mathbf{a}(\theta_D)}{\partial \theta_D}$, and $\dot{\mathbf{b}}(\theta_A) = \frac{\partial \mathbf{b}(\theta_A)}{\partial \theta_A}$. The elements of the Fisher information matrix are given by (see **Appendix** 2.6.3 for more details)

$$\begin{aligned}
[\mathbf{F}(\mathbf{\Theta})]_{1,1} =& \frac{8\pi^2 |\beta|^2 TN\sigma_x^2}{\lambda^2\sigma_n^2}\cos^2(\theta_D)\sum_{k=1}^{M} a_k^2\left(1+\frac{|\beta|^2 TM\sigma_x^2\sigma_e^4}{\sigma_n^2+|\beta|^2 TM\sigma_x^2\sigma_e^2}\right),\\
[\mathbf{F}(\mathbf{\Theta})]_{2,2} =& \frac{\frac{8\pi^2}{\lambda^2}|\beta|^2 TM\sigma_x^2}{\sigma_n^2+|\beta|^2 TM\sigma_x^2\sigma_e^2}\cos^2\theta_A\sum_{k=1}^{N} b_k^2,\\
[\mathbf{F}(\mathbf{\Theta})]_{3,3} =& N\left(\frac{2\beta_R TM\sigma_x^2\sigma_e^2}{\sigma_n^2+|\beta|^2 TM\sigma_x^2\sigma_e^2}\right)^2+\frac{2TNM\sigma_x^2}{\sigma_n^2+|\beta|^2 TM\sigma_x^2\sigma_e^2},\\
[\mathbf{F}(\mathbf{\Theta})]_{4,4} =& N\left(\frac{2\beta_I TM\sigma_x^2\sigma_e^2}{\sigma_n^2+|\beta|^2 TM\sigma_x^2\sigma_e^2}\right)^2+\frac{2TNM\sigma_x^2}{\sigma_n^2+|\beta|^2 TM\sigma_x^2\sigma_e^2},\\
[\mathbf{F}(\mathbf{\Theta})]_{3,4} =& \{\mathbf{F}(\mathbf{\Theta})\}_{4,3} = 4N\beta_R\beta_I\left(\frac{TM\sigma_x^2\sigma_e^2}{\sigma_n^2+|\beta|^2 TM\sigma_x^2\sigma_e^2}\right)^2,
\end{aligned} \tag{2.25}$$

and all the other elements of the Fisher information matrix are equal to zero leading to a strong block diagonal structure (only β_R and β_I are coupled).

Consequently, the Cramér-Rao bounds (*i.e.*, the diagonal elements of the inversion of the Fisher information matrix) are given by

$$\begin{cases}
CRB(\theta_D) &= \frac{\lambda^2\sigma_n^2\left(\sigma_n^2+|\beta|^2TM\sigma_x^2\sigma_e^2\right)}{8\pi^2|\beta|^2TN\sigma_x^2\left(\sigma_n^2+|\beta|^2TM\sigma_x^2\sigma_e^2(1+\sigma_e^2)\right)\cos^2(\theta_D)\sum_{k=1}^{M}a_k^2},\\
CRB(\theta_A) &= \frac{\sigma_n^2+|\beta|^2TM\sigma_x^2\sigma_e^2}{\frac{8\pi^2}{\lambda^2}|\beta|^2TM\sigma_x^2\cos^2\theta_A\sum_{k=1}^{N}b_k^2},\\
CRB(\beta_R) &= \frac{1+\beta_I^2\sigma_e^2 d}{Nd(1+|\beta|^2\sigma_e^4 d)},\\
CRB(\beta_I) &= \frac{1+\beta_R^2\sigma_e^2 d}{Nd(1+|\beta|^2\sigma_e^4 d)},
\end{cases} \tag{2.26}$$

where $d = \frac{2TM\sigma_x^2}{\sigma_n^2+|\beta|^2TM\sigma_x^2\sigma_e^2}$.

2.3.3 Simulation results

In order to analyze the Cramér-Rao bounds behavior, we perform in this Section some simulations. The scenario is the following : the transmit and the receive arrays are uniform linear arrays of $M = 4$ and $N = 4$ sensors, respectively, with inter-element spacing (in unit of wavelengths) is 0.5. The orthogonal MIMO radar waveforms are generated using Hadamard codes with $T = 32$ snapshots. We put the angle-of-departure and the angle-of-arrival of the target at $\theta_D = 67.5^o$ and $\theta_A = 22.5^o$ and we assume that $\beta = 1+j$. The total transmitted power is $M\sigma_x^2 = 1$. Figure 2.8 shows the Cramér-Rao bounds for parameters of interest versus the Array Signal-to-Noise Ratio (ASNR) where we define $ASNR = \frac{MN\sigma_x^2}{\sigma_n^2}$. Note that we do not plot $CRB(\beta_I)$ since it has the same behavior as $CRB(\beta_R)$. For

comparison, we also draw the performance of the maximum likelihood estimator (MLE) evaluated over 1000 Monte Carlo trials. This first simulation represents the behavior of the Cramér-Rao bounds and of the MLE without modeling error, *i.e.*, with $\sigma_e^2 = 0$. We note that one observes the classical behavior of the Cramér-Rao bounds which decrease linearly when the ASNR increase. We also note that the MLE reaches asymptotically the Cramér-Rao bound (as $ASNR \to \infty$) [RFCL06] and we observe the classical threshold of the MSE of the MLE at low ASNR.

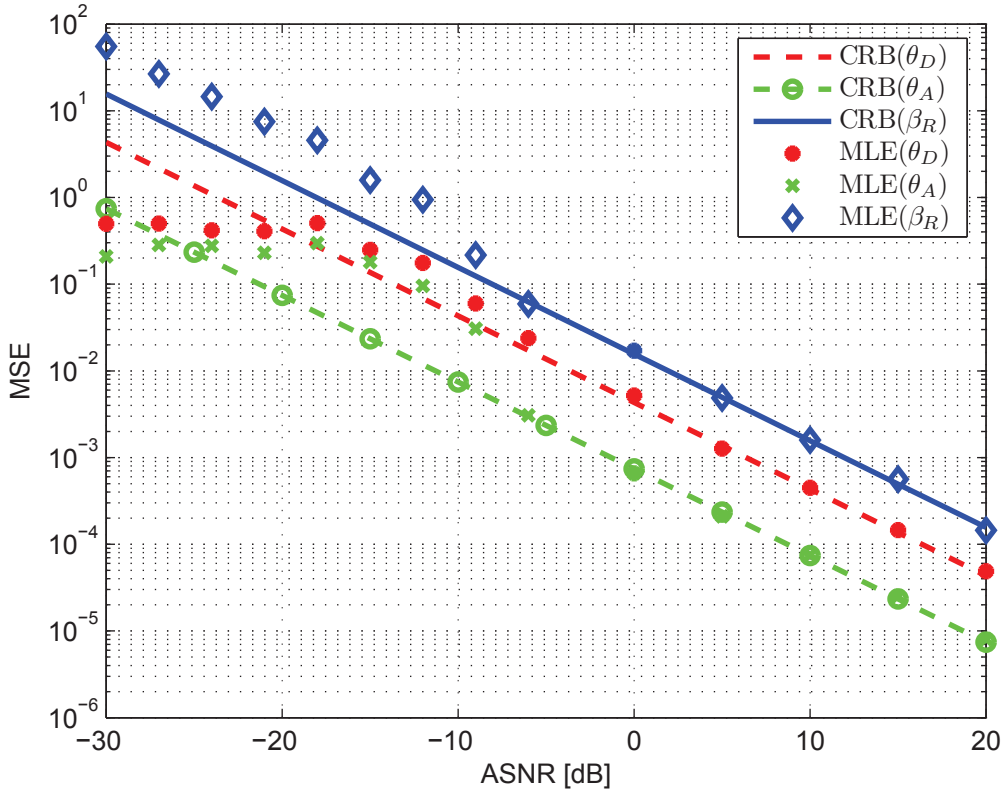

FIGURE 2.8 – Maximum Likelihood estimator empirical mean square error and Cramér-Rao bounds versus ASNR without modelling error

Figure 2.9 shows the behavior of the Cramér-Rao bounds and of the MLE with error modeling where $\sigma_e^2 = 0.1$. Again, we observe the asymptotic efficiency of the MLE but, when $ANSR \to \infty$, the Cramér-Rao bound and the MSE of the MLE of the angle-of-arrival θ_A do not fall into zero and converge to a fixed limit that can be derived from Eqn. (2.26) and which is equal to

$$\lim_{ASNR \to \infty} CRB\left(\theta_A\right) = \frac{\sigma_e^2}{\frac{8\pi^2}{\lambda^2} \cos^2 \theta_A \sum_{k=1}^{N} b_k^2}. \tag{2.27}$$

Note that this value is independent of β. This convergence means that for a given "power" level of modeling error σ_e^2, if the ASNR is over a certain threshold value, no improvement on the estimation performance can be done. Quantitatively, we calculate this threshold

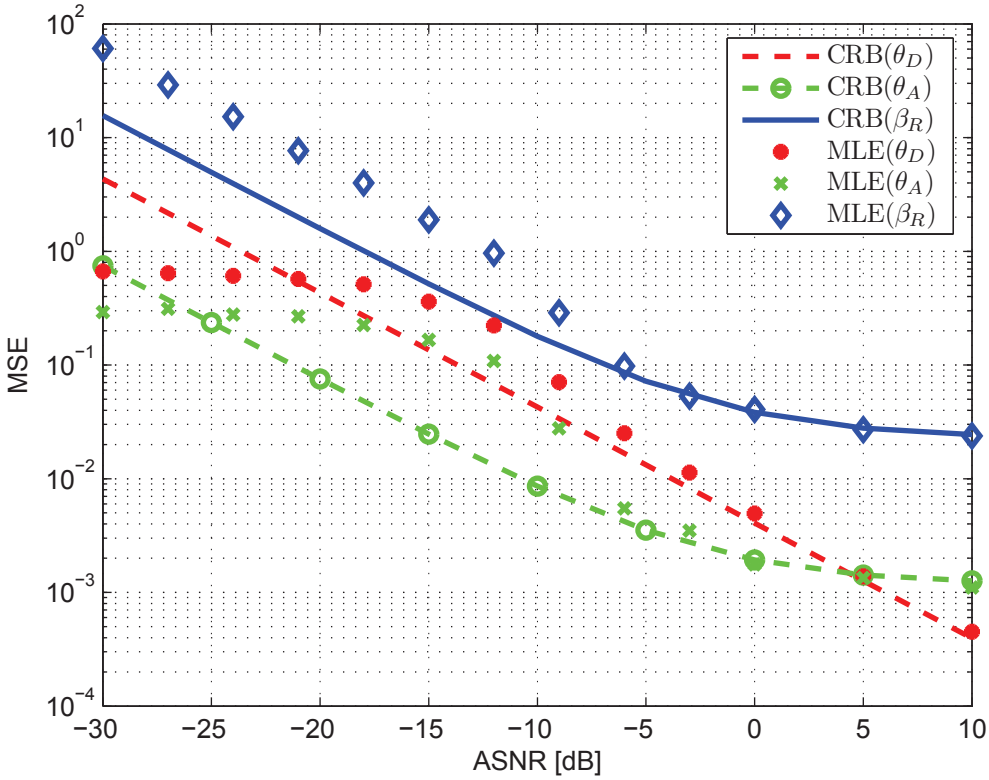

FIGURE 2.9 – Maximum Likelihood estimator empirical mean square error and Cramér-Rao bounds versus ASNR with $\sigma_e^2 = 0.1$.

value of the ANSR denoted $ASNR_{threshold}$ as the value at which, $CRB(\theta_A) = (1+\epsilon) \times \lim_{ASNR\to\infty} CRB(\theta_A)$. We obtain the following simple closed-form expression

$$ASNR_{threshold} = 10\log_{10}\frac{N}{\epsilon\sigma_e^2 T\left|\beta\right|^2}. \tag{2.28}$$

This expression shows that $ASNR_{threshold}$ is linear (in dB) w.r.t. σ_e^2. Note that the same behavior occurs on β_R and β_I, *i.e.*, when $ANSR \to \infty$, the Cramér-Rao bound and the MSE of the MLE do not fall into zero and converge to a fixed limit which is given by

$$\lim_{ASNR\to\infty} CRB(\beta_R) = \frac{\sigma_e^2\left(\left|\beta\right|^2 + 2\sigma_e^2\beta_I\right)}{2N\left(1+2\sigma_e^2\right)}, \tag{2.29}$$

and

$$\lim_{ASNR\to\infty} CRB(\beta_I) = \frac{\sigma_e^2\left(\left|\beta\right|^2 + 2\sigma_e^2\beta_R\right)}{2N\left(1+2\sigma_e^2\right)}. \tag{2.30}$$

Consequently, for a scenario where the number of sensors is fixed and the array aperture

too, the sensors' positions can be used to decrease this limit. Finally, we plotted on Figure 2.10 the Cramér-Rao bounds versus σ_e^2 with $ASNR = 20dB$. Again, we note that both θ_A and β are affected by the modeling error while θ_D is not affected.

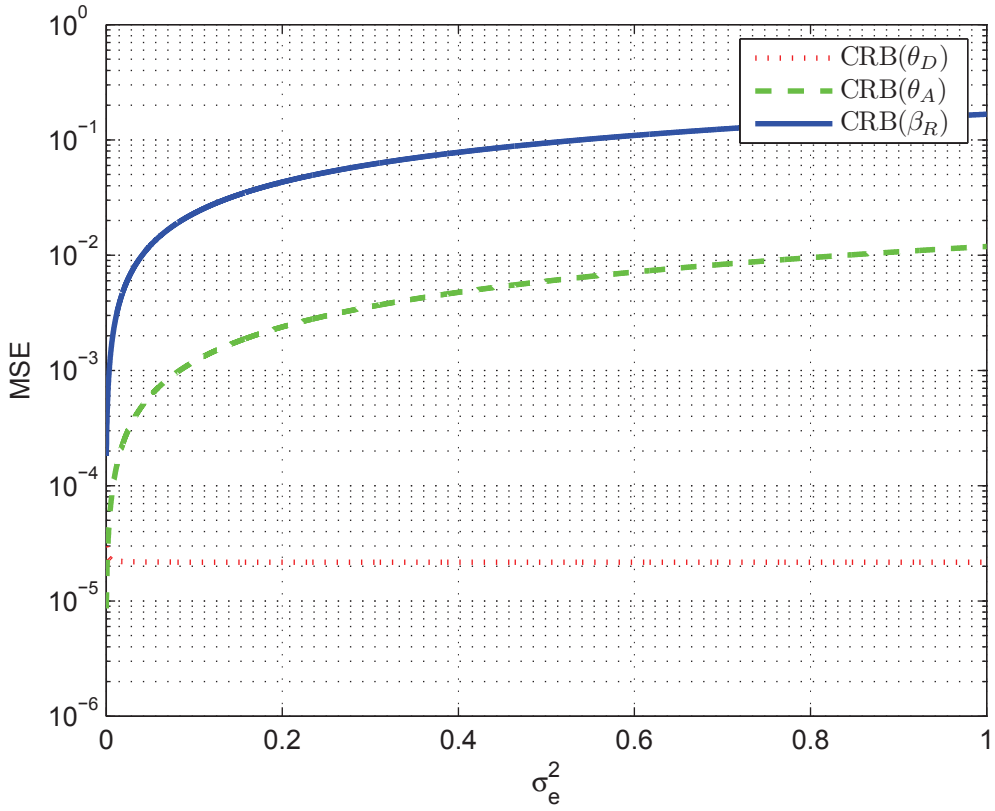

FIGURE 2.10 – Cramér-Rao bounds versus σ_e^2 with $ASNR = 20dB$

2.3.4 Summary

An investigation, by way of the Cramér-Rao bound, of the influence of modeling error at the receiver of a widely separated MIMO radar to localize a target was conducted. For that purpose, we have derived closed-form expressions of the Fisher information matrix and shown its block diagonal structure to deduce the Cramér-Rao bounds expressions of the angle-of-arrival and of the angle-of-departure. We have shown that, under a certain signal-to-noise ratio, the performance of the system can not be improved. Finally, we have proposed a simple formula to evaluate this critical value of the signal-to-noise ratio.

2.4 Performance Bounds for The Pulse Phase Estimation of X-Ray Pulsars

This Section is organized as follows : Section 2.4.1 presents the mathematical model of the X-ray pulsar signal, and also the likelihood of the observations. In Section 2.4.2, we exploit the deterministic bound for the pulse phase and we give the closed-form expression

of the Quinlan-Chaumette-Larzabal bound (QCLB) [CGQL08] [QCL06] since the QCLB is one of the tightest deterministic bounds. In section 2.4.3, we derive the closed-form expression of the Weiss-Weinstein bound (WWB) [WW85] to analyze the behavior of the global MSE. Next, simulations are presented in Section 2.4.4 to confirm the good ability of the derived bounds to predict the performance of the MLE. Finally, Section 2.4.5 draws the conclusions.

2.4.1 X-ray Signal Model

In this Section, we give a brief background about the mathematical observation model provided and justified in [GS07]. This will lead to the likelihood function which will be the cornerstone of our analysis. Let us call k the number of photons detected at the detectors in a fixed time interval (a, b). The photon TOAs are modeled as a non-homogeneous Poisson process (NHPP) with a time-varying rate $\lambda(t) \geq 0$. This means that k follows a Poisson distribution $p(k;(a,b))$ with associated parameter $\int_a^b \lambda(t)dt$:

$$p(k;(a,b)) = \frac{\left[\int_a^b \lambda(t)dt\right]^k \exp\left[-\int_a^b \lambda(t)dt\right]}{k!} \tag{2.31}$$

The rate function $\lambda(t)$ denotes the aggregate rate of all photons arriving at the detector from the X-ray pulsar and background, expressed in photons per second (ph/s). In practice, the rate function $\lambda(t)$ has the following form :

$$\lambda(t) = \lambda_b + \lambda_s h(\phi_{obs}(t)) \qquad \text{(ph/s)}, \tag{2.32}$$

where λ_s and λ_b are called the *effective source rate* and *effective background arrival rate*, respectively ; $h(\phi(t))$ is the normalized pulse profile function, and $\phi_{obs}(t)$ is the phase observed at the detector. Note that, thanks to the database obtained from years, the shape and period of the pulse profile are known very accurately [PUL]. The pulse profile function $h(\phi(t))$ (see figure 2.11) is defined as a periodic function with its period equal to one cycle, i.e., $h(\phi(t))$ is defined on the interval $\phi \in [0, 1)$, and we have $h(m + \phi(t)) = h(\phi(t))$ for all integers m. Besides, the function $h(\phi(t))$ is normalized, i.e, $\int_0^1 h(\phi)d\phi = 1$, and $\min_\phi h(\phi(t)) = 0$.

The observed phase at the detector is given by $\phi_{obs}(t) = \phi_0 + \int_{t_0}^t f(\tau)d\tau$, where ϕ_0 is the initial phase, where t_0 is the start of the observation interval, and where $f(t)$ is the observed signal frequency which depends on the constant source frequency and the variant Doppler frequency shift. Note that, in this section, we concentrate on the initial phase estimation problem, then, we assume that the observed frequency is a known constant. This is the constant-frequency model as in [ES10] where the observed phase at the detector can be rewritten as $\phi_{obs} = \phi_0 + (t - t_0)f$.

The Poisson rate function can, now, be considered as a function of the only unknown parameter, the initial phase, as below $\lambda(t;\phi_0) = \lambda_b + \lambda_s h(\phi_0 + (t - t_0)f)$. Since λ_b and λ_s are known from the database, then, the remaining challenge here is to estimate the initial phase ϕ_0. This is what has been done in [GS07] and [ES10] where two estimators, the MLE and the NLS, are studied and their performance has been compared to the CRB in terms of MSE. In this work, other bounds, such as QCL and WWB, are exploited to have a better benchmark. For this reason, we derive below the likelihood function.

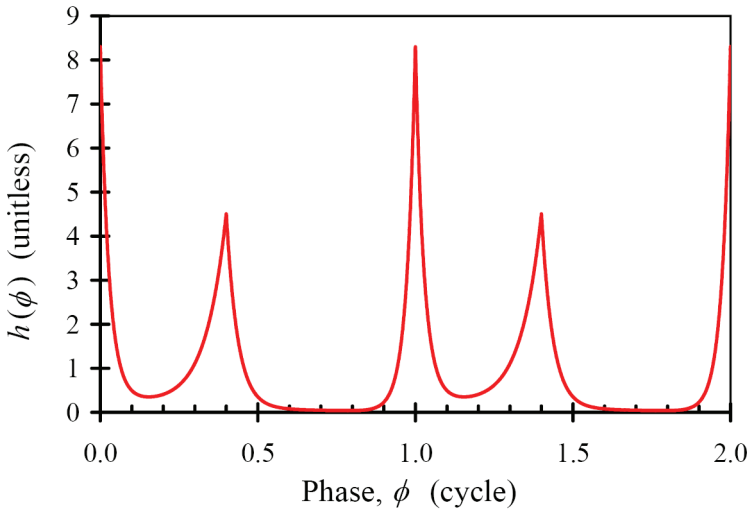

FIGURE 2.11 – Normalized pulse profile function of the Crab pulsar

The observation interval (t_0, t_0+T_{obs}) is partitioned into N equal-length segments. We define x_n, $n = 0, 1, \ldots, N-1$, as the number of photons detected in the n-th segment, and $\Delta t \equiv T_{obs}/N$ as the segment size. If N is large enough, the Poisson rate $\lambda(t, \phi_0)$ can be assumed constant in the n-th segment, i.e. $\lambda_n(\phi_0) = \lambda(t_n; \phi_0)$, where $t_n = t_0 + n\Delta t$. The probability mass function (pmf) for each Poisson random variable x_n, $n = 0, 1, \ldots, N-1$, can be written as : $p(x_n = x; \phi_0) = \frac{[\lambda_n(\phi_0)\Delta t]^x}{x!} \exp(-\lambda_n(\phi_0)\Delta t)$, where x is a non-negative integer. Under the assumption of independent observations, the likelihood of the full set of observations $\mathbf{x} = [x_0, x_1, \ldots, x_{N-1}]$ is given by

$$p(\mathbf{x}; \phi_0) = \prod_{n=0}^{N-1} \frac{[\lambda_n(\phi_0)\Delta t]^{x_n}}{x_n!} \exp(-\lambda_n(\phi_0)\Delta t). \tag{2.33}$$

In Section 2.4.2 and Section 2.4.3, we will derive the lower bounds based on (2.33) in the deterministic context and Bayesian context, respectively.

2.4.2 Deterministic Bound

In this Section, we consider the so-called deterministic bounds for pulse phase estimation. Mathematically, the Barankin bound (BB) [Bar49] is known to be tighter than the CRB, however, it is not computable. In classical array processing, to obtain a computable BB, several approximations of BB were proposed [CGQL08]. Consequently, in this section, we derive the QCLB [CGQL08] which is one of the tightest bounds among the Barankin family. This approximation is obtained following the search of an optimum over a set of test points, denoted as $[\theta_0, \ldots, \theta_{N-1}]$.

The Nth-order QCLB of the unknown parameter ϕ_0 satisfies the following relation $E_{\mathbf{x};\phi_0}\left[(\hat{\phi} - \phi_0)^2\right] \geq B^N_{QCL}(\phi_0)$, where $E_{\mathbf{x};\phi_0}\left[(\hat{\phi} - \phi_0)^2\right] = \sum_{x_0=0}^{\infty} \cdots \sum_{x_{N-1}=0}^{\infty} (\hat{\phi} - \phi_0)^2 p(\mathbf{x}; \phi_0)$ is the variance of any unbiased estimators $\hat{\phi}$ of ϕ_0. Hereafter, we use, for simplicity, $\sum_{\mathbf{x}=0}^{\infty}$ instead of $\sum_{x_0=0}^{\infty} \cdots \sum_{x_{N-1}=0}^{\infty}$.

The bound B^N_{QCL} is calculated as follows [CGQL08] : $B^N_{QCL} = \mathbf{v}^T \mathbf{M}^{-1}_{QCL} \mathbf{v}$ where

$$\left\{ \begin{array}{l} \mathbf{v} = [\mathbf{\Phi}^T, 1, \ldots, 1]^T \in \mathbb{R}^{2N\times 1} \text{ where } \mathbf{\Phi} = [\xi_0 \ldots \xi_{N-1}]^T, \text{ where } \xi_n = \theta_n - \phi_0,\ n = 0 \ldots N-1, \\ \mathbf{M}_{QCL} = \left[\begin{array}{cc} \mathbf{M}_{MS} & \mathbf{H}^T \\ \mathbf{H} & \mathbf{M}_{EFI} \end{array} \right] \in \mathbb{R}^{2N\times 2N} \end{array} \right. , \tag{2.34}$$

where

$$\mathbf{M}_{MS} = E_{\mathbf{x};\phi_0}\left[\left(\begin{array}{c} \frac{p(\mathbf{x};\theta_0)}{p(\mathbf{x};\phi_0)} \\ \vdots \\ \frac{p(\mathbf{x};\theta_{N-1})}{p(\mathbf{x};\phi_0)} \end{array} \right) \left(\begin{array}{c} \frac{p(\mathbf{x};\theta_0)}{p(\mathbf{x};\phi_0)} \\ \vdots \\ \frac{p(\mathbf{x};\theta_{N-1})}{p(\mathbf{x};\phi_0)} \end{array} \right)^T \right], \tag{2.35}$$

$$\mathbf{M}_{EFI} = E_{\mathbf{x};\phi_0}\left[\left(\begin{array}{c} \frac{\partial \ln p(\mathbf{x};\theta_0)}{\partial\theta_0} \frac{p(\mathbf{x};\theta_0)}{p(\mathbf{x};\phi_0)} \\ \vdots \\ \frac{\partial \ln p(\mathbf{x};\theta_{N-1})}{\partial\theta_{N-1}} \frac{p(\mathbf{x};\theta_{N-1})}{p(\mathbf{x};\phi_0)} \end{array} \right) \left(\begin{array}{c} \frac{\partial \ln p(\mathbf{x};\theta_0)}{\partial\theta_0} \frac{p(\mathbf{x};\theta_0)}{p(\mathbf{x};\phi_0)} \\ \vdots \\ \frac{\partial \ln p(\mathbf{x};\theta_{N-1})}{\partial\theta_{N-1}} \frac{p(\mathbf{x};\theta_{N-1})}{p(\mathbf{x};\phi_0)} \end{array} \right)^T \right], \tag{2.36}$$

$$\mathbf{H} = E_{\mathbf{x};\phi_0}\left[\left(\begin{array}{c} \frac{\partial \ln p(\mathbf{x};\theta_0)}{\partial\theta_0} \frac{p(\mathbf{x};\theta_0)}{p(\mathbf{x};\phi_0)} \\ \vdots \\ \frac{\partial \ln p(\mathbf{x};\theta_{N-1})}{\partial\theta_{N-1}} \frac{p(\mathbf{x};\theta_{N-1})}{p(\mathbf{x};\phi_0)} \end{array} \right) \left(\begin{array}{c} \frac{p(\mathbf{x};\theta_0)}{p(\mathbf{x};\phi_0)} \\ \vdots \\ \frac{p(\mathbf{x};\theta_{N-1})}{p(\mathbf{x};\phi_0)} \end{array} \right)^T \right], \tag{2.37}$$

where $\mathbf{M}_{MS}$ is the McAulay–Seidman matrix, $\mathbf{M}_{EFI}$ is the extended Fisher information matrix, and $\mathbf{H}$ is a kind of "hybrid" matrix [CGQL08]. The set $\theta_n, n = 1, \ldots, N-1$ is the so-called set of the test point. After the calculation which is detailed in Appendix one obtains the closed-form expressions of elements (k, l) of matrix $\mathbf{M}_{MS}$ (see Appendix 2.6.4), $\mathbf{M}_{EFI}$ (see Appendix 2.6.5), and $\mathbf{H}$ (see Appendix 2.6.6) as follows :

$$\mathbf{M}_{MS}(k,l) = \exp\left\{ T_{obs} \int_0^1 \lambda(\phi) - \lambda(\xi_k + \phi) - \lambda(\xi_l + \phi) + \frac{\lambda(\xi_k + \phi)\lambda(\xi_l + \phi)}{\lambda(\phi)} d\phi \right\}, \tag{2.38}$$

$$\begin{aligned} \mathbf{M}_{EFI}(k,l) = \mathbf{M}_{MS}(k,l) \Bigg[& T_{obs}^2 \int_0^1 \frac{\partial\lambda(\phi+\xi_k)}{\partial\xi_k} \frac{\lambda(\phi+\xi_l)}{\lambda(\phi)} d\phi \int_0^1 \frac{\partial\lambda(\phi+\xi_l)}{\partial\xi_l} \frac{\lambda(\phi+\xi_k)}{\lambda(\phi)} d\phi \\ & + T_{obs}^2 \int_0^1 \frac{\partial\lambda(\phi+\xi_k)}{\partial\xi_k} d\phi \int_0^1 \frac{\partial\lambda(\phi+\xi_l)}{\partial\xi_l} d\phi - T_{obs}^2 \int_0^1 \frac{\partial\lambda(\phi+\xi_l)}{\partial\xi_l} d\phi \int_0^1 \frac{\partial\lambda(\phi+\xi_k)}{\partial\xi_k} \frac{\lambda(\phi+\xi_l)}{\lambda(\phi)} d\phi, \\ & - T_{obs}^2 \int_0^1 \frac{\partial\lambda(\phi+\xi_k)}{\partial\xi_k} d\phi \int_0^1 \frac{\partial\lambda(\phi+\xi_l)}{\partial\xi_l} \frac{\lambda(\phi+\xi_k)}{\lambda(\phi)} d\phi + T_{obs} \int_0^1 \frac{\partial\lambda(\phi+\xi_k)}{\partial\xi_k} \frac{\partial\lambda(\phi+\xi_l)}{\partial\xi_l} \frac{1}{\lambda(\phi)} d\phi \Bigg] \end{aligned} \tag{2.39}$$

and

$$\mathbf{H}(k,l) = \mathbf{M}_{MS}(k,l) \left[T_{obs} \int_0^1 \frac{\partial\lambda(\phi+\xi_k)}{\partial\xi_k} \frac{\lambda(\phi+\xi_l)}{\lambda(\phi)} d\phi - T_{obs} \int_0^1 \frac{\partial\lambda(\phi+\xi_k)}{\partial\xi_k} d\phi \right]. \tag{2.40}$$

In the expression of the QCLB, we can see the existence of an integral which can be computed easily and rapidly in a numerical way. Note that, it was also the case in the CRB calculus proposed in [GS07] and [ES10]. In Section 2.4.4, we plot the QCLB versus several observation times and compare it to the CRB and the MSE of the MLE.

2.4.3 Bayesian bound

As an alternative to the deterministic framework, we propose to handle the problem in the Bayesian framework which will provide a tight minimal bound over all the range of observation time and a good prediction of the observation time threshold. In particular, we assume that the parameter of interest ϕ_0 is random with an *a priori* uniform probability density function (pdf) over the support $[0, 1]$. Note that not all the Bayesian bounds proposed in the literature are able to take into account the case when the parameters of interest are supposed to be uniformly distributed. Therefore, among various types of Bayesian bounds [TB07], we concentrate, in this Section, on the Weiss-Weinstein bound (WWB) (see [WW85] [RO07a] [RO07b]), which can deal with the uniformly distributed prior assumption and is one of the tightest bound of the Weiss and Weinstein family [RFL05] [RFL$^+$08].

The Weiss-Weinstein bound, denoted WWB, for the unknown parameter ϕ_0 satisfies the following relation $E_{\mathbf{x};\phi_0}\left[(\hat{\phi}-\phi_0)^2\right] \geq WWB$, where $E_{\mathbf{x};\phi_0}\left[(\hat{\phi}-\phi_0)^2\right] = \int_{\mathbf{\Theta}} \sum_{\mathbf{x}=0}^{\infty} (\hat{\phi}-\phi_0)^2 p(\mathbf{x},\phi_0) d\phi_0$ is the variance of any estimators of ϕ_0, where $p(\mathbf{x},\phi_0)$ being the joint pdf and $\mathbf{\Theta}$ is the parameter space. Note that, contrary to the deterministic bounds, no assumption is made on the estimator $\hat{\phi}$, e.g., $\hat{\phi}$ can be biased. The WWB is calculated by [WW85]

$$WWB = \underset{u,s}{sup} \frac{u^2 \exp(2\eta(s,u))}{\exp(\eta(2s,u)) + \exp(\eta(2-2s,-u)) - 2\exp(\eta(s,2u))}, \tag{2.41}$$

where $s \in [0,1]$, where u is the test point chosen such that $\phi_0 + u \in [0,1)$, and $\eta(\alpha,\beta)$ is defined by

$$\begin{aligned}
\eta(\alpha,\beta) &= \ln \int_{\mathbf{\Theta}} \sum_{\mathbf{x}=0}^{\infty} p(\mathbf{x},\phi_0+\beta)^{\alpha} p(\mathbf{x},\phi_0)^{1-\alpha} d\phi_0 \\
&= \ln \int_{\mathbf{\Theta}} \sum_{\mathbf{x}=0}^{\infty} p(\mathbf{x};\phi_0+\beta)^{\alpha} p(\phi_0+\beta)^{\alpha} p(\mathbf{x};\phi_0)^{1-\alpha} p(\phi_0)^{1-\alpha} d\phi_0 \\
&= \ln \int_{\mathbf{\Theta}} \eta'(\alpha,\beta) p(\phi_0+\beta)^{\alpha} p(\phi_0)^{1-\alpha} d\phi_0,
\end{aligned} \tag{2.42}$$

where we define $\eta'(\alpha,\beta) = \sum_{\mathbf{x}=0}^{\infty} p(\mathbf{x};\phi_0+\beta)^{\alpha} p(\mathbf{x};\phi_0)^{1-\alpha}$. The closed-form expression of $\eta'(\alpha,\beta)$ is given by (see Appendix 2.6.7 for details)

$$\eta'(\alpha,\beta) = \exp\left\{ T_{obs} \int_0^1 \left(-\alpha\lambda(\phi+\beta) - (1-\alpha)\lambda(\phi) + \lambda(\phi+\beta)^{\alpha}\lambda(\phi)^{1-\alpha} \right) d\phi \right\}. \tag{2.43}$$

Note that, the dependance of $\eta'(\alpha,\beta)$ on ϕ_0 is now removed, then, the integral in (2.42)

can be calculated easily. Finally, the Weiss-Weinstein bound for the unknown parameter ϕ_0 is given by

$$WWB = \sup_{u,s} \frac{u^2(1-u)^2\eta'^2(s,u)}{(1-u)\eta'(2s,u) + (1-u)\eta'(2-2s,-u) - 2(1-2u)\eta'(s,2u)}. \quad (2.44)$$

As it appears in the QCLB [see (2.38)-(2.40)], integrals also exist in the expression of the WWB but they can be numerically integrated.

2.4.4 Numerical Results

To evaluate the proposed bounds, we compare them to the performance of the MLE of the pulse phase which is given by $\hat{\phi} = \arg\max_{\phi_0 \in \mathbf{\Theta}} \sum_{n=0}^{N-1} [x_n \ln[\lambda_n(\phi_0)\Delta t] - \lambda_n(\phi_0)\Delta t]$. The performance of the MLE is simulated using 1000 Monte Carlo runs. The observed frequency is $f = 29.85$ Hz and the pulsar period is 33.5 ms. The photon rates are $\lambda_b = 5$ (ph/s) and $\lambda_s = 15$ (ph/s). The number of test point is 100. As the phase is defined on the $[0, 1]$ interval, the phase error value is calculated modulo one cycle, i.e., $min[mod(\phi_0 - \hat{\phi}, 1), mod(\hat{\phi} - \phi_0, 1)]$. For example, the error between 0.9 cycle and 0.1 cycle should be 0.2 cycle, and not 0.8 cycle.

In Figure 2.12, we compare the QCLB to the CRB and to the MSE of the MLE versus the observation time. The initial phase, $\phi_0 = 0.9$ cycle, is chosen arbitrarily. It can be seen that the QCL provides a good prediction of the threshold location compared to the MSE of the MLE. We also plot in Figure 2.13 the QCLB with various numbers of test point. One can see that using more test points achieves a slightly better bound but increases the numerical complexity.

Figure 2.14 shows the WWB and the empirical global MSE of the MLE of ϕ_0 versus the observation time. It can be seen that the WWB predicts well not only the threshold position, but also the MSE of the MLE in all range of observation time (asymptotic and threshold regions). Note that the tightest WWB is achieved when $s = 1/2$.

2.4.5 Summary

Accurate estimation of the initial phase of the pulse arriving at the detector appears to be the key challenge in a system using X-ray pulsars to perform the autonomous deep space navigating. Therefore, we have derived the closed-form expressions of the lower bounds on the MSE and analyzed their behavior for the problem of X-ray pulse phase estimation. Indeed, both deterministic (QCLB) and Bayesian bounds (WWB) have been considered. We have shown that both types of lower bound provide good prediction of the threshold location depending on the estimation framework.

2.5 Conclusion

In this Chapter, we have examined the lower bounds in two different contexts :

- The first one is the target localization using the MIMO radar for which we have developed the Weiss-Weinstein bound for Bayesian parameter and the CRB for deterministic parameter in the presence of modeling errors. For the Bayesian case, we have shown that the Weiss-Weinstein bound for the parameter of interest provides a

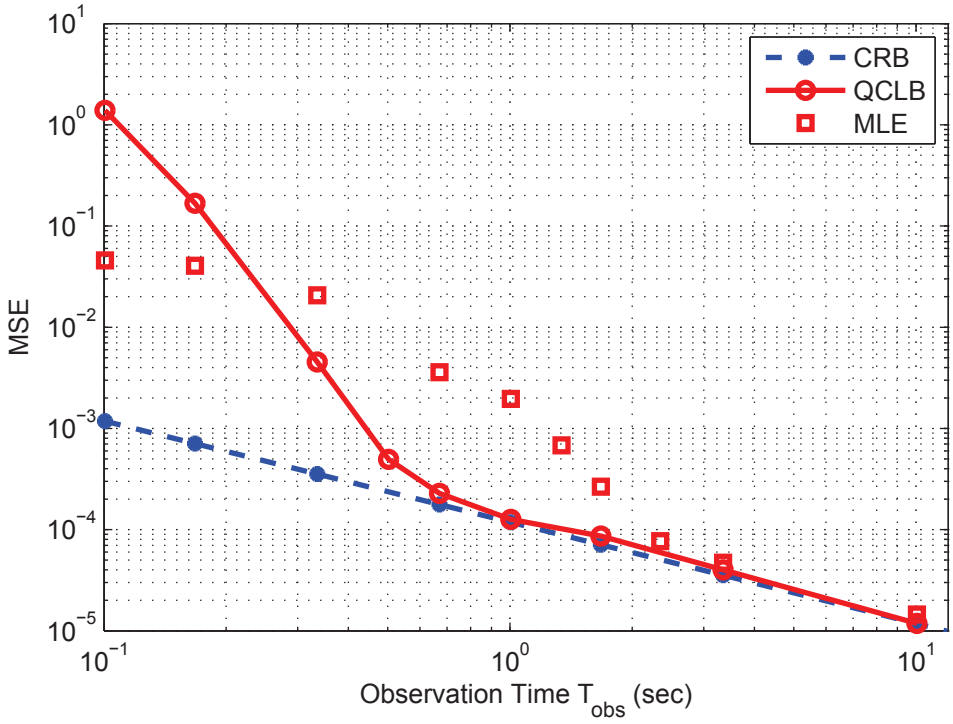

FIGURE 2.12 – QCLB, CRB and empirical MSE of the MLE of ϕ_0 versus observation time

good prediction of the MSE of the MLE in all regions of the ASNR. It also predicts the threshold ASNR location near the one indicated by the maximum *a posteriori* estimator. We also introduced a numerical procedure to optimize antenna geometry of MIMO radar in terms of the MSE. For the case with modeling errors, we have derived closed-form expressions of the Fisher information matrix and shown its block diagonal structure to deduce the Cramér-Rao bounds expressions of the angle-of-arrival and of the angle-of-departure. We have shown that, under a certain signal-to-noise ratio, the performance of the system can not be improved. Finally, we have proposed a simple formula to evaluate this critical value of the signal-to-noise ratio.

- The second context is the pulse phase estimation of X-ray pulsars for which we have derived the closed-form expressions of the Quinlan-Chaumette-Larzabal bound for the deterministic parameter and the Weiss-Weinstein bound for the Bayesian parameter. We have shown that both types of lower bound provide good prediction of the threshold location depending on the estimation framework while the computational complexity remains very low in comparison to the maximum likelihood estimator.

2.6 Appendix

2.6.1 Proof of Equ. (2.8)

Note that

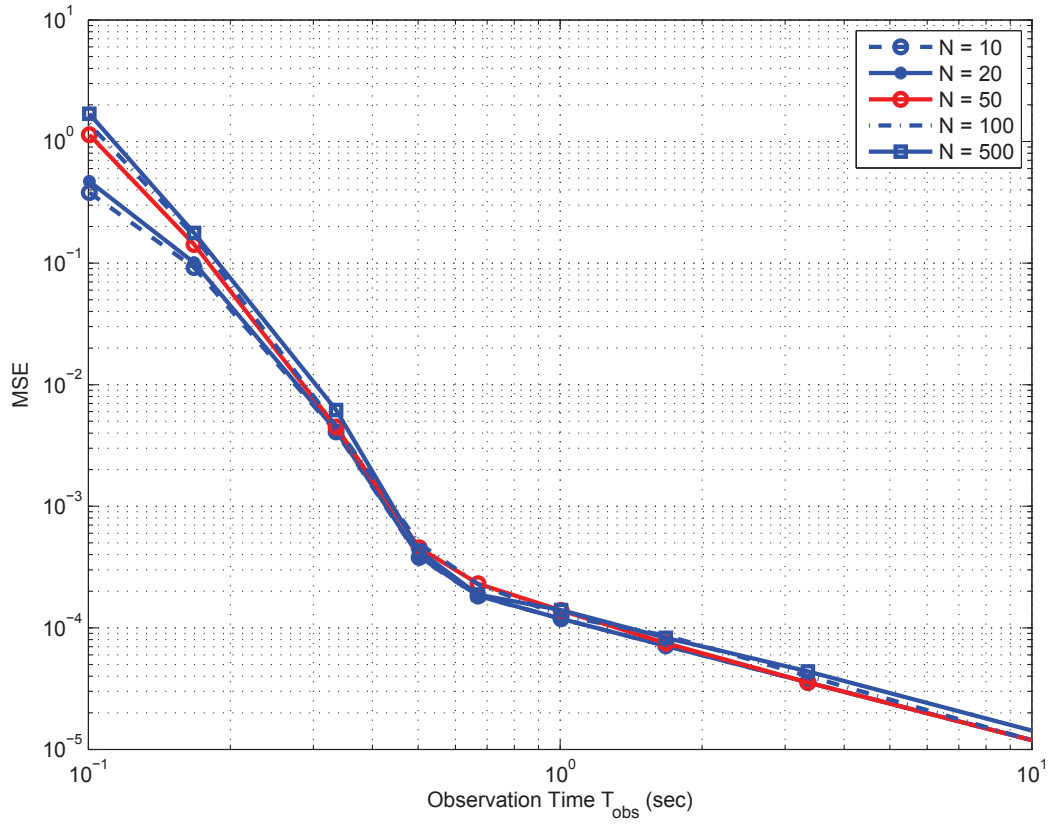

FIGURE 2.13 – QCLB of ϕ_0 versus observation time

$$p(\mathbf{Y};\boldsymbol{\Theta}+\boldsymbol{\alpha})^{\frac{1}{2}}p(\mathbf{Y};\boldsymbol{\Theta}+\boldsymbol{\gamma})^{\frac{1}{2}} = \frac{1}{\pi^{NT}\sigma_n^{NT}}\exp\left(-\sum_{t=1}^{T}\zeta(\boldsymbol{\Theta},\boldsymbol{\alpha},\boldsymbol{\gamma},t)\right), \tag{2.45}$$

where

$$\begin{aligned}\zeta(\boldsymbol{\Theta},\boldsymbol{\alpha},\boldsymbol{\gamma},t) =& \frac{1}{2\sigma_n^2}\left[\mathbf{y}-\mathbf{f}(\boldsymbol{\Theta}+\boldsymbol{\alpha},t)\right]^H\left[\mathbf{y}-\mathbf{f}(\boldsymbol{\Theta}+\boldsymbol{\alpha},t)\right] + \frac{1}{2\sigma_n^2}\left[\mathbf{y}-\mathbf{f}(\boldsymbol{\Theta}+\boldsymbol{\gamma},t)\right]^H\left[\mathbf{y}-\mathbf{f}(\boldsymbol{\Theta}+\boldsymbol{\gamma},t)\right] \\ =& \frac{1}{\sigma_n^2}\left[\mathbf{y}^H\mathbf{y} - \frac{1}{2}\mathbf{y}^H\mathbf{f}(\boldsymbol{\Theta}+\boldsymbol{\alpha},t) - \frac{1}{2}\mathbf{y}^H\mathbf{f}(\boldsymbol{\Theta}+\boldsymbol{\gamma},t) - \frac{1}{2}\mathbf{f}(\boldsymbol{\Theta}+\boldsymbol{\alpha},t)^H\mathbf{y} - \frac{1}{2}\mathbf{f}(\boldsymbol{\Theta}+\boldsymbol{\gamma},t)^H\mathbf{y}\right. \\ &\left. + \frac{1}{2}\mathbf{f}(\boldsymbol{\Theta}+\boldsymbol{\alpha},t)^H\mathbf{f}(\boldsymbol{\Theta}+\boldsymbol{\alpha},t) + \frac{1}{2}\mathbf{f}(\boldsymbol{\Theta}+\boldsymbol{\gamma},t)^H\mathbf{f}(\boldsymbol{\Theta}+\boldsymbol{\gamma},t)\right].\end{aligned} \tag{2.46}$$

Define $\mathbf{z} = \mathbf{y} - \frac{1}{2}\mathbf{f}(\boldsymbol{\Theta}+\boldsymbol{\alpha},t) - \frac{1}{2}\mathbf{f}(\boldsymbol{\Theta}+\boldsymbol{\gamma},t)$, we have

$$\zeta(\boldsymbol{\Theta},\boldsymbol{\alpha},\boldsymbol{\gamma},t) = \frac{1}{\sigma_n^2}\mathbf{z}^H\mathbf{z} + \frac{1}{4}\zeta'(\boldsymbol{\Theta},\boldsymbol{\alpha},\boldsymbol{\gamma},t), \tag{2.47}$$

where $\zeta'(\boldsymbol{\Theta},\boldsymbol{\alpha},\boldsymbol{\gamma},t) = \frac{1}{\sigma_n^2}\left[\mathbf{f}(\boldsymbol{\Theta}+\boldsymbol{\alpha},t)-\mathbf{f}(\boldsymbol{\Theta}+\boldsymbol{\gamma},t)\right]^H\left[\mathbf{f}(\boldsymbol{\Theta}+\boldsymbol{\alpha},t)-\mathbf{f}(\boldsymbol{\Theta}+\boldsymbol{\gamma},t)\right]$. Consequently, $\zeta'(\boldsymbol{\Theta},\boldsymbol{\alpha},\boldsymbol{\gamma},t)$ does not depend on $\mathbf{Y}$, and

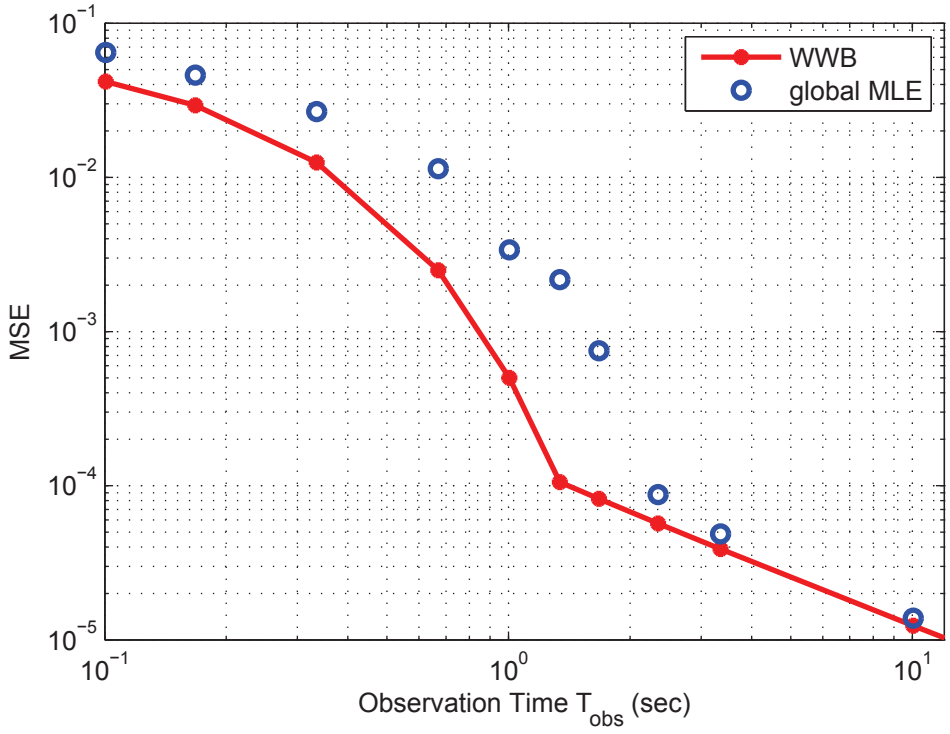

FIGURE 2.14 – WWB and empirical global MSE of MLE of ϕ_0 versus observation time

$$\begin{aligned}\eta'(\boldsymbol{\Theta},\boldsymbol{\alpha},\boldsymbol{\gamma}) =& \frac{1}{\pi^{NT}\sigma_n^{NT}}\int_{\Omega}\exp\left(-\sum_{t=1}^{T}(\frac{1}{\sigma_n^2}\mathbf{z}^H\mathbf{z}+\frac{1}{4}\zeta'(\boldsymbol{\Theta},\boldsymbol{\alpha},\boldsymbol{\gamma},t))\right)d\mathbf{Y}\\ =& \exp\left(-\sum_{t=1}^{T}\frac{1}{4}\zeta'(\boldsymbol{\Theta},\boldsymbol{\alpha},\boldsymbol{\gamma},t))\right).\end{aligned} \tag{2.48}$$

2.6.2 Proof of Equ. (2.11)

From (2.8), the set of functions involved in $[\mathbf{G}]_{11}$ are given by

$$\begin{cases}\eta'(\boldsymbol{\Theta},\mathbf{h}_1,\mathbf{h}_1)=1,\eta'(\boldsymbol{\Theta},-\mathbf{h}_1,-\mathbf{h}_1)=1,\\ \eta'(\boldsymbol{\Theta},\mathbf{h}_1,-\mathbf{h}_1)=\exp\left\{-\frac{1}{2}(\beta_R^2+\beta_I^2)T\sum_{k=1}^{M}\sum_{r=1}^{N}\frac{\sigma_k^2}{\sigma_n^2}\left[1-\cos\left(\frac{4\pi}{\lambda}h_1(a_k+b_r)\right)\right]\right\},\\ \eta'(\boldsymbol{\Theta},\mathbf{h}_1,0)=\exp\left\{-\frac{1}{2}(\beta_R^2+\beta_I^2)2T\sum_{k=1}^{M}\sum_{r=1}^{N}\frac{\sigma_k^2}{\sigma_n^2}\left[1-\cos\left(\frac{2\pi}{\lambda}h_1(a_k+b_r)\right)\right]\right\}.\end{cases} \tag{2.49}$$

Then, since all the functions η' do not depend on u, by integrating w.r.t. $\boldsymbol{\Theta}$, we obtain

$$\begin{cases}\eta(\mathbf{h}_1,\mathbf{h}_1)=\frac{2-h_1}{2},\eta(-\mathbf{h}_1,-\mathbf{h}_1)=\frac{2-h_1}{2},\\ \eta(\mathbf{h}_1,-\mathbf{h}_1)=\frac{1-h_1}{\sigma_\beta^2\frac{1}{2}T\sum_{k=1}^{M}\sum_{r=1}^{N}\frac{\sigma_k^2}{\sigma_n^2}\left[1-\cos\left(\frac{4\pi}{\lambda}h_1(a_k+b_r)\right)\right]+1},\\ \eta(\mathbf{h}_1,0)=\frac{2-h_1}{2}\frac{1}{\sigma_\beta^2\frac{1}{2}T\sum_{k=1}^{M}\sum_{r=1}^{N}\frac{\sigma_k^2}{\sigma_n^2}\left[1-\cos\left(\frac{2\pi}{\lambda}h_1(a_k+b_r)\right)\right]+1}.\end{cases} \tag{2.50}$$

The set of functions involved in $[\mathbf{G}]_{kk}, k=2,3$ are given by

$$\left\{\begin{array}{l}\eta'(\boldsymbol{\Theta},\mathbf{h}_k,\mathbf{h}_k)=1,\eta'(\boldsymbol{\Theta},-\mathbf{h}_k,-\mathbf{h}_k)=1,\\ \eta'(\boldsymbol{\Theta},\mathbf{h}_k,-\mathbf{h}_k)=\exp\left(-h_k^2NT\frac{\sum_{k=1}^M\sigma_k^2}{\sigma_n^2}\right),\\ \eta'(\boldsymbol{\Theta},\mathbf{h}_k,0)=\exp\left(-\frac{1}{4}h_k^2NT\frac{\sum_{k=1}^M\sigma_k^2}{\sigma_n^2}\right).\end{array}\right. \Rightarrow \left\{\begin{array}{l}\eta(\mathbf{h}_k,\mathbf{h}_k)=1,\eta(-\mathbf{h}_k,-\mathbf{h}_k)=1,\\ \eta(\mathbf{h}_k,-\mathbf{h}_k)=\exp\left(-h_k^2NT\frac{\sum_{k=1}^M\sigma_k^2}{\sigma_n^2}\right)\exp\left(-\frac{h_k^2}{\sigma_\beta^2}\right),\\ \eta(\mathbf{h}_k,0)=\exp\left(-\frac{1}{4}h_k^2NT\frac{\sum_{k=1}^M\sigma_k^2}{\sigma_n^2}\right)\exp\left(-\frac{h_k^2}{4\sigma_\beta^2}\right).\end{array}\right. \tag{2.51}$$

The set of functions involved in $[\mathbf{G}]_{12}$ are given by

$$\left\{\begin{array}{ll}\eta'(\boldsymbol{\Theta},\mathbf{h}_1,\mathbf{h}_2)= & \exp\left\{2T\sum_{k=1}^M\sum_{r=1}^N\frac{\sigma_k^2}{\sigma_n^2}\left[\beta_R^2\left(1-\cos\left(\frac{2\pi}{\lambda}h_1(a_k+b_r)\right)\right)\right.\right.\\ & +\beta_Rh_2\left(1-\cos\left(\frac{2\pi}{\lambda}h_1(a_k+b_r)\right)\right)+\beta_I^2\left(1-\cos\left(\frac{2\pi}{\lambda}h_1(a_k+b_r)\right)\right)\\ & \left.\left.-\beta_Ih_2\sin\left(\frac{2\pi}{\lambda}h_1(a_k+b_r)\right)+\frac{1}{2}h_2^2\right]\right\},\\ \eta'(\boldsymbol{\Theta},-\mathbf{h}_1,-\mathbf{h}_2)= & \exp\left\{2T\sum_{k=1}^M\sum_{r=1}^N\frac{\sigma_k^2}{\sigma_n^2}\left[\beta_R^2\left(1-\cos\left(\frac{2\pi}{\lambda}h_1(a_k+b_r)\right)\right)\right.\right.\\ & -\beta_Rh_2\left(1-\cos\left(\frac{2\pi}{\lambda}h_1(a_k+b_r)\right)\right)+\beta_I^2\left(1-\cos\left(\frac{2\pi}{\lambda}h_1(a_k+b_r)\right)\right)\\ & \left.\left.+\beta_Ih_2\sin\left(\frac{2\pi}{\lambda}h_1(a_k+b_r)\right)+\frac{1}{2}h_2^2\right]\exp\right\},\\ \eta'(\boldsymbol{\Theta},-\mathbf{h}_1,\mathbf{h}_2)= & \exp\left\{2T\sum_{k=1}^M\sum_{r=1}^N\frac{\sigma_k^2}{\sigma_n^2}\left[\beta_R^2\left(1-\cos\left(\frac{2\pi}{\lambda}h_1(a_k+b_r)\right)\right)\right.\right.\\ & +\beta_Rh_2\left(1-\cos\left(\frac{2\pi}{\lambda}h_1(a_k+b_r)\right)\right)+\beta_I^2\left(1-\cos\left(\frac{2\pi}{\lambda}h_1(a_k+b_r)\right)\right)\\ & \left.\left.+\beta_Ih_2\sin\left(\frac{2\pi}{\lambda}h_1(a_k+b_r)\right)+\frac{1}{2}h_2^2\right]\exp\right\},\\ \eta'(\boldsymbol{\Theta},-\mathbf{h}_1,-\mathbf{h}_2)= & \exp\left\{2T\sum_{k=1}^M\sum_{r=1}^N\frac{\sigma_k^2}{\sigma_n^2}\left[\beta_R^2\left(1-\cos\left(\frac{2\pi}{\lambda}h_1(a_k+b_r)\right)\right)\right.\right.\\ & -\beta_Rh_2\left(1-\cos\left(\frac{2\pi}{\lambda}h_1(a_k+b_r)\right)\right)+\beta_I^2\left(1-\cos\left(\frac{2\pi}{\lambda}h_1(a_k+b_r)\right)\right)\\ & \left.\left.-\beta_Ih_2\sin\left(\frac{2\pi}{\lambda}h_1(a_k+b_r)\right)+\frac{1}{2}h_2^2\right]\exp\right\}.\end{array}\right. \tag{2.52}$$

Consequently,

$$\eta(\mathbf{h}_1,\mathbf{h}_2)=\eta(-\mathbf{h}_1,\mathbf{h}_2)=\frac{2-h_1}{2}t_1t_2, \tag{2.53}$$

where

$$\begin{aligned}t_1=\exp\left(-\frac{h_2^2}{2\sigma_\beta^2}\right)\exp\left\{\frac{h_2^2}{4}\left[\frac{T}{2}\sum_{k=1}^M\sum_{r=1}^N\frac{\sigma_k^2}{\sigma_n^2}\left(1-\cos\left(\frac{2\pi}{\lambda}h_1(a_k+b_r)\right)\right)+\frac{1}{\sigma_\beta^2}\right]\right\}\\ \times\frac{\sqrt{\pi}\sigma_\beta}{4\left\{\frac{\sigma_\beta^2}{2}\left[\frac{T}{2}\sum_{k=1}^M\sum_{r=1}^N\frac{\sigma_k^2}{\sigma_n^2}\left(1-\cos\left(\frac{2\pi}{\lambda}h_1(a_k+b_r)\right)\right)+\frac{1}{\sigma_\beta^2}\right]\right\}^{\frac{1}{2}}},\end{aligned} \tag{2.54}$$

$$t_2 = \exp\left\{\frac{\left[h_2\frac{T}{2}\sum_{k=1}^{M}\sum_{r=1}^{N}\frac{\sigma_k^2}{\sigma_n^2}\sin\left(\frac{2\pi}{\lambda}h_1(a_k+b_r)\right)\right]^2}{4\left[\frac{T}{2}\sum_{k=1}^{M}\sum_{r=1}^{N}\frac{\sigma_k^2}{\sigma_n^2}\left(1-\cos\left(\frac{2\pi}{\lambda}h_1(a_k+b_r)\right)\right)+\frac{1}{\sigma_\beta^2}\right]}\right\} \times \frac{\sqrt{\pi}\sigma_\beta}{4\left\{\frac{\sigma_\beta^2}{2}\left[\frac{T}{2}\sum_{k=1}^{M}\sum_{r=1}^{N}\frac{\sigma_k^2}{\sigma_n^2}\left(1-\cos\left(\frac{2\pi}{\lambda}h_1(a_k+b_r)\right)\right)+\frac{1}{\sigma_\beta^2}\right]\right\}^{\frac{1}{2}}}. \tag{2.55}$$

Similarly, it is straightforward to see that $\eta(\mathbf{h}_1,-\mathbf{h}_2)=\eta(-\mathbf{h}_1,-\mathbf{h}_2)$ which, together with (2.53), lead to $[\mathbf{G}]_{12}=0$. We also have $[\mathbf{G}]_{21}=0$, $[\mathbf{G}]_{13}=0$, $[\mathbf{G}]_{31}=0$, $[\mathbf{G}]_{23}=0$, and $[\mathbf{G}]_{32}=0$. Therefore, the matrix $\mathbf{G}$ is diagonal with elements given by

$$[\mathbf{G}]_{11} = 2\frac{\frac{2-h_1}{2}-\frac{1-h_1}{\frac{\sigma_\beta^2}{\sigma_n^2}\frac{1}{2}T\sum_{k=1}^{M}\sum_{r=1}^{N}\sigma_k^2\left[1-\cos\left(\frac{4\pi}{\lambda}h_1(a_k+b_r)\right)\right]+1}}{\left[\frac{2-h_1}{2}\frac{1}{\frac{\sigma_\beta^2}{\sigma_n^2}\frac{1}{2}T\sum_{k=1}^{M}\sum_{r=1}^{N}\sigma_k^2\left[1-\cos\left(\frac{2\pi}{\lambda}h_1(a_k+b_r)\right)\right]+1}\right]^2}, \tag{2.56}$$

$$[\mathbf{G}]_{22} = 2\frac{1-\exp\left(-h_2^2NT\frac{\sum_{k=1}^{M}\sigma_k^2}{\sigma_n^2}\right)\exp\left(-\frac{h_2^2}{\sigma_\beta^2}\right)}{\exp\left(-\frac{1}{2}h_2^2NT\frac{\sum_{k=1}^{M}\sigma_k^2}{\sigma_n^2}\right)\exp\left(-\frac{h_2^2}{2\sigma_\beta^2}\right)}, \tag{2.57}$$

$$[\mathbf{G}]_{33} = 2\frac{1-\exp\left(-h_3^2NT\frac{\sum_{k=1}^{M}\sigma_k^2}{\sigma_n^2}\right)\exp\left(-\frac{h_3^2}{\sigma_\beta^2}\right)}{\exp\left(-\frac{1}{2}h_3^2NT\frac{\sum_{k=1}^{M}\sigma_k^2}{\sigma_n^2}\right)\exp\left(-\frac{h_3^2}{2\sigma_\beta^2}\right)}, \tag{2.58}$$

Using all the assumptions and results above, the closed-form expression of the matrix $\mathbf{WWB}$ can be written as $\mathbf{WWB} = Diag\left(\sup_{h_1}\frac{h_1^2}{[\mathbf{G}]_{11}}, \sup_{h_2}\frac{h_2^2}{[\mathbf{G}]_{22}}, \sup_{h_3}\frac{h_3^2}{[\mathbf{G}]_{33}}\right)$, with $[\mathbf{G}]_{11}, [\mathbf{G}]_{22}, [\mathbf{G}]_{33}$ given in (2.12), (2.57), and (2.58), respectively.

Note that in the original form of the Weiss-Weinstein bound (2.3), we have to optimize the matrix $\mathbf{WWB}$ w.r.t. $h_1, h_2,$ and h_3. Since $[\mathbf{G}]_{ii}$ depends only on h_i, the optimization task is reduced to $\sup_{h_k}\frac{h_k^2}{[\mathbf{G}]_{kk}}, \forall k$ which is more tractable. Next, we give a closed-form expression for $\sup_{h_k}\frac{h_k^2}{[\mathbf{G}]_{kk}}$, $k=2,3$, $\mathbf{WWB}_{kk} = \sup_{x\geq 0}\frac{x\exp(-ax)}{2[1-\exp(-2ax)]}, a>0$, where $x=h_k^2$ and $a = NT\frac{\sum_{k=1}^{M}\sigma_k^2}{2\sigma_n^2}+\frac{1}{2\sigma_\beta^2}$. If we denote $g(x)=\frac{x\exp(-ax)}{2[1-\exp(-2ax)]}$, then

$$\frac{dg(x)}{dx} = \frac{\exp(-ax)\left[1-ax-\exp(-2ax)-ax\exp(-2ax)\right]}{4[1-\exp(-2ax)]^2}, \tag{2.59}$$

which is always negative $\forall x>0$. Consequently, $g(x)$ is a monotonically decreasing function and has its maximum at $x=0$. Finally, we obtain : $\sup_{h_k}\frac{h_k^2}{[\mathbf{G}]_{kk}} = \frac{1}{2\left(NT\frac{\sum_{k=1}^{M}\sigma_k^2}{\sigma_n^2}+\frac{1}{\sigma_\beta^2}\right)}, k=2,3,$

which concludes the proof.

2.6.3 Proof of Equ. (2.25)

In order to deriving the elements of the FIM, let us introduce the following definitions and results :

- $$\dot{\mathbf{a}} = \left[\cdots - j\frac{2\pi}{\lambda} a_k \cos(\theta_D) \exp\left(-j\frac{2\pi}{\lambda} a_k \sin\theta_D \right) \cdots \right]^T, \; k = 1, \ldots, M \tag{2.60}$$

- $$\dot{\mathbf{b}} = \left[\cdots - j\frac{2\pi}{\lambda} b_k \cos(\theta_A) \exp\left(-j\frac{2\pi}{\lambda} b_k \sin\theta_A \right) \cdots \right]^T, \; k = 1, \ldots, N \tag{2.61}$$

- $$\dot{\mathbf{s}}(\theta_D) = \left[\dot{\mathbf{a}}^T(\theta_D)\mathbf{x}(1) \ldots \dot{\mathbf{a}}^T(\theta_D)\mathbf{x}(T) \right]^T,$$

- $$\begin{aligned} \mathbf{s}^H(\theta_D)\mathbf{s}(\theta_D) &= \sum_{t=1}^{T} (\mathbf{a}^T(\theta_D)\mathbf{x}(1))^H \mathbf{a}^T(\theta_D)\mathbf{x}(1) \\ &= \mathbf{a}^T(\theta_D) \sum_{t=1}^{T} \mathbf{x}(1)\mathbf{x}(1)^H \mathbf{a}^*(\theta_D) \\ &= T\sigma_x^2 \mathbf{a}^T(\theta_D)\mathbf{a}^*(\theta_D) \\ &= TM\sigma_x^2, \end{aligned} \tag{2.62}$$

- $$\begin{aligned} \dot{\mathbf{s}}^H(\theta_D)\mathbf{s}(\theta_D) &= \sum_{t=1}^{T} (\dot{\mathbf{a}}^T(\theta_D)\mathbf{x}(1))^H \mathbf{a}^T(\theta_D)\mathbf{x}(1) \\ &= \dot{\mathbf{a}}^T(\theta_D) \sum_{t=1}^{T} \mathbf{x}(1)\mathbf{x}(1)^H \mathbf{a}^*(\theta_D) \\ &= T\sigma_x^2 \dot{\mathbf{a}}^T(\theta_D)\mathbf{a}^*(\theta_D) \\ &= 0. \end{aligned} \tag{2.63}$$

- $$\dot{\mathbf{s}}^H(\theta_D)\dot{\mathbf{s}}(\theta_D) = \sum_{t=1}^{T} (\dot{\mathbf{a}}^T(\theta_D)\mathbf{x}(1))^H \dot{\mathbf{a}}^T(\theta_D)\mathbf{x}(1)$$

$$
\begin{aligned}
&= \dot{\mathbf{a}}^T(\theta_D) \sum_{t=1}^{T} \mathbf{x}(1)\mathbf{x}(1)^H \dot{\mathbf{a}}^*(\theta_D) \\
&= T\sigma_x^2 \dot{\mathbf{a}}^T(\theta_D)\dot{\mathbf{a}}^*(\theta_D) \\
&= T\sigma_x^2 \left(\frac{2\pi}{\lambda}\right)^2 \cos^2(\theta_D) \sum_{k=1}^{M} a_k^2. \qquad (2.64)
\end{aligned}
$$

- By using the Schur complement, one obtains

$$
\begin{aligned}
\mathbf{R}^{-1}(\mathbf{\Theta}) &= \frac{1}{\sigma_n^2}\left(\mathbf{I}_T - \frac{|\beta|^2\sigma_e^2}{\sigma_n^2 + |\beta|^2 TM\sigma_x^2\sigma_e^2}\mathbf{s}(\theta_D)\mathbf{s}^H(\theta_D)\right) \otimes \mathbf{I}_N \\
&= \frac{1}{\sigma_n^2}\left(\mathbf{I}_T - c\mathbf{s}(\theta_D)\mathbf{s}^H(\theta_D)\right) \otimes \mathbf{I}_N, \qquad (2.65)
\end{aligned}
$$

  where $c = \frac{|\beta|^2\sigma_e^2}{\sigma_n^2+|\beta|^2TM\sigma_x^2\sigma_e^2}$.

The elements of the FIM can be given by

- $[\mathbf{F}(\mathbf{\Theta})]_{1,1}$ is given by

$$
\begin{aligned}
[\mathbf{F}(\mathbf{\Theta})]_{1,1} =& Tr\left\{\mathbf{R}^{-1}(\mathbf{\Theta})\frac{\partial\mathbf{R}(\mathbf{\Theta})}{\partial\theta_D}\mathbf{R}^{-1}(\mathbf{\Theta})\frac{\partial\mathbf{R}(\mathbf{\Theta})}{\partial\theta_D}\right\} + 2\mathcal{R}\left\{\frac{\partial\mathbf{m}^H(\mathbf{\Theta})}{\partial\theta_D}\mathbf{R}^{-1}(\mathbf{\Theta})\frac{\partial\mathbf{m}(\mathbf{\Theta})}{\partial\theta_D}\right\} \\
=& \frac{8\pi^2|\beta|^2TN\sigma_x^2}{\lambda^2\sigma_n^2}\cos^2(\theta_D)\sum_{k=1}^{M}a_k^2 \times \left(1 + \frac{|\beta|^2TM\sigma_x^2\sigma_e^4}{\sigma_n^2 + |\beta|^2TM\sigma_x^2\sigma_e^2}\right), \qquad (2.66)
\end{aligned}
$$

since

$$
\begin{aligned}
&Tr\left\{\mathbf{R}^{-1}(\mathbf{\Theta})\frac{\partial\mathbf{R}(\mathbf{\Theta})}{\partial\theta_D}\mathbf{R}^{-1}(\mathbf{\Theta})\frac{\partial\mathbf{R}(\mathbf{\Theta})}{\partial\theta_D}\right\} \\
=& Tr\left\{\frac{|\beta|^4\sigma_e^4}{\sigma_n^4}\left((\dot{\mathbf{s}}(\theta_D)\mathbf{s}^H(\theta_D) + \mathbf{s}(\theta_D)\dot{\mathbf{s}}^H(\theta_D)) \otimes \mathbf{I}_N\right)\left((\mathbf{I}_T - c\mathbf{s}(\theta_D)\mathbf{s}^H(\theta_D)) \otimes \mathbf{I}_N\right)\right. \\
&\left.\times\left((\dot{\mathbf{s}}(\theta_D)\mathbf{s}^H(\theta_D) + \mathbf{s}(\theta_D)\dot{\mathbf{s}}^H(\theta_D)) \otimes \mathbf{I}_N\right)\left((\mathbf{I}_T - c\mathbf{s}(\theta_D)\mathbf{s}^H(\theta_D)) \otimes \mathbf{I}_N\right)\right\} \\
=& \frac{N|\beta|^4\sigma_e^4}{\sigma_n^4}Tr\left\{\left(\dot{\mathbf{s}}(\theta_D)\mathbf{s}^H(\theta_D) + \mathbf{s}(\theta_D)\dot{\mathbf{s}}^H(\theta_D)\right)\left(\mathbf{I}_T - c\mathbf{s}(\theta_D)\mathbf{s}^H(\theta_D)\right)\right. \\
&\left.\times\left(\dot{\mathbf{s}}(\theta_D)\mathbf{s}^H(\theta_D) + \mathbf{s}(\theta_D)\dot{\mathbf{s}}^H(\theta_D)\right)\left(\mathbf{I}_T - c\mathbf{s}(\theta_D)\mathbf{s}^H(\theta_D)\right)\right\} \\
=& \frac{N|\beta|^4\sigma_e^4}{\sigma_n^4}Tr\left\{\left(\dot{\mathbf{s}}(\theta_D)\mathbf{s}^H(\theta_D) + \mathbf{s}(\theta_D)\dot{\mathbf{s}}^H(\theta_D) - c\dot{\mathbf{s}}(\theta_D)\mathbf{s}^H(\theta_D)\mathbf{s}(\theta_D)\mathbf{s}^H(\theta_D)\right.\right. \\
&\left.\left. - c\mathbf{s}(\theta_D)\dot{\mathbf{s}}^H(\theta_D)\mathbf{s}(\theta_D)\mathbf{s}^H(\theta_D)\right)^2\right\} \\
=& \frac{N|\beta|^4\sigma_e^4}{\sigma_n^4}Tr\left\{\left((1 - cTM\sigma_x^2)\dot{\mathbf{s}}(\theta_D)\mathbf{s}^H(\theta_D) + \mathbf{s}(\theta_D)\dot{\mathbf{s}}^H(\theta_D)\right)^2\right\}
\end{aligned}
$$

$$
\begin{aligned}
=&\frac{N|\beta|^4\sigma_e^4}{\sigma_n^4}2(1-cTM\sigma_x^2)TM\sigma_x^2\dot{\mathbf{s}}^H(\theta_D)\dot{\mathbf{s}}(\theta_D)\\
=&\frac{8\pi^2T^2MN\sigma_x^4|\beta|^4\sigma_e^4\cos^2(\theta_D)\sum_{k=1}^M a_k^2}{\lambda^2\sigma_n^2(\sigma_n^2+|\beta|^2\sigma_e^2TM\sigma_x^2)},
\end{aligned}
\tag{2.67}
$$

and

$$
\begin{aligned}
&\mathcal{R}\left\{\frac{\partial\mathbf{m}^H(\mathbf{\Theta})}{\partial\theta_D}\mathbf{R}^{-1}(\mathbf{\Theta})\frac{\partial\mathbf{m}(\mathbf{\Theta})}{\partial\theta_D}\right\}\\
=&\mathcal{R}\left\{Tr\Big\{\mathbf{R}^{-1}(\mathbf{\Theta})\frac{\partial\mathbf{m}^H(\mathbf{\Theta})}{\partial\theta_D}\frac{\partial\mathbf{m}(\mathbf{\Theta})}{\partial\theta_D}\Big\}\right\}\\
=&\frac{1}{\sigma_n^2}\mathcal{R}\left\{Tr\Big\{\Big((\mathbf{I}_T-c\mathbf{s}(\theta_D)\mathbf{s}^H(\theta_D))\otimes\mathbf{I}_N\Big)\Big(\dot{\mathbf{s}}(\theta_D)\dot{\mathbf{s}}^H(\theta_D)\Big)\otimes\Big(\mathbf{b}(\theta_D)\mathbf{b}(\theta_D)^H\Big)\Big\}\right\}\\
=&\frac{|\beta|^2}{\sigma_n^2}\mathcal{R}\left\{Tr\Big\{\Big((\mathbf{I}_T-c\mathbf{s}(\theta_D)\mathbf{s}^H(\theta_D))\Big)\dot{\mathbf{s}}(\theta_D)\dot{\mathbf{s}}^H(\theta_D)\Big\}Tr\Big\{\Big(\mathbf{b}(\theta_D)\mathbf{b}(\theta_D)^H\Big)\Big\}\right\}\\
=&\frac{N|\beta|^2}{\sigma_n^2}\mathcal{R}\left\{Tr\Big\{\dot{\mathbf{s}}(\theta_D)\dot{\mathbf{s}}^H(\theta_D)\Big\}\right\}\\
=&\frac{4\pi^2NT|\beta|^2\sigma_x^2\cos^2(\theta_D)\sum_{k=1}^M a_k^2}{\lambda^2\sigma_n^2}.
\end{aligned}
\tag{2.68}
$$

- $[\mathbf{F}(\mathbf{\Theta})]_{2,2}$ is given by

$$
\begin{aligned}
[\mathbf{F}(\mathbf{\Theta})]_{2,2}&=Tr\left\{\mathbf{R}^{-1}(\mathbf{\Theta})\frac{\partial\mathbf{R}(\mathbf{\Theta})}{\partial\theta_A}\mathbf{R}^{-1}(\mathbf{\Theta})\frac{\partial\mathbf{R}(\mathbf{\Theta})}{\partial\theta_A}\right\}+2\mathcal{R}\left\{\frac{\partial\mathbf{m}^H(\mathbf{\Theta})}{\partial\theta_A}\mathbf{R}^{-1}(\mathbf{\Theta})\frac{\partial\mathbf{m}(\mathbf{\Theta})}{\partial\theta_A}\right\}\\
&=2\mathcal{R}\left\{\frac{\partial\mathbf{m}^H(\mathbf{\Theta})}{\partial\theta_A}\mathbf{R}^{-1}(\mathbf{\Theta})\frac{\partial\mathbf{m}(\mathbf{\Theta})}{\partial\theta_A}\right\}\\
&=\frac{2}{\sigma_n^2}\mathcal{R}\left\{Tr\Big\{\Big((\mathbf{I}_T-c\mathbf{s}(\theta_D)\mathbf{s}^H(\theta_D))\otimes\mathbf{I}_N\Big)\Big(\mathbf{s}(\theta_D)\mathbf{s}^H(\theta_D)\Big)\otimes\Big(\dot{\mathbf{b}}(\theta_D)\dot{\mathbf{b}}^H(\theta_D)\Big)\Big\}\right\}\\
&=\frac{2|\beta|^2}{\sigma_n^2}\mathcal{R}\left\{Tr\Big\{\Big(\mathbf{I}_T-c\mathbf{s}(\theta_D)\mathbf{s}^H(\theta_D)\Big)\mathbf{s}(\theta_D)\mathbf{s}^H(\theta_D)\Big\}Tr\Big\{\Big(\dot{\mathbf{b}}(\theta_D)\dot{\mathbf{b}}(\theta_D)^H\Big)\Big\}\right\}\\
&=\frac{8\pi^2|\beta|^2TM\sigma_x^2\cos^2(\theta_A)\sum_{k=1}^N b_k^2}{\lambda^2(\sigma_n^2+|\beta|^2TM\sigma_x^2\sigma_e^2)}.
\end{aligned}
\tag{2.69}
$$

- $[\mathbf{F}(\mathbf{\Theta})]_{3,3}$ is given by

$$
\begin{aligned}
[\mathbf{F}(\mathbf{\Theta})]_{3,3}&=Tr\left\{\mathbf{R}^{-1}(\mathbf{\Theta})\frac{\partial\mathbf{R}(\mathbf{\Theta})}{\partial\beta_R}\mathbf{R}^{-1}(\mathbf{\Theta})\frac{\partial\mathbf{R}(\mathbf{\Theta})}{\partial\beta_R}\right\}+2\mathcal{R}\left\{\frac{\partial\mathbf{m}^H(\mathbf{\Theta})}{\partial\beta_R}\mathbf{R}^{-1}(\mathbf{\Theta})\frac{\partial\mathbf{m}(\mathbf{\Theta})}{\partial\beta_R}\right\}\\
&=N\Big(\frac{2\beta_RTM\sigma_x^2\sigma_e^2}{\sigma_n^2+|\beta|^2TM\sigma_x^2\sigma_e^2}\Big)^2+\frac{2TMN\sigma_x^2}{\sigma_n^2+|\beta|^2TM\sigma_x^2\sigma_e^2},
\end{aligned}
\tag{2.70}
$$

since

$$
\begin{aligned}
Tr\left\{\mathbf{R}^{-1}(\mathbf{\Theta})\frac{\partial\mathbf{R}(\mathbf{\Theta})}{\partial\beta_R}\mathbf{R}^{-1}(\mathbf{\Theta})\frac{\partial\mathbf{R}(\mathbf{\Theta})}{\partial\beta_R}\right\} =& \frac{4\beta_R^2\sigma_e^4}{\sigma_n^4}Tr\Bigg\{\Big(\mathbf{I}_T - c\mathbf{s}(\theta_D)\mathbf{s}^H(\theta_D)\Big)\Big(\mathbf{s}(\theta_D)\mathbf{s}^H(\theta_D)\Big)\\
&\times\Big(\mathbf{I}_T - c\mathbf{s}(\theta_D)\mathbf{s}^H(\theta_D)\Big)\Big(\mathbf{s}(\theta_D)\mathbf{s}^H(\theta_D)\Big)\Bigg\}Tr\Big\{\mathbf{I}_N\Big\}\\
=& \frac{4N\beta_R^2\sigma_e^4}{\sigma_n^4}\Big(\mathbf{s}^H(\theta_D)\Big(\mathbf{I}_T - c\mathbf{s}(\theta_D)\mathbf{s}^H(\theta_D)\Big)\mathbf{s}(\theta_D)\Big)^2\\
=& N\Big(\frac{2\beta_R TM\sigma_x^2\sigma_e^2}{\sigma_n^2+|\beta|^2TM\sigma_x^2\sigma_e^2}\Big)^2, \qquad (2.71)
\end{aligned}
$$

and

$$
\begin{aligned}
&\mathcal{R}\left\{\frac{\partial\mathbf{m}^H(\mathbf{\Theta})}{\partial\beta_R}\mathbf{R}^{-1}(\mathbf{\Theta})\frac{\partial\mathbf{m}(\mathbf{\Theta})}{\partial\beta_R}\right\}\\
=&\mathcal{R}\left\{Tr\Big\{\mathbf{R}^{-1}(\mathbf{\Theta})\frac{\partial\mathbf{m}^H(\mathbf{\Theta})}{\partial\beta_R}\frac{\partial\mathbf{m}(\mathbf{\Theta})}{\partial\beta_R}\Big\}\right\}\\
=&\frac{1}{\sigma_n^2}\mathcal{R}\left\{Tr\Big\{\Big((\mathbf{I}_T - c\mathbf{s}(\theta_D)\mathbf{s}^H(\theta_D))\otimes\mathbf{I}_N\Big)\Big(\mathbf{s}(\theta_D)\mathbf{s}^H(\theta_D)\Big)\otimes\Big(\mathbf{b}(\theta_D)\mathbf{b}(\theta_D)^H\Big)\Big\}\right\}\\
=&\frac{1}{\sigma_n^2}\mathcal{R}\left\{Tr\Big\{\Big((\mathbf{I}_T - c\mathbf{s}(\theta_D)\mathbf{s}^H(\theta_D))\Big)\mathbf{s}(\theta_D)\mathbf{s}^H(\theta_D)\Big\}Tr\Big\{\Big(\mathbf{b}(\theta_D)\mathbf{b}(\theta_D)^H\Big)\Big\}\right\}\\
=&\frac{TMN\sigma_x^2}{\sigma_n^2+|\beta|^2TM\sigma_x^2\sigma_e^2}. \qquad (2.72)
\end{aligned}
$$

- Similarly, $[\mathbf{F}(\mathbf{\Theta})]_{4,4}$ is given by

$$
\begin{aligned}
[\mathbf{F}(\mathbf{\Theta})]_{4,4} &= Tr\left\{\mathbf{R}^{-1}(\mathbf{\Theta})\frac{\partial\mathbf{R}(\mathbf{\Theta})}{\partial\beta_I}\mathbf{R}^{-1}(\mathbf{\Theta})\frac{\partial\mathbf{R}(\mathbf{\Theta})}{\partial\beta_I}\right\} + 2\mathcal{R}\left\{\frac{\partial\mathbf{m}^H(\mathbf{\Theta})}{\partial\beta_I}\mathbf{R}^{-1}(\mathbf{\Theta})\frac{\partial\mathbf{m}(\mathbf{\Theta})}{\partial\beta_I}\right\}\\
&= N\Big(\frac{2\beta_I TM\sigma_x^2\sigma_e^2}{\sigma_n^2+|\beta|^2TM\sigma_x^2\sigma_e^2}\Big)^2 + \frac{2TMN\sigma_x^2}{\sigma_n^2+|\beta|^2TM\sigma_x^2\sigma_e^2}, \qquad (2.73)
\end{aligned}
$$

- $[\mathbf{F}(\mathbf{\Theta})]_{1,2}$ is given by

$$
\begin{aligned}
[\mathbf{F}(\mathbf{\Theta})]_{1,2} &= Tr\left\{\mathbf{R}^{-1}(\mathbf{\Theta})\frac{\partial\mathbf{R}(\mathbf{\Theta})}{\partial\theta_A}\mathbf{R}^{-1}(\mathbf{\Theta})\frac{\partial\mathbf{R}(\mathbf{\Theta})}{\partial\theta_D}\right\} + 2\mathcal{R}\left\{\frac{\partial\mathbf{m}^H(\mathbf{\Theta})}{\partial\theta_A}\mathbf{R}^{-1}(\mathbf{\Theta})\frac{\partial\mathbf{m}(\mathbf{\Theta})}{\partial\theta_D}\right\}\\
&= \frac{1}{\sigma_n^2}\mathcal{R}\left\{Tr\Big\{\Big((\mathbf{I}_T - c\mathbf{s}(\theta_D)\mathbf{s}^H(\theta_D))\otimes\mathbf{I}_N\Big)\Big(\dot{\mathbf{s}}(\theta_D)\mathbf{s}^H(\theta_D)\Big)\otimes\Big(\mathbf{b}(\theta_D)\dot{\mathbf{b}}(\theta_D)^H\Big)\Big\}\right\}\\
&= \frac{1}{\sigma_n^2}\mathcal{R}\left\{Tr\Big\{\Big((\mathbf{I}_T - c\mathbf{s}(\theta_D)\mathbf{s}^H(\theta_D))\Big)\dot{\mathbf{s}}(\theta_D)\mathbf{s}^H(\theta_D)\Big\}Tr\Big\{\Big(\mathbf{b}(\theta_D)\dot{\mathbf{b}}(\theta_D)^H\Big)\Big\}\right\}\\
&= 0 \qquad (2.74)
\end{aligned}
$$

- $[\mathbf{F}(\mathbf{\Theta})]_{2,1}$ is given by

$$\begin{aligned}[\mathbf{F}(\mathbf{\Theta})]_{2,1} &= Tr\left\{\mathbf{R}^{-1}(\mathbf{\Theta})\frac{\partial \mathbf{R}(\mathbf{\Theta})}{\partial \theta_D}\mathbf{R}^{-1}(\mathbf{\Theta})\frac{\partial \mathbf{R}(\mathbf{\Theta})}{\partial \theta_A}\right\} + 2\mathcal{R}\left\{\frac{\partial \mathbf{m}^H(\mathbf{\Theta})}{\partial \theta_D}\mathbf{R}^{-1}(\mathbf{\Theta})\frac{\partial \mathbf{m}(\mathbf{\Theta})}{\partial \theta_A}\right\} \\ &= \frac{1}{\sigma_n^2}\mathcal{R}\left\{Tr\left\{\left((\mathbf{I}_T - c\mathbf{s}(\theta_D)\mathbf{s}^H(\theta_D))\otimes \mathbf{I}_N\right)\left(\mathbf{s}(\theta_D)\dot{\mathbf{s}}^H(\theta_D)\right)\otimes\left(\dot{\mathbf{b}}(\theta_D)\mathbf{b}(\theta_D)^H\right)\right\}\right\} \\ &= \frac{1}{\sigma_n^2}\mathcal{R}\left\{Tr\left\{\left((\mathbf{I}_T - c\mathbf{s}(\theta_D)\mathbf{s}^H(\theta_D))\right)\mathbf{s}(\theta_D)\dot{\mathbf{s}}^H(\theta_D)\right\}Tr\left\{\left(\mathbf{b}(\theta_D)\dot{\mathbf{b}}(\theta_D)^H\right)\right\}\right\} \\ &= 0 \end{aligned} \tag{2.75}$$

- Similarly, we have $[\mathbf{F}(\mathbf{\Theta})]_{1,3} = [\mathbf{F}(\mathbf{\Theta})]_{3,1} = [\mathbf{F}(\mathbf{\Theta})]_{2,3} = [\mathbf{F}(\mathbf{\Theta})]_{3,2} = [\mathbf{F}(\mathbf{\Theta})]_{2,4} = [\mathbf{F}(\mathbf{\Theta})]_{4,2} = 0$.

- $[\mathbf{F}(\mathbf{\Theta})]_{3,4}$ is given by

$$\begin{aligned}[\mathbf{F}(\mathbf{\Theta})]_{3,4} &= Tr\left\{\mathbf{R}^{-1}(\mathbf{\Theta})\frac{\partial \mathbf{R}(\mathbf{\Theta})}{\partial \beta_R}\mathbf{R}^{-1}(\mathbf{\Theta})\frac{\partial \mathbf{R}(\mathbf{\Theta})}{\partial \beta_I}\right\} + 2\mathcal{R}\left\{\frac{\partial \mathbf{m}^H(\mathbf{\Theta})}{\partial \beta_R}\mathbf{R}^{-1}(\mathbf{\Theta})\frac{\partial \mathbf{m}(\mathbf{\Theta})}{\partial \beta_I}\right\} \\ &= N\Big(\frac{TM\sigma_x^2\sigma_e^2}{\sigma_n^2 + |\beta|^2TM\sigma_x^2\sigma_e^2}\Big)^2 + \frac{2TMN\sigma_x^2}{\sigma_n^2 + |\beta|^2TM\sigma_x^2\sigma_e^2}, \end{aligned} \tag{2.76}$$

since

$$\begin{aligned} Tr\left\{\mathbf{R}^{-1}(\mathbf{\Theta})\frac{\partial \mathbf{R}(\mathbf{\Theta})}{\partial \beta_R}\mathbf{R}^{-1}(\mathbf{\Theta})\frac{\partial \mathbf{R}(\mathbf{\Theta})}{\partial \beta_I}\right\} =& \frac{4\beta_R\beta_I\sigma_e^4}{\sigma_n^4}Tr\left\{\left(\mathbf{I}_T - c\mathbf{s}(\theta_D)\mathbf{s}^H(\theta_D)\right)\left(\mathbf{s}(\theta_D)\mathbf{s}^H(\theta_D)\right)\right. \\ &\left.\times\left(\mathbf{I}_T - c\mathbf{s}(\theta_D)\mathbf{s}^H(\theta_D)\right)\left(\mathbf{s}(\theta_D)\mathbf{s}^H(\theta_D)\right)\right\}Tr\left\{\mathbf{I}_N\right\} \\ =& \frac{4N\beta_R^2\sigma_e^4}{\sigma_n^4}\left(\mathbf{s}^H(\theta_D)\left(\mathbf{I}_T - c\mathbf{s}(\theta_D)\mathbf{s}^H(\theta_D)\right)\mathbf{s}(\theta_D)\right)^2 \\ =& N\beta_R\beta_I\Big(\frac{2TM\sigma_x^2\sigma_e^2}{\sigma_n^2 + |\beta|^2TM\sigma_x^2\sigma_e^2}\Big)^2, \end{aligned} \tag{2.77}$$

and

$$\begin{aligned} &\mathcal{R}\left\{\frac{\partial \mathbf{m}^H(\mathbf{\Theta})}{\partial \beta_R}\mathbf{R}^{-1}(\mathbf{\Theta})\frac{\partial \mathbf{m}(\mathbf{\Theta})}{\partial \beta_R}\right\} \\ =&\mathcal{R}\left\{Tr\left\{\mathbf{R}^{-1}(\mathbf{\Theta})\frac{\partial \mathbf{m}^H(\mathbf{\Theta})}{\partial \beta_R}\frac{\partial \mathbf{m}(\mathbf{\Theta})}{\partial \beta_R}\right\}\right\} \\ =&\frac{1}{\sigma_n^2}\mathcal{R}\left\{Tr\left\{\left((\mathbf{I}_T - c\mathbf{s}(\theta_D)\mathbf{s}^H(\theta_D))\otimes \mathbf{I}_N\right)j\left(\mathbf{s}(\theta_D)\mathbf{s}^H(\theta_D)\right)\otimes\left(\mathbf{b}(\theta_D)\mathbf{b}(\theta_D)^H\right)\right\}\right\} \\ =&\frac{1}{\sigma_n^2}\mathcal{R}\left\{jTr\left\{\left((\mathbf{I}_T - c\mathbf{s}(\theta_D)\mathbf{s}^H(\theta_D))\right)\mathbf{s}(\theta_D)\mathbf{s}^H(\theta_D)\right\}Tr\left\{\left(\mathbf{b}(\theta_D)\mathbf{b}(\theta_D)^H\right)\right\}\right\} \end{aligned}$$

$$=0. \tag{2.78}$$

- Similarly, we have $[\mathbf{F}(\mathbf{\Theta})]_{4,3} = [\mathbf{F}(\mathbf{\Theta})]_{3,4}$.

2.6.4 Derivation of (2.35)

From (2.35), the element (k,l) of the matrix $\mathbf{M}_{MS}$ is given by

$$\begin{aligned}
\mathbf{M}_{MS}(k,l) &= E_{\mathbf{x};\phi_0}\left[\frac{p(\mathbf{x};\theta_k)}{p(\mathbf{x};\phi_0)}\frac{p(\mathbf{x};\theta_l)}{p(\mathbf{x};\phi_0)}\right] \\
&= \sum_{\mathbf{x}=0}^{\infty}\frac{p(\mathbf{x};\theta_k)p(\mathbf{x};\theta_l)}{p(\mathbf{x};\phi_0)} \\
&= \prod_{n=0}^{N-1}\exp\left(\Delta t[\lambda_n(\phi_0)-\lambda_n(\theta_k)-\lambda_n(\theta_l)]\right)\sum_{\mathbf{x}=0}^{\infty}\prod_{n=0}^{N-1}\left[\frac{\lambda_n(\theta_k)\lambda_n(\theta_l)\Delta t}{\lambda_n(\phi_0)}\right]^{x_n}\frac{1}{x_n!} \\
&= \exp\left\{\Delta t\sum_{n=0}^{N-1}\lambda_n(\phi_0)-\lambda_n(\theta_k)-\lambda_n(\theta_l)+\frac{\lambda_n(\theta_k)\lambda_n(\theta_l)}{\lambda_n(\phi_0)}\right\},
\end{aligned} \tag{2.79}$$

since

$$\sum_{\mathbf{x}=0}^{\infty}\prod_{n=0}^{N-1}\left[\frac{\lambda_n(\theta_k)\lambda_n(\theta_l)\Delta t}{\lambda_n(\phi_0)}\right]^{x_n}\frac{1}{x_n!} = \prod_{n=0}^{N-1}\exp(\frac{\lambda_n(\theta_k)\lambda_n(\theta_l)}{\lambda_n(\phi_0)}\Delta t).$$

By taking the limit $\Delta t \to 0$, or equivalently $N \to \infty$, and by noting that $\lambda_n(.) = \lambda(t_n;.)$, we can convert the above summation to an integral :

$$\begin{aligned}
\mathbf{M}_{MS}(k,l) &= \exp\left\{\int_{t_0}^{t_0+T_{obs}}\left[\lambda(t,\phi_0)-\lambda(t,\theta_k)-\lambda(t,\theta_l)+\frac{\lambda(t,\theta_k)\lambda(t,\theta_l)}{\lambda(t,\phi_0)}\right]dt\right\} \\
&= \exp\left\{\int_{\phi_0}^{\phi_0+fT_{obs}}\frac{1}{f}\left[\lambda(\phi)-\lambda(\phi+\xi_k)-\lambda(\phi+\xi_l)+\frac{\lambda(\phi+\xi_k)\lambda(\phi+\xi_l)}{\lambda(\phi)}\right]d\phi\right\},
\end{aligned} \tag{2.80}$$

where $\lambda(\phi+\alpha) = \lambda_b + \lambda_s h(\phi+\alpha)$. Note that we have used in the above derivation the change of variable formula $\phi = \phi_0 + (t-t_0)f$. As the pulse profile function $h(\phi(t))$ is periodic with its period equal to one cycle, hence, when the observation time is an integer number of the pulsar period, i.e., $fT_{obs} \approx N_p$ (cycle), $\mathbf{M}_{MS}(k,l)$ can be rewritten as

$$\begin{aligned}
\mathbf{M}_{MS}(k,l) &= \exp\left\{\int_{0}^{fT_{obs}}\frac{1}{f}\left[\lambda(\phi)-\lambda(\phi+\xi_k)-\lambda(\phi+\xi_l)+\frac{\lambda(\phi+\xi_k)\lambda(\phi+\xi_l)}{\lambda(\phi)}\right]d\phi\right\} \\
&= \exp\left\{\sum_{n=1}^{N_p}\int_{n-1}^{n}\frac{1}{f}\left[\lambda(\phi)-\lambda(\xi_k+\phi)-\lambda(\xi_l+\phi)+\frac{\lambda(\xi_k+\phi)\lambda(\xi_l+\phi)}{\lambda(\phi)}\right]d\phi\right\}
\end{aligned}$$

$$= \exp\left\{ \frac{N_p}{f} \int_0^1 \left[\lambda(\phi) - \lambda(\xi_k + \phi) - \lambda(\xi_l + \phi) + \frac{\lambda(\xi_k + \phi)\lambda(\xi_l + \phi)}{\lambda(\phi)} \right] d\phi \right\}$$
$$= \exp\left\{ T_{obs} \int_0^1 \left[\lambda(\phi) - \lambda(\xi_k + \phi) - \lambda(\xi_l + \phi) + \frac{\lambda(\xi_k + \phi)\lambda(\xi_l + \phi)}{\lambda(\phi)} \right] d\phi \right\}. \tag{2.81}$$

2.6.5 Derivation of (2.36)

From (2.36), the element (k,l) of the matrix $\mathbf{M}_{EFI}$ is given by

$$\begin{aligned}
\mathbf{M}_{EFI}(k,l) &= E_{\mathbf{x};\phi_0}\left[\frac{\partial \ln p(\mathbf{x};\theta_k)}{\partial \theta_k} \frac{p(\mathbf{x};\theta_k)}{p(\mathbf{x};\phi_0)} \frac{\partial \ln p(\mathbf{x};\theta_l)}{\partial \theta_l} \frac{p(\mathbf{x};\theta_l)}{p(\mathbf{x};\phi_0)} \right] \\
&= \sum_{\mathbf{x}=0}^{\infty} \left[\sum_{p=0}^{N-1} x_p \frac{\partial \ln[\lambda_p(\theta_k)\Delta t]}{\partial \theta_k} - \frac{\partial \lambda_p(\theta_k)\Delta t}{\partial \theta_k} \right] \left[\sum_{q=0}^{N-1} x_q \frac{\partial \ln[\lambda_q(\theta_l)\Delta t]}{\partial \theta_l} - \frac{\partial \lambda_q(\theta_l)\Delta t}{\partial \theta_l} \right] \\
&\qquad \prod_{n=0}^{N-1} \left[\frac{\lambda_n(\theta_k)\lambda_n(\theta_l)\Delta t}{\lambda_n(\phi_0)} \right]^{x_n} \frac{1}{x_n!} \exp\left(\Delta t[\lambda_n(\phi_0) - \lambda_n(\theta_k) - \lambda_n(\theta_l)]\right) \\
&= C_1 + C_2 + C_3 + C_4,
\end{aligned} \tag{2.82}$$

whose components C_i, $i = 1, 2, 3, 4$, are calculated as follows

$$\begin{aligned}
C_1 =& \sum_{\mathbf{x}=0}^{\infty} \sum_{p=0}^{N-1} \sum_{q=0}^{N-1} x_p x_q \frac{\partial \ln[\lambda_p(\theta_k)\Delta t]}{\partial \theta_k} \frac{\partial \ln[\lambda_q(\theta_l)\Delta t]}{\partial \theta_l} \\
& \prod_{n=0}^{N-1} \left[\frac{\lambda_n(\theta_k)\lambda_n(\theta_l)\Delta t}{\lambda_n(\phi_0)} \right]^{x_n} \frac{1}{x_n!} \exp\left(\Delta t[\lambda_n(\phi_0) - \lambda_n(\theta_k) - \lambda_n(\theta_l)]\right) \\
=& \sum_{p=0}^{N-1} \sum_{q=0}^{N-1} \frac{\partial \ln[\lambda_p(\theta_k)\Delta t]}{\partial \theta_k} \frac{\partial \ln[\lambda_q(\theta_k)\Delta t]}{\partial \theta_k} \sum_{\mathbf{x}=0}^{\infty} x_p x_q \\
& \prod_{n=0}^{N-1} \left[\frac{\lambda_n(\theta_k)\lambda_n(\theta_l)\Delta t}{\lambda_n(\phi_0)} \right]^{x_n} \frac{1}{x_n!} \exp\left(\Delta t[\lambda_n(\phi_0) - \lambda_n(\theta_k) - \lambda_n(\theta_l)]\right).
\end{aligned} \tag{2.83}$$

Let us define

$$\begin{aligned}
A &= \sum_{\mathbf{x}=0}^{\infty} x_p x_q \prod_{n=0}^{N-1} \left[\frac{\lambda_n(\theta_k)\lambda_n(\theta_l)\Delta t}{\lambda_n(\phi_0)} \right]^{x_n} \frac{1}{x_n!} \exp\left(\Delta t[\lambda_n(\phi_0) - \lambda_n(\theta_k) - \lambda_n(\theta_l)]\right) \\
&= A(p = q) + A(p \neq q),
\end{aligned} \tag{2.84}$$

where

$$A(p = q) = \sum_{\mathbf{x}=0}^{\infty} x_p^2 \prod_{n=0}^{N-1} \left[\frac{\lambda_n(\theta_k)\lambda_n(\theta_l)\Delta t}{\lambda_n(\phi_0)} \right]^{x_n} \frac{1}{x_n!} \exp\left(\Delta t[\lambda_n(\phi_0) - \lambda_n(\theta_k) - \lambda_n(\theta_l)]\right)$$

$$
\begin{aligned}
&= \sum_{\mathbf{x}=0}^{\infty} x_p(x_p-1) \prod_{n=0}^{N-1} \left[\frac{\lambda_n(\theta_k)\lambda_n(\theta_l)\Delta t}{\lambda_n(\phi_0)}\right]^{x_n} \frac{1}{x_n!} \exp\left(\Delta t[\lambda_n(\phi_0)-\lambda_n(\theta_k)-\lambda_n(\theta_l)]\right) \\
&\quad + \sum_{\mathbf{x}=0}^{\infty} x_p \prod_{m=0}^{N-1} \left[\frac{\lambda_m(\theta_k)\lambda_m(\theta_l)\Delta t}{\lambda_m(\phi_0)}\right]^{x_m} \frac{1}{x_m!} \exp\left(\Delta t[\lambda_m(\phi_0)-\lambda_m(\theta_k)-\lambda_m(\theta_l)]\right) \\
&= \sum_{\mathbf{x}'=0}^{\infty} \left[\frac{\lambda_p(\theta_k)\lambda_p(\theta_l)\Delta t}{\lambda_p(\phi_0)}\right]^2 \prod_{n=0}^{N-1} \left[\frac{\lambda_n(\theta_k)\lambda_n(\theta_l)\Delta t}{\lambda_n(\phi_0)}\right]^{x'_n} \frac{1}{x'_n!} \exp\left(\Delta t[\lambda_n(\phi_0)-\lambda_n(\theta_k)-\lambda_n(\theta_l)]\right) \\
&\quad + \sum_{\mathbf{x}''=0}^{\infty} \left[\frac{\lambda_p(\theta_k)\lambda_p(\theta_l)\Delta t}{\lambda_p(\phi_0)}\right] \prod_{m=0}^{N-1} \left[\frac{\lambda_m(\theta_k)\lambda_m(\theta_l)\Delta t}{\lambda_m(\phi_0)}\right]^{x''_m} \frac{1}{x''_m!} \exp\left(\Delta t[\lambda_m(\phi_0)-\lambda_m(\theta_k)-\lambda_m(\theta_l)]\right) \\
&= \left[\frac{\lambda_p(\theta_k)\lambda_p(\theta_l)\Delta t}{\lambda_p(\phi_0)}\right]^2 \mathbf{M}_{MS}(k,l) + \frac{\lambda_p(\theta_k)\lambda_p(\theta_l)\Delta t}{\lambda_p(\phi_0)} \mathbf{M}_{MS}(k,l), \qquad (2.85)
\end{aligned}
$$

where $\mathbf{x}' = [x_1, \ldots, x_{p-1}, x_p - 2, x_{p+1}, \ldots, x_{N-1}]$, and $\mathbf{x}'' = [x_1, \ldots, x_{p-1}, x_p - 1, x_{p+1}, \ldots, x_{N-1}]$, and where

$$
\begin{aligned}
A(p \neq q) &= \sum_{\mathbf{x}=0}^{\infty} x_p x_q \prod_{n=0}^{N-1} \left[\frac{\lambda_n(\theta_k)\lambda_n(\theta_l)\Delta t}{\lambda_n(\phi_0)}\right]^{x_n} \frac{1}{x_n!} \exp\left(\Delta t[\lambda_n(\phi_0)-\lambda_n(\theta_k)-\lambda_n(\theta_l)]\right) \\
&= \frac{\lambda_p(\theta_k)\lambda_p(\theta_l)\Delta t}{\lambda_p(\phi_0)} \frac{\lambda_q(\theta_k)\lambda_q(\theta_l)\Delta t}{\lambda_q(\phi_0)} \sum_{\mathbf{x}=0}^{\infty} \prod_{n=0}^{N-1} \left[\frac{\lambda_n(\theta_k)\lambda_n(\theta_l)\Delta t}{\lambda_n(\phi_0)}\right]^{x'''_n} \frac{1}{x'''_n!} \exp\left(\Delta t[\lambda_n(\phi_0)-\lambda_n(\theta_k)-\lambda_n(\theta_l)]\right. \\
&= \frac{\lambda_p(\theta_k)\lambda_p(\theta_l)\Delta t}{\lambda_p(\phi_0)} \frac{\lambda_q(\theta_k)\lambda_q(\theta_l)\Delta t}{\lambda_q(\phi_0)} \mathbf{M}_{MS}(k,l), \qquad (2.86)
\end{aligned}
$$

where $\mathbf{x}''' = [x_1, \ldots, x_p - 1, \ldots, x_q - 1, \ldots, x_{N-1}]$. Note that in the above derivation, we assumed , without loss of generality, that $p < q$. Consequently, we get

$$
\begin{aligned}
C_1 = \mathbf{M}_{MS}(k,l) \Bigg\{ &\sum_{p=0}^{N-1} \sum_{q=0}^{N-1} \frac{\partial \ln[\lambda_p(\theta_k)\Delta t]}{\partial \theta_k} \frac{\partial \ln[\lambda_q(\theta_l)\Delta t]}{\partial \theta_l} \frac{\lambda_p(\theta_k)\lambda_p(\theta_l)\Delta t}{\lambda_p(\phi_0)} \frac{\lambda_q(\theta_k)\lambda_q(\theta_l)\Delta t}{\lambda_q(\phi_0)} \\
&+ \sum_{p=0}^{N-1} \frac{\partial \ln[\lambda_p(\theta_k)\Delta t]}{\partial \theta_k} \frac{\partial \ln[\lambda_p(\theta_l)\Delta t]}{\partial \theta_l} \frac{\lambda_p(\theta_k)\lambda_p(\theta_l)\Delta t}{\lambda_p(\phi_0)} \Bigg\} \\
= \mathbf{M}_{MS}(k,l) \Bigg\{ &\sum_{p=0}^{N-1} \frac{\partial \lambda_p(\theta_k)}{\partial \theta_k} \frac{\lambda_p(\theta_l)}{\lambda_p(\phi_0)} \Delta t \sum_{q=0}^{N-1} \frac{\partial \lambda_q(\theta_l)}{\partial \theta_l} \frac{\lambda_q(\theta_k)}{\lambda_q(\phi_0)} \Delta t + \sum_{p=0}^{N-1} \frac{\partial \lambda_p(\theta_k)}{\partial \theta_k} \frac{\partial \lambda_p(\theta_l)}{\partial \theta_l} \frac{1}{\lambda_p(\phi_0)} \Delta t \Bigg\}. \qquad (2.87)
\end{aligned}
$$

Using again the same calculating technique as in the derivation of the MS matrix, we get

$$
\begin{aligned}
C_1 = &\mathbf{M}_{MS}(k,l) \Bigg[T_{obs}^2 \int_0^1 \frac{\partial \lambda(\phi+\xi_k)}{\partial \xi_k} \frac{\lambda(\phi+\xi_l)}{\lambda(\phi)} d\phi \int_0^1 \frac{\partial \lambda(\phi+\xi_l)}{\partial \xi_l} \frac{\lambda(\phi+\xi_k)}{\lambda(\phi)} d\phi \\
&+ T_{obs} \int_0^1 \frac{\partial \lambda(\phi+\xi_k)}{\partial \xi_k} \frac{\partial \lambda(\phi+\xi_l)}{\partial \xi_l} \frac{1}{\lambda(\phi)} d\phi \Bigg]. \qquad (2.88)
\end{aligned}
$$

Similarly, we derive the other components

$$
\begin{aligned}
C_2 =& \sum_{\mathbf{x}=0}^{\infty} \sum_{p=0}^{N-1} \sum_{q=0}^{N-1} \frac{\partial \lambda_p(\theta_k)\Delta t}{\partial \theta_k} \frac{\partial \lambda_q(\theta_l)\Delta t}{\partial \theta_l} \\
& \prod_{n=0}^{N-1} \left[\frac{\lambda_n(\theta_k)\lambda_n(\theta_l)\Delta t}{\lambda_n(\phi_0)} \right]^{x_n} \frac{1}{x_n!} \exp\left(\Delta t[\lambda_n(\phi_0) - \lambda_n(\theta_k) - \lambda_n(\theta_l)]\right) \\
=& \mathbf{M}_{MS}(k,l) \sum_{p=0}^{N-1} \sum_{q=0}^{N-1} \frac{\partial \lambda_p(\theta_k)\Delta t}{\partial \theta_k} \frac{\partial \lambda_q(\theta_l)\Delta t}{\partial \theta_l} \\
=& \mathbf{M}_{MS}(k,l) T_{obs}^2 \int_0^1 \frac{\partial \lambda(\phi + \xi_k)}{\partial \xi_k} d\phi \int_0^1 \frac{\partial \lambda(\phi + \xi_l)}{\partial \xi_l} d\phi,
\end{aligned} \tag{2.89}
$$

$$
\begin{aligned}
C_3 =& \sum_{\mathbf{x}=0}^{\infty} x_p \sum_{p=0}^{N-1} \sum_{q=0}^{N-1} \frac{\partial \ln[\lambda_p(\theta_k)\Delta t]}{\partial \theta_k} \frac{\partial \lambda_q(\theta_l)\Delta t}{\partial \theta_l} \\
& \prod_{n=0}^{N-1} \left[\frac{\lambda_n(\theta_k)\lambda_n(\theta_l)\Delta t}{\lambda_n(\phi_0)} \right]^{x_n} \frac{1}{x_n!} \exp\left(\Delta t[\lambda_n(\phi_0) - \lambda_n(\theta_k) - \lambda_n(\theta_l)]\right) \\
=& \sum_{q=0}^{N-1} \frac{\partial \lambda_q(\theta_l)\Delta t}{\partial \theta_l} \sum_{p=0}^{N-1} \frac{\partial \ln[\lambda_p(\theta_k)\Delta t]}{\partial \theta_k} \frac{\lambda_p(\theta_k)\lambda_p(\theta_l)\Delta t}{\lambda_p(\phi_0)} \mathbf{M}_{MS}(k,l) \\
=& \mathbf{M}_{MS}(k,l) T_{obs}^2 \int_0^1 \frac{\partial \lambda(\phi + \xi_l)}{\partial \xi_l} d\phi \int_0^1 \frac{\partial \lambda(\phi + \xi_k)}{\partial \xi_k} \frac{\lambda(\phi + \xi_l)}{\lambda(\phi)} d\phi,
\end{aligned} \tag{2.90}
$$

$$
\begin{aligned}
C_4 =& \sum_{\mathbf{x}=0}^{\infty} x_q \sum_{p=0}^{N-1} \sum_{q=0}^{N-1} \frac{\partial \lambda_p(\theta_k)\Delta t}{\partial \theta_k} \frac{\partial \ln[\lambda_q(\theta_l)\Delta t]}{\partial \theta_l} \\
& \prod_{n=0}^{N-1} \left[\frac{\lambda_n(\theta_k)\lambda_n(\theta_l)\Delta t}{\lambda_n(\phi_0)} \right]^{x_n} \frac{1}{x_n!} \exp\left(\Delta t[\lambda_n(\phi_0) - \lambda_n(\theta_k) - \lambda_n(\theta_l)]\right) \\
=& \sum_{p=0}^{N-1} \frac{\partial \lambda_p(\theta_k)\Delta t}{\partial \theta_k} \sum_{q=0}^{N-1} \frac{\partial \ln[\lambda_q(\theta_l)\Delta t]}{\partial \theta_l} \frac{\lambda_q(\theta_k)\lambda_q(\theta_l)\Delta t}{\lambda_q(\phi_0)} \mathbf{M}_{MS}(k,l) \\
=& \mathbf{M}_{MS}(k,l) T_{obs}^2 \int_0^1 \frac{\partial \lambda(\phi + \xi_k)}{\partial \xi_k} d\phi \int_0^1 \frac{\partial \lambda(\phi + \xi_l)}{\partial \xi_l} \frac{\lambda(\phi + \xi_k)}{\lambda(\phi)} d\phi.
\end{aligned} \tag{2.91}
$$

Finally, plugging (2.88), (2.89), (2.90), and (2.91) into (2.82), one obtains (2.39).

2.6.6 Derivation of (2.37)

From (2.37), the element (k,l) of the matrix $\mathbf{H}$ is given by

$$
\mathbf{H}(k,l) = E_{\mathbf{x};\phi_0} \left[\frac{\partial \ln p(\mathbf{x};\theta_k)}{\partial \theta_k} \frac{p(\mathbf{x};\theta_k)}{p(\mathbf{x};\phi_0)} \frac{p(\mathbf{x};\theta_l)}{p(\mathbf{x};\phi_0)} \right]
$$

$$
\begin{aligned}
&= \sum_{\mathbf{x}=0}^{\infty} \left[\sum_{p=0}^{N-1} x_p \frac{\partial \ln[\lambda_p(\theta_k)\Delta t]}{\partial \theta_k} - \frac{\partial \lambda_p(\theta_k)\Delta t}{\partial \theta_k} \right] \\
&\quad \prod_{n=0}^{N-1} \left[\frac{\lambda_n(\theta_k)\lambda_n(\theta_l)\Delta t}{\lambda_n(\phi_0)} \right]^{x_n} \frac{1}{x_n!} \exp\left(\Delta t[\lambda_n(\phi_0) - \lambda_n(\theta_k) - \lambda_n(\theta_l)]\right) \\
&= \sum_{p=0}^{N-1} \frac{\partial \ln[\lambda_p(\theta_k)\Delta t]}{\partial \theta_k} \sum_{\mathbf{x}=0}^{\infty} x_p \prod_{n=0}^{N-1} \left[\frac{\lambda_n(\theta_k)\lambda_n(\theta_l)\Delta t}{\lambda_n(\phi_0)} \right]^{x_n} \frac{1}{x_n!} \exp\left(\Delta t[\lambda_n(\phi_0) - \lambda_n(\theta_k) - \lambda_n(\theta_l)]\right) \\
&\qquad + \sum_{p=0}^{N-1} \frac{\partial \lambda_p(\theta_k)\Delta t}{\partial \theta_k} \prod_{n=0}^{N-1} \left[\frac{\lambda_n(\theta_k)\lambda_n(\theta_l)\Delta t}{\lambda_n(\phi_0)} \right]^{x_n} \frac{1}{x_n!} \exp\left(\Delta t[\lambda_n(\phi_0) - \lambda_n(\theta_k) - \lambda_n(\theta_l)]\right) \\
&= \mathbf{M}_{MS}(k,l) \left[T_{obs} \int_0^1 \frac{\partial \lambda(\phi + \xi_k)}{\partial \xi_k} \frac{\lambda(\phi + \xi_l)}{\lambda(\phi)} d\phi - T_{obs} \int_0^1 \frac{\partial \lambda(\phi + \xi_k)}{\partial \xi_k} d\phi \right]. \quad (2.92)
\end{aligned}
$$

2.6.7 Derivation of (2.43)

We have

$$
\begin{aligned}
\eta'(\alpha,\beta) &= \sum_{\mathbf{x}=0}^{\infty} \left\{ \prod_{n=0}^{N-1} \frac{[\lambda_n(\phi_0+\beta)\Delta t]^{x_n}}{x_n!} \, exp(-\lambda_n(\phi_0+\beta)\Delta t) \right\}^{\alpha} \left\{ \prod_{m=0}^{N-1} \frac{[\lambda_m(\phi_0)\Delta t]^{x_m}}{x_m!} \, exp(-\lambda_m(\phi_0)\Delta t) \right\}^{1-\alpha} \\
&= \sum_{\mathbf{x}=0}^{\infty} \prod_{n=0}^{N-1} \frac{[\lambda_n(\phi_0+\beta)^{\alpha}\lambda_n(\phi_0)^{1-\alpha}\Delta t]^{x_n}}{x_n!} \exp\left[-\alpha\lambda_n(\phi_0+\beta)\Delta t - (1-\alpha)\lambda_n(\phi_0)\Delta t\right] \\
&= \exp\left\{ T_{obs} \int_0^1 \left(-\alpha\lambda(\phi+\beta) - (1-\alpha)\lambda(\phi) + \lambda(\phi+\beta)^{\alpha}\lambda(\phi)^{1-\alpha}\right) d\phi \right\}. \quad (2.93)
\end{aligned}
$$

Chapitre 3

Statistical resolution limit for array processing and MIMO radar

3.1 Introduction

The statistical resolution limit (SRL) is the minimal distance in terms of the parameter of interest between two signals allowing to correctly separate/estimate the parameters of interest. The problem of SRL for two closely spaced sources has attached many interests with applications such as radar, sonar, image processing. In the literature, there are mainly four different ways to obtain the SRL :

1. The first approach is based on the concept of the mean null spectrum concerning the specific high-resolution estimation algorithms [Cox, KB86, AD08]. In this approach, if we assume that two signals are parameterized by two parameters of interest θ_1 and θ_2 , the Cox's criterion [Cox] states that *two sources are resolved (w.r.t. a given high-resolution estimation algorithm) if the mean null spectrum at* θ_1 *and* θ_2 *is lower than the mean of the null spectrum at the midpoint* $\frac{\theta_1+\theta_2}{2}$. While the concept of this approach is quite simple, its application is limited to the used estimation algorithm. In following, we present three other approaches which do not depend on the algorithm.
2. The second approach is based on the detection theory using the hypothesis test formulation [SM04, SM05, LN07, AW08]. The main idea is to use a hypothesis test to decide if the two signal sources are combined into a single signal or they are resolvable. Follow this concept, in [SM05], the resolution limit on the frequency of two sinusoids is derived for a fixed probability of detection P_d and a fixed probability of false alarm P_{fa} using the Generalized Likelihood Ratio Test (GLRT). Besides, in [LN07], the angular resolution limit (ARL), i.e. the resolution limit of the angle of arrival, on resolving two closely spaced point sources is derived by considering the asymptotic performance of the GLRT. The result in this paper is also based on the contraints on the P_d and P_{fa} for a hypothesis test. Finally, in [AW08], one can find the expression of the SRL in the Bayesian context based on the first order Taylor expansion of the probability of error P_e.
3. The third approach is based on the estimation accuracy, *i. e.* the CRB [Lee92, Lee94, Smi05, Dil98]. In the literature, one can find two main criteria based on the CRB in this family :
   • The first one is called Lee's criterion which was introduced in [Lee92]. In the

context of array processing, it states that *two signals are properly resolved w.r.t the DOA θ_1 and θ_2, if the maximum standard deviation is lower than at less than half the difference between θ_1 and θ_2*. Since the standard deviations of an unbiased estimator can be approximated by $\sqrt{CRB(\theta_1)}$ and $\sqrt{CRB(\theta_2)}$ (under certain regularity conditions), the SRL in the Lee sense is $2\max(\sqrt{CRB(\theta_1)}, \sqrt{CRB(\theta_2)})$. The applications of this criterion can be found in [Lee94, Dil98] where the problem of frequency resolution is addressed. Note that the coupling between the parameters of interest, i.e. the off-diagonal term of the CRB matrix, $CRB(\theta_1, \theta_2)$, is ignored in this criterion.

- To fill this lack, the second criterion was introduced by Smith in [Smi05] taking in account this coupling effect as follows : *two signals are resolvable w.r.t the DOA if the separation between the two parameters of interest θ_1 and θ_2, denoted by δ, is less than the standard deviation of the difference between these parameters.* Hence, the SRL in the Smith sense can be obtained as the solution of the following equation

$$\delta^2 = CRB(\delta).$$

In [LN07], the SRL in the Smith sense is linked to the SRL based on the hypothesis test as in the equation below :

$$\delta^2 = \gamma CRB(\delta),$$

where γ is a translator factor depending on the P_{fa} and P_d.

4. The final approach is based on the Stein's lemma [CT, Che56] which establishes the relation between measures of the difference between two probability distributions and the P_e for a hypothesis test. In the literature, this lemma has already been used to calculate the relative entropy to study detection performance and to design waveform for MIMO radar in [TLWP09] [TTP10] and for multi-static radar in [Kay09]. Besides, in [VEB+11], the ARL on resolving two closely spaced polarized sources using vector-sensor arrays is also studied by using the relative entropy.

In this chapter, we examine the SRL based on estimation accuracy and the SRL based on the Stein's lemma. First, we derive and analyse the SRL based on the Lee's criterion and the Smith's criterion in the context of array processing. Although there are many works related to the resolvability of closely spaced sources exist in the literature (see articles cited above), to the best of our knowledge, all these works are investigated in the ideal scenario where the observation model is assumed to be correct, *i.e.* the array response is supposed to be precisely known. However, in practice, as the modeling errors always exist and degrade the system performance, it is important to investigate the impact of modeling errors in sensor system on the SRL for two closely spaced sources. One can find some works related to the modeling errors that have been done in array processing such as [RP87, VS94] and recently [FLV10]. However, to the best of our knowledge, there is no results available for the resolution limit in this practice context of array processing. To fill this lack, in this chapter, we study the influence of modeling error on the ARL for two closely spaced sources in the array processing context. Our approach follows the idea presented in [FLV10] where the error is modeled by a Gaussian random vector added to the true steering vector.

Second, we follow the approach based on the Stein's lemma to derive the SRL. This approach is new and rarely used in the literature. Hence, our goal here is to demonstrate its usefulness in investigating the SRL. For this purpose, we examine this approach in two

difference contexts : (i) in the context of array processing, the ARL based on the Stein's lemma is derived and compared to the ARL based on the Lee's and Smith's criteria, and (ii) in the context of MIMO radar whose transmitting array and receiving array are either widely spaced or collocated. Note that, when transmitting array and receiving array are widely spaced, the problem becomes Multidimensional SRL (MSRL). To the best of our knowledge, there are few works concerning the problem of SRL in the context of MIMO radar that have been done. In [Boy11], the ARL of a collocated MIMO radar is derived and analyzed using the Smith's criterion. In [EBRM12], the MSRL for two closely spaced targets with a widely spaced MIMO radar is derived by using the GLRT. Note that, until now, there is none result of the MSRL based on the algorithm criterion or the CRB in the context of widely separated MIMO radar due to the difficulty in generalizing the existing mono-dimensional works.

3.2 The SRL based on the CRB in the context of array processing in the presence of modeling errors

This Section is organized as follows : Section 3.2.1 presents the array processing model in the presence of modeling errors. In Section 3.2.2, we derive the corresponding ARL based on the Lee's and Smith's criterions. In Section 3.2.3, an analytical analysis is presented to study the ARL expressions in different specific scenarios. Next, Section 3.2.4 presents some numerical simulations to investigate the impact of medeling errors on the ARL in this context. An numerical procedure is also introduced to analyze the ARL in terms of antenna geometry. Finally, Section 3.2.5 draws some summaries of this Section.

3.2.1 Problem setup

We consider here a linear sensor array of N elements in the case of two source signals (see figure 3.1). The two source signals, denoted by $\mathbf{s}_1 = [s_1(1) \dots s_1(L)]^T$ and $\mathbf{s}_2 = [s_2(1) \dots s_2(L)]^T$ where L is the number of transmitted pulses, are assumed to be deterministic and located in the far-field w.r.t. the array. Each source is located by an angle-of-arrival denoted by θ_m, $m = 1, 2$. The distance between the n-th sensor w.r.t. a reference is denoted by d_n. In the scenario without modeling errors, the signal received at such an array for the $l-$th snapshot is given by

$$\mathbf{y}(l) = \mathbf{a}(\omega_1)s_1(l) + \mathbf{a}(\omega_2)s_2(l) + \mathbf{n}(l), \tag{3.1}$$

where $l = 1, \dots, L$. The theoretical nominal angular steering vectors have the following structures $\mathbf{a}(\omega_m) = [\exp(j\omega_m d_1) \ \dots \ \exp(j\omega_m d_N)]^T$ where $\omega_m = \frac{2\pi}{\lambda} \sin\theta_m$ with λ denoting the wavelength. The noise vector for the l-th snapshot $\mathbf{n}(l)$ is assumed to be independent and identically distributed (i.i.d.) symmetric complex Gaussian with zero-mean and covariance matrix $\sigma^2\mathbf{I}_N$. In this section, we consider that the true steering vector of the receiving array, $\mathbf{a}_t(\omega_m)$, is subject to a modeling error represented by an additive random vector $\mathbf{e_m}$, $m = 1, 2$. In other words,

$$\mathbf{a}_t(\omega_m) = \mathbf{a}(\omega_m) + \mathbf{e}_m, \tag{3.2}$$

where $\mathbf{e}_m$ is assumed to be i.i.d. complex Gaussian distributed, namely $\mathbf{e}_m \sim \mathcal{CN}(0, \sigma_e^2\mathbf{I}_N)$,

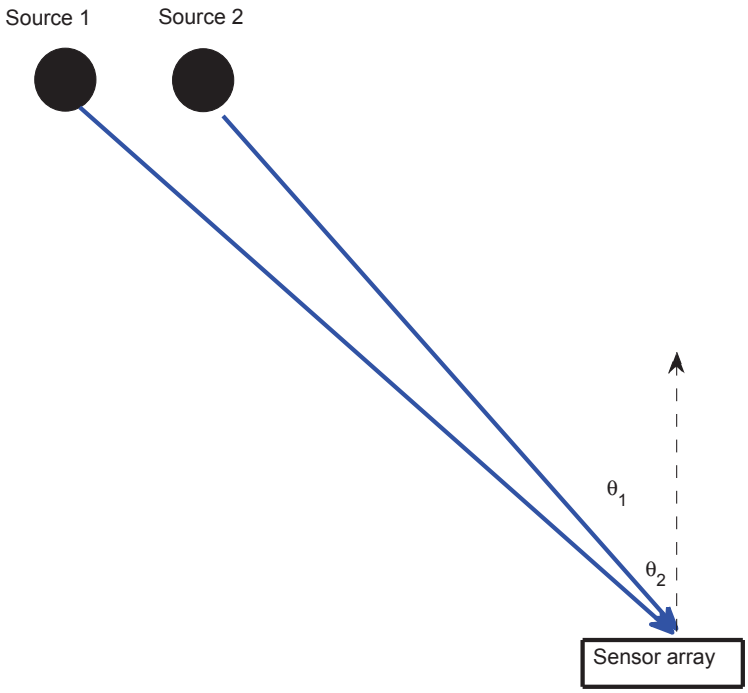

FIGURE 3.1 – Sensor array with two sources

$m = 1, 2$. Moreover, $\mathbf{e}_m$ is assumed to be statistically independent of the noise. Consequently, equation (3.1) can be written as

$$\mathbf{y}(l) = (\mathbf{a}(\omega_1) + \mathbf{e}_1)s_1(l) + (\mathbf{a}(\omega_2) + \mathbf{e}_2)s_2(l) + \mathbf{n}(t),\ l = 1 \dots L. \tag{3.3}$$

Let us define $\mathbf{y} = [\mathbf{y}^T(1) \dots \mathbf{y}^T(L)]^T$ and $\mathbf{n} = [\mathbf{n}^T(1) \dots \mathbf{n}^T(L)]^T$, and assume : $\mathbf{s}_1 \neq \mathbf{s}_2$ and $||\mathbf{s}_1||^2 = ||\mathbf{s}_2||^2 = L$, (3.3) can be rewritten as

$$\mathbf{y} = \mathbf{s}_1 \otimes \mathbf{a}(\omega_1) + \mathbf{s}_2 \otimes \mathbf{a}(\omega_2) + \tilde{\mathbf{n}} + \mathbf{n} \tag{3.4}$$

where $\otimes$ stands for the Kronecker product and $\tilde{\mathbf{n}} = \mathbf{s}_1 \otimes \mathbf{e}_1 + \mathbf{s}_2 \otimes \mathbf{e}_2$ can be viewed as a structured interference noise. From (3.4), one can see that the likelihood of the observations is complex circular Gaussian distributed with parameterized mean, *i.e.*, $\mathbf{y} \sim \mathcal{CN}(\mathbf{s}_1 \otimes \mathbf{a}(\omega_1) + \mathbf{s}_2 \otimes \mathbf{a}(\omega_2), \mathbf{C})$, where we define $\mathbf{C} = \mathbf{R} \otimes \mathbf{I}_N$ with $\mathbf{R} = \mathbf{R}_\mathbf{n} + \mathbf{R}_{\tilde{\mathbf{n}}} = \sigma^2\mathbf{I}_L + \sigma_e^2(\mathbf{s}_1\mathbf{s}_1^H + \mathbf{s}_2\mathbf{s}_2^H)$.

3.2.2 ARL based on the Cramér-Rao bound

In this section, we use the Smith's criterion [Smi05, EBRM11] and the Lee's criterion [Lee92] which are based on the estimation accuracy concept to determine the ARL for the considered model. Generally speaking, Lee and Smith's criteria are not easy to derive since the off-diagonal terms of the CRB for general arrays are a function of the ARL. So, to

obtain the ARL in the sense of Lee and Smith, we have to analytically solve a polynomial of high order [EBRM, Boy11] after linearization.

3.2.2.1 ARL based on Lee's criterion

The ARL based on the Lee's criterion is given by [Lee92]

$$\delta_L = 2\max\left\{\sqrt{\mathbf{B}(\omega_1,\omega_1)}, \sqrt{\mathbf{B}(\omega_2,\omega_2)}\right\} \tag{3.5}$$

where $\mathbf{B}$ is the 2×2 deterministic Cramer-Rao Bound Matrix and $\mathbf{B}(\omega_1,\omega_1)$ (*resp.* $\mathbf{B}(\omega_2,\omega_2)$) stands for the $(1,1)$-th (*resp.* $(2,2)$-th) element of matrix $\mathbf{B}$. In the appendix 3.5.1, we derive a closed-form expression of the linearized CRB for the considered model. In particular, using result (3.48), the Lee's criterion takes the following form :

$$\delta_L = 2\sqrt{\mathbf{B}(\omega_1,\omega_1)} = 2\sqrt{\frac{\mathbf{F}(\omega_1,\omega_1)}{\mathbf{F}(\omega_1,\omega_1)^2 - \mathbf{F}(\omega_1,\omega_2)^2}} \tag{3.6}$$

where $\mathbf{F}$ is the Fisher Information Matrix (FIM) such as $\mathbf{B} = \mathbf{F}^{-1}$. Let

$$\begin{aligned}
a &= 2\mathcal{R}\{\mathbf{s}_2^H\mathbf{R}^{-1}\mathbf{s}_1\}\sum_{n=1}^{N} d_n^2 = \frac{2\sigma^2\mathcal{R}\{\rho\}}{\sigma^4+\sigma_e^2(\sigma_e^2L^2+2\sigma^2L-\sigma_e^2|\rho|^2)}\sum_{n=1}^{N} d_n^2\\
b &= -\mathcal{I}\{\mathbf{s}_2^H\mathbf{R}^{-1}\mathbf{s}_1\}\sum_{n=1}^{N} d_n^3 = \frac{\sigma^2\mathcal{I}\{\rho\}}{\sigma^4+\sigma_e^2(\sigma_e^2L^2+2\sigma^2L-\sigma_e^2|\rho|^2)}\sum_{n=1}^{N} d_n^3\\
\mathbf{F}(\omega_1,\omega_1) &= \frac{2(\sigma^2L+\sigma_e^2(L^2-|\rho|^2))}{\sigma^4+\sigma_e^2(\sigma_e^2L^2+2\sigma^2L-\sigma_e^2|\rho|^2)}\sum_{n=1}^{N} d_n^2,
\end{aligned} \tag{3.7}$$

where $\mathcal{R}\{.\}$ and $\mathcal{I}\{.\}$ are the real and imaginary parts of a complex number and $\rho = \mathbf{s}_1^H\mathbf{s}_2$. Criterion (3.6) can be rewritten as a fourth-order polynomial according to

$$b^2\delta_L^4 + 2ab\delta_L^3 + (a^2 - \mathbf{F}(\omega_1,\omega_1)^2)\delta_L^2 + 4\mathbf{F}(\omega_1,\omega_1) = 0. \tag{3.8}$$

We follow the methodology introduced in [Boy11]. The goal is to select the root corresponding to the ARL and reject the three extraneous roots. For this purpose, first we use the property that if δ is the solution of the Lee equation, then $-\delta$ is also a solution, to simplify the problem. Let r_1 and r_2 be the other roots, we have

$$\begin{cases}
\delta^2 r_1 r_2 = \frac{4\mathbf{F}(\omega_1,\omega_1)}{b^2},\\
\delta^2(r_1+r_2) = 0,\\
r_1+r_2 = \frac{2a}{b},\\
r_1r_2 - \delta^2 = \frac{a^2-\mathbf{F}(\omega_1,\omega_1)^2}{b^2}.
\end{cases}$$

Combining the first and fourth equations, one obtains a new polynomial

$$b^2\delta^4 + (a^2 - \mathbf{F}(\omega_1,\omega_1)^2)\delta^2 + 4\mathbf{F}(\omega_1,\omega_1) = 0. \tag{3.9}$$

This is a biquadratic equation whose solutions are :

$$\delta_L^2 = \frac{1}{2b^2}\left(\mathbf{F}(\omega_1,\omega_1)^2 - a^2 \pm \sqrt{(\mathbf{F}(\omega_1,\omega_1)^2 - a^2)^2 - 16b^2\mathbf{F}(\omega_1,\omega_1)}\right). \tag{3.10}$$

To choose the sign in the above solutions, we consider the case where $\sigma_e^2 = 0$, the expressions of a, b and $\mathbf{F}(\omega_1,\omega_1)$ are given by $a = \frac{2\mathcal{R}\{\rho\}}{\sigma^2}\sum_{n=1}^{N} d_n^2$, $b = \frac{\mathcal{I}\{\rho\}}{\sigma^2}\sum_{n=1}^{N} d_n^3$, $\mathbf{F}(\omega_1,\omega_1) = \frac{2L}{\sigma^2}\sum_{n=1}^{N} d_n^2$. Consequently, (3.10) can be rewritten as

$$\delta_L^2 = \frac{\left(2\sum_{n=1}^{N} d_n^2\right)^2(L^2 - \mathcal{R}\{\rho\}^2)}{2\left(\sum_{n=1}^{N} d_n^3\mathcal{I}\{\rho\}\right)^2} \pm \frac{1}{2}\sqrt{\left(\frac{\left(2\sum_{n=1}^{N} d_n^2\right)^2(L^2 - \mathcal{R}\{\rho\}^2)}{\left(\sum_{n=1}^{N} d_n^3\mathcal{I}\{\rho\}\right)^2}\right)^2 - \frac{32\sigma^2\sum_{n=1}^{N} d_n^2 L}{\left(\sum_{n=1}^{N} d_n^3\mathcal{I}\{\rho\}\right)^2}}. \tag{3.11}$$

To get $\delta_L \to 0$ when $SNR \to \infty$, the convenient solution is the one with the negative sign.

3.2.2.2 ARL based on the Smith's criterion

The ARL based on the Smith's criterion is given by [Smi05]

$$\delta_S = \sqrt{\gamma(\mathbf{B}(\omega_1,\omega_1) + \mathbf{B}(\omega_2,\omega_2) - 2\mathbf{B}(\omega_1,\omega_2))} \tag{3.12}$$

where γ is a translation factor [LN07] which can be estimated numerically by solving the equation $Q^{-1}_{\mathcal{X}_1^2}(P_{fa}) = Q^{-1}_{\mathcal{X}_1^2(\gamma)}(P_d)$, where $Q^{-1}_{\mathcal{X}_1^2}$ is the inverse of the right tail of the chi-square distribution, denoted by $\mathcal{X}_1^2$, and P_{fa} and P_d are the probability of false alarm and detection, respectively. Using the results given in the appendix 3.5.1, the Smith's criterion for the considered model is given

$$\delta_S = \sqrt{\frac{2\gamma}{\mathbf{F}(\omega_1,\omega_1) - (a + b\delta_S)}}. \tag{3.13}$$

Finally, criterion (3.13) can be rewritten as a third-order polynomial :

$$b\delta^3 + (a - \mathbf{F}(\omega_1,\omega_1))\delta^2 + 2\gamma = 0. \tag{3.14}$$

We also use the same property as in deriving the ARL based on the Lee's criterion : if δ is the solution of the Smith equation, then $-\delta$ is also a solution. Let r be the other root, we have

$$\begin{cases} \delta^2 r = \frac{2\gamma}{b}, \\ r = \frac{-a + \mathbf{F}(\omega_1,\omega_1)}{b}. \end{cases}$$

Finally, the ARL based on the Smith's criterion is given by

$$\delta_S = \sqrt{\frac{2\gamma}{\mathbf{F}(\omega_1,\omega_1) - a}}, \tag{3.15}$$

where a and $\mathbf{F}(\omega_1,\omega_1)$ are given in (3.7). Note that in the case without modeling errors, i.e. $\sigma_e^2=0$, the terms a, b and $\mathbf{F}(\omega_1,\omega_1)$ are given by using (3.47) as follows

$$\begin{aligned} a &= \frac{2\mathcal{R}\{\rho\}}{\sigma^2}\sum_{n=1}^{N} d_n^2, \\ b &= \frac{\mathcal{I}\{\rho\}}{\sigma^2}\sum_{n=1}^{N} d_n^3, \\ \mathbf{F}(\omega_1,\omega_1) &= \frac{2L}{\sigma^2}\sum_{n=1}^{N} d_n^2, \end{aligned} \tag{3.16}$$

Remark : the ARL based on the Lee's and Smith's criteria for the case without modeling errors can be given by

$$\begin{aligned} \delta_L(\sigma_e^2=0) &= \sqrt{\frac{2(\sum_{n=1}^{N} d_n^2)^2(L^2-\mathcal{R}\{\rho\}^2)}{(\sum_{n=1}^{N} d_n^3\mathcal{I}\{\rho\})^2} - 2\sqrt{\frac{(\sum_{n=1}^{N} d_n^2)^4(L^2-\mathcal{R}\{\rho\}^2)^2}{(\sum_{n=1}^{N} d_n^3\mathcal{I}\{\rho\})^4} - \frac{2\sigma^2\sum_{n=1}^{N} d_n^2 L}{(\sum_{n=1}^{N} d_n^3\mathcal{I}\{\rho\})^2}}} \\ \delta_S(\sigma_e^2=0) &= \sqrt{\frac{\gamma\sigma^2}{\sum_{n=1}^{N} d_n^2(L-\mathcal{R}\{\rho\})}}. \end{aligned} \tag{3.17}$$

3.2.3 Analytical analysis

3.2.3.1 Central-symmetric array analysis

If the antenna array is assumed to be central-symmetric linear and the center of array is chosen as the reference point, *i.e.* $\sum_{n=1}^{N} d_n = 0$ and we denote $\sigma_a^2 = \frac{1}{N}||\mathbf{d}||^2$ where $||\mathbf{d}|| = \sqrt{\mathbf{d}^T\mathbf{d}}$ with $\mathbf{d} = [d_1,\ldots,d_N]^T$, the CRB is no longer a function of the ARL. More precisely, the off-diagonal terms $\mathbf{F}(\omega_1,\omega_2) = \mathbf{F}(\omega_2,\omega_1)$ in the FIM are for this particular array not a function of the ARL since $\sum_{n=1}^{N} d_n^3 = 0$ (see the appendix 3.5.1). Consequently, the formula of the ARL based on the Lee's and Smith's criteria are

$$\begin{aligned} \delta_L &= \sqrt{\frac{2\mathbf{s}_1^H\mathbf{R}^{-1}\mathbf{s}_1}{N\sigma_a^2((\mathbf{s}_1^H\mathbf{R}^{-1}\mathbf{s}_1)^2 - \mathcal{R}^2\{\mathbf{s}_1^H\mathbf{R}^{-1}\mathbf{s}_2\})}}, \\ \delta_S &= \sqrt{\frac{\gamma}{N\sigma_a^2(\mathbf{s}_1^H\mathbf{R}^{-1}\mathbf{s}_1 - \mathcal{R}\{\mathbf{s}_1^H\mathbf{R}^{-1}\mathbf{s}_2\})}}. \end{aligned} \tag{3.18}$$

ARL for the exact model

Finally, the ARL based on the Lee's and Smith's criteria in the context of symmetric array for the case without modeling errors can be given by

$$\begin{aligned} \delta_L(\sigma_e^2=0) &= \sqrt{\frac{2\sigma^2}{N\sigma_a^2\left(L-\frac{\mathcal{R}^2\{\rho\}}{L}\right)}}, \\ \delta_S(\sigma_e^2=0) &= \sqrt{\frac{\gamma\sigma^2}{N\sigma_a^2(L-\mathcal{R}\{\rho\})}}. \end{aligned} \tag{3.19}$$

Orthogonal sources

Note that if the two sources are orthogonal, *ie.* $\rho = 0$, we have

$$\begin{aligned}\delta_L(\sigma_e^2 = 0) &= \sqrt{\frac{2}{NL}}\frac{\sigma}{\sigma_a},\\ \delta_S(\sigma_e^2 = 0) &= \sqrt{\frac{\gamma}{NL}}\frac{\sigma}{\sigma_a}.\end{aligned} \tag{3.20}$$

One can see that the ARL obtained in this case do not depend on the sources but on the configuration of the array, the probability of false alarm and the probability of detection.

3.2.3.2 ARL at high SNR

As we can see in figures 3.2 and 3.3, when SNR is low, the noise component dominates, hence, the impact of modeling errors is negligible. Therefore, it is interesting to examine the case of high SNR where the noise component is small and the impact of modeling errors becomes visible. In this section, we propose closed-form expressions of the ARL in the case of high SNR (*ie.* $\sigma^2 \to 0$). From (3.7), one can see that $\lim\limits_{SNR\to\infty} a = \lim\limits_{SNR\to\infty} b = 0$, hence (3.8) and (3.14) can be rewritten as

$$\begin{aligned}-\mathbf{F}(\omega_1,\omega_1)^2\delta_L^2 + 4\mathbf{F}(\omega_1,\omega_1) = 0,\\ -\mathbf{F}(\omega_1,\omega_1)\delta_S^2 + 2\gamma = 0.\end{aligned} \tag{3.21}$$

Consequently, one obtains the limits of the ARL based on the Lee's and Smith's criteria when $SNR \to \infty$

$$\begin{aligned}\lim_{SNR\to\infty}\delta_L &= \sqrt{\frac{4}{\mathbf{F}(\omega_1,\omega_1)}} = \sqrt{2}\frac{\sigma_e}{||\mathbf{d}||},\\ \lim_{SNR\to\infty}\delta_S &= \sqrt{\frac{2\gamma}{\mathbf{F}(\omega_1,\omega_1)}} = \sqrt{\gamma}\frac{\sigma_e}{||\mathbf{d}||}.\end{aligned} \tag{3.22}$$

This convergence means that for a given "power" level of modeling error σ_e^2, if the SNR is over a certain threshold value, no improvement on the ARL can be done. Another remark here is that the limits of the ARLs proposed above are linear in σ_e and do not depend on the number of pulse or the source signals. Finally, if parameter $\gamma = 2$, the two ARL are equal.

3.2.3.3 Orthogonal sources

If the two sources are orthogonal, *ie.* $\rho = \mathbf{s}_1^H\mathbf{s}_2 = 0$, one can see that $a = b = 0$ and $\mathbf{F}(\omega_1,\omega_1) = \frac{2||\mathbf{d}||(\sigma^2 L+\sigma_e^2 L^2)}{\sigma^4+\sigma_e^2(\sigma_e^2 L^2+2\sigma^2 L)}$. Consequently, the ARL based on the Lee's and Smith's criteria in this case are given by

$$\begin{aligned}\delta_L(s=0) &= \sqrt{\frac{4}{\mathbf{F}(\omega_1,\omega_1)}}\\ &= \sqrt{\frac{2(\sigma^4+\sigma_e^2(\sigma_e^2L^2+2\sigma^2L))}{||\mathbf{d}||^2(\sigma^2L+\sigma_e^2L^2)}},\end{aligned}$$

$$\delta_S(s=0) = \sqrt{\frac{2\gamma}{\mathbf{F}(\omega_1,\omega_1)}} = \sqrt{\frac{\gamma(\sigma^4+\sigma_e^2(\sigma_e^2L^2+2\sigma^2L))}{||\mathbf{d}||^2(\sigma^2L+\sigma_e^2L^2)}}. \tag{3.23}$$

3.2.4 Numerical results

In this section, some numerical results are presented to analyze and compare the behavior of the ARL determined by using different approaches. The scenario is the following : the sensor array is uniform linear array and is composed of $N = 10$ sensors, with inter-element spacing (in unit of wavelengths) is 0.5. The first sensor is chosen as the reference point. The number of snapshots $L = 100$. The probability of false alarm and the probability of detection are $P_{fa} = 0.01$ and $P_d = 0.99$, respectively. First, figure 3.2 plots the ARL δ versus SNR(dB) for both cases with and without modeling errors in the context of non-symmetric array.

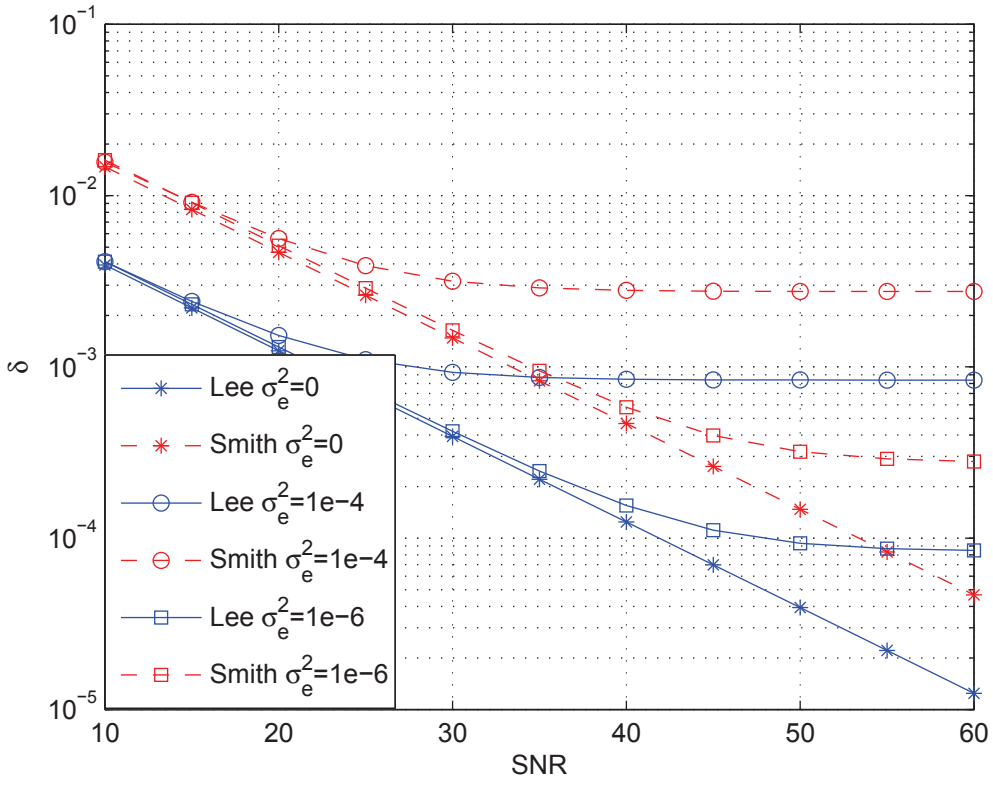

FIGURE 3.2 – ARL versus SNR(dB) in the context of non-symmetric array

We also plot in figure 3.3 the ARL δ versus SNR(dB) for both cases with and without modeling errors in the context of central-symmetric array. For all methods, one can observe in figure 3.2 that when $SNR \to \infty$, the ARL in the case of modeling errors do not fall into zero (contrary to the classical case without error modeling) and converge to fixed limits that are given in (3.22). Next, figure 3.4 plots the ARL based on Lee's and Smith's criteria versus SNR(dB) in the context of central-symmetric array for two scenarios : orthogonal

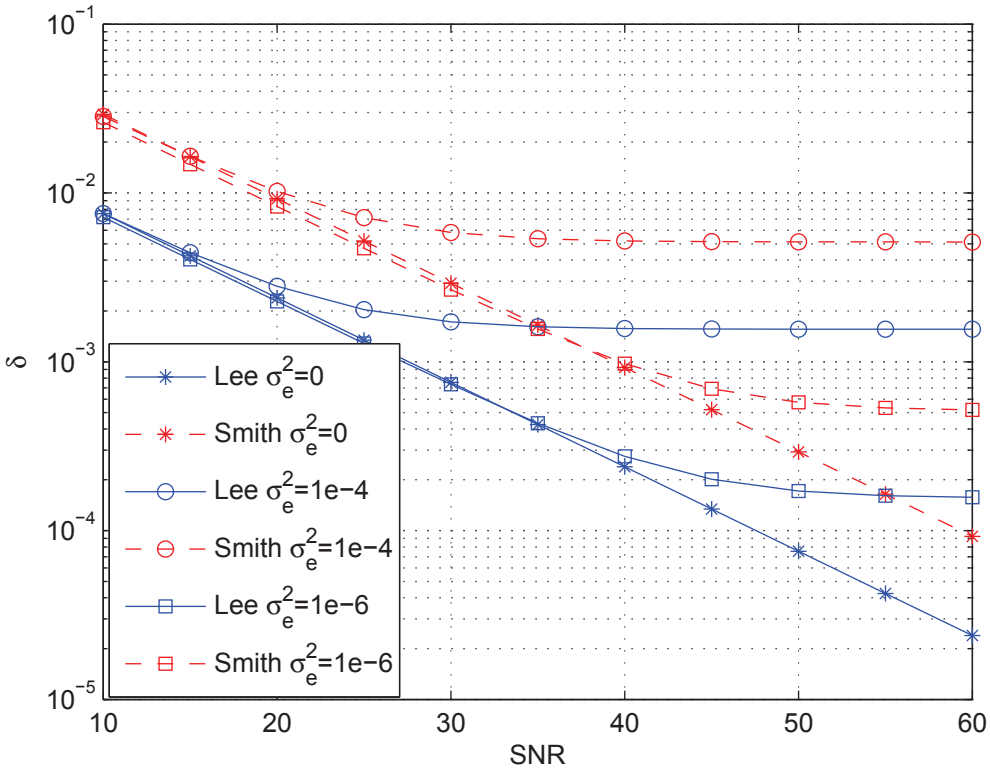

FIGURE 3.3 – ARL versus SNR(dB) in the context of central-symmetric array

sources and non-orthogonal sources. We fixed the error variance at $\sigma_e^2 = 1e-6$. One can see that the orthogonality of sources does not have much influence on the ARL, especially at high SNR, the two scenarios have the same ARL.

In figure 3.5, we plot the ARL based on the Lee's and Smith's criteria versus σ_e^2 with $SNR = 50dB$ in the context of central-symmetric array. We note that the variance of modeling errors have to be restrained in order to keep an acceptable level of the ARL.

Comparing the two figures 3.3 and 3.2, one can see a difference between the ARL for non-symmetric and central-symmetric arrays which means that an optimization based on the array geometry can be performed to achieve an optimal ARL. For this purpose, we consider different linear array geometries keeping the number of sensor N fixed and the array aperture fixed (i.e. the positions of the 2 extreme sensors of the linear array are fixed). First, we can see that in the so-called converging region, both ARL expressions in (3.22) are inversely proportional to $\sum_{n=1}^{N} d_n^2$. Hence, the ARL is minimized when the sensors are placed as far from the reference sensor as possible. In our context, the so-called optimal array can be built as follows : one extreme sensor is considered as the reference sensor and $N-2$ remaining sensors are placed near the other extreme sensor. Next, in the so-called non-converging region, the expression of the ARL based on the Smith's criterion in (3.15) is inversely proportional to $\mathbf{F}(\omega_1, \omega_1) - a$ which is proportional to $\sum_{n=1}^{N} d_n^2$. This leads to the same optimal array as in the converging region. For the optimization of the ARL based on the Lee's criterion in the non-converging region, as its expression in (3.11) with negative sign does not show a simple explicit relation to the positions of array sensor, we here employ a numerical search. The system has the following configuration :

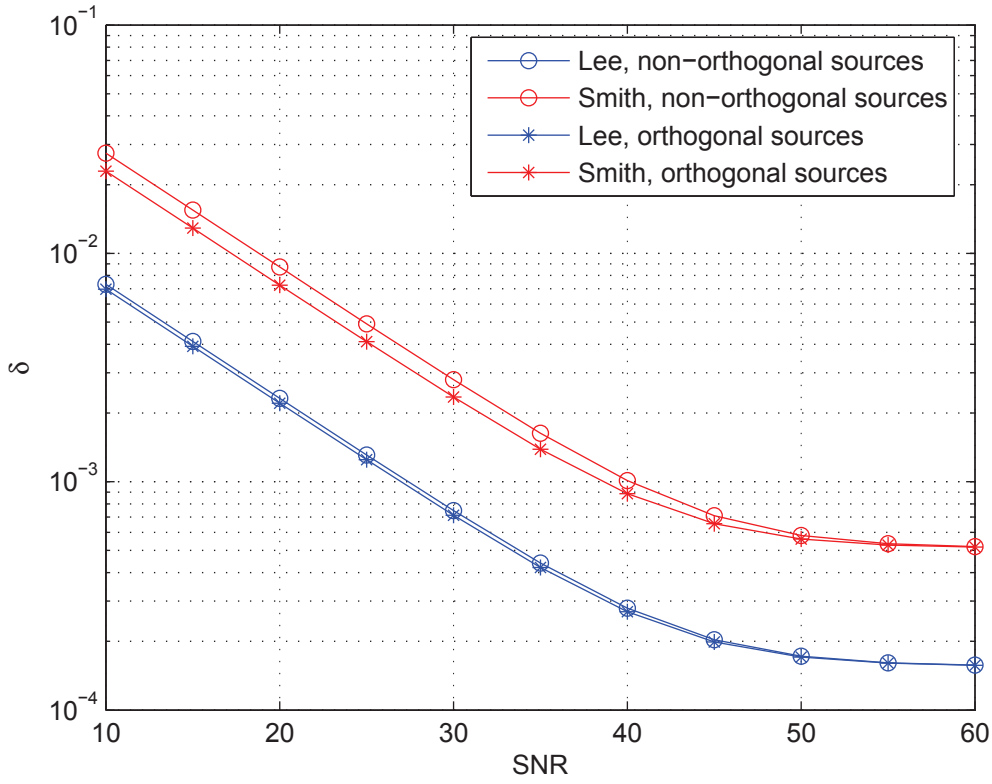

FIGURE 3.4 – ARL versus SNR(dB) in the context of central-symmetric array for two scenarios : orthogonal sources and non-orthogonal sources

the number of observations is $L = 100$, the array aperture is fixed at $D = 23$, the number of sensors is $N = 8$. In other words, there are 22 positions available for the 6 other sensors (74613 possibilities). We have generated all the array configurations and computed the associated ARL. Interestingly, once again, the above optimal array leads to the lowest ARL. In summary, the array geometry that achieved the lowest ARL based on the Lee's and Smith's criteria is the optimal array described above. Figure 3.6 displays the ARL based on the Lee's and Smith's criteria versus SNR for various geometries of the array : the optimal array, the symmetric array and the minimum redundancy (MR) array. Indeed, for this configuration, it can be seen that it exists four MR arrays. We have computed the ARL associated to these four possibilities and plotted the best one in terms of ARL for comparison purpose. One can see that the optimal array achieves the lowest ARL among these arrays.

3.2.5 Summary

In this Section, we have studied the impact of modeling errors on the behavior of the ARL for two closely spaced sources in the context of array processing. Particularly, we used two methods based on the well-known Lee and Smith's criteria using the CRB to derive closed-form expression of the ARL w.r.t. the error variance. We showed that, as the signal-to-noise ratio increases, for each method, the ARL does not fall into zero (contrary to the classical case without modeling errors) and converge to a fixed limit depending

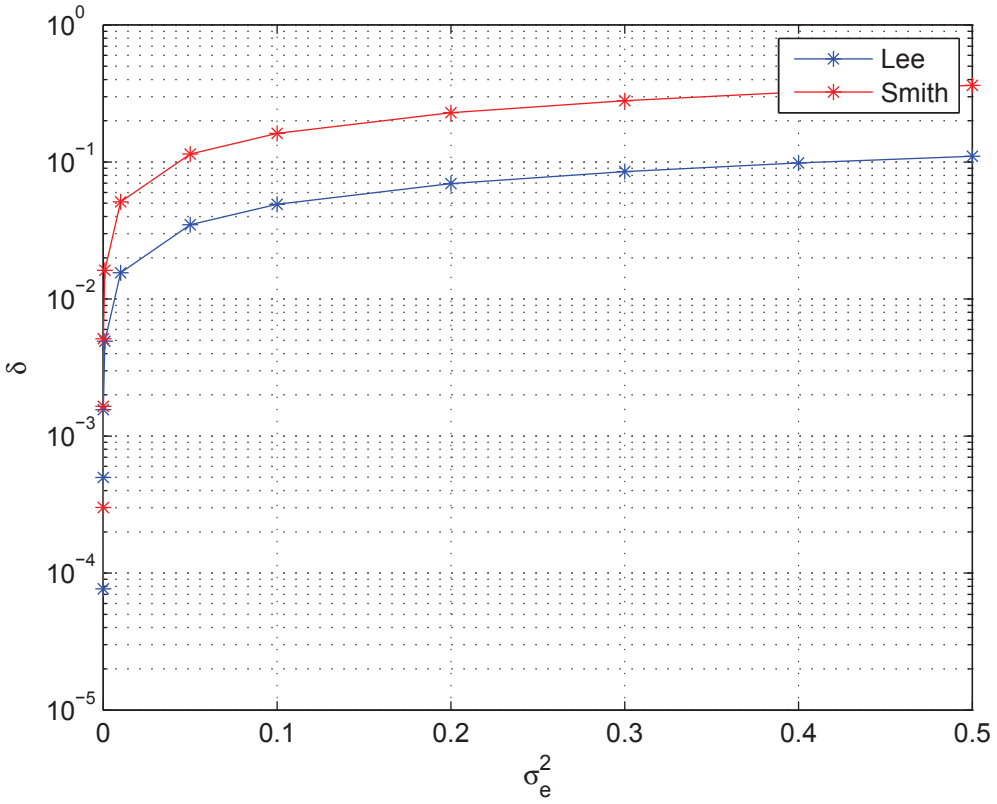

FIGURE 3.5 – ARL versus σ_e^2 in the context of central-symmetric array

on the method for which we gave a closed-form expression. It can be seen that at high SNR, the ARL in the Lee and Smith sense are linear in the error variance. We have also investigated the influence of array geometry on the ARL based on the Lee's and Smith's criteria.

3.3 The SRL based on the Stein's lemma in the context of array processing and MIMO radar

3.3.1 The SRL based on the Stein's lemma in the context of array processing

This Section is organized as follows : Section 3.3.1.1 presents a linearized observation and binary hypothesis test using the array processing model without the modeling errors in (3.1). Next, in Section 3.3.1.2, we use the Stein's lemma to derive the Chernoff distance ($\mathcal{CD}$), then, the ARL for a fixed probability of error. In Section 3.3.1.3 and 3.3.1.4, comparisons in terms of closed-form expressions and numerical results between this approach and the approach based on the CRB previously discussed in Section 3.2 are introduced to show the relevance of the Stein's lemma criterion and the Smith's criterion. Finally, Section 3.3.1.5 gives some summaries of this Section.

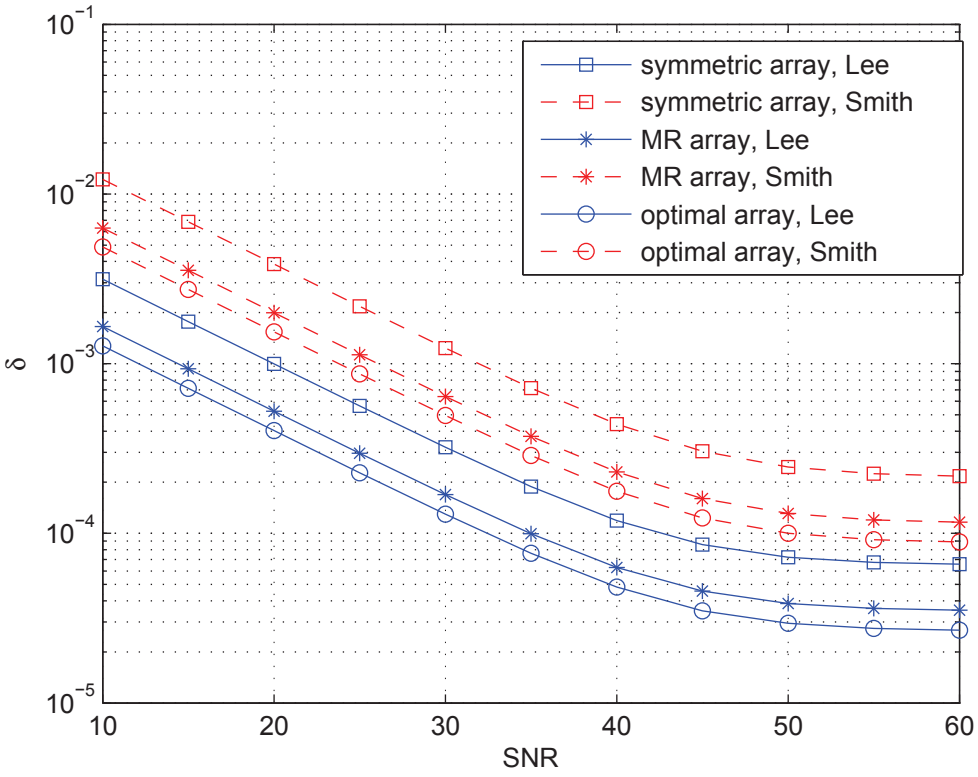

FIGURE 3.6 – ARL versus SNR(dB) for various array geometries

3.3.1.1 Linearized observation and new binary hypothesis test

The problem of resolving two closely spaced sources can be formulated as a binary hypothesis test as follows :

$$\begin{cases} \mathcal{H}_0 : & \delta = 0, \\ \mathcal{H}_1 : & \delta \neq 0. \end{cases} \tag{3.24}$$

As the fact that δ is small, by using the first order Taylor expansion around the so-called center parameters $\omega_c = \frac{\omega_1+\omega_2}{2}$, i.e. $\mathbf{a}(\omega_1) \overset{1}{=} \mathbf{a}(\omega_c) - \frac{j}{2}\delta\dot{\mathbf{a}}(\omega_c)$ and $\mathbf{a}(\omega_2) \overset{1}{=} \mathbf{a}(\omega_c) + \frac{j}{2}\delta\dot{\mathbf{a}}(\omega_c)$ where symbol $\overset{1}{=}$ stands for first-order approximation and $\dot{\mathbf{a}}(\omega_c) = \frac{\partial \mathbf{a}(\omega_c)}{\partial \omega_c}$, one can obtain the linear approximation of (3.1) as follows [1]

$$\mathbf{y} \overset{1}{=} \mathbf{a}(\omega_c) \otimes (\mathbf{s}_1 + \mathbf{s}_2) + \frac{j}{2}\delta\dot{\mathbf{a}}(\omega_c) \otimes (\mathbf{s}_2 - \mathbf{s}_1) + \mathbf{n}.$$

The linearized binary hypothesis test can be rewritten as

$$\begin{cases} \mathcal{H}_0 : & \mathbf{y} \sim \mathcal{CN}(\mathbf{a}(\omega_c) \otimes (\mathbf{s}_1 + \mathbf{s}_2), \sigma^2\mathbf{I}_{LN}), \\ \mathcal{H}_1 : & \mathbf{y} \sim \mathcal{CN}(\mathbf{a}(\omega_c) \otimes (\mathbf{s}_1 + \mathbf{s}_2) + \frac{j}{2}\delta\dot{\mathbf{a}}(\omega_c) \otimes (\mathbf{s}_2 - \mathbf{s}_1), \sigma^2\mathbf{I}_{LN}). \end{cases} \tag{3.25}$$

1. If the sources are equal, we need to consider a second-order Taylor expansion of the steering vectors. But this leads to untractable mathematical derivations.

3.3.1.2 Stein's lemma based analysis of ARL

From the Stein's lemma [CT, Che56], we have the asymptotic [2] relation between the $\mathcal{CD}$ relying the two probability density functions for the test (3.25) and a given probability of error for a binary hypothesis test as follows

$$\mathcal{CD}(p(y_n(l)|\mathcal{H}_0)||p(y_n(l)|\mathcal{H}_1)) = -\lim_{NL\to\infty} \frac{1}{NL}\ln(P_e), \tag{3.26}$$

where $\mathcal{CD}(p(y_n(l)|\mathcal{H}_0)||p(y_n(l)|\mathcal{H}_1))$ is the Chernoff distance (for the sake of simplicity, we hereafter use $\mathcal{CD}_n(l)$ to denote the distance), $p(y_n(l)|\mathcal{H}_i)$ is the pdf of element $y_n(l)$ associated to hypothesis $\mathcal{H}_i$ and P_e denotes a given probability of error. The Chernoff distance between two complex Gaussian distributions with parameterized means, *ie.*

$$y_n(l)|\mathcal{H}_0 \sim \mathcal{CN}((s_1(l)+s_2(l))\exp(j\omega_c d_n), \sigma^2),$$

and

$$y_n(l)|\mathcal{H}_1 \sim \mathcal{CN}((s_1(l)+s_2(l))\exp(j\omega_c d_n) + \frac{j}{2}\delta\frac{\partial\exp(j\omega_c d_n)}{\partial\omega_c}(s_2(l)-s_1(l)), \sigma^2),$$

is given by [CKNS89]

$$\begin{aligned}
\mathcal{CD}_n(l) &= \max_{0\le k\le 1} -\ln\int_\Omega [p(y_n(l)|\mathcal{H}_0)]^{1-k}[p(y_n(l)|\mathcal{H}_1)]^k dy_n(l) \\
&= \max_{0\le k\le 1} \frac{k(1-k)}{\sigma^2}\left|\frac{j}{2}\delta\frac{\partial\exp(j\omega_c d_n)}{\partial\omega_c}(s_2(l)-s_1(l))\right|^2 \\
&= \frac{\delta^2}{16\sigma^2}d_n^2|s_2(l)-s_1(l)|^2.
\end{aligned} \tag{3.27}$$

Note that we have used in the above derivation the fact that $\frac{\delta^2}{4\sigma^2}d_n^2|s_2(l)-s_1(l)|^2$ does not depend on k and it is straightforward to see that $k(1-k)$ is maximized when $k=1/2$. Consequently, the $\mathcal{CD}$ between $p(\mathbf{y}|\mathcal{H}_0)$ and $p(\mathbf{y}|\mathcal{H}_1)$ is given by

$$\begin{aligned}
\mathcal{CD} &= \sum_{n=1}^{N}\sum_{l=1}^{L}\mathcal{CD}_n(l) \\
&= \sum_{n=1}^{N}\sum_{l=1}^{L}\frac{\delta^2}{16\sigma^2}d_n^2|s_2(l)-s_1(l)|^2 \\
&= \frac{\delta^2}{16\sigma^2}\sum_{n=1}^{N}d_n^2\sum_{l=1}^{L}|s_2(l)-s_1(l)|^2 \\
&= \frac{\delta^2}{16\sigma^2}N\sigma_a^2||\mathbf{s}_2-\mathbf{s}_1||^2.
\end{aligned} \tag{3.28}$$

2. Note that the asymptotic context is not very severe since it is not necessary to consider a large number of sensors, N, and/or a large number of snapshots, L, but only a large product, NL, between these two quantities.

From (3.26) and (3.28), we obtain

$$\frac{\delta^2}{16\sigma^2} N\sigma_a^2 ||\mathbf{s}_2 - \mathbf{s}_1||^2 = -\lim_{NL\to\infty} \ln(P_e).$$

Finally, the ARL based on the $\mathcal{CD}$ is given by

$$\begin{aligned} \delta_C &= \sqrt{\frac{-16\sigma^2 \ln(P_e)}{N\sigma_a^2 ||\mathbf{s}_2 - \mathbf{s}_1||^2}} \\ &= \sqrt{\frac{-8\sigma^2 \ln(P_e)}{N\sigma_a^2 (L - \mathcal{R}\{\mathbf{s}_1^H \mathbf{s}_2\})}}. \end{aligned} \tag{3.29}$$

In the next Section, we introduce analytical comparison between the ARL based on Stein's lemma and the ARL based on Lee's and Smith's criteria.

3.3.1.3 Analytic comparisons

1. **Ratios between the ARL**
   It can be seen that the ARL based on three criteria are proportional and the factors can be derived from (3.20) and (3.29) as

$$\begin{aligned} \frac{\delta_C}{\delta_S} &= 2\sqrt{\frac{-2\ln(P_e)}{\gamma}}, \\ \frac{\delta_C}{\delta_L} &= 2\sqrt{-\ln(P_e)\beta}, \\ \frac{\delta_L}{\delta_S} &= \sqrt{\frac{2}{\gamma\beta}}. \end{aligned} \tag{3.30}$$

   where $\beta = 1 + \frac{\mathcal{R}\{\mathbf{s}_1^H \mathbf{s}_2\}}{L}$. While the first factor depends only on the probability of error and γ (which depends on the probability of false alarm and of detection), the other factors that related to the Lee's criterion depend also on the number of snapshots and the sources.

2. **Unified expressions of the ARL**
   If the two sources are orthogonal, *ie.* $\mathbf{s}_1^H \mathbf{s}_2 = 0$ or/and if the number of snapshots is large enough *ie.*, $L \gg \mathcal{R}\{\mathbf{s}_1^H \mathbf{s}_2\}$, we have $\beta \approx 1$ and the ARL given here can be unified according to

$$\delta = \sqrt{\frac{\xi\sigma^2}{NL\sigma_a^2}},$$

   where

$$\xi = -8\ln(P_e) \quad \text{for the Chernoff's ARL} \tag{3.31}$$
$$\xi = \gamma(P_{fa}, P_d) \quad \text{for the Smith's ARL} \tag{3.32}$$
$$\xi = 2 \quad \text{for the Lee's ARL} \tag{3.33}$$

and the ratios between these ARL are given by

$$\begin{aligned}\frac{\delta_C}{\delta_S} &= 2\sqrt{\frac{-2\ln(P_e)}{\gamma}},\\ \frac{\delta_C}{\delta_L} &= 2\sqrt{-\ln(P_e)},\\ \frac{\delta_L}{\delta_S} &= \sqrt{\frac{2}{\gamma}}.\end{aligned} \tag{3.34}$$

One can see the ARL obtained above do not depend on the sources but on the configuration of the array, the power of noise, the probability of false alarm and the probability of detection.

3.3.1.4 Numerical illustrations

In this Section, some numerical results are presented to analyze and compare the behavior of the ARL determined by the different approaches proposed above. The scenario is the following : the sensor array is central-symmetric uniform linear array and is composed of $N = 10$ sensors, with inter-element spacing (in unit of wavelengths) is 0.5, the number of snapshots $L = 100$, the probability of false alarm and the probability of detection are $P_{fa} = 0.01$ and $P_d = 0.99$, respectively, we obtain the probability of error $P_e = \frac{1}{2}P_{fa} + \frac{1}{2}(1 - P_d) = 0.01$. First, figure 3.7 plots the ARL δ versus the SNR(dB)

One can see on figure 3.7 that the ARL based on the Chernoff distance and the Smith's criterion are very closed. Considering a fixed value of the probability of detection $P_d = 0.99$, we plot on figure 3.8 the ARL based on the Chernoff distance and the Smith's criterion versus the probability of false alarm. One can see that at a certain value of P_{fa}, the ARL based on these two criteria can be identical.

3.3.1.5 Summary

In this Section, we have derived and analyzed a closed-form expression of the ARL, denoted by δ, for two closely spaced targets in the context of array processing using the method based on the Stein's lemma. This method is based on the link between the Chernoff distance and a given probability of error associated to the binary hypothesis test : $\mathcal{H}_0 : \delta = 0$ versus $\mathcal{H}_1 : \delta \neq 0$. The analysis has provided new interesting insights on the ARL in this context. It has been seen that the ARL based on the Chernoff distance and the Smith's criterion have a similar behavior and they are proportional by a factor which depends on the probabilities of false alarm and of detection and not of the signal parameters. We also show that for orthogonal sources and/or a large number of snapshots, it is possible to give a unified expression of the ARL for the three considered approaches.

3.3.2 The SRL based on the Stein's lemma in the context of MIMO radar

This Section is organized as follows : Section 3.3.2.1 models the observations after matched filtering of a MIMO radar. Next, Section 3.3.2.2 presents a linearized binary hypothesis test in this context. After that, We use the Stein's lemma to derive the Chernoff distance ($\mathcal{CD}$) in Section 3.3.2.3, and, the ARL w.r.t the amplitudes in Section 3.3.2.4. In

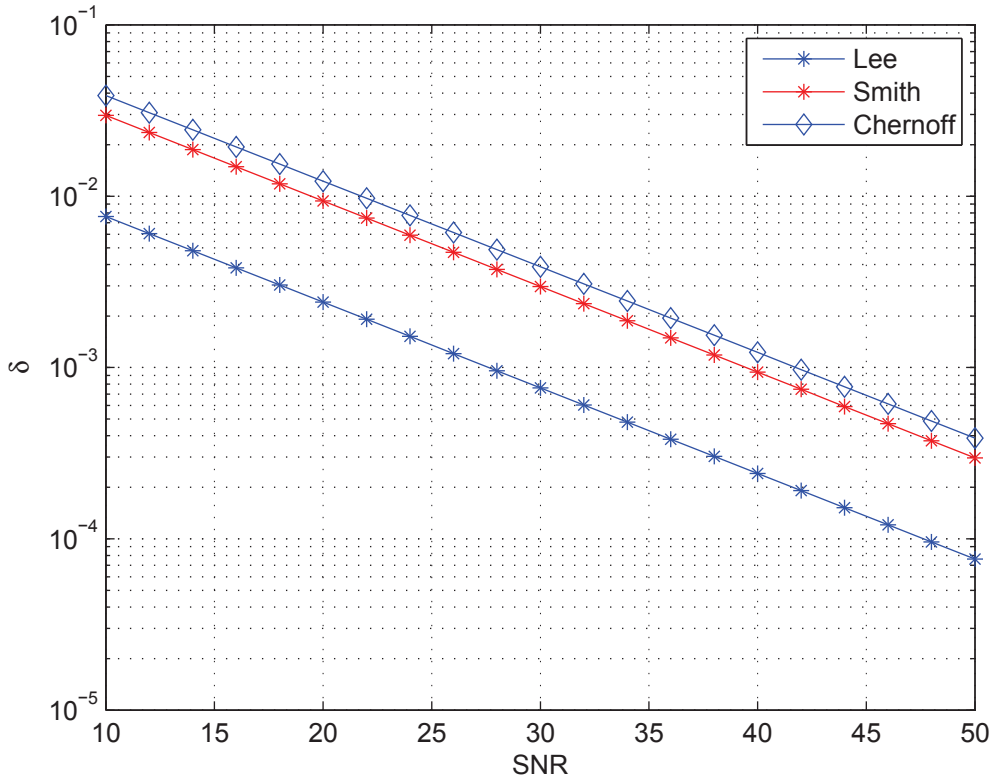

FIGURE 3.7 – ARL versus the SNR(dB)

Section 3.3.2.5, we present some numerical simulations to investigate analyse the behavior of the TMRL in this context. Finally, Section 3.3.2.6 gives some summaries of this Section.

3.3.2.1 Widely spaced MIMO radar setup

We consider here a MIMO radar system with widely spaced linear arrays [3] in the case of two point targets (see figure 3.9). The numbers of antennas in transmitter and receiver are denoted N_T and N_R, respectively. The distances between the i-th sensor w.r.t. a reference are denoted by $d_i^{(T)}$ and $d_i^{(R)}$ for the transmitter and the receiver, respectively. Each point target is located by two parameters : the angle-of-departure denoted by θ_m^T and the angle-of-arrival denoted by θ_m^R, $m = 1, 2$. In this context, the signal at the receiver of such a MIMO radar for the $l-$th pulse is given by

$$\mathbf{X}_l = \sum_{m=1}^{2} \rho_m \exp(j2\pi f_m l)\mathbf{a}_R(\omega_m^{(R)})(\mathbf{a}_T(\omega_m^{(T)}))^T\mathbf{S} + \mathbf{W}_l \tag{3.35}$$

where $l = 0 \dots L-1$ with L is the number of transmitted pulses, and ρ_m, f_m denote the complex amplitude related to the radar-cross-section (RCS) of the target and the normalized Doppler frequency of the m-th target, respectively. The steering vectors have the following structures $\mathbf{a}_T(\omega_m^{(T)}) = [\exp(j\omega_m^{(T)}d_1^{(T)}) \dots \exp(j\omega_m^{(T)}d_{N_T}^{(T)})]^T$, and $\mathbf{a}_R(\omega_m^{(R)}) =$

3. the collocated MIMO radar scenario is tackled in Appendix 3.5.3.

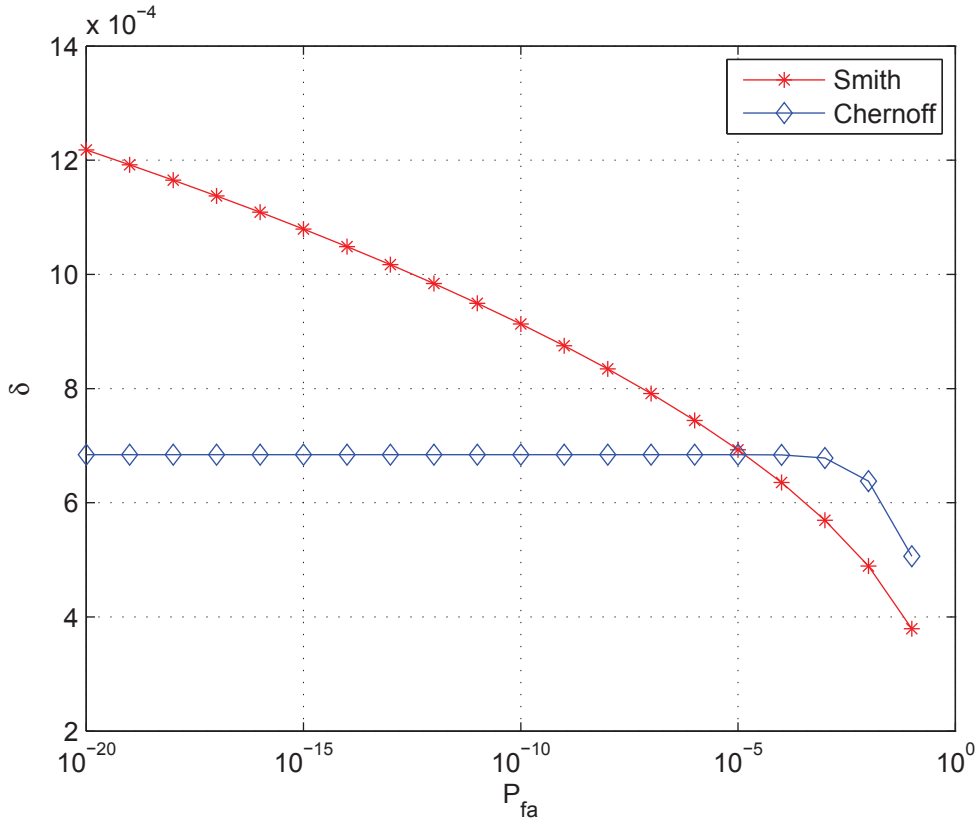

FIGURE 3.8 – ARL versus P_{fa} at SNR $= 45dB$

$[\exp(j\omega_m^{(R)} d_1^{(R)}) \ \ldots \ \exp(j\omega_m^{(R)} d_{N_R}^{(R)})]^T$ where $\omega_m^{(T)} = \frac{2\pi}{\lambda} \sin\theta_m^T$, and $\omega_m^{(R)} = \frac{2\pi}{\lambda} \sin\theta_m^R$ with λ denoting the wavelength. The matrix $\mathbf{S} = [\mathbf{s}_1 \ldots \mathbf{s}_{N_T}]^T$ contains N_T transmitted waveforms where each waveform is a vector of T snapshots. We assume that these waveforms are orthogonal so that $\frac{1}{T}\mathbf{S}\mathbf{S}^H = \mathbf{I}_{N_T}$ [LS09]. The noise matrix for the l-th pulse $\mathbf{W}_l$ is assumed to be independent and identically distributed symmetric complex Gaussian with zero-mean and covariance matrix $\sigma^2\mathbf{I}_{N_R}$. The output of (3.35) after matched filtering is given by $\mathbf{y}_l = \text{vec}(\mathbf{Y}_l) = \frac{1}{\sqrt{T}}\text{vec}(\mathbf{X}_l\mathbf{S}^H)$.

The observation can then be rewritten as a PARAFAC model [Boy11, NS10] :

$$\mathbf{y} = \left[\mathbf{y}_0^T \ldots \mathbf{y}_{L-1}^T\right]^T = \sum_{m=1}^{2} \alpha_m \mathbf{c}(f_m) \otimes \mathbf{a}_T(\omega_m^{(T)}) \otimes \mathbf{a}_R(\omega_m^{(R)}) + \mathbf{z}, \tag{3.36}$$

where $\alpha_m = \sqrt{T}\rho_m$, $\mathbf{z} = [\mathbf{z}_0^T \ldots \mathbf{z}_{L-1}^T]^T$ with $\mathbf{z}_l = \text{vec}(\frac{1}{\sqrt{T}}\mathbf{W}_l\mathbf{S}^H)$ and $\mathbf{c}(f_m) = [1 \ \exp(i2\pi f_m) \ \ldots$ $\exp(i2\pi f_m(L-1))]^T$ in which $\otimes$ denotes the Kronecker product. Since $\mathbf{W}_l$ is assumed to be i.i.d. symmetric complex Gaussian with zero-mean and covariance matrix $\sigma^2\mathbf{I}_{N_R}$, we obtain that $E\{\mathbf{z}\mathbf{z}^H\} = \sigma^2\mathbf{I}_{LN_TN_R}$. Consequently, the likelihood of the observations $\mathbf{y}$ is complex Gaussian distributed with mean $\sum_{m=1}^{2} \alpha_m \mathbf{c}(f_m) \otimes \mathbf{a}_T(\omega_m^{(T)}) \otimes \mathbf{a}_R(\omega_m^{(R)})$ and covariance $\sigma^2\mathbf{I}_{LN_TN_R}$.

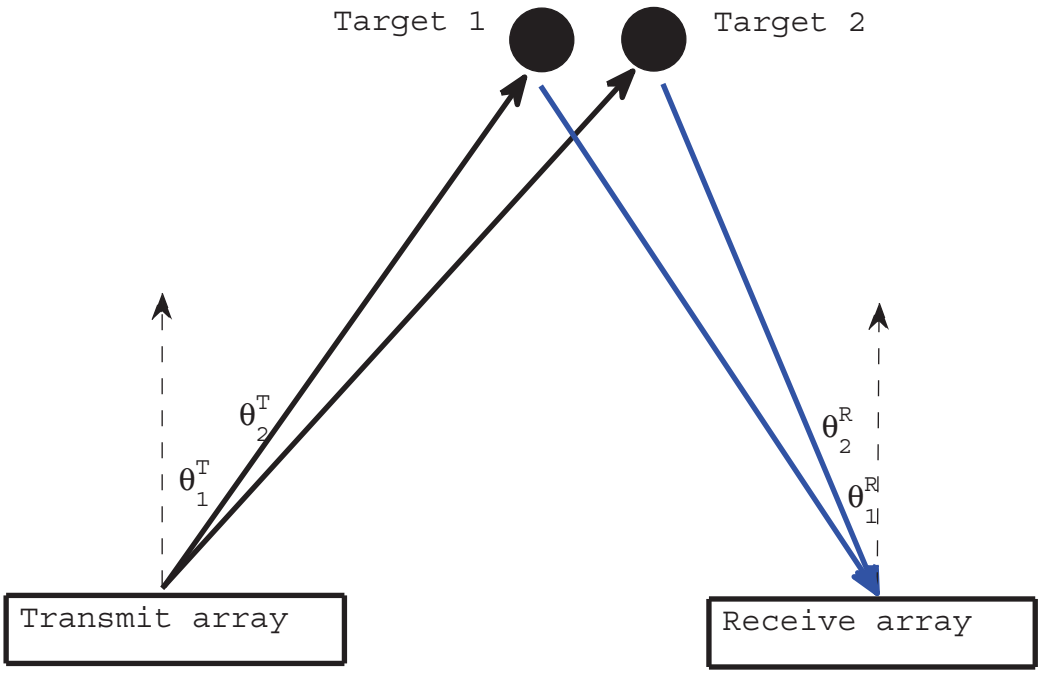

FIGURE 3.9 – Widely separated MIMO radar with two targets

3.3.2.2 Linearized detection hypothesis test

If we denote $\delta_T = \omega_2^{(T)} - \omega_1^{(T)}$ and $\delta_R = \omega_2^{(R)} - \omega_1^{(R)}$, the problem of resolving two closely spaced sources can be formulated as a binary hypothesis test as follows :

$$\begin{cases} \mathcal{H}_0 : & (\delta_T, \delta_R) = (0,0), \\ \mathcal{H}_1 : & (\delta_T, \delta_R) \neq (0,0). \end{cases} \tag{3.37}$$

Assume that δ_T and δ_R are small, by using the first-order Taylor expansion around the so-called center parameters $\omega_c^{(T)} = \frac{\omega_1^{(T)}+\omega_2^{(T)}}{2}$ and $\omega_c^{(R)} = \frac{\omega_1^{(R)}+\omega_2^{(R)}}{2}$, hence, $\omega_1^{(T)} = \omega_c^{(T)} - \frac{\delta_T}{2}$, $\omega_2^{(T)} = \omega_c^{(T)} + \frac{\delta_T}{2}$, $\omega_1^{(R)} = \omega_c^{(R)} - \frac{\delta_R}{2}$, and $\omega_2^{(R)} = \omega_c^{(R)} + \frac{\delta_R}{2}$, one can obtain the linear approximation of (3.36) as follows

$$\mathbf{y} \simeq \mathbf{G}\mathbf{Q}\boldsymbol{\delta} + \mathbf{z} \tag{3.38}$$

where $\boldsymbol{\delta} = [1\ \delta_T\ \delta_R\ \delta_T\delta_R]^T$, where $\mathbf{Q} = \text{Diag}\Big(\alpha_1+\alpha_2, \frac{j}{2}(\alpha_2-\alpha_1), \frac{j}{2}(\alpha_2-\alpha_1), -\frac{1}{4}(\alpha_1+\alpha_2)\Big)$, and where $\mathbf{G} = [\mathbf{g}_1\ \mathbf{g}_2\ \mathbf{g}_3\ \mathbf{g}_4]$ with $\mathbf{g}_1 = \mathbf{c}(f) \otimes \mathbf{a}_T(\omega_c^{(T)}) \otimes \mathbf{a}_R(\omega_c^{(R)})$, $\mathbf{g}_2 = \mathbf{c}(f) \otimes \dot{\mathbf{a}}_T(\omega_c^{(T)}) \otimes \mathbf{a}_R(\omega_c^{(R)})$, $\mathbf{g}_3 = \mathbf{c}(f) \otimes \mathbf{a}_T(\omega_c^{(T)}) \otimes \dot{\mathbf{a}}_R(\omega_c^{(R)})$, $\mathbf{g}_4 = \mathbf{c}(f) \otimes \dot{\mathbf{a}}_T(\omega_c^{(T)}) \otimes \dot{\mathbf{a}}_R(\omega_c^{(R)})$. Let $\boldsymbol{\delta}_0 = [1\ 0\ 0\ 0]^T$, then (3.37) can be rewritten as :

$$\begin{cases} \mathcal{H}_0 : & \mathbf{y} \sim \mathcal{CN}(\mathbf{G}\mathbf{Q}\boldsymbol{\delta}_0, \sigma^2\mathbf{I}), \\ \mathcal{H}_1 : & \mathbf{y} \sim \mathcal{CN}(\mathbf{G}\mathbf{Q}\boldsymbol{\delta}, \sigma^2\mathbf{I}). \end{cases} \tag{3.39}$$

3.3.2.3 Chernoff distance for detection test (3.39)

From the Stein's lemma [CT] [Che56], we have the asymptotic [4] relation between the Chernoff distance (CD) relying the two probability density functions (pdf) and a given probability of error for a hypothesis test as follows $\mathcal{CD}(p(\mathbf{y}|\mathcal{H}_0)||p(\mathbf{y}|\mathcal{H}_1)) = -\ln(P_e)$ where the Chernoff distance is defined as $\mathcal{CD}(p(\mathbf{y}|\mathcal{H}_0)||p(\mathbf{y}|\mathcal{H}_1))$, and where P_e denotes a given probability of error. In our context, the Chernoff distance can be calculated as a function of δ_T and δ_R as follows (see the Appendix 3.5.2)

$$\begin{aligned}\mathcal{CD} =& \frac{L}{16\sigma^2}\Bigg(N_R \left|\alpha_2-\alpha_1\right|^2 \sum_{n_t=1}^{N_T}\left(d_{n_t}^{(T)}\right)^2 \delta_T^2 + 2\left|\alpha_2-\alpha_1\right|^2 \sum_{n_t=1}^{N_T} d_{n_t}^{(T)} \sum_{n_r=1}^{N_R} d_{n_r}^{(R)} \delta_T\delta_R \\ &+ N_T \left|\alpha_2-\alpha_1\right|^2 \sum_{n_r=1}^{N_R}\left(d_{n_r}^{(R)}\right)^2 \delta_R^2 + \frac{1}{4}\left|\alpha_2+\alpha_1\right|^2 \sum_{n_t=1}^{N_T}\left(d_{n_t}^{(T)}\right)^2 \sum_{n_r=1}^{N_R}\left(d_{n_r}^{(R)}\right)^2 \delta_T^2\delta_R^2\Bigg).\end{aligned} \tag{3.40}$$

The behavior of the $\mathcal{CD}$ seems hard to study for general array geometries so our analysis will be focused on symmetric (possibly non-uniform) arrays. We here consider the case where both arrays are assumed to be central-symmetric linear and the center of both arrays is chosen as the reference point, *i.e.* $\sum_{n_t=1}^{N_T} d_{n_t}^{(T)} = 0$ and $\sum_{n_r=1}^{N_R} d_{n_r}^{(R)} = 0$. Denoting $\sigma_T^2 = \frac{1}{N_T}\sum_{n_t=1}^{N_T}\left(d_{n_t}^{(T)}\right)^2$ and $\sigma_R^2 = \frac{1}{N_R}\sum_{n_r=1}^{N_R}\left(d_{n_r}^{(R)}\right)^2$, the expression of the CD can be rewritten as

$$\mathcal{CD} = \frac{LN_TN_R}{16\sigma^2}\left(\left|\alpha_2-\alpha_1\right|^2\sigma_T^2\delta_T^2 + \left|\alpha_2-\alpha_1\right|^2\sigma_R^2\delta_R^2 + \frac{1}{4}\left|\alpha_2+\alpha_1\right|^2\sigma_T^2\sigma_R^2\delta_T^2\delta_R^2\right). \tag{3.41}$$

3.3.2.4 Analysis *w.r.t* the amplitudes

We consider two cases with regard to the relation between amplitude coefficients α_1 and α_2. We also denote the signal to noise ratio in dB by $SNR = 10\log_{10}\left(\frac{|\alpha_1|^2+|\alpha_2|^2}{2\sigma^2}\right)$.

1. If $\alpha_1 = \alpha_2 = \alpha$, equation (3.41) becomes

$$\frac{LN_TN_R}{32\sigma^2}\left|\alpha\right|^2\sigma_T^2\sigma_R^2\delta_T^2\delta_R^2 = -\ln(P_e). \tag{3.42}$$

Consider δ_T as fixed and $\delta_T > 0$, $\delta_R > 0$, one obtains δ_R in function of δ_T as follows

$$\delta_R = \frac{4\sqrt{-2\ln(P_e)}10^{-\frac{SNR}{20}}}{\delta_T\sigma_T\sigma_R\sqrt{LN_TN_R}}. \tag{3.43}$$

The locus of MSRL in this case is a rectangular parabola. In this scenario, we have $\delta_R = O(1/\delta_T)$ and $\delta_T = O(1/\delta_R)$ which mean that if we have a small resolution along the transmission (*resp.* reception) array, we have a large resolution along the reception (*resp.* transmission) array. It is easy to see that δ_R is minimized when both $N_T\sigma_T^2$ and $N_R\sigma_R^2$ are maximized. For antennas with fixed apertures, the maxima happens when the elements of both arrays are placed as far as possible *w.r.t* the reference points (*i.e.* the centers of the arrays in the considered geometry).

4. Note that this assumption is not severe in the context of MIMO radar since we generally dispose of a large (LN_TN_R) number of observations.

2. If $\alpha_1 \neq \alpha_2$, since the resolution limits are considered to be small, *i.e.* $\delta_T \ll 1$ and $\delta_R \ll 1$, the term containing $\delta_T^2\delta_R^2$ in (3.41) can be omitted and the Stein's lemma can be rewritten as

$$\frac{\delta_T^2}{d_T^2} + \frac{\delta_R^2}{d_R^2} = 1, \tag{3.44}$$

where $d_T^2 = \frac{-16\sigma^2 \ln(P_e)}{LN_TN_R|\alpha_2-\alpha_1|^2\sigma_T^2}$ and $d_R^2 = \frac{-16\sigma^2 \ln(P_e)}{LN_TN_R|\alpha_2-\alpha_1|^2\sigma_R^2}$. Equation (3.44) means that the locus of δ_T and δ_R is an ellipse centered at $(0\,,0)$ whose the axes are $2d_T$ and $2d_R$. Without loss of generality, if we consider δ_T fixed and assume that $\delta_R > 0$, one obtains δ_R in function of δ_T as follows

$$\delta_R = d_R\sqrt{1 - \frac{\delta_T^2}{d_T^2}}, \tag{3.45}$$

under the condition $\delta_T^2 < d_T^2$. Note that if $\sigma_T^2 = \sigma_R^2$, *i.e.* $d_T^2 = d_R^2 = d^2$, (3.44) becomes $\delta_T^2 + \delta_R^2 = d^2$ which means that the locus in this case is a circle.

3.3.2.5 Numerical results

In this Section, some simulations are presented to analyse the behavior of the MSRL. The scenario is the following : the transmit and the receive arrays are uniform linear arrays of $N_T = 4$ and $N_R = 10$ sensors, respectively, with inter-element spacing (in unit of wavelengths) is 0.5, the probability of error is fixed : $P_e = 0.02$, and the number of pulses $L = 10$. First, figure 3.10 plots the locus of δ_T and δ_R in both case $\alpha_1 = \alpha_2$ and $\alpha_1 \neq \alpha_2$. The locus of δ_T and δ_R is the curve obtained by intersecting the surface $z = \mathcal{CD}(\delta_T\,, \delta_R)$ with the plane $z = -\ln(P_e)$. One can see that the locus in the case $\alpha_1 = \alpha_2$ is a rectangular hyperbola while the locus in the case $\alpha_1 \neq \alpha_2$ is an ellipse.

Next, figure 3.11 plots δ_R versus δ_T when $SNR = 40$dB in both cases $\alpha_1 = \alpha_2$ and $\alpha_1 \neq \alpha_2$. Note that, in figure A.9(a), we also draw a vertical line that divides the curve into two regions where $\delta_R > \delta_T$ on the left hand and $\delta_R < \delta_T$ on the right hand. The value of the MSRL at the intersection between the vertical line and the curve can be analytically derived and is given by

$$\delta_T = \delta_R = \frac{d_T d_R}{\sqrt{d_T^2 + d_R^2}} = \sqrt{\frac{-16\sigma^2 \ln(P_e)}{LN_TN_R|\alpha_2 - \alpha_1|^2(\sigma_T^2 + \sigma_R^2)}}.$$

We can see here a trade-off between δ_T and δ_R. Comparing fig. A.9(a) to fig. A.9(b), we can see that when $\alpha_1 \neq \alpha_2$, one obtains better resolution limits than in the case $\alpha_1 = \alpha_2$.

Finally, we present a comparison between the collocated arrays context (TRL) and the widely spaced arrays context (MSRL). Particularly, we plot in figure 3.12, δ_R versus SNR (δ_T is considered fixed) for the case of the MSRL and δ versus SNR for the case of the TRL with two configurations : (A) $N_T = 4$ and $N_R = 10$ and (B) $N_T = 10$ and $N_R = 4$ and in two scenarios : $\alpha_1 = \alpha_2$ and $\alpha_1 \neq \alpha_2$. By resolving the equation $\delta_R = \delta$ for a given δ_T, we obtain that $\delta_R > \delta$ when $SNR \in [0, SNR_t]$ and $\delta_R < \delta$ when $SNR \in [SNR_t, \infty]$ where SNR_t is given by :

$$\begin{cases} \alpha_1 = \alpha_2 = \alpha : SNR_t = 10\log_{10}\left(\frac{-16\ln(P_e)}{\delta_T^2\sigma_T^2\sigma_R^2 LN_TN_R}\right), \\ \alpha_1 \neq \alpha_2 : SNR_t = 10\log_{10}\left(\frac{-16\ln(P_e)(|\alpha_1|^2+|\alpha_2|^2)}{\delta_T^2(\sigma_T^2+\sigma_R^2)|\alpha_2-\alpha_1|^2 LN_TN_R}\right). \end{cases}$$

3.3.2.6 Summary

In this paper, we have derived a closed-form expression of the Chernoff distance for a MIMO Radar with widely spaced linear arrays, then, we have applied the Stein's lemma to obtain the MSRL for two closely spaced targets. The analysis has provided interesting characteristics of the MSRL in this context. It has been seen that the behavior of MSRL is different in two cases $\alpha_1 = \alpha_2$ and $\alpha_1 \neq \alpha_2$. Numerical results have shown that the MSRL is better when amplitudes of two targets are not identical.

3.4 Conclusion

In this Chapter, we derived the closed-form expressions of the SRL based on estimation accuracy and the SRL based on the Stein's lemma :

- First, we derived and analyzed the angular resolution limit (ARL) based on the Lee's criterion and the Smith's criterion in the context of array processing in the presence of modeling errors. We showed that, as the signal-to-noise ratio increases, the ARL does not fall into zero (contrary to the classical case without modeling errors) and converge to a fixed limit depending on the method for which we gave a closed-form expression. It can be seen that at high SNR, the ARL in the Lee and Smith sense are linear in the error variance. We have also investigated the influence of array geometry on the ARL based on the Lee's and Smith's criteria.

- Second, we followed the approach based on the Stein's lemma to derive the SRL. We examined this approach in two difference contexts : (i) in the context of array processing, the ARL based on the Stein's lemma is derived and compared to the ARL based on the Lee's and Smith's criteria. It has been seen that the ARL based on the Chernoff distance and the Smith's criterion have a similar behavior and they are proportional by a factor which depends on the probabilities of false alarm and of detection and not of the signal parameters. We also show that for orthogonal sources and/or a large number of snapshots, it is possible to give a unified expression of the ARL for the three considered approaches. (ii) In the context of MIMO radar, the ARL is derived when the transmitting array and the receiving array are either widely spaced or collocated. It has been seen that the behavior of resolution limit is different when the amplitudes of the targets are identical or not. Numerical results have shown that the resolution limit is better when the amplitudes of two targets are not identical.

3.5 Appendix

3.5.1 CRB Derivation

The vector of unknown parameters is $\boldsymbol{\omega} = [\omega_1\, \omega_2]^T$. It is well known that for a Gaussian parameterized model, the CRB is the inverse of the Fisher information matrix (FIM), defined by $\mathbf{F}(\boldsymbol{\omega})$. Hence, to calculate the CRB, first, we calculate the set of elements of the FIM using the Slepian-Bang formula (see, *e.g.*, [Kay93]) as follows

$$
\begin{aligned}
\mathbf{F}(\omega_1,\omega_1) &= 2\mathcal{R}\Big\{(\mathbf{s}_1^H \otimes \dot{\mathbf{a}}(\omega_1)^H)\mathbf{C}^{-1}(\mathbf{s}_1 \otimes \dot{\mathbf{a}}(\omega_1))\Big\} \\
&= 2\sum_{n=1}^{N} d_n^2 \mathbf{s}_1^H \mathbf{R}^{-1}\mathbf{s}_1, \\
\mathbf{F}(\omega_2,\omega_2) &= 2\mathcal{R}\Big\{(\mathbf{s}_2^H \otimes \dot{\mathbf{a}}(\omega_2)^H)\mathbf{C}^{-1}(\mathbf{s}_2 \otimes \dot{\mathbf{a}}(\omega_2))\Big\} \\
&= 2\sum_{n=1}^{N} d_n^2 \mathbf{s}_2^H \mathbf{R}^{-1}\mathbf{s}_2, \\
\mathbf{F}(\omega_1,\omega_2) &= 2\mathcal{R}\Big\{(\mathbf{s}_1^H \otimes \dot{\mathbf{a}}(\omega_1)^H)\mathbf{C}^{-1}(\mathbf{s}_2 \otimes \dot{\mathbf{a}}(\omega_2))\Big\} \\
&= 2\mathcal{R}\Big\{\sum_{n=1}^{N} d_n^2 \exp(\frac{j}{2}d_n\delta)\mathbf{s}_1^H \mathbf{R}^{-1}\mathbf{s}_2\Big\} \\
&\overset{1}{=} 2\mathcal{R}\Big\{\sum_{n=1}^{N} d_n^2 (1+\frac{j}{2}d_n\delta)\mathbf{s}_1^H \mathbf{R}^{-1}\mathbf{s}_2\Big\} \\
&= 2\sum_{n=1}^{N} d_n^2 \mathcal{R}\big\{\mathbf{s}_1^H \mathbf{R}^{-1}\mathbf{s}_2\big\} + \delta\mathcal{R}\big\{j\mathbf{s}_1^H \mathbf{R}^{-1}\mathbf{s}_2\big\}\sum_{n=1}^{N} d_n^3, \\
\mathbf{F}(\omega_2,\omega_1) &= 2\mathcal{R}\Big\{(\mathbf{s}_2^H \otimes \dot{\mathbf{a}}(\omega_2)^H)\mathbf{C}^{-1}(\mathbf{s}_1 \otimes \dot{\mathbf{a}}(\omega_1))\Big\} \\
&= 2\mathcal{R}\Big\{\sum_{n=1}^{N} d_n^2 \exp(\frac{j}{2}d_n\delta)\mathbf{s}_2^H \mathbf{R}^{-1}\mathbf{s}_1\Big\} \\
&\overset{1}{=} 2\mathcal{R}\Big\{\sum_{n=1}^{N} d_n^2 (1+\frac{j}{2}d_n\delta)\mathbf{s}_2^H \mathbf{R}^{-1}\mathbf{s}_1\Big\} \\
&= 2\sum_{n=1}^{N} d_n^2 \mathcal{R}\big\{\mathbf{s}_2^H \mathbf{R}^{-1}\mathbf{s}_1\big\} + \delta\mathcal{R}\big\{j\mathbf{s}_2^H \mathbf{R}^{-1}\mathbf{s}_1\big\}\sum_{n=1}^{N} d_n^3,
\end{aligned}
$$

where $\mathcal{R}\{.\}$ is the real part of a complex number.The off terms of the CRB are linearized thanks to a first-order Taylor expansion since δ is small. Note that, by using the Schur complement, the inversion of the matrix $\mathbf{R}$ can be given by

$$
\begin{aligned}
\mathbf{R}^{-1} &= \frac{1}{\sigma^2}\big(\mathbf{I}_L + \frac{\sigma_e^2}{\sigma^2}[\mathbf{s}_1\,\mathbf{s}_2][\mathbf{s}_1\,\mathbf{s}_2]^H\big)^{-1} \\
&= \frac{1}{\sigma^2}\Big(\mathbf{I}_L - \frac{\sigma_e^2}{\sigma^2}[\mathbf{s}_1\,\mathbf{s}_2]\big(\mathbf{I}_2 + \frac{\sigma_e^2}{\sigma^2}[\mathbf{s}_1\,\mathbf{s}_2]^H[\mathbf{s}_1\,\mathbf{s}_2]\big)^{-1}[\mathbf{s}_1\,\mathbf{s}_2]^H\Big) \\
&= \frac{1}{\sigma^2}\left(\mathbf{I}_L - \frac{\sigma_e^2}{\sigma^2}[\mathbf{s}_1\,\mathbf{s}_2]\begin{bmatrix} 1+\frac{\sigma_e^2}{\sigma^2}||\mathbf{s}_1||^2 & \frac{\sigma_e^2}{\sigma^2}\mathbf{s}_1^H\mathbf{s}_2 \\ \frac{\sigma_e^2}{\sigma^2}\mathbf{s}_2^H\mathbf{s}_1 & 1+\frac{\sigma_e^2}{\sigma^2}||\mathbf{s}_2||^2 \end{bmatrix}^{-1}[\mathbf{s}_1\,\mathbf{s}_2]^H\right) \\
&= \frac{1}{\sigma^2}\left(\mathbf{I}_L - \frac{\sigma_e^2}{\sigma^2\Big(\big(1+\frac{\sigma_e^2}{\sigma^2}L\big)^2 - \frac{\sigma_e^4}{\sigma^4}|\rho|^2\Big)}\Big(\big(1+\frac{\sigma_e^2}{\sigma^2}L\big)\mathbf{s}_1\mathbf{s}_1^H - \frac{\sigma_e^2}{\sigma^2}\mathbf{s}_2\mathbf{s}_2^H\mathbf{s}_1\mathbf{s}_1^H - \frac{\sigma_e^2}{\sigma^2}\mathbf{s}_1\mathbf{s}_1^H\mathbf{s}_2\mathbf{s}_2^H \right.\right. \\
&\qquad\qquad \left.\left. + \big(1+\frac{\sigma_e^2}{\sigma^2}L\big)\mathbf{s}_2\mathbf{s}_2^H\Big)\right)
\end{aligned}
$$

$$= \frac{1}{\sigma^2}\Bigg(\mathbf{I}_L - \frac{\sigma_e^2}{\sigma^2\Big(\big(1+\frac{\sigma_e^2}{\sigma^2}L\big)^2 - \frac{\sigma_e^4}{\sigma^4}|\rho|^2\Big)}\Bigg(\Big(\big(1+\frac{\sigma_e^2}{\sigma^2}L\big) - \frac{\sigma_e^2}{\sigma^2}\mathbf{s}_2\mathbf{s}_2^H\Big)\mathbf{s}_1\mathbf{s}_1^H + \Big(\big(1+\frac{\sigma_e^2}{\sigma^2}L\big) - \frac{\sigma_e^2}{\sigma^2}\mathbf{s}_1\mathbf{s}_1^H\Big)\mathbf{s}_2\mathbf{s}_2^H\Big)\Bigg), \tag{3.46}$$

where $s = \mathbf{s}_1^H\mathbf{s}_2$. After some derivation, one obtains

$$\begin{aligned}\mathbf{s}_1^H\mathbf{R}^{-1}\mathbf{s}_1 = \mathbf{s}_2^H\mathbf{R}^{-1}\mathbf{s}_2 &= \frac{\sigma^2 L + \sigma_e^2(L^2 - |\rho|^2)}{\sigma^4 + \sigma_e^2(\sigma_e^2L^2 + 2\sigma^2L - \sigma_e^2|\rho|^2)},\\ \mathbf{s}_2^H\mathbf{R}^{-1}\mathbf{s}_1 = \mathbf{s}_1^H\mathbf{R}^{-1}\mathbf{s}_2 &= \frac{\sigma^2 s}{\sigma^4 + \sigma_e^2(\sigma_e^2L^2 + 2\sigma^2L - \sigma_e^2|\rho|^2)}.\end{aligned} \tag{3.47}$$

Using the result from (3.47), one can see that $\mathbf{F}(\omega_1,\omega_2) = \mathbf{F}(\omega_2,\omega_1)$ and $\mathbf{F}(\omega_1,\omega_1) = \mathbf{F}(\omega_2,\omega_2)$. Inverting the FIM, one can obtain the elements of the CRB, denoted by $\mathbf{B}$, as follows

$$\begin{aligned}\mathbf{B}(\boldsymbol{\omega}) &= \mathbf{F}^{-1}(\boldsymbol{\omega})\\ &\overset{1}{=} \frac{1}{\mathbf{F}(\omega_1,\omega_1)^2 - \mathbf{F}(\omega_1,\omega_2)^2}\begin{bmatrix}\mathbf{F}(\omega_1,\omega_1) & -\mathbf{F}(\omega_1,\omega_2)\\ -\mathbf{F}(\omega_1,\omega_2) & \mathbf{F}(\omega_1,\omega_1)\end{bmatrix}.\end{aligned} \tag{3.48}$$

3.5.2 Chernoff Distance Derivation

The CD between two Gaussian distributions with parameterized means, $\mathbf{y}|\mathcal{H}_0 \sim \mathcal{CN}(\boldsymbol{\mu}_0, \sigma^2\mathbf{I})$ and $\mathbf{y}|\mathcal{H}_1 \sim \mathcal{CN}(\boldsymbol{\mu}_1, \sigma^2\mathbf{I})$, is given by [CT]

$$\mathcal{CD}(p(\mathbf{y}|\mathcal{H}_0)||p(\mathbf{y}|\mathcal{H}_1)) = \underset{0\le k\le 1}{max} - \log\eta(k), \tag{3.49}$$

where

$$\begin{aligned}\eta(k) &= \int_\Omega [p(\mathbf{y}|\mathcal{H}_0)]^{1-k}[p(\mathbf{y}|\mathcal{H}_1)]^k d\mathbf{y}\\ &= \int_\Omega \frac{1}{\pi^{LN_TN_R}|\sigma^2\mathbf{I}|}\exp\Bigg(-\frac{1-k}{\sigma^2}(\mathbf{y}-\boldsymbol{\mu}_0)^H(\mathbf{y}-\boldsymbol{\mu}_0) - \frac{k}{\sigma^2}(\mathbf{y}-\boldsymbol{\mu}_1)^H(\mathbf{y}-\boldsymbol{\mu}_1)\Bigg)d\mathbf{y}.\end{aligned} \tag{3.50}$$

$$= \exp\Big(\frac{(k-1)k}{\sigma^2}||\boldsymbol{\mu}_1 - \boldsymbol{\mu}_0||^2\Big). \tag{3.51}$$

Consequently, (3.49) can be rewritten as

$$\mathcal{CD}(p(\mathbf{y}|\mathcal{H}_0)||p(\mathbf{y}|\mathcal{H}_1)) = \underset{0\le k\le 1}{max} - \frac{(k-1)k}{\sigma^2}||\boldsymbol{\mu}_1 - \boldsymbol{\mu}_0||^2. \tag{3.52}$$

Since $\frac{1}{\sigma^2}(\boldsymbol{\mu}_1-\boldsymbol{\mu}_0)^H(\boldsymbol{\mu}_1-\boldsymbol{\mu}_0)$ does not depend on k and it is easy to see that $-(k-1)k$ is maximized when $k = 1/2$, the Chernoff's distance between two Gaussian distributions with parameterized means is given by $\mathcal{CD}(p(\mathbf{y}|\mathcal{H}_0)||p(\mathbf{y}|\mathcal{H}_1)) = \frac{1}{4\sigma^2}||\boldsymbol{\mu}_1 - \boldsymbol{\mu}_0||^2$. In our context, we have $\boldsymbol{\mu}_0 = \mathbf{GQ}\boldsymbol{\delta}_0$ and $\boldsymbol{\mu}_1 = \mathbf{GQ}\boldsymbol{\delta}$, consequently, one obtains (3.40).

3.5.3 ARL Derivation for collocated MIMO radar

In the context of collocated MIMO radar, each point target is now located by only one angle ω_m, $m = 1\,, 2$, hence, the problem of TMRL becomes mono-dimensional, *i.e.*, $\delta_T = \delta_R = \delta$. After some calculations, the analysis *w.r.t* the amplitudes for this context is simplified as follows :

1. $\alpha_1 = \alpha_2 = \alpha : \delta = \sqrt[4]{\frac{-32\ln(P_e)10^{-\frac{SNR}{10}}}{LN_TN_R\sigma_T^2\sigma_R^2}}$
2. $\alpha_1 \neq \alpha_2 : \delta = \sqrt{\frac{-16\sigma^2\ln(P_e)}{LN_TN_R|\alpha_2-\alpha_1|^2(\sigma_T^2+\sigma_R^2)}}$

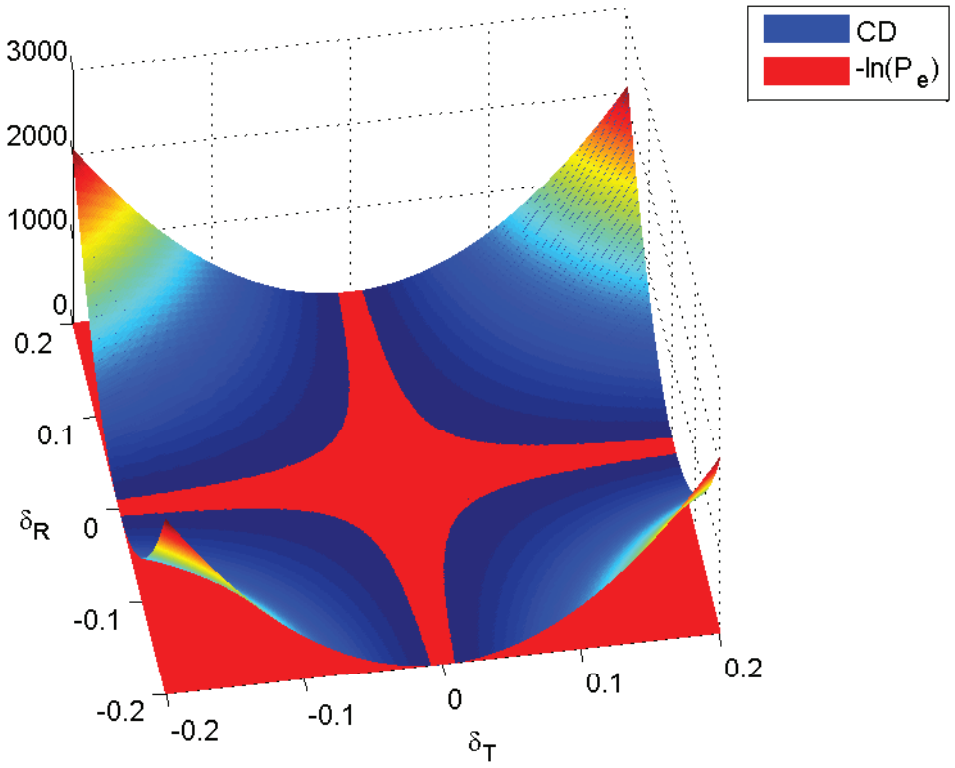

(a) $\alpha_1 = \alpha_2$

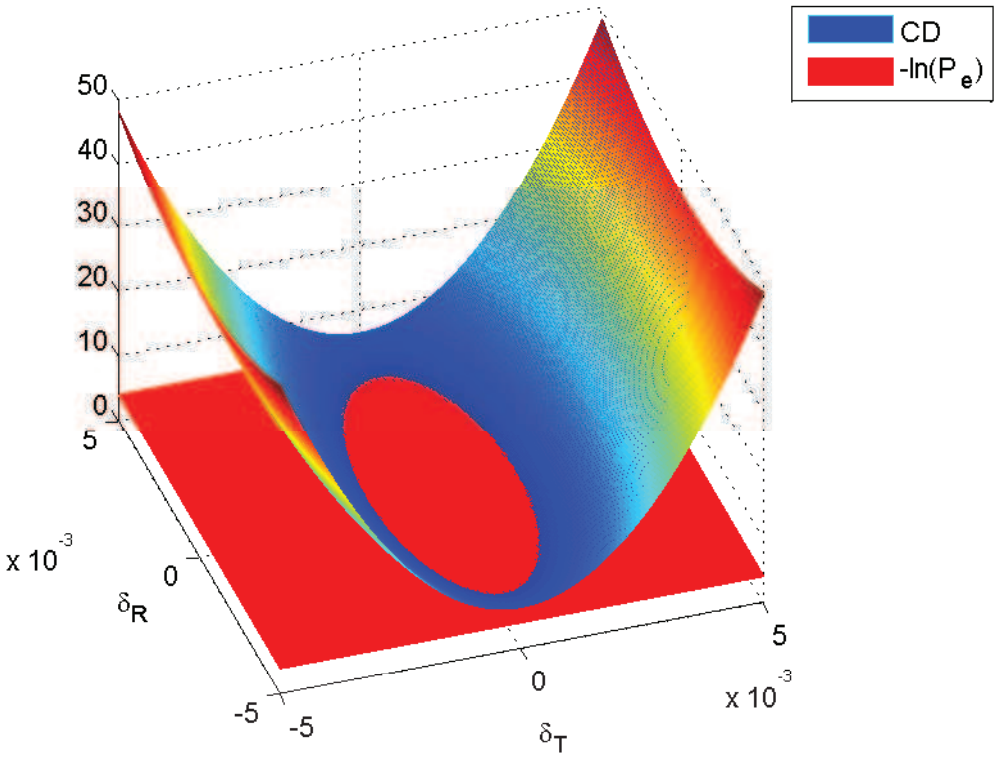

(b) $\alpha_1 \neq \alpha_2$

FIGURE 3.10 – $\mathcal{CD}$ with respect to δ_T and δ_R for $SNR = 40$dB, $P_e = 0.02$.

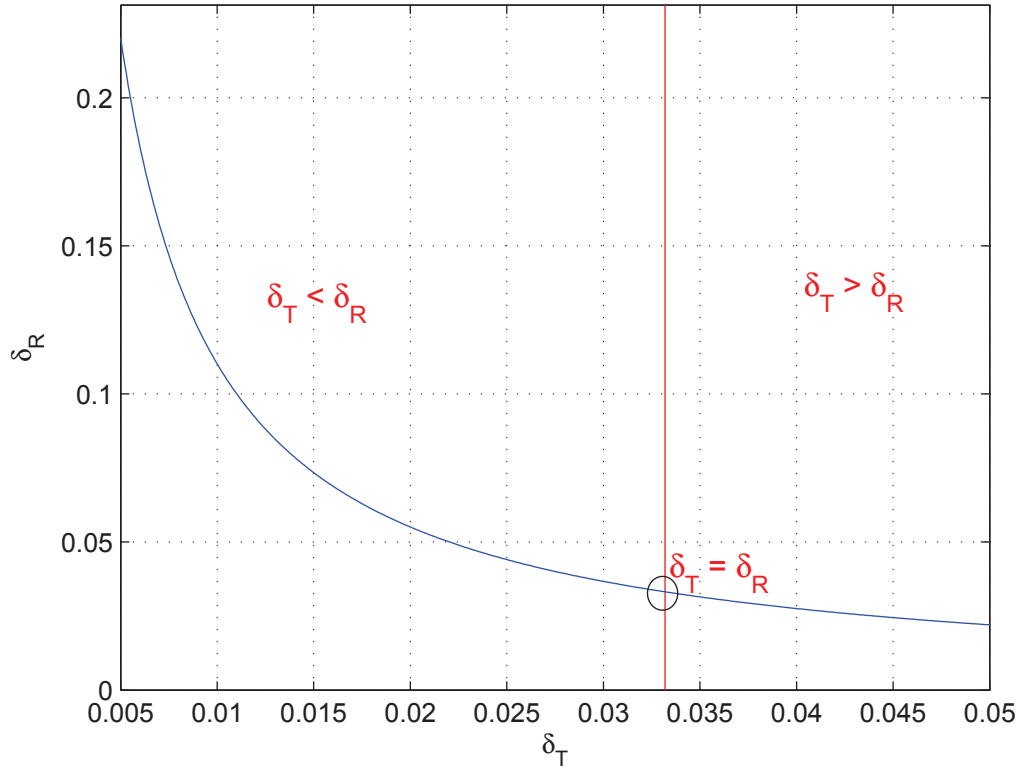

(a) $\alpha_1 = \alpha_2$

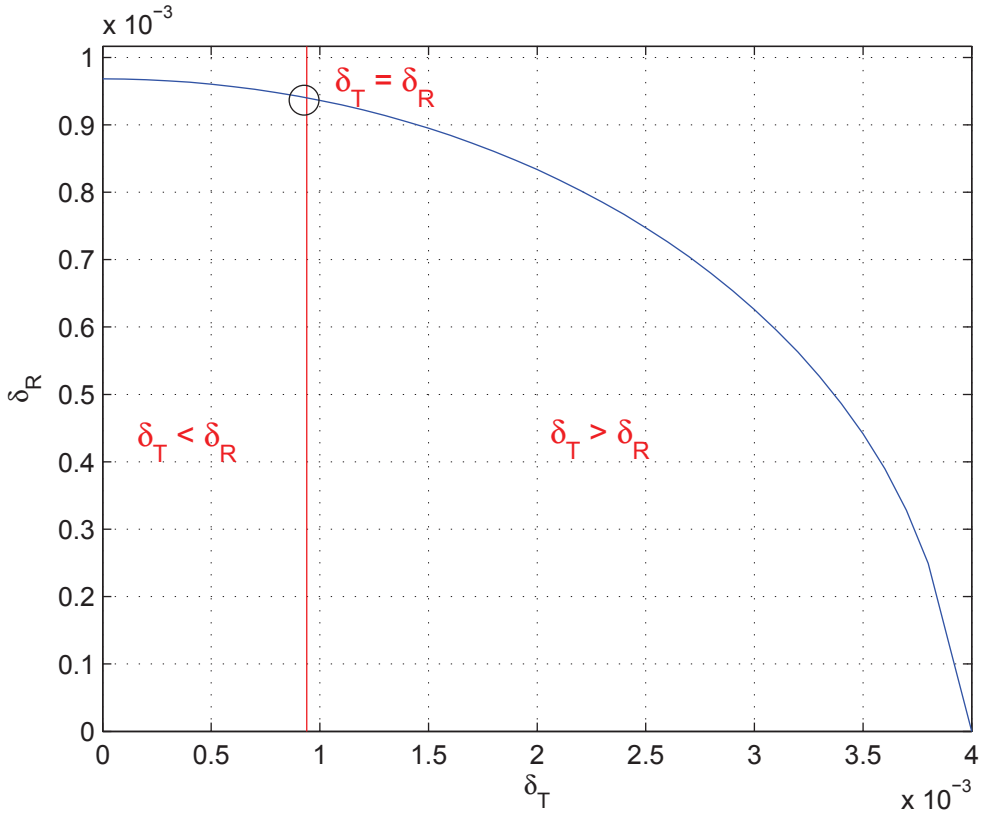

(b) $\alpha_1 \neq \alpha_2$

FIGURE 3.11 – δ_R versus δ_T for $SNR = 40$dB, $P_e = 0.02$

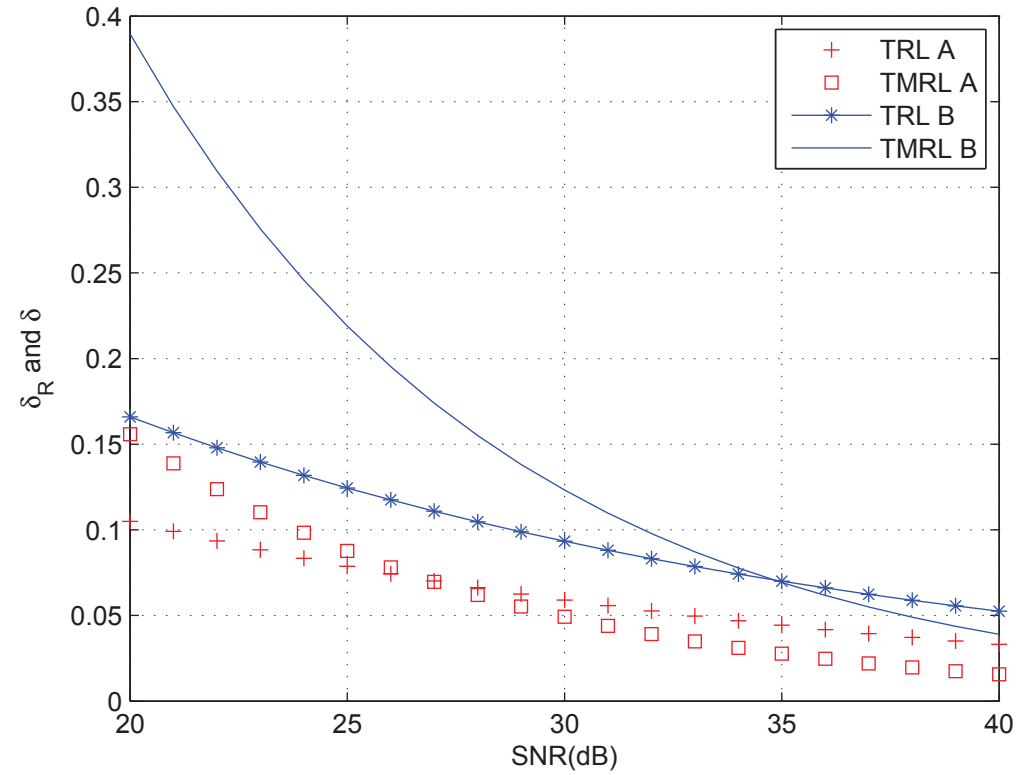

(a) $\alpha_1 = \alpha_2$

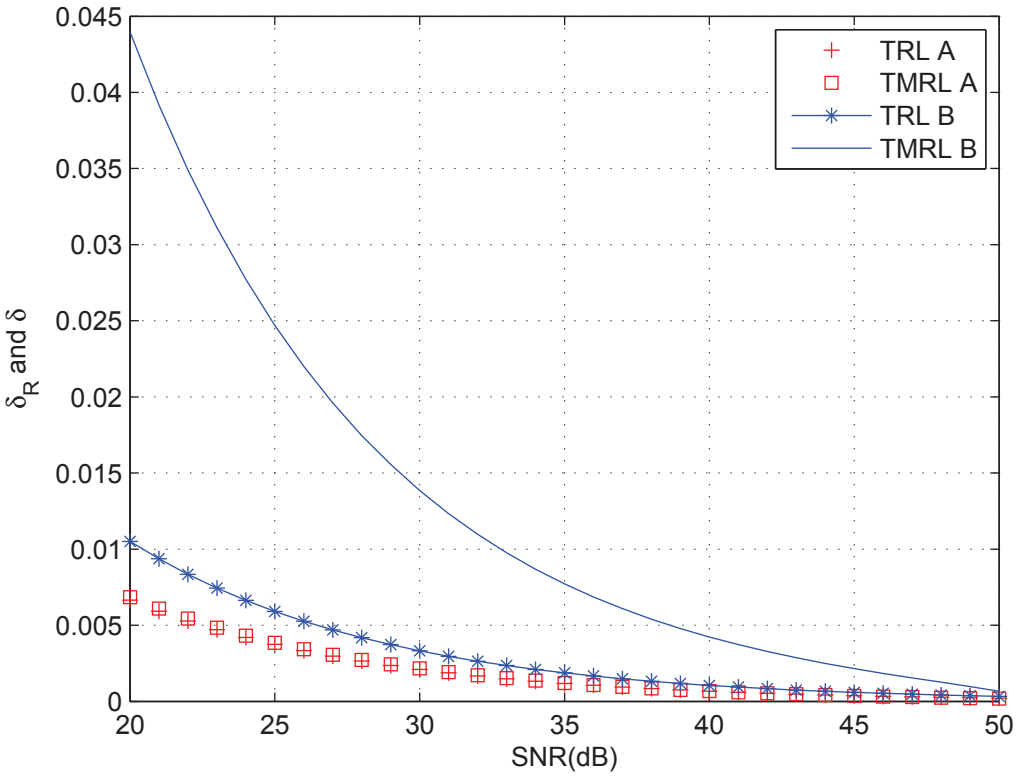

(b) $\alpha_1 \neq \alpha_2$

FIGURE 3.12 – δ_R and δ versus SNR for $P_e = 0.02$

Chapitre 4

Conclusion and perspectives

This thesis concerns the applications of theoretical tools in signal processing. For this purpose, we have studied the lower bounds on the estimation performance and the statistical resolution limit for two closely spaced sources. We have shown the usefulness of these theoretical tools in answering many different practical problems. The contributions of this thesis were presented in two chapters.

- In Chapter 2, we have examined the lower bounds in two different contexts. The first one is the target localization using the MIMO radar for which we have developed the Weiss-Weinstein bound for Bayesian parameter and the CRB for deterministic parameter in the presence of modeling errors. For the Bayesian case, we have shown that the Weiss-Weinstein bound for the parameter of interest provides a good prediction of the MSE in all regions. It also predicts the threshold SNR location near the threshold SNR indicated by the maximum *a posteriori* estimator. We also introduced a numerical procedure to optimize antenna geometry of MIMO radar in terms of the MSE. For the case with modeling errors, we have derived closed-form expressions of the Fisher information matrix and shown its block diagonal structure to deduce the Cramér-Rao bound expressions of the angle-of-arrival and of the angle-of-departure. We have shown that, under a certain signal-to-noise ratio, the performance of the system cannot be improved. Finally, we have proposed a simple formula to evaluate this critical value of the signal-to-noise ratio. The second context is the pulse phase estimation of X-ray pulsars for which we have derived the closed-form expressions of the Quinlan-Chaumette-Larzabal bound for the deterministic parameter and the Weiss-Weinstein bound for the Bayesian parameter. We have shown that both types of lower bound provide good prediction of the threshold location depending on the estimation framework while the computational complexity remains very low in comparison to the maximum likelihood estimator.

- In Chapter 3, we derived the closed-form expressions of the SRL based on estimation accuracy and the SRL based on the Stein's lemma. First, we derived and analyzed the angular resolution limit (ARL) based on the Lee's criterion and the Smith's criterion in the context of array processing in the presence of modeling errors. We showed that, as the signal-to-noise ratio increases, the ARL does not fall into zero (contrary to the classical case without modeling errors) and converges to a fixed limit depending on the method for which we gave a closed-form expression. It can be seen that at high SNR, the ARL in the Lee and Smith sense are linear in the error variance. We have also investigated the influence of array geometry on the ARL

based on the Lee's and Smith's criteria. Second, we followed the approach based on the Stein's lemma to derive the SRL. We examined this approach in two different contexts : (i) in the context of array processing, the ARL based on the Stein's lemma is derived and compared to the ARL based on the Lee's and Smith's criteria. It has been seen that the ARL based on the Chernoff distance and the Smith's criterion have a similar behavior and they are proportional by a factor which depends on the probabilities of false alarm and of detection and not of the signal parameters. We also show that for orthogonal sources and/or a large number of snapshots, it is possible to give a unified expression of the ARL for the three considered approaches. (ii) In the context of MIMO radar, the ARL is derived when the transmitting array and the receiving array are either widely spaced or collocated. It has been seen that the behavior of resolution limit is different when the amplitudes of the targets are identical or not. Numerical results have shown that the resolution limit is better when the amplitudes of two targets are not identical.

Followed the above contributions, the perspectives of this thesis are :

- Concerning the estimation performance of MIMO radar
  - The impact of modeling errors on the estimation performance of MIMO radar regardless of the type of modeling errors (phase errors or array errors) and of the type of system configuration (non-linear array, collocated arrays, ...) : in this thesis, the impact of modeling errors on the estimation performance of MIMO radar has been studied for a specific scenario, however an extended investigation is necessary to have better insight of this problem.
  - The Weiss-Weinstein bound on the estimation performance of MIMO radar for more than one source and for tracking problems : a general closed-form expression for WWB for two and more sources is required to fill this lack.
- Concerning the lower bounds for the pulse phase estimation of X-Ray pulsars taking in account the variation of observed signal frequency : in this thesis, to compare our results with other works in the literature, the observed signal frequency is assumed to be fixed. In practice, when the spacecraft is moving, the observed signal frequency varies slightly due to the Doppler effect. Hence, derivations of lower bounds for this problem with varied observed signal frequency is required since it may have an important impact on the estimation performance.
- Concerning the statistical resolution limit :
  - The impact of modeling errors on the SRL for MIMO radar : as it can be seen in this thesis, the modeling errors have an important impact on the estimation performance of MIMO radar. Therefore, a study of MIMO radar in the presence of modeling errors in terms of SRL is necessary.
  - The general expression of the SRL based on the Stein's lemma : in this thesis, closed-form expressions of the SRL based on the Stein's lemma are derived for some specific scenarios. Nevertheless, it is interesting to obtain an expression of the SRL based on this method for a general gaussian distribution.

Annexe A

Résumé

A.1 Introduction

A.1.1 Généralité

Le traitement statistique du signal est un domaine ayant de nombreuses applications dans la science et l'ingénierie. Un des buts importants du traitement du signal est d'extraire des informations pertinentes, généralement appelées paramètres d'intérêt, à partir d'un ensemble de mesures affectés par un bruit. Ces paramètres inconnus peuvent être un angle d'arrivée, une phase, un retard, etc .... La théorie de l'estimation offre un cadre formel pour résoudre ce type de problèmes. Plus particulièrement, en estimation paramétrique, nous fixons un modèle d'observation physique qui est généralement une fonction non linéaire des paramètres d'intérêt. Ensuite, à partir de la distribution de probabilité de ce modèle, nous employons un algorithme, c'est à dire une règle d'estimation, pour estimer les paramètres d'intérêt. Dans la littérature, il existe deux catégories d'estimateurs : les estimateurs optimaux (maximum de vraisemblance) et les estimateurs sous-optimaux (MUSIC). L'expérience montre que, bien que la première catégorie soit plus précise, la deuxième catégorie exige une charge de calcul moindre.

L'estimation d'un paramètre s'effectue généralement à travers la recherche d'un maximum global d'un critère dépendant de l'estimateur. La précision d'un estimateur (ou la différence entre la valeur estimée et la vraie valeur du paramètre d'intérêt) peut être quantifié par son erreur quadratique moyenne (EQM). On peut voir dans la littérature [Van68] que la variation d'EQM d'un estimateur pour un problème non-linéaire peut être divisé en trois régions par rapport au rapport signal sur bruit (RSB) ou par rapport au nombre d'observations. Dans la première région, lorsque le RSB ou le nombre d'observations est élevé, l'EQM est petite et cette région est appelé asymptotique. Ensuite, lorsque le RSB ou le nombre d'observations diminue, l'erreur d'estimation augmente rapidement, menant à l'effet du décrochement. Par conséquent, on appelle cette région la zone de décrochement. Enfin, la région dite de non-information est la zone où le RSB ou le nombre d'observations est très faible, l'observation se réduit à la composante de bruit. Ainsi, la distribution des estimées est quasi-uniforme sur le support du paramètre et l'EQM devient plate.

En général, l'EQM d'un estimateur est évaluée en utilisant des tirages de Monte Carlo. Dans chaque tirage, le paramètre estimé est recherché en tant que le maximum global d'un critère dependant l'estimateur. Par conséquent, dans un problème multi-paramètres, il nécessite une recherche multidimensionnelle, menant à une très grande charge de calcul. En outre, la méthode de Monte Carlo ne nous permet pas d'avoir une expression ana-

lytique de l'EQM, qui est essentielle pour optimiser les performances du système. Cela exige de mettre en place une autre solution qui est indépendante de tout estimateurs et qui peut donner un panorama des performances d'estimation en termes d'EQM. En traitement du signal, les bornes inférieures de l'EQM qui donnent la variance minimale qu'un estimateur peut atteindre constituent une bonne alternative. Les bornes inférieures de l'EQM peuvent être divisées en deux catégories par rapport aux hypothèses sur les paramètres [CGQL08]. Lorsque les paramètres inconnus sont supposés déterministes, les bornes dites déterministes qui évaluent le comportement "local" de l'estimateur ont été proposées. Un exemple de cette catégorie est la borne de Cramér-Rao (BCR). L'autre catégorie, les bornes bayésiennes, traite le cas où les paramètres inconnus sont supposés aléatoires avec une densité de probabilité *a priori*, de sorte qu'ils puissent évaluer le comportement "global" de l'estimateur.

Comme mentionné ci-dessus, dans la théorie de l'estimation, la borne inférieure de l'EQM semble avoir les capacités nécessaires pour étudier les performances d'estimation du système au lieu d'utiliser des tirages de Monte Carlo. Toutefois, en pratique, nombreuses questions émergent. Pouvons-nous dériver les expressions analytiques de ces bornes inférieures pour des problèmes pratiques ? Comment peuvent être utilisées ces bornes pour optimiser la performance du système ? Comment peut-on prédire le point de décrochement à l'aide de ces bornes ? Motivées par ces questions, la première partie de cette thèse examine certains problèmes pratiques pour démontrer l'utilité des bornes inférieures à caractériser et optimiser des performances d'estimation en termes de l'EQM.

Dans la littérature, une autre approche pour étudier la performance d'un système, à côté du critère de l'EQM, est le seuil statistique de résolution limite (SRL). Le SRL est la distance minimale en termes de paramètres d'intérêts entre les deux signaux permettant de séparer/estimer correctement les paramètres d'intérêt. Le problème de la SRL pour deux sources proches a sucité beaucoup d'intérêts avec des applications dans le radar, le sonar et le traitement d'image. Il y a plusieurs moyens de décrire et de dériver le SRL dans la littérature. La première façon est basée sur le pseudo-spectre des algorithmes d'estimation [Cox, KB86, AD08]. Bien que le concept de cette approche soit assez simple, son application est limitée à l'algorithme d'estimation utilisé. Par conséquent, la deuxième (et dernière) partie de cette thèse examine d'autres approches, indépendantes de l'algorithme d'estimation, pour dériver les expressions analytiques de la SRL et d'optimiser le système en utilisant ces expressions.

A.1.2 Liste des publications

Les contributions de cette thèse sont publiées (ou soumises) dans :

Revue internationale

- [TRBML12] N. D. Tran, A. Renaux, R. Boyer, S. Marcos and P. Larzabal, "Weiss-Weinstein bound for MIMO radar with colocated linear arrays for SNR threshold prediction", Elsevier Signal Processing, Volume : 92, Issue : 5, May 2012, pp. 1353-1357.
- [TRBML] N. D. Tran, A. Renaux, R. Boyer, S. Marcos and P. Larzabal, "Performance Bounds for The Pulse Phase Estimation of X-Ray Pulsars", IEEE Transactions on Aerospace and Electronic Systems, en mineur révision.
- [TBRMLb] N. D. Tran, R. Boyer, S. Marcos and P. Larzabal, "Angular Resolution Limit for array processing in the presence of modeling errors", IEEE Transactions

on Signal Processing, soumis.

Conférence

- [TRBML11a] N. D. Tran, A. Renaux, R. Boyer, S. Marcos and P. Larzabal, "MIMO radar in the presence of modelling error : a Cramér-Rao bound investigation", in Proc. of IEEE International Conference on Acoustics, Speech, and Signal Processing, ICASSP-11, Prague, Czech Republic.
- [TRBML11b] N. D. Tran, A. Renaux, R. Boyer, S. Marcos and P. Larzabal, "Radar MIMO en présence d'erreurs de modèles : une approche par les bornes de Cramér-Rao", in Proc. of Colloque GRETSI 2011, Bordeaux, France.
- [TBRMLc] N. D. Tran, R. Boyer, A. Renaux, S. Marcos and P. Larzabal, " Theoretical Multidimentional Resolution Limit for MIMO Radar based on the Chernoff distance", IEEE Workshop on Statistical Signal Processing, SSP-2012, Chicago, USA, accepté.
- [TBRMLd] N. D. Tran, R. Boyer, S. Marcos and P. Larzabal, "Angular Resolution Limit for array processing : estimation and information theory approaches", European Signal Processing Conference, EUSIPCO-2012, Bucharest, Rumania, accepté.

A.2 Applications des bornes inférieures de l'EQM au radar MIMO et à l'estimation de phase de signaux pulsars à rayon X

A.2.1 Introduction

Dans la littérature du traitement du signal, les bornes inférieures de l'EQM sont parfois utilisées pour estimer l'EQM elle même qui est parfois plus difficile à obtenir. Rigoureusement, les bornes inférieures de l'EQM donnent la variance minimale qu'un estimateur peut atteindre et elles peuvent être divisées en deux catégories selon les hypothèses sur les paramètres [CGQL08]. Lorsque les paramètres inconnus sont supposés déterministe, les bornes déterministes qui évaluent le comportement "local" de l'estimateur ont été proposés. Des exemples de cette catégorie sont la borne de Cramér-Rao (BCR) et les bornes de la famille Barankin comme la borne de McAulay-Seidman [MS69] et la borne de Quinlan-Chaumette-Larzabal (BQCL) [CGQL08]. L'autre catégorie, les bornes bayésiennes, traitent le cas où les paramètres inconnus sont supposés aléatoires avec une densité de probabilité *a priori*, de sorte qu'elles puissent évaluer le comportement "global" de l'estimateur. Les représentants de cette catégorie sont la borne de Weiss-Weinstein (BWW) [WW85] et la borne de Ziv-Zakai [ZZ69].

Pour des bornes déterministes, la BCR est la première à avoir été proposée et aussi la plus populaire en raison de sa simplicité de calcul et du fait que dans la région asymptotique, cette borne peut être atteinte sous certains conditions par l'estimateur du maximum de vraisemblance (MV). Toutefois, la limitation de la BCR montre que lorsque le RSB ou le nombre d'observations se réduit à une limite critique, le phénomène de décrochement des performances en terme d'EQM apparaît. Ce phénomène peut s'expliquer par la déformation de la fonction de coût utilisée par les estimateurs où un extremum global apparaît en un point éloigné de la vraie valeur du paramètre [RB74]. Typiquement, la valeur du point de décrochement peut être prédite en utilisant d'autres bornes plus précises que la BCR comme les bornes de la famille Barankin. Mathématiquement, la

borne Barankin (BB) [Bar49] est connue pour être plus précise que la BCR, cependant, elle n'est pas calculable directement. En traitement d'antenne classique, pour obtenir une BB calculable, plusieurs approximations ont été proposées [CGQL08] et l'une des bornes la plus précise dans la famille Barankin est la BQCL [CGQL08] qui, avec la BCR, seront examinées dans ce travail.

Comme une alternative au cas déterministe, les bornes bayésiennes fournissent une approximation de l'EQM sur toute les régions du RSB ou du temps d'observation avec une bonne prédiction du point de décrochement. Les bornes bayésiennes traitent le cas où les paramètres inconnus sont supposés aléatoires avec une densité de probabilité *a priori*. Par conséquent, l'avantage des bornes bayésiennes sur les bornes déterministes, résident dans leur capacité à donner des limites fondamentales d'un estimateur en termes de l'EQM sur toute les régions du RSB ou du nombre d'observations. On peut trouver dans la littérature les types différentes de bornes bayésiennes tel que : la borne de Ziv-Zakai [ZZ69], la borne de Bell-Steinberg-Ephraïm-Van [BSET97], la borne de Bobrovsky-Zakai [BZ76], la borne d'Abel bayésienne [RFLR06], et la borne de Weiss-Weinstein (BWW) [WW85,RO07a,RO07b]. On notera que toutes ces bornes bayésiennes ne sont pas capables de prendre en compte le cas d'un *a priori* uniforme sur les paramètres d'intérets.

L'objectif principal de ce chapitre est de démontrer l'utilité des bornes inférieures pour la caractérisation et la prédiction des performances d'estimation en termes de l'EQM, dans le cas de paramètres déterministes et aléatoires. Par conséquent, nous considérons ici deux applications dans deux domaines différents. La première est la localisation de sources à l'aide d'un radar MIMO, qui est une technologie émergente dans le traitement d'antenne. L'autre application est l'estimation de la phase de signaux pulsars à rayon X qui est une solution potentielle pour la navigation autonome dans l'espace. On notera que les travaux concernant les signaux pulsars présentés dans ce chapitre apportent également de nouvelles formes analytiques dans un cas non-gaussien puisque dans ce problème, les observations sont modélisées avec une distribution de Poisson généralisée. A notre connaissance, il y a très peu de résultats sur des bornes inférieures concernant à ce genre de densité de probabilité. On peut citer ici les travaux dans [AL01] et [Mar97] où le comportement de la BCR ainsi qu'une approximation simple de la borne Barankin sont étudiés dans le contexte de la tomographie par émission. Cependant, ces articles ne considèrent pas le cas bayésien.

La première contribution de ce chapitre est d'étudier les performances d'estimation d'un radar MIMO en termes d'EQM. Depuis qu'il a été introduit [FHB+04], le radar MIMO a reçu beaucoup d'attention de la part des chercheurs et des praticiens. Un radar MIMO est un système composé de plusieurs voies d'émission indépendantes entre elles et d'un ensemble de récepteurs. Cette technologie a été initialement proposée dans les années 80 par des Français (Radar à Impulsion et Antenne Synthétique (RIAS) développé par l'ONERA [DGA89]) mais était limité par les possibilités de traitement disponibles à l'époque. Le sujet est revenu récemment sur le devant de la scène grâce à l'amélioration constante des outils de calculs. En particulier, il a été démontré que ce type de système permet une amélioration significative des performances qu'elles soient de détection ou de localisation par rapport aux antennes phases classiques (on citera l'ouvrage collectif récent [LS09]).

Pour la localisation de sources, la supériorité des performances du radar MIMO par rapport à un réseau d'antennes phasé classique a déjà été étudiée à l'aide des bornes inférieures de l'EQM. À notre connaissance, tous les travaux existants dans la littérature concernent uniquement le cas de paramètres déterministes. Dans [FHB+04], les calculs préliminaires de la BCR ont été introduits. Le système considéré était composé d'antennes

linéaires et uniformes (ALU). Dans [GHB08] et [HBGH08], un radar MIMO avec des antennes largement séparées a été étudiée et la BCR a été calculée pour les paramètre angulaire et de vitesse de la cible. Par ailleurs, Jian Li *et al.* ont étudié l'optimisation de forme d'onde d'un radar MIMO basée sur la BCR en utilisant des ALU colocalisées [LXS+08, Boy11]. Alors que tous les travaux ci-dessus ont exploité la région asymptotique de l'EQM, la borne de Barankin a été calculée pour donner une approximation du seuil de décrochement en terme de RSB dans le scénario d'une antenne colocalisée circulaire [Tab06, LS09] (chapitre 4).

Toutes ces travaux susmentionné se sont limités au cas où les paramètres inconnus sont supposés déterministe. Pour avoir une analyse complète des performances d'un radar MIMO dans un contexte bayésienn, nous nous concentrons, dans la section A.2.2, sur la Borne de Weiss-Weinstein (BWW), qui est l'une des bornes bayésiennes les plus précises [RFL05, RFL+08]. Le scénario concerne l'estimation de la direction d'arrivée (DDA) et du coefficient lié à la surface équivalente radar (SER) d'une cible en utilisant un radar MIMO avec les antennes colocalisées. Nos résultats sont dérivés dans le cas d'antenne linéaire (possiblement non uniforme). Nous proposons tout d'abord une borne stricte pour laquelle il n'est pas possible d'obtenir une expression analytique. Quand une intégration numérique n'est pas possible, nous proposons également une expression analytique basée sur une approximation.

Comme susmentionné, un système radar MIMO permet d'obtenir des performances d'estimation et de détection supérieures par rapport à une antenne phasée classique. Toutefois, ces bonnes performances ne peuvent être atteintes que lorsque le modèle d'observation du radar MIMO est connu avec précision car les techniques puissantes de détection/estimation utilisées sont souvent basés sur des algorithmes optimaux, tels que la technique du maximum de vraisemblance. En effet, dans la littérature, le modèle d'observation du système est supposé précisement connu (par exemple la position des capteurs). Toutefois, en pratique, le modèle supposé peut être différent du vrai modèle à cause de la variation des positions des éléments de l'antenne ou du fait que les capteurs ne sont pas omnidirectionnels. Même si ce décalage est généralement corrigé par une étape de calibration, les imperfections dans le réseau d'antenne existent toujours et dégradent les performances du système. Par ailleurs, une procédure de calibration est généralement coûteuse. Par conséquent, il est important d'étudier l'impact des erreurs de modélisation dans les systèmes radar MIMO afin de quantifier les limites sur les performances. L'étude de l'influence des erreurs de modèles dans le contexte du radar MIMO a déjà donné lieu à quelques travaux, en particulier, [GHP09], [HB10], [GHP10] et [AN10]. Toutefois, ces résultats concernent seulement l'erreur de synchronisation de phase entre l'ensemble des émetteurs et des récepteurs. En outre, dans le cadre plus classique du traitement d'antenne pour la localisation passive de sources, certains travaux ont été réalisés. On peut citer par exemple [RP87], [VS94] et plus récemment [FLV10]. Notre approche suit l'idée proposée dans [FLV10] où l'erreur affectant le vecteur directionnel est modélisée par un vecteur aléatoire gaussien ajouté au vecteur directionnel idéal. Nous dérivons des expressions analytiques des bornes de Cramér-Rao pour la localisation d'une source par un radar MIMO lorsque l'émetteur et le récepteur sont largement espacés.

Nous montrons que, lorsque le rapport signal sur bruit augmente, la BCR et l'EQM de l'estimateur du maximum de vraisemblance (EMV) ne tendent pas vers zéro (contrairement au cas classique sans les erreurs de modèles) et convergent vers une limite fixe dont nous donnons une expression analytique. En outre, nous donnons une expression analytique simple de la valeur critique du rapport signal sur bruit où cette limitation des

performances apparaît.

La contribution finale de ce chapitre est une étude de l'estimation de la phase de signaux pulsars à rayon X qui est une solution potentielle pour permettre une navigation précise et autonome dans l'espace profond. La solution actuelle, la navigation guidée au sol, est très précise mais dépend fortement de la communication avec la station au sol, et par conséquent, n'est pas robuste à une perte de contact. Par ailleurs, des erreurs importantes peuvent se produire dans les zones d'ombre ou à grande distance de la terre. Alors que les systèmes de navigation par satellite, tels que le Global Positioning System (GPS), aident les appareils opérant à l'intérieur de l'orbite de la constellation GPS, une solution similaire pour les véhicules spatiaux est encore une question ouverte. Dans ce contexte, un système qui utiliserait les signaux provenant de sources célestes est un candidat potentiel pour résoudre ce problème. Parmi les différents types de sources célestes, les pulsars, découverts en 1967, sont des objets célestes qui émettent des signaux très régulières, stables, et périodiques. Leur comportement a été observé pendant des années, afin que la forme et la période de leur profil d'impulsion soient connus de façon très précise. Cette propriété est très importante pour le navigation. Dans la littérature, deux types de pulsars ont été examinés pour le navigation : les sources qui émettent dans la bande radio et de sources qui émettent dans la bande X. Nous considérons ici les pulsars à rayon X pour leur faisabilité dans la mise en œuvre (grâce à des détecteurs de taille plus petits par rapport à ceux de la bande radio) et une meilleure précision [RWP06].

Lors d'une navigation basée sur des signaux pulsar, le signal observé est un temps d'arrivée (TDA) de l'impulsion (ou la phase d'impulsion) au niveau du détecteur. Le traitement de ce signal par rapport à la base de données enregistrées nous donne l'information spécifique de l'emplacement du véhicule spatial. Le principal problème dans ce genre de navigation est d'estimer très précisément la phase initiale de l'impulsion, et ce défi a été examiné dans la littérature. Dans [GS07], le modèle statistique du TDA de l'impulsion a été développé et l'estimation de la phase d'impulsion est étudiée par la dérivation et l'analyse de l'estimateur du maximum de vraisemblance (EMV) et de la borne de Cramér-Rao. Dans [ES10], l'estimateur des moindres carrés non linéaires (MCNL) est proposé et comparé à l'EMV en termes de complexité de calcul et d'EQM en fonction de temps d'observation. Dans ces deux documents, on peut observer, en termes d'EQM, le phénomène de décrochement qui apparaît quand le temps d'observation est inférieur à un seuil critique. Puisque la BCR ne peut pas capturer ce phénomène, dans la section A.2.4, nous exploitons à la fois les bornes déterministe et bayésienne pour analyser le comportement de l'EQM et prédire la position du décrochement. En particulier, nous dérivons l'expression analytique de la BQCL (cas déterministe) et de la BWW (cas bayésien), puis nous présentons quelques simulations pour confirmer la bonne capacité des bornes dérivées à prédire la performance de l'EMV.

A.2.2 Borne de Weiss-Weinstein dans le context de radar MIMO avec les antennes collocalisées

A.2.2.1 Modèle des observations

Nous considérons un radar MIMO dont l'émetteur et le récepteur sont collocalisés (voir figure 2.3). Les deux réseaux d'antennes sont supposés linéaires avec un nombre de capteurs à l'émission et à la réception noté M et N, respectivement. Dans ce contexte, l'angle de départ et l'angle d'arrivée sont identiques, donc, une source est localisée par un seul paramètre θ. Par conséquent, le modèle d'observation est donné par [LS09] :

$$\mathbf{y}(t) = \beta \mathbf{b}(\theta)\mathbf{a}^T(\theta)\mathbf{x}(t) + \mathbf{n}(t) = \beta \mathbf{C}(\theta)\mathbf{x}(t) + \mathbf{n}(t) \ , \ t = 1 \dots T, \tag{A.1}$$

où T est le nombre d'observations, β est une amplitude complexe liée à la surface équivalente radar (SER) de la cible. Le vecteur $\mathbf{x}(t)$ contient les M formes d'onde transmises avec la matrice de covariance empirique suivante : $\mathbf{R}_x = \frac{1}{T}\sum_{t=1}^{T} \mathbf{x}(t)\mathbf{x}^H(t) = Diag(\boldsymbol{\sigma}_s^2)$, où $\boldsymbol{\sigma}_s^2 = [\sigma_1^2, \dots, \sigma_M^2]^T$.
Les vecteurs directionnels pour l'émetteur et le récepteur ont les structures suivantes $\mathbf{a}(\theta) = [\exp(-j\frac{2\pi}{\lambda}a_1 \sin\theta), \dots, \exp(-j\frac{2\pi}{\lambda}a_M \sin\theta)]^T$, et $\mathbf{b}(\theta) = [\exp\left(-j\frac{2\pi}{\lambda}b_1 \sin\theta\right), \dots, \exp\left(-j\frac{2\pi}{\lambda}b_N \sin\theta\right)]^T$, où λ est la longueur d'onde, et les quantités a_i, $i = 1 \dots M$, et b_j, $j = 1 \dots N$, sont les positions nominales des capteurs (par rapport à un point de référence) du réseau d'antennes d'émission et de réception, respectivement. Enfin, les vecteurs de bruit $\{\mathbf{n}(t)\}_{t=1}^T$ sont supposés Gaussiens, circulaires, i.i.d., de moyenne nulle et de matrice de covariance $\mathbf{R}_n = \sigma_n^2 \mathbf{I}_N$.

Dans le context bayésien, le paramètre inconnu θ est supposé avoir une distribution uniforme *a priori* sur le support $[0\ , \pi]$. Pour plus de simplicité dans le calcul, nous définissons $u = \sin(\theta)$ comme le paramètre d'intérêt au lieu de travailler directement avec θ. Notez que, la densité de probabilité pour u est $p(u) = \frac{1}{\pi\sqrt{1-u^2}}$. β est supposé avoir une distribution gaussienne, circulaire et complexe, de moyenne nulle et de variance σ_β^2, c'est-à-dire $\beta \sim \mathcal{CN}(0, \sigma_\beta^2)$. On note $\mathbf{C}(\theta) = \mathbf{b}(\theta)\mathbf{a}^T(\theta) \in \mathbb{C}^{N\times M}$. Les éléments de $\mathbf{C}(\theta)$ sont donnés par $[\mathbf{C}(\theta)]_{k,l} = \left[\exp(-j\frac{2\pi}{\lambda}(a_l + b_k)\sin\theta)\right]$. Les éléments du vecteur des paramètres inconnus $\boldsymbol{\Theta} = [u, \beta_R, \beta_I]^T$ avec $\beta_R = Re\{\beta\}, \beta_I = Im\{\beta\}$, sont considérés comme statistiquement indépendants tels que la densité de probabilité jointe $p(\boldsymbol{\Theta}) = p(u)p(\beta_R)p(\beta_I)$.
Finalement, la fonction de vraisemblance pour ce modèle est donnée par

$$p(\mathbf{Y}; \boldsymbol{\Theta}) = \frac{1}{\pi^{NT}\sigma_n^{NT}} \exp\left(-\frac{1}{\sigma_n^2}\sum_{t=1}^{T}(\mathbf{y}(t) - \beta\mathbf{C}(\theta)\mathbf{x}(t))^H(\mathbf{y}(t) - \beta\mathbf{C}(\theta)\mathbf{x}(t))\right). \tag{A.2}$$

où $\mathbf{Y} = [\mathbf{y}(1), \mathbf{y}(2), \dots, \mathbf{y}(T)]$.

A.2.2.2 Borne de Weiss-Weinstein

BWW numérique

La borne de Weiss-Weinstein [WW85], notée **BWW**, des paramètres inconnus $\boldsymbol{\Theta} = [u, \beta_R, \beta_I]^T$ est une matrice 3×3 telle que

$$E\left\{\left(\hat{\boldsymbol{\Theta}} - \boldsymbol{\Theta}\right)\left(\hat{\boldsymbol{\Theta}} - \boldsymbol{\Theta}\right)^T\right\} \geq \mathbf{BWW} = \sup_{\substack{\mathbf{h}_i, s_i \\ i=1,2,3}} \mathbf{H}\mathbf{G}^{-1}\mathbf{H}^T, \tag{A.3}$$

où $E\left\{\left(\hat{\boldsymbol{\Theta}} - \boldsymbol{\Theta}\right)\left(\hat{\boldsymbol{\Theta}} - \boldsymbol{\Theta}\right)^T\right\}$ est l'EQM de l'estimateur bayésien $\hat{\boldsymbol{\Theta}}$ et $\mathbf{H} = [\mathbf{h}_1, \mathbf{h}_2, \mathbf{h}_3]$ est la matrice 3×3 de points tests. Les éléments de la matrice $\mathbf{G}$ sont donnés par

$$[\mathbf{G}]_{kl} = \frac{E\left\{[L^{s_k}(\mathbf{Y}; \boldsymbol{\Theta} + \mathbf{h}_k, \boldsymbol{\Theta}) - L^{1-s_k}(\mathbf{Y}; \boldsymbol{\Theta} - \mathbf{h}_k, \boldsymbol{\Theta})][L^{s_l}(\mathbf{Y}; \boldsymbol{\Theta} + \mathbf{h}_l, \boldsymbol{\Theta}) - L^{1-s_l}(\mathbf{Y}; \boldsymbol{\Theta} - \mathbf{h}_l, \boldsymbol{\Theta})]\right\}}{E\left\{L^{s_k}(\mathbf{Y}; \boldsymbol{\Theta} + \mathbf{h}_k, \boldsymbol{\Theta})\right\} E\left\{L^{s_l}(\mathbf{Y}; \boldsymbol{\Theta} + \mathbf{h}_l, \boldsymbol{\Theta})\right\}}, \tag{A.4}$$

où $L(\mathbf{Y}; \boldsymbol{\Theta} + \mathbf{h}_i, \boldsymbol{\Theta}) = \frac{p(\mathbf{Y}, \boldsymbol{\Theta} + \mathbf{h}_i)}{p(\mathbf{Y}, \boldsymbol{\Theta})}$, et $s_i \in [0, 1], i = 1, 2, 3$.

Rigoureusement, la quantité $\mathbf{HG}^{-1}\mathbf{H}^T$ doit être maximisée en fonction de $\mathbf{h}_i$ et s_i menant à une très grande charge de calcul. Cependant, il est montré [WW88, Xu01] qu'en choisissant $s_i = \frac{1}{2}, \forall i = 1, 2, 3$, et une matrice diagonale $\mathbf{H}$, on obtient une borne qui reste précise. Par conséquent, on supposera que $s_i = 1/2$, $\forall i$, et $\mathbf{H} = Diag([h_1, h_2, h_3]^T)$. Dans ce cas, les éléments de la matrice $\mathbf{G}$ sont donnés par

$$[\mathbf{G}]_{kl} = \frac{\eta(\mathbf{h}_k, \mathbf{h}_l) + \eta(-\mathbf{h}_k, -\mathbf{h}_l) - \eta(\mathbf{h}_k, -\mathbf{h}_l) - \eta(-\mathbf{h}_k, \mathbf{h}_l)}{\eta(\mathbf{h}_k, \mathbf{0})\eta(\mathbf{h}_l, \mathbf{0})},$$

où on note que $\eta(\boldsymbol{\alpha}, \boldsymbol{\gamma}) = \int_{\boldsymbol{\Upsilon}} \int_{\boldsymbol{\Omega}} p(\mathbf{Y}, \boldsymbol{\Theta} + \boldsymbol{\alpha})^{\frac{1}{2}} p(\mathbf{Y}, \boldsymbol{\Theta} + \boldsymbol{\gamma})^{\frac{1}{2}} d\mathbf{Y} d\boldsymbol{\Theta}$, où $\boldsymbol{\Omega}$ et $\boldsymbol{\Upsilon}$ sont les espaces des observations et des paramètres, respectivement, et où $\boldsymbol{\alpha} = [\alpha_1, \alpha_2, \alpha_3]^T$, et $\boldsymbol{\gamma} = [\gamma_1, \gamma_2\gamma_3]^T$.
En notant

$$\eta'(\boldsymbol{\Theta}, \boldsymbol{\alpha}, \boldsymbol{\gamma}) = \int_{\boldsymbol{\Omega}} p(\mathbf{Y}; \boldsymbol{\Theta} + \boldsymbol{\alpha})^{\frac{1}{2}} p(\mathbf{Y}; \boldsymbol{\Theta} + \boldsymbol{\gamma})^{\frac{1}{2}} d\mathbf{Y}, \tag{A.5}$$

$\eta(\boldsymbol{\alpha}, \boldsymbol{\gamma})$ est donné par

$$\eta(\boldsymbol{\alpha}, \boldsymbol{\gamma}) = \int_{\boldsymbol{\Upsilon}} \eta'(\boldsymbol{\Theta}, \boldsymbol{\alpha}, \boldsymbol{\gamma}) p(\boldsymbol{\Theta} + \boldsymbol{\alpha})^{\frac{1}{2}} p(\boldsymbol{\Theta} + \boldsymbol{\gamma})^{\frac{1}{2}} d\boldsymbol{\Theta}. \tag{A.6}$$

En utilisant (A.2) dans (2.6), on obtient l'expression analytique pour η' comme suit (voir **Appendice** 2.6.1 pour le calcul détaillé)

$$\eta'(\boldsymbol{\Theta}, \boldsymbol{\alpha}, \boldsymbol{\gamma}) = \exp\left(-\frac{1}{4\sigma_n^2} \sum_{t=1}^{T} \left[\mathbf{f}(\boldsymbol{\Theta} + \boldsymbol{\alpha}, t) - \mathbf{f}(\boldsymbol{\Theta} + \boldsymbol{\gamma}, t)\right]^H \left[\mathbf{f}(\boldsymbol{\Theta} + \boldsymbol{\alpha}, t) - \mathbf{f}(\boldsymbol{\Theta} + \boldsymbol{\gamma}, t)\right] \right), \tag{A.7}$$

où $\mathbf{f}(\boldsymbol{\Theta}, t) = \beta \mathbf{C}(\theta)\mathbf{x}(t)$. Par conséquent,

$$\eta(\boldsymbol{\alpha}, \boldsymbol{\gamma}) = \int_{\boldsymbol{\Upsilon}} \eta'(\boldsymbol{\Theta}, \boldsymbol{\alpha}, \boldsymbol{\gamma}) \frac{1}{\pi((1 - (u + \alpha_1)^2))^{\frac{1}{4}} ((1 - (u + \gamma_1)^2))^{\frac{1}{4}}} \frac{1}{\pi\sigma_\beta^2} \tag{A.8}$$

$$\exp\left(-\frac{(\beta_R - \alpha_2)^2 + (\beta_R - \gamma_2)^2}{\sigma_\beta^2} \right) \exp\left(-\frac{(\beta_I - \alpha_3)^2 + (\beta_I - \gamma_3)^2}{\sigma_\beta^2} \right) du d\beta_R d\beta_I. \tag{A.9}$$

On peut voir que dans ce cas, l'expression de la BWW n'est pas analytique (voir aussi [NT94] où la même chose apparaît dans le context de traitement d'antenne classique). C'est pourquoi nous proposons dans la suite une approximation dont nous obtiendrons une expression analytique pour la borne.

Approximation analytique de la borne

Nous proposons ici une approche différente où nous supposons que u a une loi uniforme *a priori*. Notons que cette approche a déjà été utilisé dans plusieurs travaux [Ath01, AE01, XBB04, BET96]. Nous montrons aussi par simulation (voir la partie simulation) que les deux approches donnent les bornes très proches et la même prédiction du seuil de décrochement.

Par conséquent, la matrice de **BWW** est donnée par (voir **Appendice** 2.6.2 pour les détails) :

$$\mathbf{BWW} = Diag\left(\sup_{h_1}\frac{h_1^2}{[\mathbf{G}]_{11}}, \frac{1}{2\left(TRSBR+\frac{1}{\sigma_\beta^2}\right)}, \frac{1}{2\left(TRSBR+\frac{1}{\sigma_\beta^2}\right)}\right), \tag{A.10}$$

où le rapport de signal à bruit du réseau $RSBR$ est noté par PN/σ_n^2 où $P=\sum_{k=1}^{M}\sigma_k^2$ est le puissance émise totale, et où $[\mathbf{G}]_{11}$ est donné par

$$[\mathbf{G}]_{11} = 4\frac{\left[(2-h_1)f(2,h_1)-2(1-h_1)\right]f(1,h_1)^2}{(2-h_1)^2 f(2,h_1)}, \tag{A.11}$$

où $f(\varphi,h_1)=\sigma_\beta^2\frac{1}{2}T\sum_{k=1}^{M}\sum_{r=1}^{N}\frac{\sigma_k^2}{\sigma_n^2}\left[1-\cos\left(\frac{\varphi 2\pi}{\lambda}h_1(a_k+b_r)\right)\right]+1$.

A.2.2.3 Résultats de simulations

Les simulations sont effectuées pour 3 scénarios comme suit : le transmetteur est composé de $M=8$ capteurs (scénario A et B) et $M=5$ capteurs (scénario C) avec un espacement inter-capteur de $0.5M$ longueur d'onde, et le récepteur est composé de $N=8$ capteurs (scénario A et B) et $M=5$ capteurs (scénario C) avec un espacement inter-capteur de 0.5 longueur d'onde. Cette configuration est connue comme un réseau virtuel de Nyquist. Les formes d'ondes orthogonales du radar MIMO sont générées en utilisant des codes de Hadamard avec $T=64$ (scenario A) and $T=32$ (scenario B and C) observations. La puissance totale émise est de $M\sigma_x^2=1$. h_1 est choisi dans le support $[-1,1]$. La figure A.1 montre l'approximation de la BWW pour θ avec $s=1/2$ et l'EQM globale de l'estimateur du maximum a posteriori (MAP) évalué par 1000 tirage de Monte Carlo en fonction du RSBR pour les 3 scénarios. Nous traçons aussi l'optimisation numérique de l'approximation de la BWW. Nous observons que la BWW donne une bonne prédiction de l'EQM dans tous les régions du RSBR. Nous notons aussi que le seuil de RSBR prédit par la BWW est proche celui indiqué par le MAP.

La figure A.2 présente la comparaison de la vraie BWW (calculée par intégration numérique) et l'approximation de la BWW dans les 3 scénarios. Nous observons que les bornes sont très proches et donnent les mêmes prédictions du seuil de l'EQM. Notons que dans notre simulations, le temps nécessaire à l'obtention de la borne à été divisé par 100.

A.2.3 Radar MIMO en présence d'erreurs de modèles : une approche par les bornes de Cramér-Rao

A.2.3.1 Modèle des observations

Nous considérons un radar MIMO dont les émetteurs et les récepteurs sont largement espacés. Les deux réseaux d'antennes sont supposés linéaires avec un nombre de capteurs à l'émission et à la réception noté M et N, respectivement. Dans ce contexte, une source est localisée par deux paramètres : l'angle de départ noté θ_D et l'angle d'arrivée noté θ_A. Par conséquent, le modèle d'observation est donné par [LS09] :

$$\mathbf{y}(t) = \beta\mathbf{b}(\theta_A)\mathbf{a}^T(\theta_D)\mathbf{x}(t)+\mathbf{n}(t),\ t=1\dots T, \tag{A.12}$$

où T est le nombre d'observations, β est une amplitude complexe liée à la surface équivalente radar (SER) de la cible. Le vecteur $\mathbf{x}(t)$ contient les M formes d'onde transmises avec la

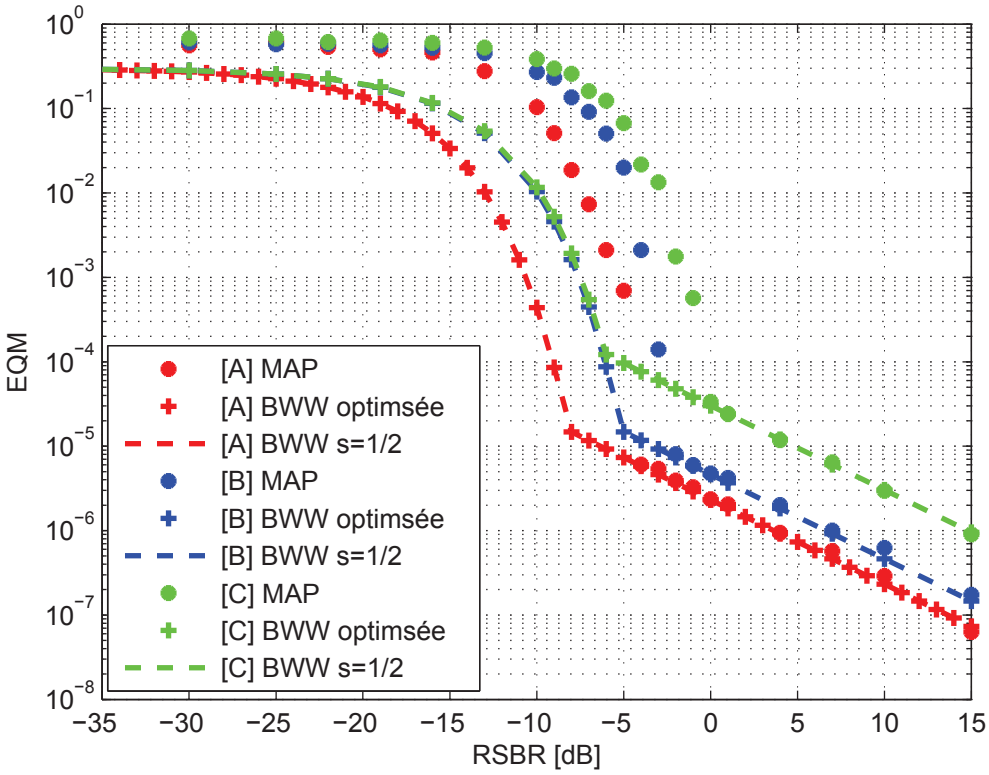

FIGURE A.1 – l'approximation de la BWW de θ et l'EQM globale de MAP évalué en fonction de RSBR

matrice de covariance empirique suivante :
$\mathbf{R}_x = \frac{1}{T}\sum_{t=1}^{T}\mathbf{x}(t)\mathbf{x}^H(t) = \sigma_x^2\mathbf{I}_M$.
Les vecteurs directionnels pour l'émetteur et le récepteur ont les structures suivantes $\mathbf{a}(\theta_D) = [\exp(-j\frac{2\pi}{\lambda}a_1\sin\theta_D),\ldots,\exp(-j\frac{2\pi}{\lambda}a_M\sin\theta_D)]^T$, et $\mathbf{b}(\theta_A) = [\exp\left(-j\frac{2\pi}{\lambda}b_1\sin\theta_A\right),\ldots,\exp\left(-j\frac{2\pi}{\lambda}b_N\sin\theta_A\right)]^T$, où λ est la longueur d'onde, et les quantités a_i, $i = 1\ldots M$, et b_j, $j = 1\ldots N$, sont les positions nominales des capteurs (par rapport à un point de référence) du réseau d'antennes d'émission et de réception, respectivement. Enfin, les vecteurs de bruit $\{\mathbf{n}(t)\}_{t=1}^{T}$ sont supposés Gaussiens, circulaires, i.i.d., de moyenne nulle et de matrice de covariance $\mathbf{R}_n = \sigma_n^2\mathbf{I}_N$.
Dans cette section, nous considérons que le vecteur directionnel nominal de réception, $\mathbf{b}(\theta_A)$, est soumis à une erreur de modèle représentée par un vecteur aléatoire additif $\mathbf{e}$. En d'autres termes, $\mathbf{b}_v(\theta_A) = \mathbf{b}(\theta_A) + \mathbf{e}$, où $\mathbf{e}$ est supposé circulaire et Gaussien, à savoir $\mathbf{e} \sim \mathcal{CN}(0, \sigma_e^2\mathbf{I}_N)$. De plus, $\mathbf{e}$ est supposé statistiquement indépendant du vecteur de bruit $\mathbf{n}(t)$, $\forall t$. Le vecteur de paramètres inconnus est $\mathbf{\Theta} = [\theta_D, \theta_A, \beta_R, \beta_I]^T$ où β_R et β_I sont les parties réelle et imaginaire de β.
Enfin, notons que [1], dans ce cas, la vraisemblance des observations est circulaire complexe

1. C'est tout à fait différent du cas classique (dans le contexte du radar MIMO ou dans le contexte du traitement d'antennes) où seule la moyenne ou la matrice de covariance sont paramétrées. Notons aussi que l'analyse de l'erreur de modélisation à la fois sur l'émetteur et le récepteur semble être un travail très complexe. En effet, dans ce cas, le vecteur des observations est la somme d'un vecteur déterministe plus un vecteur Gaussien, plus le produit de deux vecteurs Gaussiens dépendant du premier vecteur Gaussien.

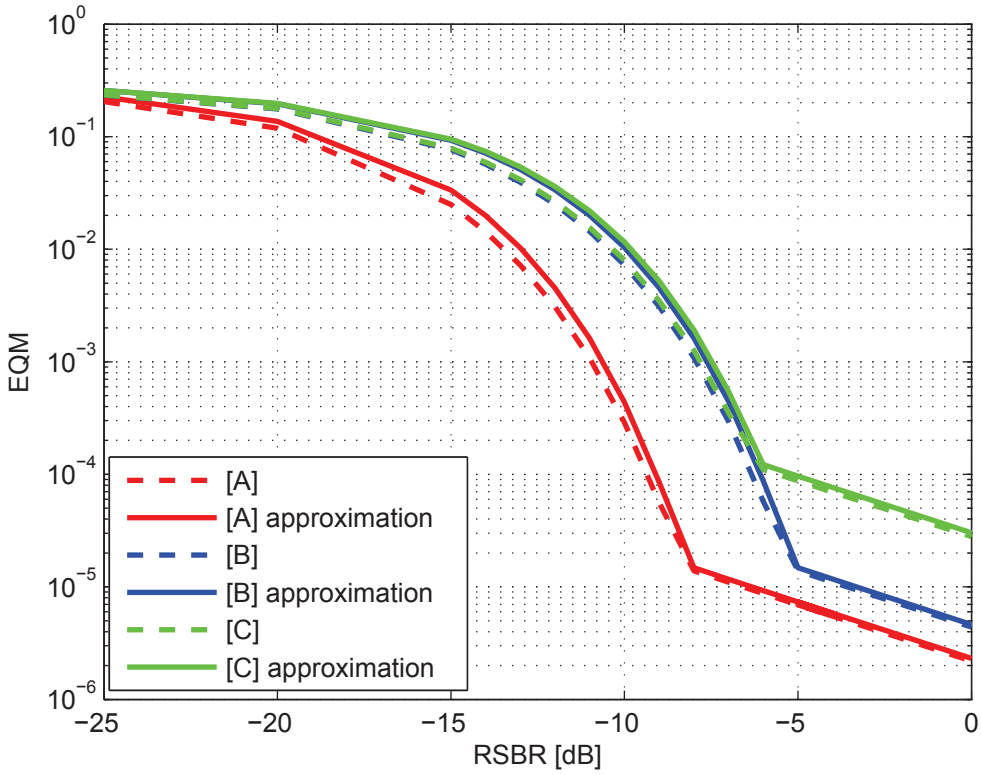

FIGURE A.2 – BWW de θ et l'approximation de la BWW en fonction de RSBR

Gaussienne avec une moyenne et une matrice de covariance paramétrés, *i.e.*, en posant $\mathbf{y} = \left[\mathbf{y}^T(1)\dots\mathbf{y}^T(T)\right]^T \in \mathbb{C}^{NT}$, $\mathbf{y}|\,\boldsymbol{\Theta} \sim \mathcal{CN}(\mathbf{m}(\boldsymbol{\Theta}), \mathbf{R}(\boldsymbol{\Theta}))$ où $\mathbf{m}(\boldsymbol{\Theta}) = vec([\beta\mathbf{b}_v(\theta_A)\mathbf{a}^T(\theta_D)\mathbf{x}(1)\dots\beta\mathbf{b}_v(\theta_A)\mathbf{a}^T(\theta_D)\mathbf{x}(T)])$, où $vec\,(.)$ est l'opérateur de vectorisation d'une matrice et où $\mathbf{R}(\boldsymbol{\Theta}) = |\beta|^2\,\sigma_e^2\mathbf{s}(\theta_D)\mathbf{s}^H(\theta_D)\otimes\mathbf{I}_N + \sigma_n^2\mathbf{I}_{NT}$, et $\mathbf{s}(\theta_D) = \left[\mathbf{a}^T(\theta_D)\mathbf{x}(1)\dots\mathbf{a}^T(\theta_D)\mathbf{x}(T)\right]^T$. On note que le vecteur de paramètres complet paramètrise la moyenne, tandis que seulement θ_D, β_R, et β_I paramètrisent la matrice de covariance des observations.

A.2.3.2 Borne de Cramér-Rao

Pour un modèle paramétré gaussien général telle que $\mathbf{y}|\,\boldsymbol{\Theta} \sim \mathcal{CN}(\mathbf{m}(\boldsymbol{\Theta}), \mathbf{R}(\boldsymbol{\Theta}))$, il est bien connu que l'élément (i,j) de la matrice de l'information de Fisher $\mathbf{F}\,(\boldsymbol{\theta})$ est donné par la formule de Slepian-Bang (voir, par exemple, [Kay93])

$$[\mathbf{F}\,(\boldsymbol{\Theta})]_{i,j} = Tr\left\{\mathbf{R}^{-1}(\boldsymbol{\Theta})\frac{\partial\mathbf{R}(\boldsymbol{\Theta})}{\partial[\boldsymbol{\Theta}]_i}\mathbf{R}^{-1}(\boldsymbol{\Theta})\frac{\partial\mathbf{R}(\boldsymbol{\Theta})}{\partial[\boldsymbol{\Theta}]_j}\right\} + 2\mathcal{R}\left\{\frac{\partial\mathbf{m}^H(\boldsymbol{\Theta})}{\partial[\boldsymbol{\Theta}]_i}\mathbf{R}^{-1}(\boldsymbol{\Theta})\frac{\partial\mathbf{m}(\boldsymbol{\Theta})}{\partial[\boldsymbol{\Theta}]_j}\right\}, \tag{A.13}$$

où $\{\boldsymbol{\theta}\}_{i=1,\dots,4}$ définit l'élément i^{eme} du vecteur $\boldsymbol{\Theta}$. Sans perte de généralité, les points de référence pour les réseaux de transmission et de réception sont choisis tels que

$$\mathbf{a}^H(\theta_D)\dot{\mathbf{a}}(\theta_D) = 0 \text{ and } \mathbf{b}^H(\theta_A)\dot{\mathbf{b}}(\theta_A) = 0, \tag{A.14}$$

où on définit $\dot{\mathbf{a}}(\theta_D) = \frac{\partial\mathbf{a}(\theta_D)}{\partial\theta_D}$, and $\dot{\mathbf{b}}(\theta_A) = \frac{\partial\mathbf{b}(\theta_A)}{\partial\theta_A}$. Après calcul, les éléments de la matrice

de l'information de Fisher sont donnés par (voir **Appendice** 2.6.3 pour le calcul détailé)

$$
\begin{aligned}
[\mathbf{F}(\mathbf{\Theta})]_{1,1} =& \frac{8\pi^2 |\beta|^2 TN\sigma_x^2}{\lambda^2\sigma_n^2}\cos^2(\theta_D)\sum_{k=1}^{M} a_k^2\left(1+\frac{|\beta|^2 TM\sigma_x^2\sigma_e^4}{\sigma_n^2+|\beta|^2 TM\sigma_x^2\sigma_e^2}\right),\\
[\mathbf{F}(\mathbf{\Theta})]_{2,2} =& \frac{\frac{8\pi^2}{\lambda^2}|\beta|^2 TM\sigma_x^2}{\sigma_n^2+|\beta|^2 TM\sigma_x^2\sigma_e^2}\cos^2\theta_A\sum_{k=1}^{N} b_k^2,\\
[\mathbf{F}(\mathbf{\Theta})]_{3,3} =& N\left(\frac{2\beta_R TM\sigma_x^2\sigma_e^2}{\sigma_n^2+|\beta|^2 TM\sigma_x^2\sigma_e^2}\right)^2+\frac{2TNM\sigma_x^2}{\sigma_n^2+|\beta|^2 TM\sigma_x^2\sigma_e^2},\\
[\mathbf{F}(\mathbf{\Theta})]_{4,4} =& N\left(\frac{2\beta_I TM\sigma_x^2\sigma_e^2}{\sigma_n^2+|\beta|^2 TM\sigma_x^2\sigma_e^2}\right)^2+\frac{2TNM\sigma_x^2}{\sigma_n^2+|\beta|^2 TM\sigma_x^2\sigma_e^2},\\
[\mathbf{F}(\mathbf{\Theta})]_{3,4} =& \{\mathbf{F}(\mathbf{\Theta})\}_{4,3} = 4N\beta_R\beta_I\left(\frac{TM\sigma_x^2\sigma_e^2}{\sigma_n^2+|\beta|^2 TM\sigma_x^2\sigma_e^2}\right)^2,
\end{aligned}
\tag{A.15}
$$

et tous les autres éléments de la matrice de l'information de Fisher sont égaux à zéro conduisant à une structure bloc diagonale (seuls les paramètres β_R et β_I sont couplés tandis que toutes les autres combinaisons sont découplées).

Après inversion de la matrice d'information de Fisher, nous montrons que les bornes de Cramér-Rao pour les paramètres inconnus sont données par

$$
\begin{cases}
BCR(\theta_D) &= \frac{\lambda^2\sigma_n^2\left(\sigma_n^2+|\beta|^2TM\sigma_x^2\sigma_e^2\right)}{8\pi^2|\beta|^2TN\sigma_x^2\left(\sigma_n^2+|\beta|^2TM\sigma_x^2\sigma_e^2(1+\sigma_e^2)\right)\cos^2(\theta_D)\sum_{k=1}^{M}a_k^2},\\
BCR(\theta_A) &= \frac{\sigma_n^2+|\beta|^2TM\sigma_x^2\sigma_e^2}{\frac{8\pi^2}{\lambda^2}|\beta|^2TM\sigma_x^2\cos^2\theta_A\sum_{k=1}^{N}b_k^2},\\
BCR(\beta_R) &= \frac{1+\beta_I^2\sigma_e^2 d}{Nd(1+|\beta|^2\sigma_e^4 d)},\\
BCR(\beta_I) &= \frac{1+\beta_R^2\sigma_e^2 d}{Nd(1+|\beta|^2\sigma_e^4 d)},
\end{cases}
\tag{A.16}
$$

where $d=\frac{2TM\sigma_x^2}{\sigma_n^2+|\beta|^2TM\sigma_x^2\sigma_e^2}$.

A.2.3.3 Résultats de Simulation

Afin d'analyser le comportement des bornes de Cramér-Rao susmentionnées, on considère ici certains résultats de simulation. Le scénario est le suivant : l'émetteur et le récepteur sont des antennes linéaires uniformes avec $M=N=4$ capteurs, respectivement, et avec un espacement inter-capteur d'une demi longueur d'onde. Les formes d'ondes orthogonales de radar MIMO sont générées en utilisant des codes de Hadamard avec $T=32$ observations. Les vraies valeurs de l'angle du départ et de l'angle d'arrivée de la cible sont $\theta_D=67,5^o$ et $\theta_A=22,5^o$, et nous supposons que $\beta=1+j$. La puissance totale émise est de $M\sigma_x^2=1$. La figure A.3 montre le comportement des bornes de Cramér-Rao pour les paramètres d'intérêt en fonction du rapport signal sur bruit de réseau (RSBR) c'est-à-dire $RSBR=\frac{MN\sigma_x^2}{\sigma_n^2}$. Notons que nous ne traçons pas $BCR(\beta_I)$ car il a le même comportement que $BCR(\beta_R)$. Nous traçons également l'erreur quadratique moyenne empirique de l'estimateur du maximum de vraisemblance évalué au travers de 1000 tirages de Monte Carlo. Cette première simulation représente le comportement des bornes de Cramér-Rao et de l'estimateur du maximum de vraisemblance sans erreur de modèles, c'est-à-dire avec $\sigma_e^2=0$. Nous notons que l'on retrouve le comportement classique des bornes de Cramér-Rao qui diminuent de façon linéaire lorsque le RSBR (en dB) augmente. Nous notons

également que l'estimateur du maximum de vraisemblance atteint asymptotiquement la borne de Cramér-Rao (lorsque $RSBR \to \infty$) [RFCL06].

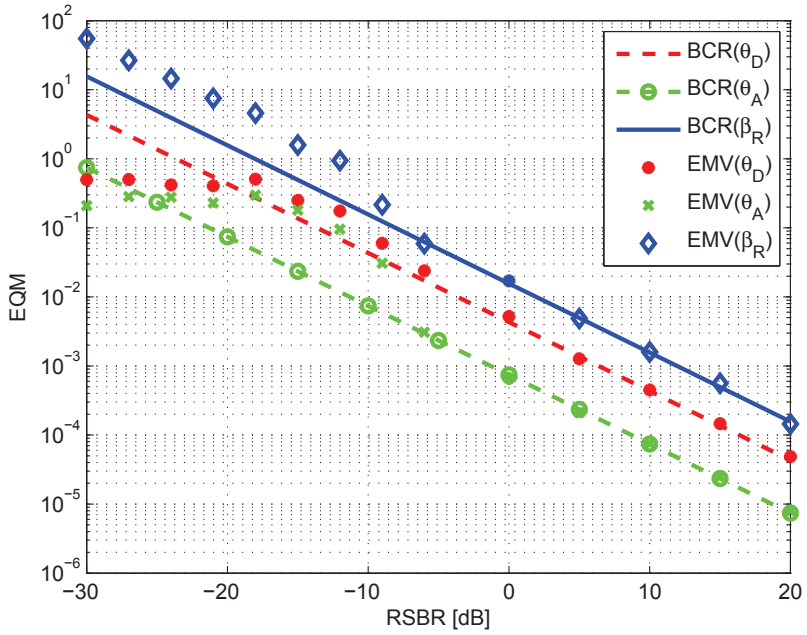

FIGURE A.3 – l'EQM de l'EMV et BCR en fonction du RSBR sans l'erreurs de modèles

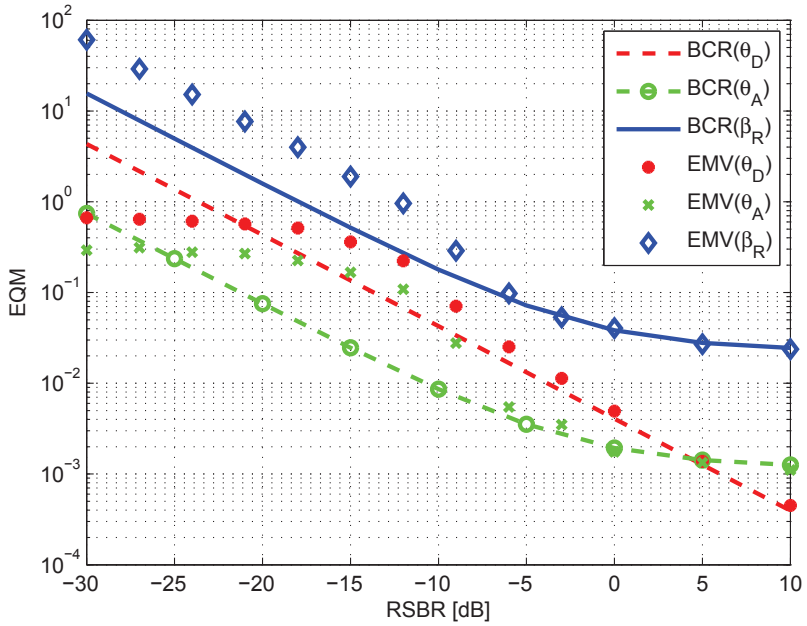

FIGURE A.4 – l'EQM de l'EMV et BCR en fonction du RSBR lorsque $\sigma_e^2 = 0.1$

La figure A.4 montre le comportement des bornes de Cramér-Rao et de l'erreur quadratique moyenne de l'estimateur du maximum de vraisemblance lorsque $\sigma_e^2 = 0.1$. Encore une fois, nous observons l'efficacité asymptotique de l'estimateur du maximum de vraisemblance, mais, lorsque $RSBR \to \infty$, la borne de Cramér-Rao ainsi que l'erreur quadratique moyenne de l'estimateur du maximum de vraisemblance de l'angle d'arrivée θ_A ne tendent pas vers zéro et convergent vers une limite fixe qui peut être obtenue à partir de l'Eqn. (A.16) et qui est égale à

$$\lim_{RSBR\to\infty} BCR\left(\theta_A\right) = \frac{\sigma_e^2}{\frac{8\pi^2}{\lambda^2}\cos^2\theta_A \sum_{k=1}^{N} b_k^2}. \tag{A.17}$$

Notons que cette valeur est indépendante de β. Cette convergence signifie que pour un niveau de "puissance" donné de l'erreur de modélisation σ_e^2, au delà d'une certaine valeur de RSBR, aucune amélioration en terme de performance ne peut plus être attendue. Par contre on notera que la position des capteurs peut être avantageusement utilisée pour diminuer cette limite. On définit cette valeur de seuil du RSBR notée $RSBR_0$ comme la valeur à laquelle, $BCR\left(\theta_A\right) = (1+\epsilon) \times \lim_{RSBR\to\infty} BCR\left(\theta_A\right)$. Nous obtenons l'expression analytique suivante

$$RSBR_0 = 10\log_{10}\frac{N}{\epsilon\sigma_e^2 T\left|\beta\right|^2}. \tag{A.18}$$

Cette expression montre que $RSBR_0$ est linéaire (en dB) concernant σ_e^2. Notons que le même comportement se produit sur β_R et β_I lorsque $ANSR \to \infty$, et nous avons

$$\lim_{RSBR\to\infty} CRB\left(\beta_R\right) = \frac{\sigma_e^2\left(\left|\beta\right|^2 + 2\sigma_e^2\beta_I\right)}{2N\left(1+2\sigma_e^2\right)}, \tag{A.19}$$

et

$$\lim_{RSBR\to\infty} CRB\left(\beta_I\right) = \frac{\sigma_e^2\left(\left|\beta\right|^2 + 2\sigma_e^2\beta_R\right)}{2N\left(1+2\sigma_e^2\right)}. \tag{A.20}$$

A.2.4 Les bornes inférieures de l'estimation de phase d'impulsion de Pulsar à rayons X

A.2.4.1 Modèle des observations

Nous présentons dans cette section le modèle mathématique d'observations donné et justifié dans [GS07]. Nous définissons k le nombre de photons détectés au niveau de détecteurs dans un intervalle de temps fixe (a, b). Les temps d'arrivée sont modelisés par un processus de Poisson non homogène (PPNH) de paramètre $\lambda(t) \geq 0$ variant dans le temps, c'est-à-dire que k suit une loi de Poisson de paramètre $\int_a^b \lambda(t)dt$

$$p(k;(a,b)) = \frac{\left[\int_a^b \lambda(t)dt\right]^k \exp\left[-\int_a^b \lambda(t)dt\right]}{k!} \tag{A.21}$$

La fonction de taux $\lambda(t)$ définit le taux total de photons arrivant au détecteur du pulsar

X et l'environment, exprimée en photons par seconde (ph/s). En pratique, la fonction de taux $\lambda(t)$ est donnée par :

$$\lambda(t) = \lambda_b + \lambda_s h(\phi_{obs}(t)) \qquad \text{(ph/s)}, \tag{A.22}$$

où λ_s et λ_b notés le *taux de source* et le *taux d'arrivé de l'environment*, respectivement ; $h(\phi(t))$ est la fonction de profil d'impulsion normalisée, et $\phi_{obs}(t)$ est la phase observée au détecteur. Nous notons que, grâce à la base de données obtenue depuis des années, la forme et la période du profil d'impulsion sont connues de façon très précise [PUL]. La fonction de profil d'impulsion $h(\phi(t))$ (voir la figure 2.11) est une fonction périodique avec sa période égale à un cycle, c'est-à-dire, $h(\phi(t))$ est définie dans l'intervalle $\phi \in [0, 1)$, et $h(m + \phi(t)) = h(\phi(t))$ pour tout m entier. D'ailleurs, la fonction $h(\phi(t))$ est normalisée, c'est-à-dire, $\int_0^1 h(\phi)d\phi = 1$, et $\min_\phi h(\phi(t)) = 0$.

La phase observée au détecteur est donnée par $\phi_{obs}(t) = \phi_0 + \int_{t_0}^{t} f(\tau)d\tau$, où ϕ_0 est la phase initiale, où t_0 est le début de l'intervalle d'observation, et où $f(t)$ est la fréquence observée du signal qui dépend de la fréquence constante de la source et de la fréquence Doppler. Notons que nous nous concentrons ici sur le problème d'estimation de la phase initiale, ensuite, nous supposons que la fréquence observée est une constante connue. On peut trouver le même modèle dans [ES10] où la phase observée est donnée par $\phi_{obs} = \phi_0 + (t - t_0)f$.

La fonction de taux peut-être considérée comme une fonction d'un paramètre, la phase initiale, comme suit $\lambda(t; \phi_0) = \lambda_b + \lambda_s h(\phi_0 + (t - t_0)f)$. Puisque λ_b et λ_s sont connus à partir la base de données, ensuite, nous devons seulement estimer la phase initiale ϕ_0. Nous dérivons ci-dessous la fonction de vraisemblance.

L'intervalle d'observation $(t_0, t_0 + T_{obs})$ est partitionné en N segments de même longueur. Nous définissons x_n, $n = 0, 1, \ldots, N - 1$ le nombre de photons détectés dans le n-eme segment, et $\Delta t \equiv T_{obs}/N$ la taille d'un segment. Si N est assez grand, le taux $\lambda(t, \phi_0)$ peut-être considéré constant dans le n-eme segment, c'est-à-dire $\lambda_n(\phi_0) = \lambda(t_n; \phi_0)$, où $t_n = t_0 + n\Delta t$. La fonction de masse pour chaque variable aléatoire de Poisson x_n, $n = 0, 1, \ldots, N - 1$, est donnée par : $p(x_n = x; \phi_0) = \frac{[\lambda_n(\phi_0)\Delta t]^x}{x!} \exp(-\lambda_n(\phi_0)\Delta t)$, où x est un entier non négatif. Avec l'hypothèse d'indépendance des observations, la vraisemblance de observations $\mathbf{x} = [x_0, x_1, \ldots, x_{N-1}]$ est donnée par

$$p(\mathbf{x}; \phi_0) = \prod_{n=0}^{N-1} \frac{[\lambda_n(\phi_0)\Delta t]^{x_n}}{x_n!} \exp(-\lambda_n(\phi_0)\Delta t). \tag{A.23}$$

A.2.4.2 Borne Déterministe

Nous considérons ici les bornes déterministes pour l'estimation de phase d'impulsion. Mathématiquement, la borne de Barankin (BB) [Bar49] est connue être plus précise que la BCR, cependant, elle n'est pas calculable directement. En traitement d'antenne classique, pour obtenir une BB calculable, plusieurs approximations ont été proposées [CGQL08]. En conséquence, nous dérivons dans ce travail la BQCL [CGQL08] qui est l'approximation la plus précise de la BB. Cette approximation est obtenue au travers de la recherche d'un maximum sur un jeu de points de test, noté par $[\theta_0, \ldots, \theta_{N-1}]$.

La BQCL à l'ordre N d'un paramètre inconnu ϕ_0 satisfait la relation suivante $E_{\mathbf{x};\phi_0}\left[(\hat{\phi} - \phi_0)^2\right] \geq B^N_{QCL}(\phi_0)$, où $E_{\mathbf{x};\phi_0}\left[(\hat{\phi} - \phi_0)^2\right] = \sum_{x_0=0}^{\infty} \cdots \sum_{x_{N-1}=0}^{\infty} (\hat{\phi} - \phi_0)^2 p(\mathbf{x}; \phi_0)$ est la variance d'un

estimateur non-biaisé $\hat{\phi}$ de ϕ_0. Pour une question de simplicité, nous noterons $\sum_{\mathbf{x}=0}^{\infty}$ au lieu de $\sum_{x_0=0}^{\infty}\cdots\sum_{x_{N-1}=0}^{\infty}$.

La borne B_{QCL}^N est introduite dans [CGQL08] est donnée par : $B_{QCL}^N = \mathbf{v}^T\mathbf{M}_{QCL}^{-1}\mathbf{v}$ où

$$\begin{cases} \mathbf{v} = [\mathbf{\Phi}^T, 1, \ldots, 1]^T \in \mathbb{R}^{2N\times 1} \text{ où } \mathbf{\Phi} = [\xi_0 \ldots \xi_{N-1}]^T, \text{ et } \xi_n = \theta_n - \phi_0,\ n = 0 \ldots N-1, \\ \mathbf{M}_{QCL} = \begin{bmatrix} \mathbf{M}_{MS} & \mathbf{H}^T \\ \mathbf{H} & \mathbf{M}_{EFI} \end{bmatrix} \in \mathbb{R}^{2N\times 2N} \end{cases},$$

où

$$\mathbf{M}_{MS} = E_{\mathbf{x};\phi_0}\left[\begin{pmatrix} \frac{p(\mathbf{x};\theta_0)}{p(\mathbf{x};\phi_0)} \\ \vdots \\ \frac{p(\mathbf{x};\theta_{N-1})}{p(\mathbf{x};\phi_0)} \end{pmatrix}\begin{pmatrix} \frac{p(\mathbf{x};\theta_0)}{p(\mathbf{x};\phi_0)} \\ \vdots \\ \frac{p(\mathbf{x};\theta_{N-1})}{p(\mathbf{x};\phi_0)} \end{pmatrix}^T\right], \tag{A.24}$$

$$\mathbf{M}_{EFI} = E_{\mathbf{x};\phi_0}\left[\begin{pmatrix} \frac{\partial \ln p(\mathbf{x};\theta_0)}{\partial\theta_0}\frac{p(\mathbf{x};\theta_0)}{p(\mathbf{x};\phi_0)} \\ \vdots \\ \frac{\partial \ln p(\mathbf{x};\theta_{N-1})}{\partial\theta_{N-1}}\frac{p(\mathbf{x};\theta_{N-1})}{p(\mathbf{x};\phi_0)} \end{pmatrix}\begin{pmatrix} \frac{\partial \ln p(\mathbf{x};\theta_0)}{\partial\theta_0}\frac{p(\mathbf{x};\theta_0)}{p(\mathbf{x};\phi_0)} \\ \vdots \\ \frac{\partial \ln p(\mathbf{x};\theta_{N-1})}{\partial\theta_{N-1}}\frac{p(\mathbf{x};\theta_{N-1})}{p(\mathbf{x};\phi_0)} \end{pmatrix}^T\right] \tag{A.25}$$

$$\mathbf{H} = E_{\mathbf{x};\phi_0}\left[\begin{pmatrix} \frac{\partial \ln p(\mathbf{x};\theta_0)}{\partial\theta_0}\frac{p(\mathbf{x};\theta_0)}{p(\mathbf{x};\phi_0)} \\ \vdots \\ \frac{\partial \ln p(\mathbf{x};\theta_{N-1})}{\partial\theta_{N-1}}\frac{p(\mathbf{x};\theta_{N-1})}{p(\mathbf{x};\phi_0)} \end{pmatrix}\begin{pmatrix} \frac{p(\mathbf{x};\theta_0)}{p(\mathbf{x};\phi_0)} \\ \vdots \\ \frac{p(\mathbf{x};\theta_{N-1})}{p(\mathbf{x};\phi_0)} \end{pmatrix}^T\right], \tag{A.26}$$

où $\mathbf{M}_{MS}$ est la matrice de McAulay–Seidman, $\mathbf{M}_{EFI}$ est la matrice d'information de Fisher, et $\mathbf{H}$ est une matrice "hybride" [CGQL08]. L'ensemble $\theta_n, n = 1, \ldots, N-1$ est le jeu des points de tests. Utilisant les calculs donnés en **Appendice**, nous obtenons l'expressions analytiques des éléments (k, l) de la matrice $\mathbf{M}_{MS}$ (voir **Appendice** 2.6.4), $\mathbf{M}_{EFI}$ (voir **Appendice** 2.6.5), et $\mathbf{H}$ (voir **Appendice** 2.6.6) comme suit :

$$\mathbf{M}_{MS}(k,l) = \exp\left\{T_{obs}\int_0^1 \lambda(\phi) - \lambda(\xi_k+\phi) - \lambda(\xi_l+\phi) + \frac{\lambda(\xi_k+\phi)\lambda(\xi_l+\phi)}{\lambda(\phi)}d\phi\right\},$$

$$\begin{aligned}\mathbf{M}_{EFI}(k,l) = \mathbf{M}_{MS}(k,l)\Bigg[&T_{obs}^2\int_0^1 \frac{\partial\lambda(\phi+\xi_k)}{\partial\xi_k}\frac{\lambda(\phi+\xi_l)}{\lambda(\phi)}d\phi\int_0^1 \frac{\partial\lambda(\phi+\xi_l)}{\partial\xi_l}\frac{\lambda(\phi+\xi_k)}{\lambda(\phi)}d\phi \\ &+ T_{obs}^2\int_0^1 \frac{\partial\lambda(\phi+\xi_k)}{\partial\xi_k}d\phi\int_0^1 \frac{\partial\lambda(\phi+\xi_l)}{\partial\xi_l}d\phi - T_{obs}^2\int_0^1 \frac{\partial\lambda(\phi+\xi_l)}{\partial\xi_l}d\phi\int_0^1 \frac{\partial\lambda(\phi+\xi_k)}{\partial\xi_k}\frac{\lambda(\phi+\xi_l)}{\lambda(\phi)}d\phi\ , \\ &- T_{obs}^2\int_0^1 \frac{\partial\lambda(\phi+\xi_k)}{\partial\xi_k}d\phi\int_0^1 \frac{\partial\lambda(\phi+\xi_l)}{\partial\xi_l}\frac{\lambda(\phi+\xi_k)}{\lambda(\phi)}d\phi + T_{obs}\int_0^1 \frac{\partial\lambda(\phi+\xi_k)}{\partial\xi_k}\frac{\partial\lambda(\phi+\xi_l)}{\partial\xi_l}\frac{1}{\lambda(\phi)}d\phi\Bigg]\end{aligned}$$

et

$$\mathbf{H}(k,l) = \mathbf{M}_{MS}(k,l)\left[T_{obs}\int_0^1 \frac{\partial\lambda(\phi+\xi_k)}{\partial\xi_k}\frac{\lambda(\phi+\xi_l)}{\lambda(\phi)}d\phi - T_{obs}\int_0^1 \frac{\partial\lambda(\phi+\xi_k)}{\partial\xi_k}d\phi\right].$$

Dans l'expressions de la BQCL, nous voyons l'existence d'une intégrale qui peut-être calculée facilement et rapidement en utilisant le calcul numérique. Notons que le même cas à été observé dans le calcul de la BCR proposé dans [GS07] et [ES10].

A.2.4.3 Borne Bayésienne

La borne de Weiss-Weinstein, noté BWW, pour un paramètre inconnu ϕ_0 satisfait la relation suivante $E_{\mathbf{x};\phi_0}\left[(\hat{\phi}-\phi_0)^2\right] \geq BWW$, où $E_{\mathbf{x};\phi_0}\left[(\hat{\phi}-\phi_0)^2\right] = \int_{\mathbf{\Theta}} \sum_{\mathbf{x}=0}^{\infty} (\hat{\phi}-\phi_0)^2 p(\mathbf{x},\phi_0) d\phi_0$ est l'EQM d'un estimateur de ϕ_0, où $p(\mathbf{x},\phi_0)$ est densité de probabilité jointe et $\mathbf{\Theta}$ est l'espace des paramètres. Notons que, contrairement au cas deterministe, l'estimateur $\hat{\phi}$ peut-être biaisé. La BWW [WW85] est donnée par

$$BWW = \sup_{u,s} \frac{u^2 \exp(2\eta(s,u))}{\exp(\eta(2s,u)) + \exp(\eta(2-2s,-u)) - 2\exp(\eta(s,2u))}, \tag{A.27}$$

où $s \in [0,1]$, où u est le point de test choisi tel que $\phi_0 + u \in [0,1)$, et $\eta(\alpha,\beta)$ est défini par

$$\begin{aligned}
\eta(\alpha,\beta) &= \ln \int_{\mathbf{\Theta}} \sum_{\mathbf{x}=0}^{\infty} p(\mathbf{x},\phi_0+\beta)^{\alpha} p(\mathbf{x},\phi_0)^{1-\alpha} d\phi_0 \\
&= \ln \int_{\mathbf{\Theta}} \sum_{\mathbf{x}=0}^{\infty} p(\mathbf{x};\phi_0+\beta)^{\alpha} p(\phi_0+\beta)^{\alpha} p(\mathbf{x};\phi_0)^{1-\alpha} p(\phi_0)^{1-\alpha} d\phi_0 \\
&= \ln \int_{\mathbf{\Theta}} \eta'(\alpha,\beta) p(\phi_0+\beta)^{\alpha} p(\phi_0)^{1-\alpha} d\phi_0,
\end{aligned} \tag{A.28}$$

où nous définissons $\eta'(\alpha,\beta) = \sum_{\mathbf{x}=0}^{\infty} p(\mathbf{x};\phi_0+\beta)^{\alpha} p(\mathbf{x};\phi_0)^{1-\alpha}$. L'expression analytique de $\eta'(\alpha,\beta)$ est donnée par (voir **Appendice** 2.6.7 pour le calcul détaillé)

$$\eta'(\alpha,\beta) = \exp\left\{ T_{obs} \int_0^1 \left(-\alpha\lambda(\phi+\beta) - (1-\alpha)\lambda(\phi) + \lambda(\phi+\beta)^{\alpha}\lambda(\phi)^{1-\alpha} \right) d\phi \right\}.$$

Notons que $\eta'(\alpha,\beta)$ ne dépend plus de ϕ_0, donc, l'intégrale dans (A.28) peut être calculée facilement.

Enfin, la BWW pour le paramètre inconnu ϕ_0 est donnée par

$$BWW = \sup_{u,s} \frac{u^2(1-u)^2 \eta'^2(s,u)}{(1-u)\eta'(2s,u) + (1-u)\eta'(2-2s,-u) - 2(1-2u)\eta'(s,2u)}. \tag{A.29}$$

Encore une fois nous pouvons observer la présence d'intégrales dans l'expression de la BWW comme dans la BQCL, mais celles-ci peuvent être calculées numériquement.

A.2.4.4 Résultats de Simulation

Afin d'analyser le comportement des bornes susmentionnées,, nous les comparons avec les performances de l'estimateur du maximum de vraisemblance donné par $\hat{\phi} = \arg\max_{\phi_0 \in \mathbf{\Theta}} \sum_{n=0}^{N-1} [x_n \ln[\lambda_n(\phi_0)\Delta t] - \lambda_n(\phi_0)\Delta t]$. Les performances de l'estimateur du maximum de vraisemblance sont évaluées au travers de 1000 tirages de Monte Carlo. Le

fréquence est fixée à $f = 29.85$ Hz et la période de pulse est de 33.5 ms. Les taux de photons sont $\lambda_b = 5$ (ph/s) et $\lambda_s = 15$ (ph/s). Le nombre de points tests est fixé à 100 répartis uniformement sur l'espace du paramètre. Puisque la phase est définie dans l'intervalle $[0, 1]$, l'erreur de la phase est calculée modulo un cycle, c'est-à-dire, $min[mod(\phi_0 - \hat{\phi}, 1), mod(\hat{\phi} - \phi_0, 1)]$. Par exemple, l'erreur entre 0.9 cycle et 0.1 cycle est de 0.2 cycle, et pas 0.8 cycle.

Dans la figure A.5 nous comparons la BQCL, la BCR et l'EQM de l'EMV de ϕ_0 en fonction de temps d'observation. La phase initiale , $\phi_0 = 0.9$ cycle, est choisie arbitrairement. Nous observons que la BQCL offre une bonne prédiction du décrochement d'EQM de l'EMV.

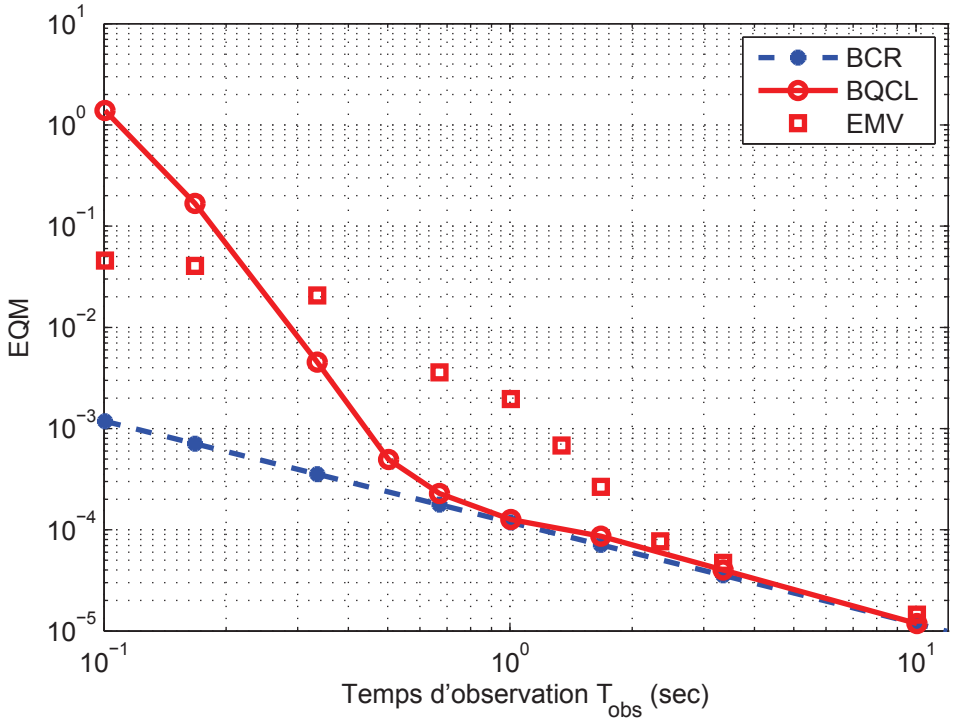

FIGURE A.5 – BQCL, BCR et EQM de l'EMV de ϕ_0 en fonction de temps d'observation.

Dans la figure A.6 nous traçons la BWW et l'EQM empirique globale de l'EMV de ϕ_0 en fonction du temps d'observation. Nous observons que la BWW prédit bien la position du seuil ainsi que l'EQM de l'EMV dans toutes les régions du temps d'observation.

A.2.5 Conclusion

Dans cette section, nous avons étudié les bornes inférieures de l'EQM dans deux contextes différents :

- D'abord, nous avons développé la borne de Weiss-Weinstein (pour le cas bayésien) dans le contexte du radar MIMO et la borne de Cramér-Rao (pour le cas déterministe) dans le context du radar MIMO en présence d'erreur de modèle. Pour le cas bayésien, nous avons montré que la BWW donne une bonne prédiction de l'EQM du MAP dans toutes les régions du RSBR. Elle peut prédire aussi le seuil de décrochement

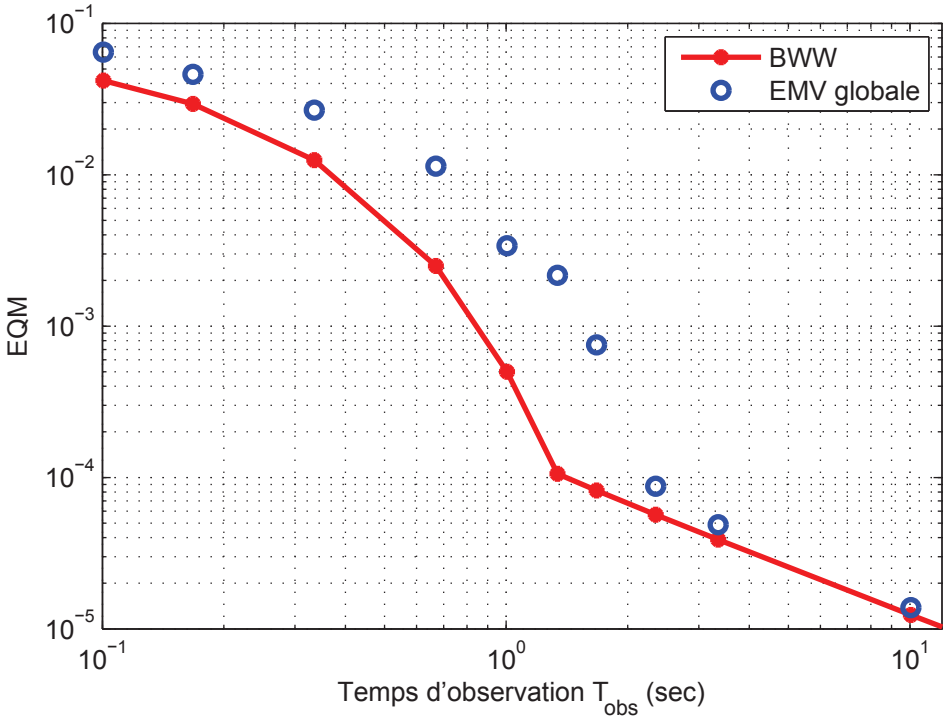

FIGURE A.6 – BWW et EQM global empirique de l'EMV de ϕ_0 en fonction du temps d'observation.

du MAP. Dans le contexte des erreurs de modèle, nous avons dérivé les expressions analytiques de la matrice d'information de Fisher et montré sa structure diagonale bloc. Cela nous a permis de déduire les expressions des bornes de Cramér-Rao de l'angle d'arrivée et de l'angle de départ. Nous avons montré que, à partir d'un certain rapport signal à bruit, les performances du système ne peuvent plus être améliorées. Enfin, nous avons proposé une formule simple pour évaluer cette valeur critique du rapport signal à bruite.

- Dans le deuxième contexte, nous avons dérivé les expressions analytiques de la borne de Quinlan-Chaumette-Larzabal (pour le cas déterministe) et de la BWW (pour le cas bayésien) pour l'estimation de la phase de signaux pulsar à rayon X. Nous avons montré que les deux bornes sont à même de prédire la position du de décrochement des estimateurs.

A.3 Seuil statistique de résolution limite et applications

A.3.1 Introduction

Le seuil statistique de résolution limite (SRL) est caractéristique de la distance minimale dans l'espace des paramètres d'intéret entre deux signaux proches permettant de les séparer/estimer correctement. Le problème de la dérivation du SRL pour deux sources proches a été l'objet de beaucoup d'intérets dans le cadre de nombreuses applications telles que le radar, le sonar, le traitement d'image... Dans la littérature, il existe principalement

quatre approches pour obtenir le SRL :

1. La première approche est basée sur le l'analyse du pseudo-spectre des estimateurs à haute résolution [Cox, KB86, AD08]. Dans ce contexte, nous supposons que deux signaux sont paramétrés chacun par un paramètre d'intéret, dénoté par θ_1 pour la première source et θ_2 pour la seconde, le critère de Cox [Cox] indique que *deux sources sont résolues (conditionellement à un estimateur à haute résolution donné) si la moyenne des valeurs du pseudo-spectre aux points θ_1 et θ_2 sont inférieures à la valeur du pseudo-spectre correspondante au barycentre $\frac{\theta_1+\theta_2}{2}$*. Bien que ce concept soit intuitif et assez simple, la portée de cette approche est limitée car dédiée à un estimateur donné.
   Dans la suite, nous présentons trois autres approches ne souffrant pas de cette limitation puisque basées sur la notion de performances limites.
2. La deuxième approche est basée sur la précision de l'estimation, c'est-à-dire la BCR du SRL [Lee92, Lee94, Smi05, Dil98]. Dans la littérature, on peut distinguer deux critères :
   - Le critère de Lee, qui a été introduit dans [Lee92], stipule que dans le contexte où nous disposons de deux signaux proches paramètrés chacun par un seul paramètre d'intérêt, *ces signaux sont correctement résolus par rapport aux paramètres d'intérêt θ_1 et θ_2, si l'écart-type maximal est inférieur à au moins deux fois la différence entre θ_1 et θ_2*. L'écart-type d'un estimateur $\hat{\theta}$ sans biais peut être approché par $\sqrt{BCR(\theta)}$ (sous certaines conditions de régularité). Le SRL au sens de Lee est définie selon $2\max(\sqrt{BCR(\theta_1)}, \sqrt{BCR(\theta_2)})$. Des applications de ce critère peuvent être trouvées dans [Lee94, Dil98] où le problème de la résolution limite en fréquence est adressée. Notez que le couplage entre les paramètres d'intérêt, c'est à dire le terme hors diagonale de la matrice BCR, dénoté par $BCR(\theta_1, \theta_2)$, est ignoré dans ce critère.
   - Un second critère a été introduit par Smith dans [Smi05] ayant pour objectif de prendre en compte l'effet de couplage. Celui-ci stipule que *deux signaux sont correctement résolus par rapport aux paramètres d'intérêt si la différence entre θ_1 et θ_2, notée δ, est inférieure à l'écart-type de la différence entre ces paramètres.* Par conséquent, le SRL au sens de Smith peut être obtenu comme la solution de l'équation suivante :
   $$\delta^2 = \gamma CRB(\delta),$$
   où γ est un facteur translation dépendant de P_{fa} et P_d [LN07].
3. La troisième approche est basée sur la théorie de la détection en formulant le problème du SRL selon un test d'hypothèse binaire [SM04, SM05, LN07, AW08]. L'idée principale est de décider si deux signaux sont combinés en un seul signal sous l'hypothèses $\mathcal{H}_0$, c'est-à-dire $\delta = 0$ ou si ces deux signaux peuvent être résolus sous l'hypothèses $\mathcal{H}_1$, c'est-à-dire $\delta \neq 0$. En se basant sur ce formalisme, le SRL de la fréquence de deux sinusoides est dérivé dans [SM05] pour une probabilité de détection P_d et une probabilité de fausse alarme P_{fa} données en utilisant le test du rapport de vraisemblance généralisé (TRVG). Par ailleurs, dans [LN07], le SRL angulaire, c'est-à-dire le SRL par rapport à la direction d'arrivée (DDA), pour la résolution de deux sources proches est proposé en considérant certaines propriétés asymptotiques du TRVG. Il est intéressant de noter que dans ce travail, les auteurs montrent que le problème du SRL du point de vue de la détection peut être en fait vu (asymptotiquement) comme un problème d'estimation. Autrement dit, le paramètre

de décentrage, représentant la "distance" entre deux hypothèses statistiques est relié à la BCR du SRL. Enfin, dans [AW08], on peut trouver l'expression du SRL dans un contexte Bayésien basé sur le développement de Taylor à l'ordre un de la probabilité d'erreur P_e.

4. La dernière approche est basée sur le lemme de Stein [CT, Che56] qui établit le lien entre une mesures de distance entre chacune des distributions de probabilité caractérisant une hypothèse statistique et le logarithme de la probabilité d'erreur P_e ou de la probabilité de fausse alarme P_{fa}. Dans la littérature, ce lemme a été utilisé comme critère d'optimisation pour la recherche de formes d'onde optimales en radar MIMO dans [TLWP09, TTP10] et dans le contexte du radar multi-statique dans [Kay09]. Par ailleurs, dans [VEB+11], le SRL angulaire pour deux sources polarisées proches est également étudié.

Dans ce travail, nous examinons le SRL dans deux contexte.

– Premièrement, nous dérivons et analysons le SRL basé sur le critère de Lee et le critère de Smith dans le contexte du traitement d'antenne. En préambule, il est proposé des formes analytiques du critères de Lee et de Smith pour le traitement d'antenne. Ensuite et bien qu'il existe de nombreux travaux liés à la résolution de sources proches, il faut noter que ces travaux sont proposés dans un contexte idéal où le modèle d'observation est supposé être connu sans erreur. Toutefois, en pratique, les erreurs de modéle existent toujours et dégradent les performances du système, il est donc important d'étudier l'impact des erreurs de modéle sur le SRL. A notre connaissance, l'introduction des erreurs de modèle dans le SRL n'a jamais été proposée, ni étudiée dans la litérature. Notre approche suit l'idée présentée dans [FLV10] où l'erreur de modèle prise en compte sous la forme d'une perturbation additive aléatoire Gaussienne entache le vecteur directionnel.

– Deuxièmement, nous exploitons le lemme de Stein afin de dériver le SRL. Cette approche est assez nouvelle et très peu utilisée jusqu'ici dans la littérature. Par conséquent, notre objectif est de démontrer son utilité dans le contexte du SRL. A cet effet, nous examinons cette approche dans le contexte : (i) du traitement d'antenne où le SRL angulaire basée sur ce lemme est proposé et comparé au SRL angulaire basé sur les critères de Lee et de Smith, et (ii) dans le le contexte du MIMO radar dont les antennes en transmission et en réception sont soit largement espacées ou collocalisées. Notez que, lorsque les antennes en transmission et réception sont largement espacées, le problème devient multidimensionnel, c'est-à-dire que nous devons considérer le SRL dans le contexte où il existe plus d'un paramètre d'intérêt par source. A notre connaissance, il existe très peu de travaux traitants le problème du SRL dans le contexte du radar MIMO. Dans [Boy11], le SRL angulaire d'un radar MIMO collocalisé est présenté et analysé en utilisant le critère de Smith. Dans [EBRM12], le SRL multidimensionnel pour deux sources proches dans le contexte du radar MIMO avec des antennes en transmission et réception largement espacées a été obtenu en utilisant le TRVG. Notez que, jusqu'à présent, il n'existe aucun résultat sur le SRL basé sur des critères issus directement de l'analyse du pseudo-spectre d'estimateurs ou sur la BCR du SRL dans le contexte du radar MIMO. Ceci s'explique en raison de la difficulté à généraliser les critères existants du SRL donnés dans un contexte mono-dimensionnels aux situations multidimensionnels (c'est-à-dire dans les cas où il y a plus d'un paramètre d'intérêt par source).

A.3.2 SRL basés sur la BCR dans le contexte du traitement d'antenne en présence d'erreur de modèle

A.3.2.1 Modèle des observations

Nous considérons un réseau d'antennes linaire avec N capteurs dans le cas de deux sources (voir la figure 3.1) notées $\mathbf{s}_1 = [s_1(1) \dots s_1(L)]^T$ et $\mathbf{s}_2 = [s_2(1) \dots s_2(L)]^T$ où L est le nombre d'observations. Chaque source est supposée être déterministe, en champ lointain, bande étroite, localisée par un angle-d'arrivé noté θ_m, $m = 1, 2$. La distance entre le n-ème capteur par rapport à un capteur de référence est noté d_n. Dans le scénario sans l'erreur de modèle, le signal observé par le réseau à la l-ème observation est donné par

$$\mathbf{y}(l) = \mathbf{a}(\omega_1)s_1(l) + \mathbf{a}(\omega_2)s_2(l) + \mathbf{n}(l), \tag{A.30}$$

où $l = 1, \dots, L$. Le vecteur directionnel nominal est $\mathbf{a}(\omega_m) = [\exp(j\omega_m d_1) \ \dots \ \exp(j\omega_m d_N)]^T$ où $\omega_m = \frac{2\pi}{\lambda} \sin\theta_m$ et λ dénotant la longueur d'onde. Le vecteur de bruit pour la l-iémé observation noté $\mathbf{n}(l)$ est supposé complexe Gaussien, circulaire, i.i.d., de moyenne nulle et de matrice de covariance $\sigma^2\mathbf{I}_N$.

Dans ce travail, nous considérons que le vecteur directionnel nominal est entaché d'une erreur selon :

$$\mathbf{a}_t(\omega_m) = \mathbf{a}(\omega_m) + \mathbf{e}_m, \tag{A.31}$$

où $\mathbf{e}_m$ est supposé, complexe, circulaire et Gaussien, c'est-à-dire $\mathbf{e}_m \sim \mathcal{CN}(0, \sigma_e^2\mathbf{I}_N)$, $m = 1, 2$. De plus, il est réaliste de supposer que $\mathbf{e}_m$ est statistiquement indépendant du vecteur de bruit. Par conséquent, l'equation (A.30) est donnée par

$$\mathbf{y}(l) = (\mathbf{a}(\omega_1) + \mathbf{e}_1)s_1(l) + (\mathbf{a}(\omega_2) + \mathbf{e}_2)s_2(l) + \mathbf{n}(t). \tag{A.32}$$

Nous définissons $\mathbf{y} = [\mathbf{y}^T(1) \dots \mathbf{y}^T(L)]^T$ et $\mathbf{n} = [\mathbf{n}^T(1) \dots \mathbf{n}^T(L)]^T$, et nous supposons : $\mathbf{s}_1 \neq \mathbf{s}_2$ et $||\mathbf{s}_1||^2 = ||\mathbf{s}_2||^2 = L$, l'équation (3.3) est donnée alors par

$$\mathbf{y} = \mathbf{s}_1 \otimes \mathbf{a}(\omega_1) + \mathbf{s}_2 \otimes \mathbf{a}(\omega_2) + \tilde{\mathbf{n}} + \mathbf{n} \tag{A.33}$$

où $\otimes$ dénote le produit de Kronecker et $\tilde{\mathbf{n}} = \mathbf{s}_1 \otimes \mathbf{e}_1 + \mathbf{s}_2 \otimes \mathbf{e}_2$. L'observation est circulaire complexe Gaussienne telle que, *i.e.*, $\mathbf{y} \sim \mathcal{CN}(\mathbf{s}_1 \otimes \mathbf{a}(\omega_1) + \mathbf{s}_2 \otimes \mathbf{a}(\omega_2), \mathbf{C})$, où $\mathbf{C} = \mathbf{R} \otimes \mathbf{I}_N$ avec $\mathbf{R} = \mathbf{R}_\mathbf{n} + \mathbf{R}_{\tilde{\mathbf{n}}} = \sigma^2\mathbf{I}_L + \sigma_e^2(\mathbf{s}_1\mathbf{s}_1^H + \mathbf{s}_2\mathbf{s}_2^H)$.

A.3.2.2 SRL angulaire basé sur la BCR

A.3.2.2.1 Critère de Lee Le SRL basé sur le critère de Lee est donné par [Lee92]

$$\delta_L = 2\max\left\{\sqrt{\mathbf{B}(\omega_1, \omega_1)}, \sqrt{\mathbf{B}(\omega_2, \omega_2)}\right\} \tag{A.34}$$

où $\mathbf{B}$ est la matrice de BCR déterministe de taille 2×2 et $\mathbf{B}(\omega_1, \omega_1)$ (*resp.* $\mathbf{B}(\omega_2, \omega_2)$) est l'élément $(1, 1)$ (*resp.* $(2, 2)$) de la matrice $\mathbf{B}$. Dans **Appendice** 3.5.1, nous avons dérivé

l'expression analytique de BCR linéarisée pour un SRL suffisamment petit. Exploitant le résultat (3.48), le critère de Lee est donné par :

$$\delta_L = 2\sqrt{\mathbf{B}(\omega_1,\omega_1)} = 2\sqrt{\frac{\mathbf{F}(\omega_1,\omega_1)}{\mathbf{F}(\omega_1,\omega_1)^2 - \mathbf{F}(\omega_1,\omega_2)^2}} \tag{A.35}$$

où $\mathbf{F}$ est la matrice d'information de Fisher telle que $\mathbf{B} = \mathbf{F}^{-1}$. Nous définissons

$$\begin{aligned} a &= 2\mathcal{R}\{\mathbf{s}_2^H\mathbf{R}^{-1}\mathbf{s}_1\}\sum_{n=1}^{N} d_n^2 = \frac{2\sigma^2\mathcal{R}\{\rho\}}{\sigma^4+\sigma_e^2(\sigma_e^2L^2+2\sigma^2L-\sigma_e^2|\rho|^2)}\sum_{n=1}^{N} d_n^2 \\ b &= -\mathcal{I}\{\mathbf{s}_2^H\mathbf{R}^{-1}\mathbf{s}_1\}\sum_{n=1}^{N} d_n^3 = \frac{\sigma^2\mathcal{I}\{\rho\}}{\sigma^4+\sigma_e^2(\sigma_e^2L^2+2\sigma^2L-\sigma_e^2|\rho|^2)}\sum_{n=1}^{N} d_n^3 \\ \mathbf{F}(\omega_1,\omega_1) &= \frac{2(\sigma^2L+\sigma_e^2(L^2-|\rho|^2))}{\sigma^4+\sigma_e^2(\sigma_e^2L^2+2\sigma^2L-\sigma_e^2|\rho|^2)}\sum_{n=1}^{N} d_n^2, \end{aligned} \tag{A.36}$$

où $\mathcal{R}\{.\}$ et $\mathcal{I}\{.\}$ sont les parties réelles et imaginaires d'un nombre complexe et $\rho = \mathbf{s}_1^H\mathbf{s}_2$. Le critère de Lee (A.35) après linéarisation (pour un SRL suffisamment petit) peut être récrit comme un polynôme d'ordre 4 comme suit

$$b^2\delta_L^4 + 2ab\delta_L^3 + (a^2 - \mathbf{F}(\omega_1,\omega_1)^2)\delta_L^2 + 4\mathbf{F}(\omega_1,\omega_1) = 0. \tag{A.37}$$

Utilisant la méthodologie présentée dans [Boy11], on sait que si δ est une racine de l'équation de Lee, $-\delta$ est aussi une racine. Utilisant cette propriété, on peut montrer que le polynôme (A.37) est équivalent à la résolution d'une équation bi-quadratique. Après calculs, les racines de (A.37) sont données par

$$\delta_L^2 = \frac{1}{2b^2}\left(\mathbf{F}(\omega_1,\omega_1)^2 - a^2 \pm \sqrt{(\mathbf{F}(\omega_1,\omega_1)^2-a^2)^2 - 16b^2\mathbf{F}(\omega_1,\omega_1)}\right). \tag{A.38}$$

Pour déterminer le signe dans l'expression ci-dessus, on utilisera la condition que $\delta_L \to 0$ quand $RSB \to \infty$ pour $\sigma_e^2 = 0$. Cet argument semble réaliste en l'absence d'erreur de modèle. Dans ce cas, nous avons

$$\delta_L^2 = \frac{\left(2\sum_{n=1}^{N} d_n^2\right)^2(L^2-\mathcal{R}\{\rho\}^2)}{2\left(\sum_{n=1}^{N} d_n^3\mathcal{I}\{\rho\}\right)^2} \pm \frac{1}{2}\sqrt{\left(\frac{\left(2\sum_{n=1}^{N} d_n^2\right)^2(L^2-\mathcal{R}\{\rho\}^2)}{\left(\sum_{n=1}^{N} d_n^3\mathcal{I}\{\rho\}\right)^2}\right)^2 - \frac{32\sigma^2\sum_{n=1}^{N} d_n^2L}{\left(\sum_{n=1}^{N} d_n^3\mathcal{I}\{\rho\}\right)^2}}. \tag{A.39}$$

Si $\delta_L \to 0$, le terme à droite du signe négatif sous la racine tend vers zéro. Il est donc logique de choisir le signe négatif.

A.3.2.2.2 Critère de Smith Le SRL basé sur le critère de Smith est donné par [Smi05]

$$\delta_S = \sqrt{\gamma(\mathbf{B}(\omega_1,\omega_1) + \mathbf{B}(\omega_2,\omega_2) - 2\mathbf{B}(\omega_1,\omega_2))} \tag{A.40}$$

où γ est un facteur translation [LN07] qui peut être déterminé numériquement en résolvant l'équation $Q^{-1}_{\mathcal{X}^2_1}(P_{fa}) = Q^{-1}_{\mathcal{X}^2_{1(\gamma)}}(P_d)$, où $Q^{-1}_{\mathcal{X}^2_1}$ est l'inverse de la surface de la queue de distribution à droite de la loi $\mathcal{X}^2_1$, et P_{fa} et P_d sont les probabilités de fausse alarme et de détection, respectivement. Utilisant les résultats de **Appendice** 3.5.1, le critère de Smith est donné par

$$\delta_S = \sqrt{\frac{2\gamma}{\mathbf{F}(\omega_1,\omega_1) - (a + b\delta_S)}}. \tag{A.41}$$

Par conséquent,

$$b\delta^3 + (a - \mathbf{F}(\omega_1,\omega_1))\delta^2 + 2\gamma = 0. \tag{A.42}$$

Utilisant la même méthodologie que précédemment, le SRL basé sur le critère de Smith est donné par

$$\delta_S = \sqrt{\frac{2\gamma}{\mathbf{F}(\omega_1,\omega_1) - a}}, \tag{A.43}$$

où a et $\mathbf{F}(\omega_1,\omega_1)$ sont donnés dans (3.7).
Le SRL basé sur le critère de Smith pour le cas sans l'erreur de modèle est

$$\delta_S(\sigma_e^2 = 0) = \sqrt{\frac{\gamma\sigma^2}{(L - \mathcal{R}\{\rho\})\sum_{n=1}^{N} d_n^2}}. \tag{A.44}$$

A.3.2.3 Résultats de simulation

Le scénario de ces simulations numériques est le suivant : l'antenne est linéaire uniforme et composée de $N = 10$ capteurs, avec un espacement inter-capteur d'une demi longueur d'onde, le capteur de référence est le premier capteur. Le nombre d'observations est $L = 100$, $P_{fa} = 0.01$ et $P_d = 0.99$. Nous traçons sur la figure 3.2 le SRL en fonction du RSB(dB) avec et sans l'erreur de modèle.

Nous observons que lorsque $RSB \to \infty$, les SRL dans le cas avec erreur de modèle ne tendent pas vers zéro (au contraire du cas sans erreur de modèle) et convergent vers les limites suivantes :

$$\begin{aligned}
\lim_{RSB\to\infty} \delta_L &= \sqrt{\frac{4}{\mathbf{F}(\omega_1,\omega_1)}} = \sqrt{2}\frac{\sigma_e}{||\mathbf{d}||}, \\
\lim_{RSB\to\infty} \delta_S &= \sqrt{\frac{2\gamma}{\mathbf{F}(\omega_1,\omega_1)}} = \sqrt{\gamma}\frac{\sigma_e}{||\mathbf{d}||}.
\end{aligned} \tag{A.45}$$

Ceci signifie que pour un niveau de "puissance" donné de l'erreur de modèle σ_e^2, au delà d'une certaine valeur de RSB, aucune amélioration en terme de SRL ne peut être attendue. Une autre remarque est que les SRL à fort RSB sont linéaire en fonction de σ_e et ne dépendent pas du nombre d'observation ou des puissances de sources.

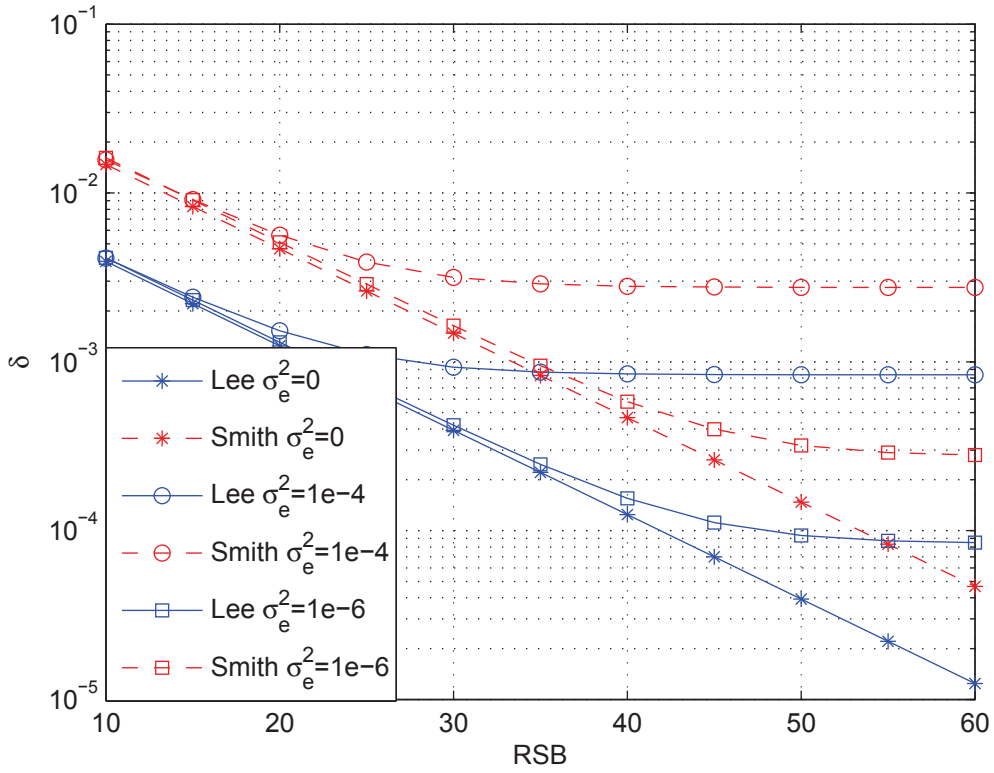

FIGURE A.7 – SRL en fonction de RSB(dB)

A.3.3 SRL basé sur le lemme de Stein

A.3.3.1 Contexte du traitement d'antenne

A.3.3.1.1 Formulation du test d'hypothèses binaire Nous abordons ici le problème de la dérivation du SRL dans le contexte du traitement d'antenne sans erreur de modèle dans A.30. Le test d'hypothèses pour ce problème peut s'écrire comme suit

$$\begin{cases} \mathcal{H}_0 : & \delta = 0, \quad \text{soit 1 source} \\ \mathcal{H}_1 : & \delta \neq 0, \quad \text{soit 2 sources.} \end{cases} \tag{A.46}$$

Pour δ suffisamment petit, le développement en série de Taylor des vecteurs directionnels au voisinage du point, $\omega_c = \frac{\omega_1+\omega_2}{2}$, est donné par $\mathbf{a}(\omega_1) \overset{1}{=} \mathbf{a}(\omega_c) - \frac{j}{2}\delta\dot{\mathbf{a}}(\omega_c)$ et $\mathbf{a}(\omega_2) \overset{1}{=} \mathbf{a}(\omega_c) + \frac{j}{2}\delta\dot{\mathbf{a}}(\omega_c)$ où le symbole $\overset{1}{=}$ signifie "approximation d'ordre un" et $\dot{\mathbf{a}}(\omega_c) = \frac{\partial \mathbf{a}(\omega_c)}{\partial \omega_c}$. Nous obtenons alors l'approximation linéaire de (A.30) comme suit

$$\mathbf{y} \overset{1}{=} \mathbf{a}(\omega_c) \otimes (\mathbf{s}_1 + \mathbf{s}_2) + \frac{j}{2}\delta\dot{\mathbf{a}}(\omega_c) \otimes (\mathbf{s}_2 - \mathbf{s}_1) + \mathbf{n}.$$

Par conséquent, le test d'hypothèse bianire linéairisé est donné par

$$\begin{cases} \mathcal{H}_0 : & \mathbf{y} \sim \mathcal{CN}(\mathbf{a}(\omega_c) \otimes (\mathbf{s}_1 + \mathbf{s}_2), \sigma^2\mathbf{I}_{LN}), \\ \mathcal{H}_1 : & \mathbf{y} \sim \mathcal{CN}(\mathbf{a}(\omega_c) \otimes (\mathbf{s}_1 + \mathbf{s}_2) + \frac{j}{2}\delta\dot{\mathbf{a}}(\omega_c) \otimes (\mathbf{s}_2 - \mathbf{s}_1), \sigma^2\mathbf{I}_{LN}). \end{cases} \tag{A.47}$$

A.3.3.1.2 Calcul du SRL basé sur le lemme de Stein Exploitant le lemme de Stein [CT, Che56], nous obtenons la relation asymptotique [2] entre la distance de Chernoff $\mathcal{CD}$ reliant deux densités de probabilité pour le test (A.47) et une probabilité d'erreur, P_e, donnée comme suit

$$\mathcal{CD}(p(y_n(l)|\mathcal{H}_0)||p(y_n(l)|\mathcal{H}_1)) = -\lim_{NL\to\infty} \frac{1}{NL}\ln(P_e), \tag{A.48}$$

où $\mathcal{CD}(p(y_n(l)|\mathcal{H}_0)||p(y_n(l)|\mathcal{H}_1))$ est la distance de Chernoff (dans la suite, par souci de garder des notations concises, nous utilisons la notation $\mathcal{CD}_n(l)$), $p(y_n(l)|\mathcal{H}_i)$ est le densité de probabilité de $y_n(l)$ associée à l'hypothèse $\mathcal{H}_i$. La distance de Chernoff entre deux distributions Gaussiennes complexes à moyenne paramétrée et de mêmes variances, *ie.*

$$y_n(l)|\mathcal{H}_0 \sim \mathcal{CN}((s_1(l)+s_2(l))\exp(j\omega_c d_n), \sigma^2),$$

et

$$y_n(l)|\mathcal{H}_1 \sim \mathcal{CN}((s_1(l)+s_2(l))\exp(j\omega_c d_n) + \frac{j}{2}\delta\frac{\partial\exp(j\omega_c d_n)}{\partial\omega_c}(s_2(l)-s_1(l)), \sigma^2),$$

est donnée par [CKNS89]

$$\begin{aligned}
\mathcal{CD}_n(l) &= \max_{0\le k\le 1} -\ln\int_\Omega [p(y_n(l)|\mathcal{H}_0)]^{1-k}[p(y_n(l)|\mathcal{H}_1)]^k dy_n(l) \\
&= \max_{0\le k\le 1} \frac{k(1-k)}{\sigma^2}\left|\frac{j}{2}\delta\frac{\partial\exp(j\omega_c d_n)}{\partial\omega_c}(s_2(l)-s_1(l))\right|^2 \\
&= \frac{\delta^2}{16\sigma^2} d_n^2 |s_2(l)-s_1(l)|^2.
\end{aligned} \tag{A.49}$$

Notons que dans le calcul ci-dessus nous avons utilisé le fait que $\frac{\delta^2}{4\sigma^2}d_n^2|s_2(l)-s_1(l)|^2$ ne dépend pas de k et que le produit $k(1-k)$ est maximisé quand $k=1/2$. Par conséquent, la distance de Chernoff entre $p(\mathbf{y}|\mathcal{H}_0)$ et $p(\mathbf{y}|\mathcal{H}_1)$ est donnée par

$$\begin{aligned}
\mathcal{CD} &= \sum_{n=1}^{N}\sum_{l=1}^{L}\mathcal{CD}_n(l) \\
&= \sum_{n=1}^{N}\sum_{l=1}^{L}\frac{\delta^2}{16\sigma^2}d_n^2|s_2(l)-s_1(l)|^2 \\
s &= \frac{\delta^2}{16\sigma^2}\sum_{n=1}^{N}d_n^2\sum_{l=1}^{L}|s_2(l)-s_1(l)|^2 \\
&= \frac{\delta^2}{16\sigma^2}N\sigma_a^2||\mathbf{s}_2-\mathbf{s}_1||^2.
\end{aligned} \tag{A.50}$$

En se basant sur les expressions (3.26) et (3.28), nous obtenons

2. Notons que le contexte asymptotique n'est pas fortement limitatif puisqu'il suffit que le produit NL soit grand et n'implique pas forcement un grand nombre de capteurs et/ou d'observations.

$$\frac{\delta^2}{16\sigma^2} N\sigma_a^2 ||\mathbf{s}_2 - \mathbf{s}_1||^2 = -\lim_{NL\to\infty} \ln(P_e).$$

Finalement, le SRL basé sur le lemme de Stein est donné par

$$\begin{aligned} \delta_C &= \sqrt{\frac{-16\sigma^2 \ln(P_e)}{N\sigma_a^2 ||\mathbf{s}_2 - \mathbf{s}_1||^2}} \\ &= \sqrt{\frac{-8\sigma^2 \ln(P_e)}{N\sigma_a^2 (L - \mathcal{R}\{\mathbf{s}_1^H \mathbf{s}_2\})}}. \end{aligned} \tag{A.51}$$

A.3.3.1.3 Résultats de simulations Nous présentons ici la comparaison entre les SRL basés sur les approches issues du critères de Lee, de Smith et du Lemme de Stein. Pour cela, nous considérons un réseau linéaire uniforme, centro-symétrique composé de $N = 10$ capteurs, avec un espacement inter-capteur d'une demi longueur d'onde, le nombre d'observations est $L = 100$, $P_{fa} = 0.01$ et $P_d = 0.99$, donc, $P_e = \frac{1}{2}P_{fa} + \frac{1}{2}(1 - P_d) = 0.01$. Nous traçons sur la figure A.8 les SRL en fonction du RSB(dB). Nous observons que le SRL basé sur la distance de Chernoff et celui basé sur le critère de Smith sont proches. Il est aussi clair que le critère de Lee qui ignore le terme de couplage est considéré comme optimiste vis-à-vis du critère de Smith.

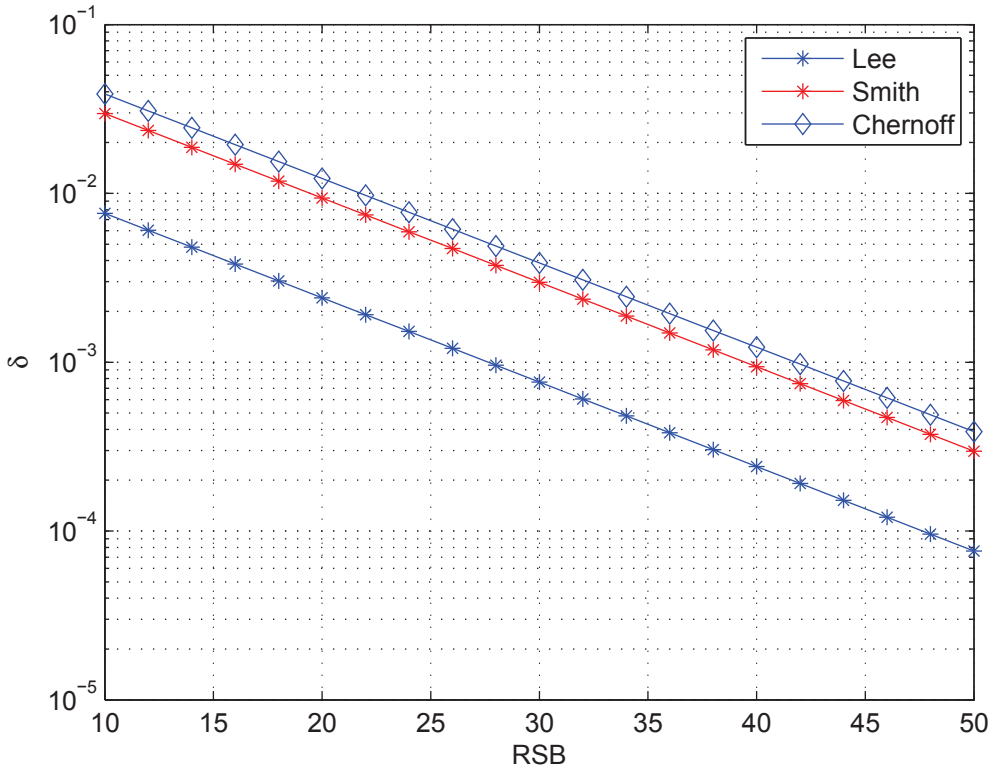

FIGURE A.8 – SRL en fonction de RSB(dB)

A.3.3.2 Contexte du radar MIMO

A.3.3.2.1 Modèle des observations de radar MIMO dont l'émetteur et le récepteur sont largement espacés Nous considérons ici un radar MIMO dont l'émetteur et le récepteur sont largement espacés avec deux cibles (voir la figure 3.9). Les deux réseaux d'antennes sont supposés linéaires avec un nombres de capteurs à l'émission et à la réception notés N_T and N_R, respectivement. Les distances entre le i-ème capteur par rapport à un capteur de référence sont notées $d_i^{(T)}$ et $d_i^{(R)}$ pour l'émetteur et le récepteur, respectivement. Dans ce contexte, chaque source est localisée par deux paramètres : l'angle de départ noté $\theta_m^{(T)}$ et l'angle d'arrivée noté $\theta_m^{(R)}$, $m = 1, 2$. Par conséquent, le signal au niveau du récepteur à la l-ème observation est donné par

$$\mathbf{X}_l = \sum_{m=1}^{2} \rho_m \exp(j2\pi f_m l)\mathbf{a}_R(\omega_m^{(R)})(\mathbf{a}_T(\omega_m^{(T)}))^T\mathbf{S} + \mathbf{W}_l \tag{A.52}$$

où $l = 0 \dots L-1$ avec L est le nombre pulses, ρ_m, f_m sont l'amplitude complexe liée à la surface équivalente radar de la cible et la fréquence Doppler normalisée de la m-ème cible, respectivement. Les vecteurs directionnels pour l'émetteur et le récepteur ont les structures suivantes : $\mathbf{a}_T(\omega_m^{(T)}) = [\exp(j\omega_m^{(T)} d_1^{(T)}) \dots \exp(j\omega_m^{(T)} d_{N_T}^{(T)})]^T$, et $\mathbf{a}_R(\omega_m^{(R)}) = [\exp(j\omega_m^{(R)} d_1^{(R)}) \dots \exp(j\omega_m^{(R)} d_{N_R}^{(R)})]^T$ où $\omega_m^{(T)} = \frac{2\pi}{\lambda}\sin\theta_m^{(T)}$, et $\omega_m^{(R)} = \frac{2\pi}{\lambda}\sin\theta_m^{(R)}$. La matrice $\mathbf{S} = [\mathbf{s}_1 \dots \mathbf{s}_{N_T}]^T$ contient N_T formes d'onde transmises où chaque forme d'onde est un vecteur composé de T observations. Nous supposons que ces formes d'onde sont orthogonales telles que $\frac{1}{T}\mathbf{S}\mathbf{S}^H = \mathbf{I}_{N_T}$ [LS09]. La matrice de bruit pour la l-ème observation, $\mathbf{W}_l$, est supposée Gaussienne, i.i.d., symétrique, de moyenne nulle et de matrice de covariance $\sigma^2\mathbf{I}_{N_R}$. Le signal de (A.52) après le filtrage adapté est donné par $\mathbf{y}_l = \text{vec}(\mathbf{Y}_l) = \frac{1}{\sqrt{T}}\text{vec}(\mathbf{X}_l\mathbf{S}^H)$. Le modèle de l'observation suit le modèle PARAFAC [Boy11, NS10] selon :

$$\mathbf{y} = \left[\mathbf{y}_0^T \dots \mathbf{y}_{L-1}^T\right]^T = \sum_{m=1}^{2} \alpha_m \mathbf{c}(f_m) \otimes \mathbf{a}_T(\omega_m^{(T)}) \otimes \mathbf{a}_R(\omega_m^{(R)}) + \mathbf{z}, \tag{A.53}$$

où $\alpha_m = \sqrt{T}\rho_m$, $\mathbf{z} = [\mathbf{z}_0^T \dots \mathbf{z}_{L-1}^T]^T$ avec $\mathbf{z}_l = \text{vec}(\frac{1}{\sqrt{T}}\mathbf{W}_l\mathbf{S}^H)$ et $\mathbf{c}(f_m) = [1\ \exp(i2\pi f_m) \dots \exp(i2\pi f_m(L-1))]^T$ où $\otimes$ est le produit de Kronecker. Nous obtenons que $E\{\mathbf{z}\mathbf{z}^H\} = \sigma^2\mathbf{I}_{LN_TN_R}$. Par conséquent, la statistique de l'observation $\mathbf{y}$ est Gaussienne complexe de moyenne $\sum_{m=1}^{2} \alpha_m \mathbf{c}(f_m) \otimes \mathbf{a}_T(\omega_m^{(T)}) \otimes \mathbf{a}_R(\omega_m^{(R)})$ et de covariance $\sigma^2\mathbf{I}_{LN_TN_R}$.

A.3.3.2.2 Formulation du test d'hypothèses binaire linéarisé Les SRL pour le problème considéré sont $\delta_T = \omega_2^{(T)} - \omega_1^{(T)}$ et $\delta_R = \omega_2^{(R)} - \omega_1^{(R)}$. Le test d'hypothèse binaire peut s'écrire comme suit

$$\begin{cases} \mathcal{H}_0 : & (\delta_T, \delta_R) = (0, 0), \\ \mathcal{H}_1 : & (\delta_T, \delta_R) \neq (0, 0). \end{cases} \tag{A.54}$$

Supposons que δ_T et δ_R sont suffisamment petits, le développement en série de Taylor des vecteurs directionnels aux voisinages des points, $\omega_c^{(T)} = \frac{\omega_1^{(T)} + \omega_2^{(T)}}{2}$ et $\omega_c^{(R)} = \frac{\omega_1^{(R)} + \omega_2^{(R)}}{2}$, est donné par $\omega_1^{(T)} = \omega_c^{(T)} - \frac{\delta_T}{2}$, $\omega_2^{(T)} = \omega_c^{(T)} + \frac{\delta_T}{2}$, $\omega_1^{(R)} = \omega_c^{(R)} - \frac{\delta_R}{2}$, et $\omega_2^{(R)} = \omega_c^{(R)} + \frac{\delta_R}{2}$, l'approximation linéaire de (A.53) est alors :

$$\mathbf{y} \simeq \mathbf{GQ}\boldsymbol{\delta} + \mathbf{z} \tag{A.55}$$

où $\boldsymbol{\delta} = [1\ \delta_T\ \delta_R\ \delta_T\delta_R]^T$, où $\mathbf{Q} = \text{Diag}\Big(\alpha_1+\alpha_2, \frac{j}{2}(\alpha_2-\alpha_1), \frac{j}{2}(\alpha_2-\alpha_1), -\frac{1}{4}(\alpha_1+\alpha_2)\Big)$, et où $\mathbf{G} = [\mathbf{g}_1\ \mathbf{g}_2\ \mathbf{g}_3\ \mathbf{g}_4]$ avec $\mathbf{g}_1 = \mathbf{c}(f)\otimes\mathbf{a}_T(\omega_c^{(T)})\otimes\mathbf{a}_R(\omega_c^{(R)})$, $\mathbf{g}_2 = \mathbf{c}(f)\otimes\dot{\mathbf{a}}_T(\omega_c^{(T)})\otimes\mathbf{a}_R(\omega_c^{(R)})$, $\mathbf{g}_3 = \mathbf{c}(f)\otimes\mathbf{a}_T(\omega_c^{(T)})\otimes\dot{\mathbf{a}}_R(\omega_c^{(R)})$, $\mathbf{g}_4 = \mathbf{c}(f)\otimes\dot{\mathbf{a}}_T(\omega_c^{(T)})\otimes\dot{\mathbf{a}}_R(\omega_c^{(R)})$.

Soit $\boldsymbol{\delta}_0 = [1\ 0\ 0\ 0]^T$ alors (A.54) est donné par :

$$\begin{cases} \mathcal{H}_0 : & \mathbf{y} \sim \mathcal{CN}(\mathbf{GQ}\boldsymbol{\delta}_0, \sigma^2\mathbf{I}), \\ \mathcal{H}_1 : & \mathbf{y} \sim \mathcal{CN}(\mathbf{GQ}\boldsymbol{\delta}, \sigma^2\mathbf{I}). \end{cases} \tag{A.56}$$

A.3.3.2.3 Distance de Chernoff pour le test (A.56) En se basant sur le lemme de Stein [CT, Che56], nous obtenons la relation asymptotique[3] entre la distance de Chernoff $\mathcal{CD}$ reliant deux densités de probabilité pour le test (A.47) et une probabilité d'erreur, P_e, fixée comme suit (voir **Appendice** 3.5.2 pour le calcul détaillé) :

$$\begin{aligned} -\ln(P_e) = &\frac{L}{16\sigma^2}\Bigg(N_R\left|\alpha_2-\alpha_1\right|^2 \sum_{n_t=1}^{N_T}\left(d_{n_t}^{(T)}\right)^2\delta_T^2 + 2\left|\alpha_2-\alpha_1\right|^2\sum_{n_t=1}^{N_T} d_{n_t}^{(T)}\sum_{n_r=1}^{N_R} d_{n_r}^{(R)}\delta_T\delta_R \\ &+ N_T\left|\alpha_2-\alpha_1\right|^2\sum_{n_r=1}^{N_R}\left(d_{n_r}^{(R)}\right)^2\delta_R^2 + \frac{1}{4}\left|\alpha_2+\alpha_1\right|^2\sum_{n_t=1}^{N_T}\left(d_{n_t}^{(T)}\right)^2\sum_{n_r=1}^{N_R}\left(d_{n_r}^{(R)}\right)^2\delta_T^2\delta_R^2\Bigg). \end{aligned} \tag{A.57}$$

Nous considérons ici le cas où l'émetteur et le récepteur sont supposés linéaires, centro-symétriques et le capteur de réference de chacun des deux réseaux est choisi comme le capteur central, *i.e.* $\sum_{n_t=1}^{N_T} d_{n_t}^{(T)} = 0$ et $\sum_{n_r=1}^{N_R} d_{n_r}^{(R)} = 0$. Définissons alors $\sigma_T^2 = \frac{1}{N_T}\sum_{n_t=1}^{N_T}\left(d_{n_t}^{(T)}\right)^2$ et $\sigma_R^2 = \frac{1}{N_R}\sum_{n_r=1}^{N_R}\left(d_{n_r}^{(R)}\right)^2$, nous obtenons

$$-\ln(P_e) = \frac{LN_TN_R}{16\sigma^2}\left(\left|\alpha_2-\alpha_1\right|^2\sigma_T^2\delta_T^2 + \left|\alpha_2-\alpha_1\right|^2\sigma_R^2\delta_R^2 + \frac{1}{4}\left|\alpha_2+\alpha_1\right|^2\sigma_T^2\sigma_R^2\delta_T^2\delta_R^2\right). \tag{A.58}$$

A.3.3.2.4 Analyse des SRL en fonction de l'amplitudes Nous étudions les SRL en fonction des amplitudes α_1 et α_2. Nous notons le $RSB = 10\log_{10}\left(\frac{|\alpha_1|^2+|\alpha_2|^2}{2\sigma^2}\right)$ en dB.

1. Si $\alpha_1 = \alpha_2 = \alpha$, l'équation (A.58) est donnée par

$$\frac{LN_TN_R}{32\sigma^2}\left|\alpha\right|^2\sigma_T^2\sigma_R^2\delta_T^2\delta_R^2 = -\ln(P_e). \tag{A.59}$$

Pour δ_T fixé et $\delta_T > 0$, $\delta_R > 0$, nous obtenons δ_R en fonction de δ_T comme suit

$$\delta_R = \frac{4\sqrt{-2\ln(P_e)}10^{-\frac{RSB}{20}}}{\delta_T\sigma_T\sigma_R\sqrt{LN_TN_R}}. \tag{A.60}$$

3. Notons que la contrainte "asymptotique" n'est pas sévère puisque même pour un nombre de capteurs en transmission, en réception et de pulses réduits, le produit LN_TN_R est grand.

2. Si $\alpha_1 \neq \alpha_2$, puisque $\delta_T \ll 1$ et $\delta_R \ll 1$, le terme contenant $\delta_T^2\delta_R^2$ (voir A.58) peut être omis et nous obtenons

$$\frac{\delta_T^2}{d_T^2} + \frac{\delta_R^2}{d_R^2} = 1, \tag{A.61}$$

où $d_T^2 = \frac{-16\sigma^2 \ln(P_e)}{LN_TN_R|\alpha_2-\alpha_1|^2\sigma_T^2}$ et $d_R^2 = \frac{-16\sigma^2 \ln(P_e)}{LN_TN_R|\alpha_2-\alpha_1|^2\sigma_R^2}$. Pour δ_T fixé et $\delta_R > 0$, nous obtenons δ_R en fonction de δ_T comme suit

$$\delta_R = d_R\sqrt{1 - \frac{\delta_T^2}{d_T^2}}, \tag{A.62}$$

sous la condition $\delta_T^2 < d_T^2$.

A.3.3.2.5 Résultats de simulation Nous considérons un radar MIMO dont l'émetteur et le récepteur sont linéaires, uniformes et composés de $N_T = 4$ et $N_R = 10$ capteurs, respectivement, avec un espacement inter-capteur d'une demi longueur d'onde, $P_e = 0.02$, et $L = 10$. Nous traçons sur la figure A.9 δ_R en fonction de δ_T pour $RSB = 40$dB dans les deux cas suivants : (i) $\alpha_1 = \alpha_2$ et (ii) $\alpha_1 \neq \alpha_2$. En comparant la figure A.9(a) à la figure A.9(b), nous observons que si $\alpha_1 \neq \alpha_2$, nous obtenons un SRL meilleur que dans le cas $\alpha_1 = \alpha_2$.

A.3.3.3 Conclusion

Dans ce travail, nous avons proposé des expressions analytiques pour le SRL basé sur la BCR et basé sur le lemme de Stein.

- Premièrement, nous avons dérivé at analysé le SRL sous forme analytique en se basant sur les critères de Lee et de Smith dans le contexte du traitement d'antenne. Nous présentons aussi une analyse des SRL en présence d'erreurs de modèle. Nous avons montré que les SRLs ne tendent pas vers zéro (au contraire du cas où il n'y a pas d'erreur de modèle) et convergent à haut RSB vers des limites fixes qui dépendent de la méthode utilisée. Nous avons donné aussi les expressions analytiques de ces limites et prouvé qu'à fort RSB, les SRLs au sens de Lee et de Smith sont linéaires en fonction de la variance de l'erreur de modèle.

- Deuxièmement, nous avons utilisé le lemme de Stein pour dériver le SRL dans deux contextes : (i) le traitement d'antenne où nous avons dérivé le SRL et comparé le SRL issu du Lemme de Stein avec les SRLs basés sur la BCR et (ii) le radar MIMO où nous avons observé que le SRL dépend fortement de l'égalité ou la différence entre les amplitudes des cibles. On a montré aussi que le SRL dépend de la différence d'amplitude des cibles.

A.4 Conclusion et perspectives

Cette thèse concerne l'application des utiles théorique dans le traitement d'antenne. Pour cela, nous avons considéré les bornes inférieures de la performance de l'estimation et le seuil statistique de résolution limite pour deux sources proches. Nous avons montré

l'utilité des utiles théoriques dans dans la résolution de plusieurs problèmes pratiques. Les contributions de cette thèse ont été présentées dans deux chapitres :

- Dans chapitre 2, nous avons considéré les bornes inférieures dans deux contextes. Le première contexte est la localisation de source en utilisant le radar MIMO. Pour cela, nous avons développé la borne de Weiss-Weinstein pour le cas bayésien et le borne de Cramér-Rao pour le cas déterministe en présence d'erreurs de modèle. Pour le cas bayésien, nous avons montré que la BWW du paramètre d'intérêt donne une bonne prédiction de l'EQM dans tout les région de RSB. Elle peut prédire aussi le seuil de RSBR proche duquel caractéristique du MAP. Dans le contexte en présence de l'erreur de modèle, nous avons dérivé les expressions analytiques de la matrice d'information de Fisher et montré sa structure diagonale bloc. Cela nous a permis de déduire les expressions des bornes de Cramér-Rao de l'angle d'arrivée et de l'angle de départ. Nous avons montré que, à partir d'un certain rapport signal à bruit, les performances du système ne peuvent plus être améliorées. Enfin, nous avons proposé une formule simple pour évaluer cette valeur critique du rapport signal à bruite. Dans le deuxième contexte, nous avons dérivé les expressions analytiques de la borne de Quinlan-Chaumette-Larzabal (pour le cas déterministe) et la BWW (pour le cas déterministe) de l'estimation de phase d'impulsion pour le pulsar X. Nous avons montré que les deux bornes prédisant bien la position du seuil d'EQM et le charge de calcul est faible en comparaison avec l'EMV.

- Dans chapitre 3, nous avons proposé des expressions analytiques pour le SRL basé sur la BCR et basé sur le lemme de Stein. Premièrement, nous avons dérivé at analysé le SRL sous forme analytique en se basant sur les critères de Lee et de Smith dans le contexte du traitement d'antenne. Nous présentons aussi une analyse des SRL en présence d'erreurs de modèle. Nous avons montré que les SRLs ne tendent pas vers zéro (au contraire du cas où il n'y a pas d'erreur de modèle) et convergent à haut RSB vers des limites fixes qui dépendent de la méthode utilisée. Nous avons donné aussi les expressions analytiques de ces limites et prouvé qu'à fort RSB, les SRLs au sens de Lee et de Smith sont linéaires en fonction de la variance de l'erreur de modèle. Deuxièmement, nous avons utilisé le lemme de Stein pour dériver le SRL dans deux contextes : (i) le traitement d'antenne où nous avons dérivé le SRL et comparé le SRL issu du Lemme de Stein avec les SRLs basés sur la BCR et (ii) le radar MIMO où nous avons observé que le SRL dépend fortement de l'égalité ou la différence entre les amplitudes des cibles. On a montré aussi que le SRL est meilleur si les amplitudes (surfaces équivalentes) des cibles sont différentes.

Les perspectives de cette thèse sont :

- Concernant la performance de l'estimation de radar MIMO
  - L'influence de l'erreur de modèle sur la performance de l'estimation de radar MIMO pour plusieurs types de l'erreur de modèle (l'erreur de phase ou l'erreur de réseau) et pour plusieurs type de système de radar (réseau non-linéaire, réseau collocalisé, ...) : dans cette thèse, nous avons considéré un scénario spécifique (l'erreur de réseau avec les antennes largement espacées), cependant, une étude générale est nécessaire pour ce type de problème.
  - La borne de Weiss-Weinstein sur la performance de l'estimation de radar MIMO avec plusieurs source et pour le problème de pistage : une expression analytique générale pour la BWW dans le contexte de plusieurs sources est nécessaire pour une étude plus profonde dans le cas bayésien.

- Concernant les bornes inférieurs pour l'estimation de phase d'impulsion de pulsar X en prenant en compte la variation de la fréquence observé : dans cette thèse, pour la comparaison avec les travaux dans littérature, la fréquence observé est supposée connue. En pratique, cette fréquence varie légèrement à cause de l'effet de Doppler. Cette variation peut affecter la performance de l'estimation. Puis, la dérivation de la borne inférieure pour ce problème est nécessaire.
- Concernant le SRL
  - L'influence de l'erreur de modèle sur le SRL de radar MIMO : on a montré dans cette thèse que l'erreur de modèle influence fortement les performances de l'estimation de radar MIMO. Par conséquent, une étude de radar MIMO en présence de l'erreur de modèle en terme du SRL est nécessaire.
  - L'expression analytique générale du SRL basé sur lemme de Stein pour traitement d'antenne et radar MIMO.

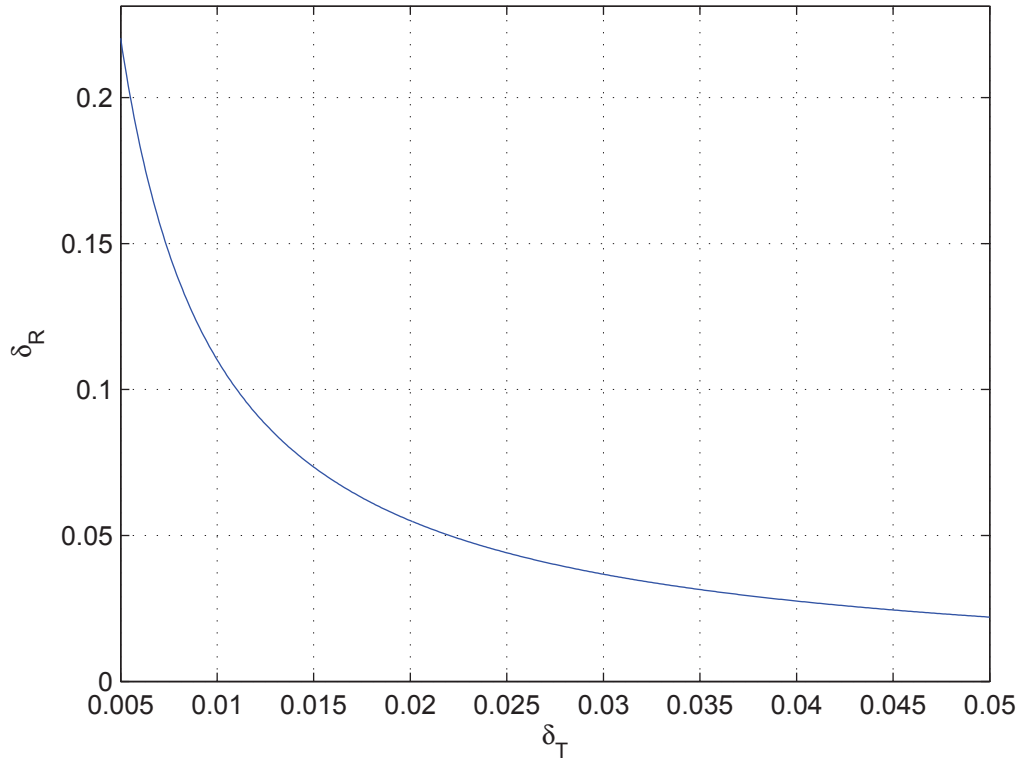

(a) $\alpha_1 = \alpha_2$

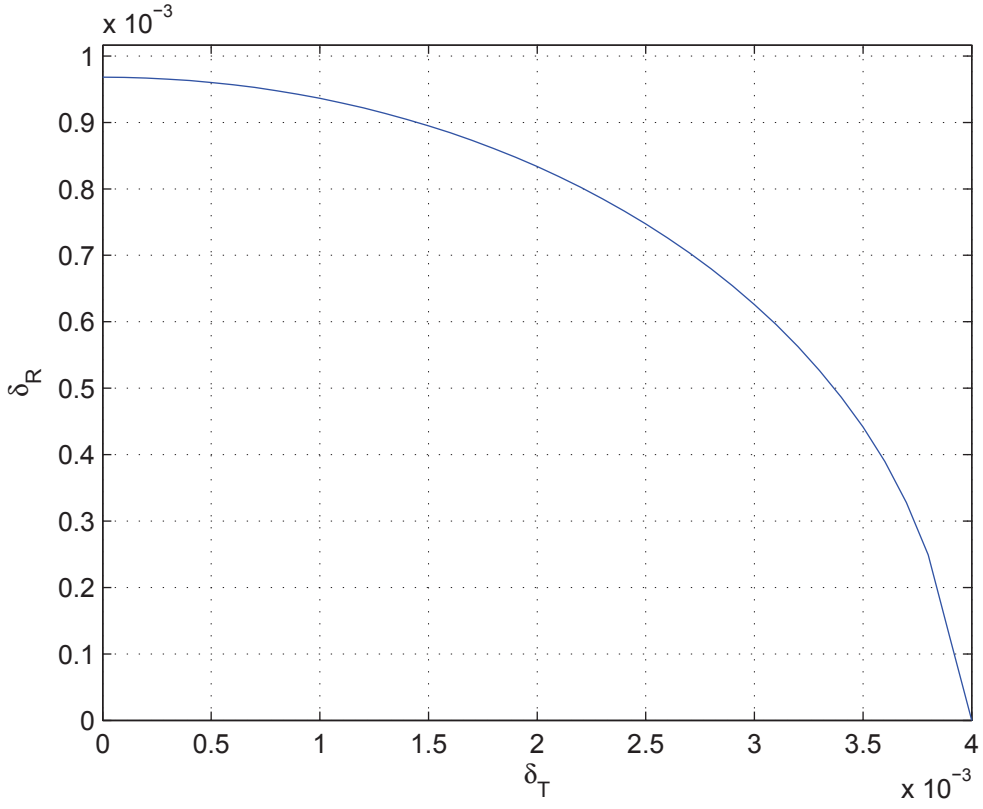

(b) $\alpha_1 \neq \alpha_2$

FIGURE A.9 – δ_R en fonction de δ_T

Notations

Acronyms

- **MSE** : mean square error
- **SNR** : signal to noise ratio
- **ASNR** : array signal to noise ratio
- **MIMO** : multiple input multiple output
- **GPS** : global positioning system
- **MLE** : maximum likelihood estimator
- **MAP** : maximum *a priori*
- **NLS** : non-linear least square
- **FIM** : Fisher information matrix
- **CRB** : Cramér-Rao bound
- **BB** : Barankin bound
- **QCLB** : Quinlan Chaumettre Larzabal bound
- **WWB** : Weiss Weinstein bound
- **TOA** : time of arrival
- **NHPP** : non-homogeneous Poisson process
- **SRL** : statistical resolution limit
- **MSRL** : multidimensional statistical resolution limit
- **ARL** : angular resolution limit
- **GLRT** : generalized likelihood ratio test
- **CD** : Chernoff's distance

General mathematical symbols

- $\mathbb{C}$ indicates the complex field.
- $\mathbb{R}$ indicates the real field.
- $\mathcal{R}\{z\}$ indicates the real part of a complex number z.
- $\mathcal{I}\{z\}$ indicates the imaginary part of a complex number z.
- The symbol * indicates the conjugate operator.
- $|.|$ indicates the absolute value.

Matrix operators and symbols

- a, A, italic letter indicates a scalar quantity.
- $\mathbf{a}$, bold lower case letter indicates a vector.
- $\mathbf{A}$, bold upper case letter indicates a matrix.
- $\mathbf{A}^T$ is the transpose of $\mathbf{A}$.
- $\mathbf{A}^H$ is the conjugate transpose of $\mathbf{A}$.
- $\mathbf{I}_N$ denotes the $N \times N$ identity matrix. .
- $|\mathbf{A}|$ indicates the determinant of matrix $\mathbf{A}$.
- $||.||$ indicates the norm of a vector.
- $A_{i,j}$ denotes theelement at the i^{th} row et j^{th} column of the matrix $\mathbf{A}$.
- $\otimes$ indicates the Kronecker product.
- $vec\,(.)$ indicates the vec operator.

Relative symbols for probability

- $\mathcal{N}(\mathbf{m}, \mathbf{C})$ indicates a multivariate Gaussian law with $\mathbf{m}$ mean et $\mathbf{C}$ covariance matrix.
- $\Pr(.)$ denotes a probability.
- $p(x)$ denotes a probability density function.
- $p(x, y)$ denotes a joint probability density function.
- $p(x|\, y)$ denotes a conditional probability density function.
- $\mathbb{E}[.]$ indicates an expectation operator.
- $\mathbb{E}_{\mathbf{y},\theta}[.]$ indicates an expectation operator w.r.t. the joint distribution $p(\mathbf{y},\theta)$.
- $\mathbb{E}_{\mathbf{y}|\theta}[.]$ indicates an expectation operator w.r.t. the conditional distribution $p(\mathbf{y}|\,\theta)$.

Table des figures

Bibliographie

[AD08] H. Abeida and J. Delmas. Statistical performance of music-like algorithms in resolving noncircular sources. *IEEE Transactions on Signal Processing*, (9) :4317–4329, 2008.

[AE01] F. Athley and C. Engdahl. Direction-of-arrival estimation using separated subarrays. In *34th IEEE Asilomar Conf. on SSC*, pages 585–589, 2001.

[AL01] R. Aharoni and D. Lee. On the achievability of the Cramér–Rao bound for poisson distribution. *IEEE Transactions on Information Theory*, 47(5) :2096–2100, 2001.

[AN10] Murat Akçakaya and Arye Nehorai. MIMO radar detection and adaptive design under a phase synchronization mismatch. *IEEE Transactions on Signal Processing*, (10) :4994–5005, October 2010.

[Ath01] Fredrik Athley. Optimization of element positions for direction finding with sparse arrays. In *Proc. 11th IEEE Signal Statistical Signal Processing Workshop on Statistical Signal Processing*, pages 516–519, 2001.

[AW08] A. Amar and A. Weiss. Fundamental limitations on the resolution of deterministic signals. *IEEE Transactions on Signal Processing*, (11) :5309–5318, 2008.

[Bar49] E. W. Barankin. Locally best unbiased estimates. *The Annals of Mathematical Statistics*, 20(4) :477–501, December 1949.

[BET96] K. Bell, Y. Ephraim, and H. L. Van Trees. Explicit Ziv Zakai lower bound for bearing estimation. 44 :2810–2824, November 1996.

[Boy11] R. Boyer. Performance bounds and angular resolution limit for the moving colocated MIMO radar. *IEEE Transactions on Signal Processing*, 59(4) :1539–1552, April 2011.

[BSET97] K. Bell, Y. Steinberg, Y. Ephraim, and H. L. Van Trees. Extended Ziv-Zakai lower bound for vector parameter estimation. 43 :624–638, March 1997.

[BZ76] B. Z. Bobrovsky and M. Zakaï. A lower bound on the estimation error for certain diffusion processes. *IEEE Transactions on Information Theory*, 22(1) :45–52, January 1976.

[CGQL08] E. Chaumette, J. Galy, A. Quinlan, and P. Larzabal. A new Barankin bound approximation for the prediction of the threshold region performance of maximum likelihood estimators. *IEEE Transactions on Signal Processing*, 56(11) :5319–5333, November 2008.

[Che56] H. Chernoff. Large-sample theory : parametric case. *Ann. Math. Statist.*, 28 :1–22, 1956.

[CKNS89] J.K Chung, P.L Kannappan, C.T Ng, and P.K Sahoo. Measures of distance between probability distributions. *Journal of Mathematical Analysis and Applications*, 138(1) :280–292, February 1989.

[Cox] H. Cox. Resolving power and sensitivity to mismatch of optimum array processors.

[Cra46] H. Cramér. *Mathematical Methods of Statistics*, volume 9 of *Princeton Mathematics*. Princeton University Press, New-York, September 1946.

[CT] T. Cover and J. Thomas. *Elements of Information Theory*. Wiley, New York.

[DGA89] J. Dorey, G. Garnier, and G. Auvray. RIAS, a synthetic impulse antenna radar. In *Proc. Int. Radar Conf.*, pages 556–562, Paris, 1989.

[Dil98] E. Dilaveroglu. Nonmatrix cramér–rao bound expressions for highresolution frequency estimators. *IEEE Transactions on Signal Processing*, (2) :463–474, 1998.

[EBRM] M. N. El Korso, R. Boyer, A. Renaux, and S. Marcos. Statistical resolution limit of the uniform linear cocentered orthogonal loop and dipole array. *IEEE Transactions on Signal Processing*.

[EBRM11] M. N. El Korso, R. Boyer, A. Renaux, and S. Marcos. Statistical resolution limit for the multidimensional harmonic retrieval model : Hypothesis test and Cramer-Rao bound approaches. *EURASIP Journal on Advances in Signal Processing, special issue Advances in Angle-of-Arrival and Multidimensional Signal Processing for Localization and Communications*, (12) :1–14, 2011.

[EBRM12] M. N. El Korso, R. Boyer, A. Renaux, and S. Marcos. Statistical resolution limit for source localization with clutter interference in a MIMO radar context. *IEEE Transactions on Signal Processing*, 60(2) :987–992, February 2012.

[ES10] A. A. Emadzadeh and J. L. Speyer. On modeling and pulse phase estimation of X-ray pulsars. *IEEE Transactions on Signal Processing*, 58(9) :4484–4495, September 2010.

[FHB+04] E. Fishler, A. Haimovich, R. Blum, L. Cimini, D. Chizhik, and R. Valenzuela. MIMO radar : an idea whose time has come. In *Proc. of the IEEE Int. Conf. on Radar*, pages 71–78, April 2004.

[FLV10] A. Ferréol, P. Larzabal, and M. Viberg. Statistical analysis of the MUSIC algorithm in the presence of modeling errors, takng into account the resolution probability. *IEEE Transactions on Signal Processing*, (58) :4156–4166, August 2010.

[GHB08] H. Godrich, A.M. Haimovich, and R.S. Blum. Cramér-Rao bound on target localization estimation in MIMO radar systems. In *Conf. Information Sciences and Systems, (CISS 08)*, pages 134–139, 2008.

[GHP09] H. Godrich, A. M. Haimovich, and H. V. Poor. An analysis of phase synchronization mismatch sensitivity for coherent MIMO radar systems. In *Proc. Third International Workshop on Computational Advances in Multi-Sensor Adaptive Processing (CAMSAP)*, December 2009.

[GHP10] H. Godrich, A. M. Haimovich, and H. V. Poor. Localization performance of coherent MIMO radar systems subject to phase synchronization errors. In *4th International Symposium on Communications, Control and Signal Processing (ISCCSP)*, March 2010.

[GS07] A. R. Golshan and S. I. Sheikh. On pulsar phase estimation and tracking of variable celestial X-ray sources. In *63rd Ann. Meet. Inst. Navigat. (ION)*, pages 413–422, Cambridge, MA, 2007.

[HB10] Qian He and R. S. Blum. Cramér-Rao bound for MIMO radar target localization with phase errors. *IEEE Signal Processing Letters*, (1) :83–86, January 2010.

[HBGH08] Q. He, R.S. Blum, H. Godrich, and A.M. Haimovich. Cramér-Rao bound for target velocity estimation in MIMO radar with widely separated antennas. In *Conf. Information Sciences and Systems, (CISS 08)*, pages 123–127, 2008.

[Kay93] S. M. Kay. *Fundamentals of Statistical Signal Processing : Estimation Theory*, volume 1. Prentice-Hall, Inc., Upper Saddle River, NJ, USA, March 1993.

[Kay09] S. Kay. Waveform design for multistatic radar detection. *IEEE Transactions on Aerospace and Electronic Systems*, 45(3) :1153–1166, July 2009.

[KB86] M. Kaveh and A. Barrarell. The statistical performance of the MUSIC and the minimum-norm algorithm in resoving plane waves in noise. *IEEE Transactions on Acoustics, Speech, and Signal Processing*, (2) :331–341, 1986.

[Lee92] H. B. Lee. The Cramér-Rao bound on frequency estimates of signals closely spaced in frequency. *IEEE Transactions on Signal Processing*, (6) :1507—-1517, 1992.

[Lee94] H. B. Lee. The cramér-rao bound on frequency estimates of signals closely spaced in frequency (unconditional case). *IEEE Transactions on Signal Processing*, (6) :1569—-1572, 1994.

[LN07] Z. Liu and A. Nehorai. Statistical angular resolution limit for point sources. *IEEE Transactions on Signal Processing*, (11) :5521–5527, 2007.

[LS09] J. Li and P. Stoica. *MIMO Radar Signal Processing*. Wiley, New York, 2009.

[LSXR07] J. Li, P. Stoica, L. Xu, and W. Roberts. On parameter identifiability of MIMO radar. (14) :968–971, December 2007.

[LXS+08] J. Li, L. Xu, P. Stoica, K. W. Forsythe, and D. W. Bliss. Range compression and waveform optimization for MIMO radar : A Cramér-Rao bound based study. 56(1) :218–232, January 2008.

[Mar97] T. L. Marzetta. Computing the Barankin bound by solving an unconstrained quadratic optimization problem. In *Proc. of IEEE International Conference on Acoustics, Speech, and Signal Processing (ICASSP)*, volume 5, pages 3829–3832, Munich, DE, April 1997.

[MS69] R. J. McAulay and L. P. Seidman. A useful form of the Barankin lower bound and its application to PPM threshold analysis. *IEEE Transactions on Information Theory*, 15(2) :273–279, March 1969.

[NS10] D. Nion and N. D. Sidiropoulos. Tensor algebra and multidimensional harmonic retrieval in signal processing for MIMO radar. *IEEE Transactions on Signal Processing*, 58(11) :5693–5705, November 2010.

[NT94] H. Nguyen and H. L. Van Trees. Comparison of performance bounds for doa estimation. In *IEEE 7th SP Workshop on SSAP*, pages 313–316, June 1994.

[PUL] The European Pulsar Network Database Browser.

[QCL06] A. Quinlan, E. Chaumette, and P. Larzabal. A direct method to generate approximations of the Barankin bound. In *Proc. of IEEE International Conference on Acoustics, Speech, and Signal Processing (ICASSP)*, volume 3, pages 808–811, Toulouse, FR, May 2006.

[Rao45] C. R. Rao. Information and accuracy attainable in the estimation of statistical parameters. *Bulletin of the Calcutta Mathematical Society*, 37 :81–91, 1945.

[RB74] D. C. Rife and R. R. Boorstyn. Single tone parameter estimation from discrete time observations. *IEEE Transactions on Information Theory*, 20(5) :591–598, September 1974.

[RFCL06] A. Renaux, P. Forster, E. Chaumette, and P. Larzabal. On the high-SNR conditional maximum-likelihood estimator full statistical characterization. *IEEE Transactions on Signal Processing*, 54(12) :4840–4843, December 2006.

[RFL05] A. Renaux, P. Forster, and P. Larzabal. A new derivation of the Bayesian bounds for parameter estimation. In *Proc. of IEEE Workshop on Statistical Signal Processing (SSP)*, pages 567–572, Bordeaux, FR, July 2005.

[RFL$^+$08] A. Renaux, P. Forster, P. Larzabal, C. Richmond, and Arye Nehorai. A fresh look at the Bayesian bounds of the Weiss-Weinstein family. 56(11) :5334–5352, 2008.

[RFLR06] A. Renaux, Ph. Forster, P. Larzabal, and C.D. Richmond. The Bayesian Abel bound on the mean square error. In *Proc. of IEEE International Conference on Acoustics, Speech, and Signal Processing (ICASSP)*, Toulouse, FR, May 2006.

[RO07a] I. Rapoport and Y. Oshman. Weiss-Weinstein lower bounds for Markovian systems. part 1 : Theory. 55(5) :2016–2030, May 2007.

[RO07b] I. Rapoport and Y. Oshman. Weiss-Weinstein lower bounds for Markovian systems. part 2 : Applications to fault tolerant filtering. 55(5) :2031–2042, May 2007.

[RP87] Y. Rockah and P.M.Schultheiss. Array shape calibration using sources in unknown locations-part i : Far-field sources. *IEEE Transactions on Acoustics, Speech, and Signal Processing*, (3) :286–299, March 1987.

[RWP06] P. Ray, K. Wood, and B. Philips. Spacecraft navigation using X-ray pulsars. *Naval Research lab. (NRL) Review*, pages 95–102, 2006.

[SM04] M. Shahram and P. Milanfar. Imaging below the diffraction limit : A statistical analysis. *IEEE Transactions on Image Processing*, (5) :677–689, 2004.

[SM05] M. Shahram and P. Milanfar. On the resolvability of sinusoids with nearby frequencies in the presence of noise. *IEEE Transactions on Signal Processing*, (7) :2579–2588, 2005.

[Smi05] S. T. Smith. Statistical resolution limits and the complexified Cramér-Rao bound. *IEEE Transactions on Signal Processing*, 53(5) :1597–1609, May 2005.

[Tab06] J. Tabrikian. Barankin bounds for target localization for MIMO radars. In *Proc. 4th IEEE Workshop on Sensor Array and Multi-channel Processing*, pages 278–281, July 2006.

[TB07] V. Trees and K.L. Bell. *Bayesian Bounds for Parameter Estimation and Nonlinear Filtering/Tracking*. Wiley, New York, 2007.

[TLWP09] J. Tang, N. Li, Y. Wu, and Y. Peng. On detection performance of MIMO radar : A relative entropy-based study. *IEEE Signal Processing Letters*, 16(3) :184–187, March 2009.

[TTP10] B. Tang, J. Tang, and Y. Peng. MIMO radar waveform design in colored noise based on information theory. *IEEE Transactions on Signal Processing*, 58(9) :4684–4697, September 2010.

[Van68] H. L. Van Trees. *Detection, Estimation and Modulation Theory*, volume 1. John Wiley & Sons, New-York, NY, USA, 1968.

[VEB+11] D. T. Vu, M. N. El Korso, R. Boyer, A. Renaux, and S. Marcos. Angular resolution limit for vector-sensor arrays : Detection and information theory approaches. In *Proc. of IEEE Workshop on Statistical Signal Processing SSP (invited paper)*, Nice, France, July 2011.

[VS94] M. Viberg and A. L. Swindlehurst. Analysis of the combined effects of finite samples and model errors on array processing performance. *IEEE Transactions on Signal Processing*, (11) :3073–3083, November 1994.

[WW85] A. J. Weiss and E. Weinstein. A lower bound on the mean square error in random parameter estimation. *IEEE Transactions on Information Theory*, 31(5) :680–682, September 1985.

[WW88] E. Weinstein and A. J. Weiss. A general class of lower bounds in parameter estimation. *IEEE Transactions on Information Theory*, 34(2) :338–342, March 1988.

[XBB04] W. Xu, A. B. Baggeroer, and K. L. Bell. A bound on mean-square estimation error with background parameter mismatch. *IEEE Transactions on Information Theory*, 50(4) :621–632, April 2004.

[XLS08] L. Xu, J. Li, , and P. Stoica. Target detection and parameter estimation for MIMO radar systems. (44) :927–939, 2008.

[Xu01] W. Xu. *Performances bounds on matched-field methods for source localization and estimation of ocean environmental parameters*. PhD thesis, Massachusetts Institute of Technology, Cambridge, MA, USA, June 2001.

[ZZ69] J. Ziv and M. Zakai. Some lower bounds on signal parameter estimation. *IEEE Transactions on Information Theory*, 15(3) :386–391, May 1969.